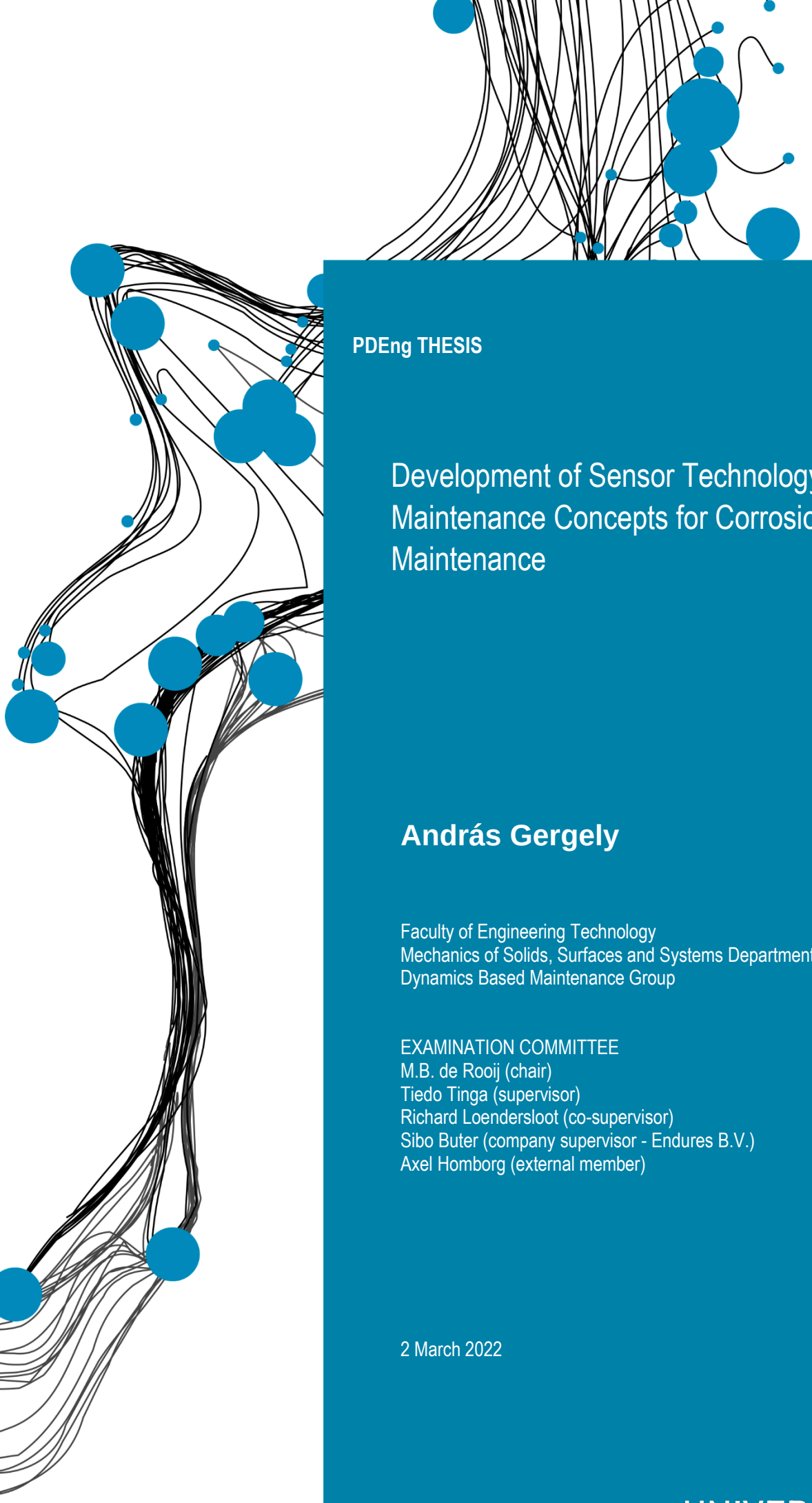

PDEng THESIS

Development of Sensor Technology & Maintenance Concepts for Corrosion-Related Maintenance

András Gergely

Faculty of Engineering Technology
Mechanics of Solids, Surfaces and Systems Department
Dynamics Based Maintenance Group

EXAMINATION COMMITTEE
M.B. de Rooij (chair)
Tiedo Tinga (supervisor)
Richard Loendersloot (co-supervisor)
Sibo Buter (company supervisor - Endures B.V.)
Axel Homborg (external member)

2 March 2022

UNIVERSITY OF TWENTE

DEVELOPMENT OF SENSOR TECHNOLOGY & MAINTENANCE CONCEPTS FOR CORROSION-RELATED MAINTENANCE

PDEng Thesis

to obtain the degree of
Professional Doctorate in Engineering (PDEng) at the University of Twente,
on the authority of the rector magnificus,
prof. dr. ir. A. Veldkamp,
on account of the decision of the graduation committee,
to be defended
on Wednesday the 02 of March 2022 at13.00 hours

by

András Gergely

born on 11 March 1976
in Kecskemét, Hungary

Preface

First, after years of chemistry related education at a technical school, I became confirmed about my enthusiasm to chemistry along with physics. I graduated as chemist and specialised in pharmaceutical science and electro-chemistry. Sometime later I developed knowledge and skills in various material science fields.

Although I deeply delved myself into subjects I worked on during my professional career and found something may not directly mean eligibility to another field of science and engineering. Generally, sensor development favours experts with background in electrical engineering and electronics, material science, mathematical and computer engineering. It was my genuine interest to be involved in such a work, but often other activities diverted me from this exciting and highly researched area. After many years of R&D work in the academic and industrial sectors, expertise and hands-on experience were acquired which allowed me to work on partly new fields of science and engineering.

To work one a military related project was my all-time dream and unexpectedly a PDEng position offered an unmissable one-off occasion to test and improve my knowledge and skills to serve a very special stakeholder which most probably could not be approached by any other means. Obviously, this position also required me to develop and extend my knowledge much further in many new areas such as electromagnetics and sensor technologies, mechanical engineering coupled with specialisation in maintenance, programming, finite and/or boundary element analysis and modelling.

This work is aimed at giving insight into and advice on the most feasible condition assessment techniques with special focus on evaluation of deterioration of paint coatings on ships and submarines, via both inspection and monitoring modes. The thesis work was performed in majority by the author. Only some last phase design validation of the prototype was carried out by other project member as referred accordingly.

Acknowledgement

I deeply indebted to and truly acknowledge my supervisor Tiedo Tinga who selected me for the PDEng position to participate in a Défense Technology Project (DTP) for the analysis and development of corrosion sensor(s) and work out maintenance concept in cooperation with the Netherlands Défense Academy on behalf of the Ministry of Défense and the Dutch Navy. He always advised and helped me with academic matters at the University of Twente as well as remained receptive for suggestions and discussions, cooperative and constructive along the entire project work.

Special thanks owe to Captain Tijdeman who allowed my stay at the Navy Premise and the Royal Naval College (formerly known as the KIM) in Den Helder during the strong Covid-19 restriction times in 2020. Without his consent and approval, major part of the laboratory experimentation, testing of the concept, sensor types and prototype hardware could not have been performed.

SUMMARY

Design work was initiated with high expectations of the stake-holders on sensing functionality of the prototype hardware, the ease of applicability in wide-range of and use-cases, working in arbitrarily both monitoring and inspection modes. After sorting and single out some of the conflicting requirements and criteria, design and development of the sensor hardware took a specific direction of dry phase material characterisation. Non-contact mode imaging and resistance assessment by contact mode measurement were tested to analyse solid state dielectric materials. The latter was partly incentivised to transfer performance and reliability of coating characterisation from test laboratories to maritime field application. Strong credit in dry phase testing with concentric probes came from the following. This method is supported by international standards and recommendations to test dielectric materials of various thickness, wide range of resistance and high robustness against transient electrical discharge, capacitive noise. The only compromise was accepted in this case to the hardware to work properly only in inspection mode.

Three design cycles were conducted, completed with assessment and validation of generation I type prototype sensors by me, whereas one additional cycle was performed to evaluate revised version of the concentric array sensor by the Endures B.V. In design cycle one, sensing characteristics of wire-based electrodes were assessed. These electrodes were inspired to test coatings via continuous monitoring mode while hosted in interior of ballast tanks which immersed with sea water by cycle patterns over time. Design cycle two was focused on assessment of interdigitated electrodes coupled into few numbers of arrays and used in non-contact mode sensing. One from two commercially available electrode array was utilised as a mono-block, while four and six pieces coupled electrically in parallel were used as interdigitated array electrodes. In design cycle three, the generation I type interdigitated and concentric array sensors were tested. These prototypes provided by a regular PCB manufacturer offered the chance of testing and validating proof of concepts in the form of a credible high-quality hardware. In outcome, correct and reliable assessment of high resistance coatings could not be performed with interdigitated electrodes via non-contact mode, although a well-controlled steady air-gap between sensor and substrate equipped with continuous grounding. On the other hand, simplified and extended form of the concentric array sensor proved to be sensitive enough, sufficiently repeatable to measure with and robust against exterior electrical noises while not necessitating electrical grounding of substrates. Therefore, this hardware was comprehensively revised and improved in many aspects by an additional design phase. Thus, in design cycle four, generation II type concentric array sensor was tested and validated on sensing characteristics compared to the outcome obtained by the wet phase setups. In general, generation II type concentric array sensor featured all benefits based on geometrical alignment of the electrodes while offered distinct advantages over gen. I prototype and much over traditional wet-phase test setups. These advantages include and not limited to the following: no shunting contribution from, measurable leakage current by condensed surface moisture between the two main in-plane test electrodes with narrow gaps,

no marked frequency dispersion in dedicated frequency range of the sensor data based on improved alignment of conductor tracks, more reliable fitting of the sensor on the surfaces of various geometries with lower probability of the electrodes not to engage with full characterisation of coatings. Although direct comparison of the CA I with the CA II was not performed, indirect comparison of the prototypes to estimate validity of the sensor readings is possible based on test data obtained with the long-exposed part of the mono-pylon. A difference of around 6×10^9 ohm cm^2 in coating resistance was obtained by testing with the CA I and II type prototypes from 10^{10} ohm cm^2 to 4×10^9 ohm cm^2. This difference is less probably or lower in scale stems from resistance drop, ionic conductivity increases of the coating after more than 11 years of continuous exposure, owing to the general good condition and the relatively low period between the CA I and CA II prototypes used for the tests. It must have been originated from the less effectively, closely fitted part of the electrodes on surface, moderate electrification of the coating, so lower measured current and overestimated resistance. The smaller lateral size of the CA II and its more of circular shape of the array allows easier and more reliable fitting of the sensor laminate on all type of surfaces with moderate rugged morphology. Improved contact of the electrode probes leads to higher degree of electrification, high current detection and so more accurate assessment. Thus, the CA II is regarded as more advanced hardware to apply for maritime use cases at field.

In regard with met design requirements, the main technical requirements of design objectives were met. Although some of the requirements such as the rate of detection or sensor availability and reliability of sensor data are difficult to prove within this work, the concentric array sensors are considered to meet such project delineated requirements. Programmatic or implementation related design requirements are believed to address appropriately by all prototypes. Nonetheless, technical requirements are in priority for condition assessment by sensors. Hence, concentric array prototypes are accepted as feasible hardware solution for sensing. As for unmet design requirements, genuine inspection device was managed to develop, not a monitoring one. The inability to obtain such a device reverts to many aspects. This could not be solved partly due to contradictory nature of the requirements and limitation on available technical aspects.

The CA prototypes developed in this PDEng program are true inspection devises, owing to its direct contact sensing mode. Nonetheless, this does not mean such sensors cannot be used for continuous monitoring, rather not advised to apply so as to avoid blocking by the sensors to mass transport of the environmental species. Continuous installation of the sensors can also have mitigated and aggravated effects. To resolve this issue, intelligent automated solutions are available for various mounting options (out of the current design space) which can lead to monitoring type application over critical areas.

In subsequent sections, there are guidelines on the main corrosion affected areas for monitoring and inspection. Critical corrosion and aging affected ship locations, structures and areas are identified. Worst affected and high-risk structures are selected as the sea, fresh and sewage water tanks bordered with double-shell hulls and biaxial joint segments of girders and stiffener web systems. As for critical

locations, these are stress concentration zones around notches, weld butts and toes, heat affected zones, biaxial type high dimensional joint sections.

Locations with tags, fasteners and crevices, welded areas and pin holes are hot-spots for initiation of corrosion and rapid spread to nearby structures. Mechanical damage of coatings often leads to fast local integrity loss in steel plates, deposition of muds, slurry and sea crustaceans on coatings on long-term. Coating failure can occur via delamination and buckle at a macro-scale. In regard with fatigue, besides steel structures over service life, coatings are also affected by brittle fracture, rupture, increasing opening and disintegration. This is inevitable due to shrinkage, decreasing ductility, increasing brittleness and fatigue cracking of coatings. Thus, large strain affected areas pose the highest integrity risk and so subjected mainly to regular sensor application. Besides aging related loss of integrity and physical protection, low-quality maintenance would highly increase severity of environment induced issues via primarily bio-fouling. Besides biogenic factor, environmental condition of the coatings is not uniform over entire surface, which leads to differentiation of states.

There are detailed guidelines on where and how to use the prototype sensor. Evaluation of the derived sensor data is given in detail for condition assessment of heavy-duty maritime coatings.

ACRONYMS

Condition Monitoring – CM

Corrective Maintenance – CoM

Corrosion Under Insulation – CUI

Delft University of Technology – TUD

Failure Mechanism and Effect Analysis – FMEA

Fault Tree Analysis – FTA

High Frequency – HF

International Maritime Organisation – IMO

Low Frequency – LF

Ministry of Defence – MoD

Maintenance Experts – ME

Maintenance Management – MM

The Royal Netherlands Aerospace Centre, National Aerospace Laboratory of the Netherlands – NLR

Non-Destructive Technique – NDT

Poly-Carbonate – PC

Poly-Methyl Methacrylate – PMMA

Preventive Maintenance – PM

System of Interest – SoI

University of Twente – UT

United State Navy – USN

TABLE OF CONTENTS

1. INTRODUCTION

1.1. Context and Background

Naval ships and submarines similar to commercial ships often experience several failure modes. There is more than a century record on it [1]. Regardless of the type of the failed system components, i.e., hull-frame, buoyance, motivation, navigation or interceptor, failure events incapacitate naval ships via annihilating full and partial mission capability, readiness, reduce mobility of assets or may even endanger crew life, although the latter is less likely than was in the 20th century [2−5]. In a distant viewpoint, severity of the events is expressed in decreasing reliability, availability, maintainability and worsened economic perspectives. Owing to decisive effect of the critical events on asset use and economics, prediction of failure events after varied timeframe of progression is priority to maintenance experts and asset management.

In the viewpoint of environmental loads, ships are affected by numerous types and amplitudes of static and dynamic loads. Mechanical loads were historically first explored and most discussed, categorised into still water and wave induced hydro-dynamic loads, fast transient loads by slamming and whipping. The internal ship load sloshing stems from movement of partly filled cargo bays and ballast tanks. Ship internal loads can vary due to fully draught and ballasted conditions, while external loads driven by dynamic pressure of the waves (induced by currents and wind). In addition, engine and propeller raised vibrations cause regular cyclic loads. Besides the mechanical loads, the marine environment exerts various loads like thermal cycling and fluctuation, vibrations, radiation and most importantly chemical loads.

The latter is perceived as the most severe factor behind numerous failure events and mechanisms over service life. Thus, naval ships and submarines are continuously exposed to severe environmental conditions [6,7] aggravated by the presence of sea water, high relative humidity and frequent precipitation/raining with its mechanical impinging impact, combined with strong waves and gusty winds [8]. Ship hull, ballast tanks, bilge and sea chest experience immersion condition by direct contact with sea water. Girders and fuel tanks experience closed chamber effect along with accumulation of corrosive chemical species and undesired sea fauna. Upper part of ships, deck, machinery are exposed to marine type atmospheric corrosion [9−11]. There are three phenomena from which two, uniform and local pitting corrosion, take place on carbon steel elements and the well passivating but locally activating aluminium and stainless-steel alloys, respectively. The third factor involves swelling, delamination and detachment of coatings [12,13] which means the end of passive protection. For a durable, safe and reliable operation at sea, the high-risk related corrosion phenomena need to be controlled.

One of the real problems is the exceptionally high rate of corrosion deterioration of almost all ship structures under marine condition. Corrosion is a prevalent damaging mechanism surpassing the impact of mechanical degradations such as fatigue caused cracking over time by a factor of ≥3. Corrosion takes

place mainly at surface and partly in bulk phase under ambient temperature. The genuine nature of localised processes is the accumulation and low controllability over time, despite the redundant protection tools. In addition, the progression rate to ultimate failure is generally difficult to predict. As an example, time-variant corrosion modelling is an effective tool to describe immersion exposure type integrity loss of steel plates, e.g., on ship hulls [14] but such models need certain input data such as end wastage, maximal corrosion allowance, and more under the actual and local conditions. It is partly because of the unknown acceleration of processes over time and local conditions different from global ones. What is more, this can act together with fatigue mechanisms. As it is learned from past experience at the US Navy (USN), localised corrosion phenomena with average pit size of 130 μm at a majority (90%) of <250 μm leads to fast growing cracks in steel plates. Despite the huge effort, no accurate prediction has been worked out on the relationship between external loads and condition of vessels, due to the highly variability of diverse loads on local areas.

The best way to avoid severe impact of the marine environment is the application of coatings [15] to block mass transport of certain species to the steel structures [16]. Nonetheless, corrosion of steel plates may take place without coating breakdown as localised actions can occur under hydrated coatings [17]. Aside from the direct physical impact and biofouling, the most deteriorative factor to coatings is the increasing service temperature. A temperature increases from 4 to 10°C can accelerate coating breakdown and shorten service life to half [18−20]. Then, subsequent corrosion of steel plates rapidly proceeds [16−22].

Thus, due to the numerous failure modes and diverse impact on the assets, the onset of failure and the recommended time for service is difficult if not impossible to predict. In general, mindful design features, sufficient load carrying capacity and a safety factor (corrosion allowance) coupled with high standard manufacturing and maintenance (crack growth management) can warrant full and safe operation over expected lifetime. In a closer view, to forgo undesired impact of localised events, corrosion monitoring or inspection offers the proper means to update the representative status of the condition of ship structures. Therefore, development of corrosion sensors(s) to assist the work of maintenance experts on accurate assessment of the condition of vessels is invaluable assistance to the asset management to organise and execute maintenance actions.

In the viewpoint of corrosion monitoring and inspection, inspection and monitoring are fundamental tools for continuous and safe long-term operation of engineering structures and high value assets. Both practices need appropriate instrumentation. Sensors represent a key part of such apparatus and so experienced recently unparalleled high demand due to burst in demand for automation, cybernetics and smart revolution of vehicles and cities. Sensors are the most dynamically extending area of scientific research and engineering, customised for a wide-range of applications. There are laboratory and field types of equipment used as NDT techniques for CM, which primarily take advantage of this rapid sensor development. As a result, maintenance experts and asset management are equipped with

leading-edge tools to ensure a good service state of engineering structures on behalf of direct and indirect stakeholders.

As for the application of corrosion sensors, a long-history of technology progress in electronics and industrial sensors make them possible. Further, the current industrial sensor market is highly motivated for further technological development. There is a large-range of MEMS sensors for condition monitoring in civil engineering. Physical parameters for sensing cover temperature, pressure, humidity, acoustics, strain, etc. Mechanical sensors detect proximity, position, level and motion of structural parts. Furthermore, chemical sensors are used for gas and bio sensing. All real-time monitoring procedures are intended to observe the environment (to forecast and measure pollution) and industrial processes for energy and infrastructure management, construction and building, factory and manufacturing processes (for smart manufacturing), chemical processing, farming and agriculture, industrial control, waste management, industrial automation, logistics and transportation (public and private). Based on the contribution of non-profit organisations, regulations and standards kept pace with and provided proper environment for advancement. Successful application of sensors can only be realised by development of telecommunication systems and software engineering. The nowadays overruling cultural trend is connected to the means of real-time, effortless and comprehensive information gathering techniques. This necessitates the use of wireless networks which are already wide-spread and diffuse into intact areas. In fact, a wireless network of sensors constitutes one important stipulation of the current project deliverables. Nevertheless, interaction of sensors, monitoring technology and the military organisations obviously includes many aspects.

In general, regardless of the initial approach and quality of design, good and regular maintenance practice plays a pivotal role in conservation of the good state of assets [23,24]. The general aim is proper planning and execution based on abundant information (data driven) on asset condition, which otherwise leads to optimised operation with high availability at reasonable cost. Nonetheless, truly helpful and accurate asset condition data can only be obtained by application of CM sensors used for monitoring or inspection or combination of these strategies. The reason for this is straightforward. The problem with maintenance organisation of maritime assets is the unpredictability of the weather conditions, and therefore of both the external and especially the internal (concentrated) physical loads accompanied with intense radiations and chemical processes which often strongly interfere with each other leading to unexpected fast and severe deteriorations. All these loads are typically cyclic and so more deteriorating than the effect of static loads. Furthermore, increased rate of disintegration of maritime exposed structures partly owes to the impact of the low occurrence of extreme events [25] which are usually omitted during the design stage. Despite a regularly updated and well-managed database, corrosion related deteriorations and failures cannot be accurately predicted in the offshore and maritime industry. This statement is true for both phenomena: uniform corrosion, but especially local deterioration like crevice and pitting corrosion.

In a historical sense, the first generation of corrosion sensors and sensing techniques were developed for the oil and gas industry [26−34] due to high integrity risk of the assets and the particularly corrosive media. Later, plenty of solutions arrived to the construction and civil engineering covering many industries like the deep-water mining facilities [35], automotive [36], concrete structures like bridges [37,38] and buildings [39−41], onshore and offshore structures [42,43], high power reactors [44], aerospace industry [45−48]. Generally, only some of those solutions are directly implementable for monitoring and most of them rather inspection capable, although continuous real-time monitoring would represent a higher value for maintenance. This is also the case for the maritime and aerospace industry. Chronologically, corrosion sensors were started to develop relatively late due to technical constrains, the lack of proper technology and incentives rather relying on experience and anecdotes. It is still often the case, because sensor mounting options would lead to altered exposure to the environment. Thus, sensor readings will not always be representative for the actual condition of the overall structure because of physical separation and restricted mass transport between the environment and mounted area.

Similar to corrosion sensors, detection technologies also evolved a lot recently but only a handful are feasible for maritime and aerospace applications. Other methods are uncompetitive for monitoring and inspection. The weight loss method is only useful for laboratory experimentation and validation [49−52] rather than real-time economic operation due to its laborious post-processing nature. On the one hand, short range ultrasonic testing performs well at spot testing for thickness and delamination. On the other hand, long-range ultrasonic testing is incompatible with maritime and aerospace applications and out of the expected accuracy range for even moderate damage size and scaling. Laboratory type classical electrochemical methods cannot be directly applied but customisation of some of those techniques may offer appropriate sensing solutions.

One of the objectives of the present work is therefore to select an appropriate technique, as will be discussed in more detail later on.

1.2. Problem Statement and Objectives

From the background on corrosion monitoring in the previous subsection, there is clearly a need for a continuous or frequently updated database on the condition of vessels heavily affected by integrity issues. Thus, main goal of the MoD and the Navy is to develop and use a set of sensors data and thus finding proper balance between preventive and corrective maintenance practice, depending on the type of locations and structures. In this sector, reliable PM supported with sensor data is considered to be the best solution. Therefore, this need translates into the request of having at least two types of sensors: one to assess condition of dielectric materials such as paint coatings and another one to test uniform and local thickness of steel plates. According to current state of the technologies, the range of electrical and magnetic material testing techniques could provide the expected degree of capabilities and performance.

Primary goal of the current PDEng project is to develop a corrosion sensor, used either in continuous monitoring or regular inspection mode, capable of assessing sensitively and reliably condition of assets, in this case paint coatings (operational need). The sensor diagnostic capabilities must be in compliance with technical requirements in inspection mode (tactical aspect).

In addition to this primary goal, there are two additional goals:

- to meet practical requirements in applicability and maintainability of the sensor, like definition of the sensor mounting options and detection peculiarities;
- to integrate the corrosion sensor(s) into maintenance practice (strategical aspect) to improve planning and execution (organisational and management needs). For a successful implementation, the relationship between sensor data and maintenance action is to be defined.

As for the importance and relevance of design solutions, relevance of this thesis work is underlined by the most recently updated expectation of the government for efficiency improvement of naval operations. This is unavoidable because versatile and multiple duties performed on a yearly basis almost annihilated usability of former knowledge and skills of maintenance experts and moderate databases (if ever existed in effectively accessible and practical way). This owes to the mainly unpredictable mission lengths and routes of service, environmental conditions and the resulting loads on vessels. Therefore, a device to detect actual condition of critically affected structures and have historical data records is highly awaited. Useful information must be readily available for all maintenance entities besides unhindered information exchange so as to increase service and lifetime of the vessels while decreasing the cost of maintenance. It is usually not evident because of a marked immediate budget sacrifice but this project could certainly come to fruition by cooperation of domestic universities and expert contractors. In addition, the government was committed to be wiser at spending public money and controlling military budget expenditure more efficiently while being a more active entity for military allies in the future.

1.3. Design Questions

The initial design objectives started with the definition of a few favourable sensor electrode configurations and extended to identification of compact AC/DC testing equipment. The former is utmost for performance and reliability of sensing while the latter for physical attainability of material testing, credibility and validity of the results. During the project, this set of objectives shrank to achievement of favourable sensor electrode configurations because the PDEng candidates in the DTP experienced severe time constraints at around half of the project timeframe. In addition, design of a state-of-the-art AC/DC equipment would have certainly required dedicated background knowledge, skills and time. Furthermore, not addressing the complete design package did not seem to be severe loss to the project due to the number of already available mobile equipment on the market, which can be readily fit with the sensor electrodes.

The following design questions can be derived from the objectives, specifying the different steps in the design process. These questions are thus related to design considerations concerning favourable

sensor electrode configurations, mounting options, practical and programmatic aspects of use by the crew, maintenance experts and possibly independent contractor consultants.

I. How can corrosion processes of maritime structures properly be monitored over time?
II. What are measurement techniques suited for condition assessment of maritime structures and corrosion related integrity losses for monitoring and inspection?
III. What are the test methods suited for evaluation of condition, deterioration of coatings?
IV. What sorts of electrode configurations are preferable for sensitive condition assessment of dielectric materials? What types of materials and sensor geometries can be favourable to accurate and reliable monitoring and inspection of deterioration of maritime coatings?
V. In programmatic and economic aspects, what types of hardware solutions can meet fast and cost-effective manufacturing of the sensor hardware?
VI. By what ways can electrolyte use for electrical testing of coatings be avoided to obliterate many practical and implementation related boundaries?
VII. What sensor mounting options are favourable for field applications (structure and sensor hardware centred aspects)?
VIII. What physical embodiments, design solutions can meet applicability and maintainability requirements of sensor hardware for the main stakeholder (ease of use and maintainability, programmatic and human centred aspects)?

1.4. Design Methodology

A systematic sequence of actions was applied to answer the important design questions, initiating with performing a detailed review followed with critical analysis of the civil and naval literature, coupled with discussion and gathering valuable information from naval maintenance and inspection experts. Based on those inputs, some heavy corrosion-affected high risk vessel structures were defined. As a next step, design boundaries and requirements for the corrosion sensors were determined.

Then, based on these requirements, three design iterations were executed. The first iteration resulted in some potentially interesting sensing concepts, which have been further elaborated and tested in the 2nd and 3rd iteration. The details of this design process will be discussed in chapter 3.

1.5. Stakeholder Analysis

The current project is financed and overviewed by the Ministry of Defense, whereas the Royal Netherlands Navy is the main stakeholder for technology development. To achieve the project objectives and deliverables within the expected timeframe, contributions from project members were regularly monitored by the project leader from NLR. With indirect interests, this party was responsible for coordination and management of the DTP, retaining full command on allocation of funds upon reaching milestones and completion of work packages.

There were two business partners representing the industrial sector: Endures BV and Damen Schelde Naval Shipbuilding – Damen Shipyards. These two entities have always had close ties with the MoD and the Dutch Navy and so are interested in reaching project goals. Endures B.V. has wide expertise in laboratory techniques and owns a corrosion inspection database, whereas the ship manufacturer remained project observer and insider consultant. These entities are indirectly and less affected by the project outcome. Short project roles and goals are given in Table 1.

Table 1. Stakeholders and independent consultant expert entities with their short-term goals

Stakeholder groups, Main entities	**Entities**	**Roles & goals**
Military sphere	Ministry of Defense	• financial sponsor of the DTP • owner of achievements of the DTP
	Royal Netherlands Navy	• operational & management user of CS
	National Aerospace Laboratory	• project coordinator, evaluator & validator of design solutions
	Netherlands Defence Academy	• one of the main contractors of design solutions
Industrial (insider) entities	Damen Schelde Naval Shipbuilding	• inventory of marine corrosion damages • to speed up initial phase of the DTP
	Endures B.V.	• inventory of typical & critical corrosion of maritime vessels • co-development of the sensor hardware • further future contracts after successful completion of the corrosion sensor hardware
Academic groups	University of Twente	• co-development of the corrosion sensor • implementation of the corrosion sensor into maintenance
	Delft University of Technology	• co-development of the corrosion sensor hardware based on expert consultancy

In the academic sector, the UT and the TUD were as subcontractors in charge of development of the corrosion sensor(s) prototype hardware. Participation of the UT was constructively supervised by expert representatives at the MoD and NLDA, contributing to my design process and hardware prototype(s). They were interested in establishing and maintaining protected environment, fostering activities in the design process and implementation phase. Long-term interests and goals of the stakeholders and other entities are summarised in Table 2.

Table 2. Long-term interests and goals of the stakeholders and independent contractors

Entity groups	Stakeholders	Roles & goals
Main beneficiaries	Ministry of Defense	• efficient navy operation; higher availability at lower maintenance cost • better view in the political atmosphere
	Royal Netherlands Navy	• safe operation • higher deploy-ability, availability • proper planning & schedule, utilisation of assets for over entire lifetime
Research institute	National Aerospace Laboratory	• support MoD with knowledge, advice & development for new technologies
Direct end-user beneficiary	Maintenance operators	• justified PM actions • reduced work load
Indirect end-user beneficiary	Marine and crew	• fewer maintenance actions
	Logistic and support	• reduced work load
Industrial parties	Endures B.V.	• to widen knowledge in sensing techniques • to earn good reference for future contracts
	Damen Schelde Naval Shipbuilding	• to obtain knowledge on corrosion affected critical structural areas of vessels • to improve ship design • main beneficiary of increased market potential after commercialisation of sensor equipped vessels
Academic groups	University of Twente	• to deepen knowledge in material science, sensor techniques & maintenance engineering • to cultivate good ties with the NLDA • to get more funding in future

1.6. Thesis Outline

The thesis is structured into eleven main chapters and around half of these contain multiple sub-chapters. First in the introduction, context and background of the thesis is established. In the subsequent sub-chapters, problem statement and stakeholder analysis are given. Final section of chapter one describes careful design considerations, questions and objectives focusing on the thesis work.

In section two, a concise literature overview is given on state-of-the-art of the potential non-destructive CM techniques with reference on the summarising table included in corresponding part of the Appendix. At the end of the review, niches and feasible terms to prototype design are underscored.

In chapter three, technical and programmatic requirements are summarised, which were established based on lean and green engineering approach. In chapter four, design method is described on development of the concept and detailed sensor hardware, planning and execution.

Chapter five covers design cycle I with description of motivation on initial sensors, outcome of the investigated independent variables, evaluation and inferences of test results and the preliminary design solutions. The subsequent chapter six is on design cycle II on outcome and interpretation of the results obtained with small-size interdigitated strip-line electrode and its array formulations. In chapter seven, three types of generation I prototype sensors were tested. Strengths and shortcomings of the hardware are discussed to reflect on motivation, development of the next generation design solution. Chapter eight presents model field test results and validation of the generation I & II formulations of a selected sensor hardware. In chapter nine, evaluation of sensor results is detailed as well as comparison of sensor features and failed targets of the requirements.

In chapter ten, recommended implementation of the sensor hardware in practice is delineated, the reasons for mounting and inspection over critical areas of maritime ships. Discussion is given on how to use sensor hardware in practice and interpretation of the sensor reading, data to facilitate seamless maintenance implementation and management.

Chapter eleven provides a concise summary with conclusions. Critical assessment of the project and thesis work is provided. In addition, recommendations on improvement of the final sensor prototype hardware are given.

This thesis work is part of a large project entitled as a Défense Technology Project for “Corrosion Monitoring” which is henceforth abbreviated and referred to subsequently as the DTP. When the term of vessel is used in the thesis, this generally may refer on both naval ships and submarines.

2. LITERATURE REVIEW

In this chapter, state-of-the-art of the scientific literature is briefly summarised on restrained selection of technologies. Firstly, the most common corrosion issues in naval vessels are identified (2.1). Then in 2.2, a number of possible non-destructive techniques are reviewed, discussing pros and cons.

2.1. Corrosion Related Issues on Naval Vessels

An exploratory move to inventory of corrosion problems and difficulties in maintenance was required by performing an overview on and identify the most critical corrosion related issues at the navy in regard with maintenance aspects and select proper sensor technologies for concept and development of detailed design. This assessment was carried out primarily by me relying on multiple maintenance assessment reports on the USN, the international literature and partly by the expert contractor Endures BV owing to extensive experience and database on all maritime corrosion related asset integrity problems.

The following information on maritime corrosion issues were found primarily in the international literature. Under normal circumstances, the time leading to breakdown of coatings [20] is generally much shorter than deterioration rate of civil trade ship [18,53−67] and naval vessel structures [16,19,21,22,68]. Regardless of the environmental impact, i.e., atmospheric or immersion exposure, the first and main means of protection to vessel steel structures is always the coatings. Organic-inorganic paint coatings and linings afford firm barrier, passive protection, physical separation of the environment from the vessel structures. Generally, paint coatings related works cover ~43% of the total maintenance cost regardless of its preventive and corrective manner [69].

The most affected vessel structures are the ones contacting with sea water, water and humidity, i.e., ballast tanks, freshwater and sewage tanks, hull (sea chest), bilge, girders and stiffeners, etc. Although this list seems to refer to extensive list (not complete), only ballast and other confined areas are difficult to reach for inspection, requires special licence and safety preparation. Thus, these areas are subjected to sensor hardware solutions. The independent contractor Endures BV pointed out mainly the same integrity problems such as coatings, water and fuel tanks, pipework of cooling systems. All these ship sections feature difficulties in diagnostics and so prognostics on condition besides maintenance cost. The literature review assisted the selection of potential techniques for conceptual sensor development.

2.2. Potential Non-Destructive Techniques

2.2.1. Ultrasonic waves

Ultrasonic inspection techniques are generally divided into three main categories, i.e., acoustic emission, short and long-range acoustics. The first is passive analogue to OCP and ECN methods, and the latter two active material testing ones. Signal intensity of the first is orders of magnitude lower than the latter two. In addition, maritime vessels feature complex structures around hull sections directly and indirectly bordered with numerous chambers, girders and stiffeners of web systems, which inherently lead to

strongly attenuated signal intensity, dissipated energy of emitted signals over relatively short distances (between location of failure and acoustic receivers). This makes almost impossible exact localisation and quantification of damages in complex vessel structures. On top of that, problem with acoustic emission is the high background noise of the marine environment [70]. All these incapacitate exploitation of this early qualitative for reliable maritime implementation. For small spot testing, short-range ultrasonic techniques are reliable and sufficiently accurate [71]. Time-flight sensing in 'pulse-echo' detection mode is suitable for single-side structure testing, while detection via 'pitch-catch' mode is often not feasible. Accurate CM is readily available over wall thickness between 1 and 40 mm to ascertain uniform wall thickness loss rates [72−74]. If there is no structural complexity then it would serve identification of planar cracks over entire cross-section of steel plates without coating removal. It does not require long training of personals and substantial support due to cheap consumables. Shortages are referred to as sensitivity to surface condition/preparation, inhomogeneities in bulk phase, probe orientation and couplant to surface, structural complexity, labour intensive manipulation and high-power supply requirement. The laser pulse excitation mode represents minor value to the industry in both performance and programmatic aspects [75−77].

Long-range guided waves ultrasonic techniques feature different set of strengths and weaknesses. There are at least 4 different groups of ultrasonic waves and few distinct modes for propagation-based testing of plates. These are strongly advised by international standards [78] for plate loss detection at inaccessible locations [79] due to complementary benefits in condition assessment to short range ultrasonic methods. None of those offers absolute material assessment. Complex behaviour of guided waves can be highlighted in susceptibility to mode conversion and transition from fundamental to harmonics at non-continuous structural sections with abrupt increase in plate thickness, while insensitive for smooth and continuous cross-section changes [80]. Difficulties with guided waves for material characterisation does not end with the required extensive knowledge and skillset coupled with regular training. Certain structural sections like sharp edges, defects and damages, intense strictures in tubes and plates, L- and T-sections often lead to mode conversions of the longitudinal, horizontal and torsional modes. As a matter of viewpoint, rich wave spectrum can be regarded as either chance and strength or limitation and shortfall depending on the frequency range for definite identification. The somewhat narrow optimal range of the ratio of phase and group velocities and plate thicknesses are obviously drawback similarly to the generally low sensitivity detection of uniform wall thickness loss (≥15%). To indicate local damages, detection threshold is usually large in size and must be comparable with the wavelength at a magnitude of ~15 mm. In reality the relatively still short investigation range, extensive surface mounting of probes with numerous cables, frequent and high-power supply for excitation and sensitive detection at moderate and 'long' distances make this method generally inapplicable [81,82]. On this matter, the electromagnetic coils transducer-based excitation (EM-AT) does not improve reasonably despite avoided coating removal [83,84].

2.2.2. Magnetic Techniques

2.2.2.1. Eddy Current Testing

Eddy current methods represent wide-scale of active testing of electrically conductive and semi-conductive materials [85−88] regardless of the absence and presence of ferromagnetic properties [89]. This is a widespread, deeply investigated and actively researched NDT area. This group of methods includes great variety of active testing modes from which many are summarised in the Excel sheet. In general, eddy current is surface sensitive to the effect of chemical state [90], anisotropy of conductivity [91] and magnetic domain structures, phase transformation in surface and the surface near bulk phase [92] due to exponential decay of magnetising and arousing field signals from a maximum analysis depth of ~6 mm. The latter depends on signal types, testing frequency, material properties like conductivity [93,94], magnetic permeability and lateral size of the probes. Primarily cracks [95,96] and other anisotropic defects and damages can be identified surface near range [97] and the presence of coatings causes no limitation [98]. Defects and damages are identified via lift-off correction. Pulsed mode [99] can help to define coating thickness accurately [100] and characterise corroded phase layers [101]. Thus, this is complementary to ultrasonic techniques which more suited for bulk phase testing. Qualitative and quantitative capabilities with 3D aligned probes cover localisation, size and orientation identification, indication of uniform and local integrity losses, i.e., cracks in three directions depending on number and orientation of magnetic field flux gate sensors [102]. Most recent development involves diverse geometries of sensor probes [103−108], array variants [109−112] with flexibility [113−115]. band selection to pulse testing modes [116], combination with TMR sensing [117], thickness assessment of metal layers via apparent eddy current conductivity spectroscopy [118], applicable to strain sensing [119] based on implementation of simulation [120,121] and modern signal-processing algorithms [122]. Overall, this group of techniques is wide-spread adopted in aerospace and shipping industry, and so DTP leaders, coordinators and consultants decided to take this one subjected to further development for aerospace implementation, dedicated to application on the NH90 helicopters at the Dutch Airforce.

2.2.2.2. Magnetic Memory Method

The passive magnetic memory method came under consideration due to sensitive detection of self-leakage of residual magnetic fields [123,124] from ferromagnetic materials affected by anisotropic magnetic field and physical load, high mobility and universal applicability. Qualitative information can be obtained from a depth of up to 7 mm [125] with detection sensitivity of ~1 nT with flux gate sensors and hand-held device with scanning at a speed of >100 m/hour. Only this technique is able to assess pitting corrosion in analysis depth of 6 mm. Flux leakage signal is proportional with the extent of deformation of magnetic domains in elastic part of the stress-strain curves [126] both in tensile and compression modes. Th effect of fatigue can be assessed [127−129] which can be valuable to assess ship hulls, ballast tanks and deck plates. This is applicable anywhere elastic to plastic transition and

permanent shift of dislocations takes place. Nevertheless, there is a large difficulty in obtaining quantitative data for maintenance experts. So, it was not taken to conceptual and detailed development [130−133].

2.2.3. Electrical Resistance

This group of techniques can be differentiated into at least four main categories as follows, the electrical resistance (ER) [134] and multiple electrical resistance or field-signature methods (FSM) [135], the direct potential difference (DCPD) [136] and the alternating current potential drop (ACPD) [137] methods. The electrical resistance measurement is specified by standards [138−140], exist in multiple implementations such as the two and four-point measurement [141−144] (dating back more than 100 years) [145], strips, various concentric sensor probes and arrays for material characterisation. Realisation of the technique provides real-time monitoring full cross-sectional impact of both uniform and localised atmospheric corrosion, integrity loss and deterioration processes. The object to monitor can be target location or modelling materials. The former realises real-time condition assessment via fitted electrodes, and the latter achieves estimation of environment corrosivity using miniaturised substrates [146−149]. Detection sensitivity is between 1 and 10 nm and the response time varies between hours and few minutes [150] while STD of sensor data is within ±20%. Direct current potential drop techniques were implemented to achieve full penetration of structures [151]. The four-point ACPD is employed in NDT testing of material properties [152−154]. The ACPD is considered as an extension of DCPD to estimate depths of defects based on varied scanning frequencies due to the skin effect. Thus, low currents can produce large potential difference [155] for characterization of emerging materials [156,157]. Latest development is the non-linear difference imaging-based crack estimation, which tolerates spatial variation of the sensing skin conductivity [158]. The electrical resistance tomography develops images of crack patterns. To increase sensing area for large-scale monitoring and to detect internal corrosion, DCPD arrays or the FSM was invented based on potential-matrix measurement [159] using electrode pairs [160,161]. The FSM provides information on location dependent changing resistance caused by local voltage drops in the system along current lines. The FSM is a potential drop technique suited for sensing uniform plate thickness losses. Application of FSM is mainly retained to land-based oil and gas transmission pipes and containers [162], fatigue crack monitoring on civil structures like steel bridges [163]. Limitations are the strong interference of low amount of salt deposition, corrosion products unfilled and filled with electrolyte on the substrate and sensor surface leading to shunting leakage current type error in detection. Preliminary information is needed to select correct probe array matching the resistance range, but sensitivity reverse proportional with lifetime of probes. Usually, weight loss method in needed prior to define selection of ER probes with suitable sensitivity and lifetime. All methods are readily applicable for plate thickness testing above 1 mm, sensitive to detect uniform material loss in the range of ~0.1%. This group was developed for the oil and gas industry and suited to evaluate atmospheric events due to insulator behaviour of the environment.

Practical implementation in maritime and aerospace industry is more than surmountable due to the need of full access to areas, permanent fitting of wire arrays over small areas and the moderately large size of the equipment. In case of aerospace industry, embedding a device like the AirCorr™ logger [164] or similar [165] is officially unauthorised by the manufacturers and its stand-alone application is not representative for the targeted location. Partly for these reasons, this design was not successful on the market and shortly after introduction of the product was phased-out, despite the Luna Sensor Suite was introduced as an award-winning design solution [166]. Based on recent developments, the inductive coupling based magnetic techniques present competitive alternatives to assess condition of metallic substrates and ferromagnetic steel plates.

2.2.4. Electrochemical Techniques

Electrochemical techniques represent major part of corrosion rate assessment methods, restrained to assess condition of the interface [167]. Passive and active DC polarisation techniques were historically first developed for laboratory and field applications. For monitoring, open-circuit electrode potential or corrosion electrode potential and electrochemical noise measurement are suited for qualitative measure of corrosivity of environment and protectiveness of engineering alloys, steel bars in concrete and coated specimens [168]. Noise measurement is not instantaneous rate assessment unlike DC resistive slopes defined in the anodic and cathodic ranges. Generally, DC techniques are compatible with the marine environment due to high conductivity of surrounding fluid phase. These are partly the reasons for such methods actively used at the USN for monitoring state of seawater ballast tanks [169]. ENM was listed for its universal use by 'no connection to substrate' configuration besides other appliable configurations suitable for laboratory and field implementations in inspection and monitoring use cases. Latest development in open circuit potential measurements is informative [170,171] for condition assessment [42,172] and time saving for inspection [173]. This is useful to define effectiveness of barrier coatings and cathodic protection systems [174] on ballast tanks [23]. Embedded solid state reference electrodes offers real-time monitoring of metallic components for over medium long periods. These electrodes are advised for corrosion monitoring, which can be composed of graphite [175] for reinforced concrete [176,177], manganese oxide [178] for cathodic protecting systems [179,180], platinum [181] and silver/silver chloride electrodes [182] for coatings existing in stable thin-layer forms [183] favourable due to reliable stability in environment of high chlorite concentration [184]. In a historical sense and general importance, such methods were started in the form of slow scan-rate DC measure by Tafel [185,186] to potential dynamic or PD scanning at the beginning of the 20th century. It was improved by Stern introducing the linear polarisation resistance or LPR [187,188] for rapid corrosion rate assessment of metals in sea water with acceptable accuracy. Active DC techniques provide acceptable accurate results on superficial instantaneous loss rate of metals based on interfacial resistance also known as the polarisation resistance. Although polarisation resistance is directly coupled and greatly affected by mass transport of the chemical components in case of macro-size electrodes and relatively large electrolysing

currents, the micron-size linear polarisation resistance or LPR sensors [189] are exempt of this characteristic. Thus, such sensors feature dominantly charge-transfer limitation which can be accurately defined by electrochemical techniques coupled with correction to surface properties. Interdigitated electrode configurations are abundant for micro-LPR sensors [190] usually coupled with electrical resistance probes for monitoring metallic section of civil and military structures [191,192]. There is civil engineering [193,194] and military applications [192,195−199] with proven validity for atmospheric corrosion evaluation. There is implementation by ElectraWatch, Inc for macro-scale monitoring of coatings to facilitate condition-based maintenance at the USN [200]. Technical details are related to series of mini-potentiostat modules coupled with two or more tape electrodes mounted on top of the coatings. Periodic report to handheld devices relies on Zigbee wireless protocol. Despite the lot of advancements and convincing applications, some works drew doubt on true validity of this sensing mode despite the introduction of many corrections.

In 2nd half of the 20th century, marked development of AC testing instruments took place. Impedance spectroscopy became available as a more informative and accurate NDT alternative and generally applicable to evaluate protection of coatings and corrosion rate of electrodes [201−205]. In cases when DC results would be noise affected by the impact of mass transport processes unknown at extent to couple with superficial electrochemistry events, i.e., Faraday processes, then a large variety of AC techniques offer remedy to differentiate these processes. Impedance testing is a powerful tool to distinct resistance contributions from different phases based on time constant of processes and to analyse reaction mechanism [206], to define charge-transfer resistance and interfacial pseudo-capacitance, and coupled further processes. This group is viewed due to exceptionally high sensitivity for surface and bulk phase events, suited to characterise corrosion at solid-liquid interphases, biofilms [207] and dielectrics such as paint coatings [208−212]. Surface condition assessment is directly expressed in the charge-transfer resistance and interfacial pseudo-capacitance. Although multi-sine [213−219], electrochemical frequency modulation [220,221] and non-linear [222,223] techniques work well under laboratory condition with reference set-ups and materials, and in research phase, further customisation is required to enable effective implementation at fields. Intensity of signal strength of the harmonic responses are at least an order of magnitude lower than fundamentals and so their use to high resistive maritime coatings and materials may look more than questionable presently. This partly means an optimal set of potentiostat-galvanostat coupled with a frequency analyser might not be possible in current state and so underperform in comparison with single-sine impedance analysis. Furthermore, non-linear EIS is usually problematic as it requires more time to scan in frequency ranges than traditional linear EIS, and it is for good a reason to improve SNR of collected data. Therefore, traditional linear impedance testing is still considered as a reference in characterisation of material properties. In civil engineering, long-term monitoring is attainable by micro-potentiostat AC/DC testers featuring ASIC-VLSI technology [224,225] which was readily available on the market around 2000 and became probably sufficiently mature over the decades. A fully-integrated on-chip solution, micro-size EIS tester

with the size of ~1.1 mm^3 (130 nm CMOS) requires power of only 10 μA at 1.2V (12 μW consumption) with stimulus generator (no off-chip auxiliary) coupled to an electrode array with lateral size of ~1×2 cm [226,227]. Wireless communicating EIS testers worked at 1.5 V with typical consumption of 300 mW, tested at the USAF with Pt electrodes (d=30 nm and width=4 mm) embedded between top and primer coatings. Taking this idea further, fully embedded sensors were elaborated [228−231] in the form of distributed sensors to monitor coatings and lap joints without leads, only wireless energy supply, communication, interrogation [232,233g. Only segments of the spectra in LF range are used for determination of coating failure. In parallel, size decreased and material selection for the sensing electrodes increased remarkably. Screen- [234] and ink-printed electrodes [235] are made of copper and silver nano-size particles, carbon nanotubes [236] and graphene [237−239]. Owing to limited timeframe of the DTP, development of a mobile impedance tester equipment was not aimed, only definition of the most favourable electrode configurations for sensor hardware formulation.

2.3. Measurement Principles

To reflect on the main differences between wet and dry phase test setups, and to underscore some of the major benefits of dry phase material test configuration, the following is described and represented in Figure 1 and Figure 2. As it is represented in Figure 1, traditional electrochemical type test setups always utilise high conductivity electrolyte (supported case) and one counter electrode for dielectric material, coating tests. The supported case is important to apply so as to avoid distortion arisen from the high resistance electrolyte and effective decoupling of the electrochemical interfacial components, i.e., the charge-transfer resistance (R_{ct}) and double layer capacitance (C_{dl}) and combine of passive model circuit elements of those in parallel topology. The third electrode is usually the lead wired metallic conducting substrates being present in high surface direct electric contact with tested coatings. In this electrode arrangement, the two main electrodes volumetrically comprise and the electrical field tests to characterise all of the materials in that volume range, which provides additional signals in the forms of geometrical cell constant and the two wet interfaces (superposition on coating properties) besides the dielectric material, although only the latter, in this case the coating is genuinely supposed and intended to test. Minor issue is the single charge-transfer resistance (R_{ct}) contribution technically measured in series with the coating resistance in initial lifetime of coatings (less comparable to each other) while later two R_{ct} measured in series with lower coating resistance (within some orders of magnitude). The latter case carries the opportunity leading to large mismatch between expected and real test results, which medium coating resistance range is otherwise the main interest of maintenance experts and asset management. The main problem is the large, the orders of magnitude difference in measured capacitive character of the system, mainly set by the electrochemical double layer pseudo capacitance (C_{dl}, ~10^{-5} F cm^{-2}) far exceeding space charge capacitive character of dielectrics, coatings (~10^{-13} ohm^{-1} cm^{-2} s^n).

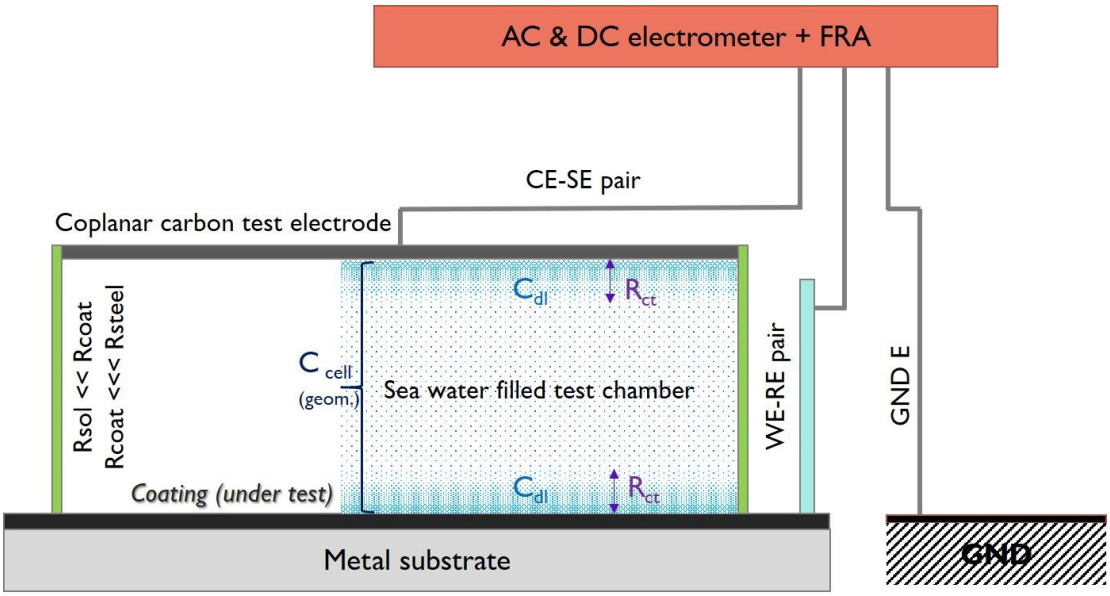

Figure 1. Traditional electrochemical test configuration with all physical components contributing to measurement signals (sensor readings).

This may lead to difficulties and inaccuracies in derivation of reliable dedicated material properties from the measurement results during field test. Further complication arises from the fact, electrical test results are unfavourably affected by strong scattering effect of the liquid-solid interface as a consequence of the huge resistance difference between coating and its environment, leading to varied rate of transmission and reflection of the electrical signals. The latter is manifested as high scatter of data in the moderate and low frequency range which genuinely feature increasing penetration into the test materials. The range of data scatter can be so much which may completely invalidate fitting and so evaluation results of the raw test data (even after advanced notice filtration). Although the argument of not committing large derivation error or performing good correction of the raw measurement data may be valid in general, any added factor to cause uncertainty in the test application and data evaluation might be seen not only questionable but rather as futile as superfluous and completely invalidating in nature in the viewpoint of reliable, credible material characterisation. To resolve all of these issues can be as simple as elegant in reality as to remove the electrolyte and test the solely dielectrics, coatings, which is in accordance with recommendations and guidelines o international standards.

Two dry state test electrode alignments are referred herein forth and represented in schematics in Figure 2. The parallel plate configuration is laboratory reference setup to test dielectric materials (Figure 2a) and another one coplanar electrode arrangement which is practically important for its universal usability in material testing for inspections and monitoring (Figure 2b).

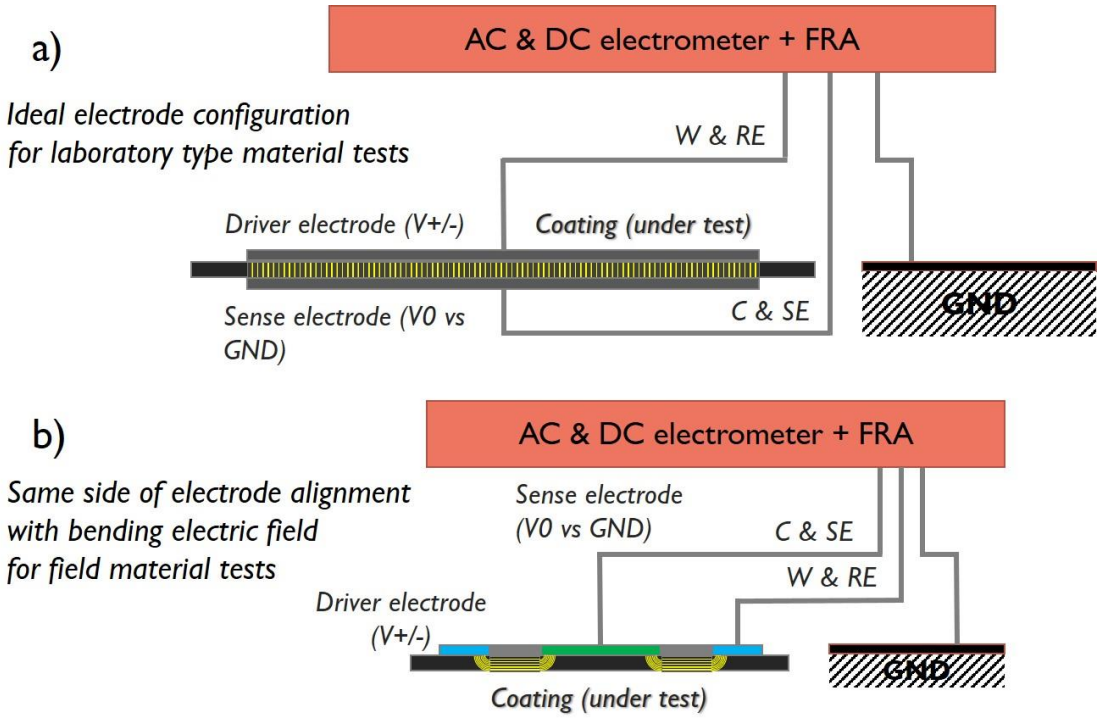

Figure 2. Traditional parallel plate electrode (a) and the inspection suited coplanar electrode alignments (b) dry phase test configurations (standard compliant) with one major measurement signal contributing factor, the coating laminate in the sensor readings (might be affected by varied contact resistance).

Although the reference setup offers assures the most representative and credible material test results with complete volumetric range testing of materials between parallel plate electrodes, such configuration can hardly be exploited in real-life situations and this shortcoming can also be resolved by varied lateral application of the sensor test electrodes. Compared to the electrochemical type wet phase testing, some of the clear advantages of such dry phase test of paint coatings with both configurations are plausibly the missing high double layer capacitance contribution in the measured signals. In addition, absence of the charge-transfer resistance is evidently also an advantage especially in later stage of coating deterioration due to its lower resistance. Representative nature of sensor readings on lower coating resistance is due to the missing effect of charge transfer resistance in series. Moreover, important practical advantage is the absence of electrolyte-coating interface, which causes orders of magnitude sudden resistance increase with reduced transmittance, and so the missing scatter of AC (in the LF range) and DC perturbation signals obtained in the measurement results. The concentric electrodes or disk-ring alignments feature further advantages like robustness against capacitive electrical noise, which ensures superior sensing performance and quality of data obtained with the generation I type concentric array prototype (presented and discussed in subsequent section of the thesis).

2.4. Final Comments

In accordance with our findings and conclusions, the following was stated in a Défense material [71,240]. Short-range ultrasonic and eddy current techniques were found sufficiently competitive with detection relative material losses of ~6% or lower (better) properly correlating with thickness loss and good spatial resolution. These were found reliable for further sensor development both for inspection and monitoring. Nonetheless, reliable material testing by these techniques without false-negative and positive indications is warranted in inspection mode rather than monitoring use case.

3. REQUIREMENTS

According to the general engineering routine, stakeholder needs and wishes representing organisational priorities were carefully learned first. Then, these were translated into both technical and implementation requirements by tools of requirements engineering and management. In a broad perspective, technical requirements of the stakeholders and end-user beneficiaries covered sensitivity and reliability of the sensor device. As was stated in section 1.2, the aim of this project is to design a sensor which is capable of sensing deterioration and onset of breakdown of coatings on ballast, fresh and sewage water tanks and pipe-work of the sea-water cooling system. Full compatibility of the sensor with the maritime environment is therefore mandatory. Further stipulation was the fast and easy communication of the sensor hardware with maintenance experts and asset management. Then, technological aspects of the requirements would come into consideration with materials of the physical embodiment and selection of certain manufacturing processes.

Practical aspects were related to the ease of practical usability, durability and maintainability. Human centred design involved easy interpretation of sensor data, knowledge transfer to maintenance practice, user-friendly operability and service-ability. Furthermore, economic aspects were connected to manufacturability with preference on low structural complexity and inexpensive materials, emphasis on long-term re-usability (physical durability) and reasonable life-time cost. These expectations are difficult to meet at the same time by the feasible design solutions and physical embodiments, especially in the viewpoint of other existing naval sensor hardware often used in single use case [241]. The latter can be understood by concluding on the options of proper detailed design solutions.

After completing the overview of stakeholder needs, requirements were set based on green engineering principles [242−244] (EPA assessment [245] on Green Engineering provided in the footnote [246]) complying with the latest engineering design attitude [247] with remind on limited resources, global maintainability, competition and high-pace market demand. In the process, cooperation with the expert consultant Endures BV helped reconsider and definition of detailed technical and practical requirements for the sensor hardware. Then, key drivers, i.e., coatings and steel structures, and coupled sensing functions were identified. Then these were transferred into requirements validated via investigation-validation cycles by answering the ‘what’ and ‘why’ and not the ‘how’ questions. Thus, requirements became traceable, quantifiable and verifiable. Tolerance limits and thresholds were included to avoid over-stringent specification and cost overrun. Further details are provided in the design method and process description in chapter 4.

3.1. Concept and Hypotheses

Due to the severe time constrains partly because of the short timeframe of the effective project work and the Covid-19 restrictions, project leaders, coordinators and contracted consultants agreed on pursuing a lean development plan involving few test matrices, the concept of testing and validation process of the

prototype design solutions. The following hypothesis was agreed on by project members. As a minimum requirement, performance and reliability testing, validation of the prototypes must show quantified results at least comparable to the outcome obtained with traditional test configurations, i.e., immersion with electrolyte (supported case) and EIS testing (besides modelling almost exactly the same conditions as immersion exposure with sea water).

3.2. Technical Aspects of Design Requirements

Quantitative aspects of the sensor function to assess protectiveness of coatings is expressed in the following requirements:

1) sensitive detection of coating deterioration and onset of breakdown, CUI,
2) representative measure of electrical resistance over full coating cross-section within the specific resistance range of 10^4 ohm cm^2 and 10^{10} ohm cm^2,
3) reliable sensor readings to obtain by using exciting voltage between 0.1 and 1 V (rms in AC test mode) and test current $>10^{-9}$ A,
4) sensor readings must be informative within the frequency range of 10^4 and 0.1 Hz with AC test (with a maximum of half an hour test time) and less than 10 minutes with DC test modes,
5) close linear sensor signals expected with increasing coating hydration (only sensitivity allowed to change with region of coating cross-section),
6) applicability to coatings with variable thickness range of 0.05 to 1 mm (by dedicated sensor array patches),
7) applicability on flat and curved surface with low and variable curvature,
8) favourably features porous lateral structure (dedicated to medium and long-term monitoring) to allow wettability of substrates by fluids and electrolytes,
9) complete lateral size shall not exceed length and width thresholds of 25×25 cm^2,
10) sensor hardware laminate thickness shall remain below 3 mm,
11) power demand of the device in active sensing mode shall not exceed 10 mW,
12) the rate of detection in time must feature excellence by uptime: ≥98% (physical readiness for use), and availability: ≥95% (working in sensing mode for detection).
13) excellent reliability of sensor readings and derived data, probability of detection of uniform and local corrosion processes: ≥95% and ≥45%, respectively. The latter is due to the fact, localised corrosion areas are the best described statistically distributed along the most active grain binderies and usually cover ratio of the overall surface.

3.3. Practical Implementation Related Design Requirements

1) full operational safety without health hazard,
2) materials used during production and operation must be in full compliance with international standards and regulations [248] along with complete recyclability after decommission.

3) low and easy or no maintenance need over sensor lifetime,
4) commercial off the shelf policy shall be supported,
5) easy installation, usability and operability by crew and maintenance experts,
6) low training needs to understand and interpret sensor data by maintenance experts and management.

The technical requirements cover quantified parameters which can be transferable to KPIs to serve examination and verification of the proposed prototype hardware solutions. The rest of the technical requirements are translated into attributes. The criteria set to evaluate sensor design involves all technical and programmatic aspects, although priority is in favour of sensing performance, effectiveness and reliability of detection over the programmatic terms (according to stakeholder preference). If objectives relating to these criteria are properly addressed and testified by laboratory and field tests, then the sensor design(s) can be regarded as successful and so accepted. Special security and privacy terms do not apply to this project.

4. DESIGN METHOD and PROCESS

In this chapter, the methodology followed in the design process is described. This implies that firstly the sensor hardware related system of interest is defined and introduced to the reader. Then, design questions are presented and discussed. In two consecutive main steps, sound design method is described while focusing on establishing feasible and proper engineering solutions. In last part, the applied design cycle is delineated in reference to the value engineering approach.

4.1. Design Considerations

According to the merit and practice of systems engineering [249], the main aspects and answers to important design questions are as follows:

1) According to the systems engineering guidelines, advanced timewise nature of expected design solution(s) is to ensure by allowing the sensor applicable under rapidly, dynamically changing environmental conditions and under various maintenance policies. Steady solutions mature in industrial engineering is to choose due to universal adoptability in both maritime (naval) and aerospace applications in the present and future. This is a hardware level feature.
2) A fundamental part of the design processes is the feedback approach to assure a proper outcome at the end of the project by repeated comparison of obtained and desired results. This will be strictly observed at times of choosing certain design directions, reaching nodes and milestones to decision making ahead of further progress.
3) Specific and generic aspects will be adopted and complied with dedicated design solution(s). Thus, the final prototype hardware is to offer a generic CM solution not restrained to the maritime

(naval) field, rather extendable to other applications which were not genuine project objectives. The ultimate generic nature of the prototype will be based on the value of high flexibility, offering solutions to numerous industrial fields.

4) Design solution(s) will have to satisfy scale-ability at various size of the organisations, i.e., crew personals, maintenance experts and asset management, whenever and whatever used at.
5) According to technical details focused rational approach, the prototype hardware is to be created based on strong scientific fundamentals. Scientific viewpoint will be guaranteed by international scientific literature and expert advice on maintenance. In addition, this will facilitate formulation of reasonable design requirements, assuring applicability at diverse fields, overlapping with the aspect of specific and generic approach and scale-ability at various organisations.
6) Lifetime usability will be a strong proviso on the prototype hardware. So, this aspect has to be added to the list of requirements. No single mount and use device are accepted. Instead, owing to the need of multiple mount-ability and durable usability besides the economic and environmental aspects is required to comply with. Therefore, hardware solutions will be developed in two specific ways to meet this requirement.
7) A minor risk of ineffective sensing performance and unreliability of detection of uniform and localised integrity losses is identified, when the design will be based solely on one physical embodiment and one detailed design solution (i.e., sensor probe and/or mobile tester equipment.) Therefore, two fundamental types and in one of those two physical embodiments are anticipated to be developed. No other risks were identified to the sensor design and device integration into the SoI, the naval maintenance concept.
8) Operational perspectives must be added to the requirements list referring to continuous usability for sensing and frequent short-term (renewed) mount-ability on targeted locations. The former is required for high-throughput utilisation over a regular working day/shift for routine labour. The latter can be critical to thin sticky-patch sensor laminates, which otherwise express limitation due to the intention to retain unaltered deterioration processes and perform representative condition assessment.
9) In terms of health and safety, strong requirements will be formulated in line with international standards (referenced ahead of this section) over the entire lifetime of the sensor from production to decommission. These require safe materials to use for production, no emission and pollution of environment, low power uptake, energy consumption and full recycle-ability at decommission.

4.2. Functional Analysis

A systematic examination and functional analysis provided guidance in arriving to justified functions of the corrosion sensor from the beginning of the design process. To assist an effective and rapid convergence to the final solution, first the less specific five ‘What’s questions’ were answered, and then the more specific five ‘W’s’ were addressed. Answers to the five ‘What’s’ are summarised in the left

hand-side of Figure 3. The first one delineates a monitoring device, prototype hardware itself and its main functions such as sensing and data processing. These functions are reviewed and confirmed to be rudimentary without redundancy to facilitate maintenance expert and asset management in decision making and organisation. The answer to the last 'What's' is a mixture of environmental compliance and minimisation of costs, although the latter is generally far from comparable with the economic scale of naval vessels.

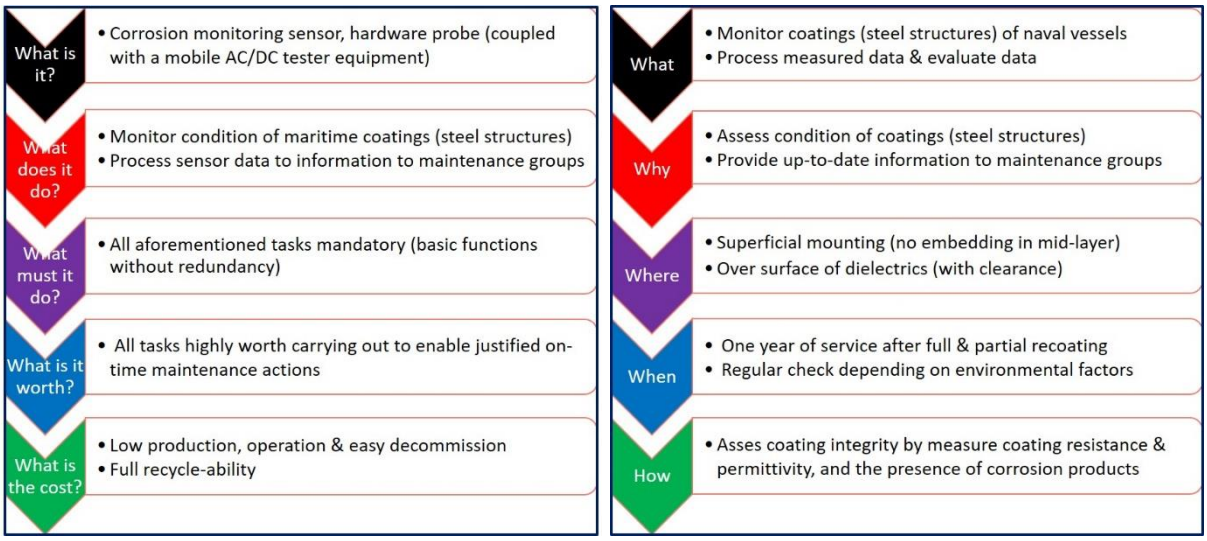

Figure 3. The 5 'What's with answers (left-hand side) in guidance leading to required functions of the corrosion sensor. The 5 'W's listed on the right-hand side are to define some details of the design solution(s).

Answers to the five 'W's are given on the right hand-side of Figure 3, which are more focused on physical and practical terms of the final design choice by making the transition from general to customer related aspects. The first two answers to 'What' and 'Why' serve to specify and check validity of sensor functions. The answer to the question 'Where' clarifies physical locations, mounting options of the sensor to monitor coatings on top surface areas with direct contact (either with adhesives and/or application of force on backside) and some clearance (with some spacers). The question of 'When' was answered from two directions. The one major part is closely defined by the use cases and scenarios experienced by naval vessels after coating application in dry docks, whereas the other one is more related to timing of routine and full-scale inspection practices by crew members and maintenance experts. The most specific term in the whole function set is the answer to the question 'How', which defines the important physics principles of the sensor hardware. What more in this choice is the extended sensing function to assess integrity deterioration of coatings and the underlying steel substrates at the same time. To sense the latter is somewhat more sensitive than the former because of the orders of magnitude higher electrical conductivity of semiconductors and higher permittivity of such corrosion products compared to intact and partially hydrated, deteriorated maritime paint coatings. Therefore, key performance indicators are assessed in regard with technical requirements and the reliability of derived sensor data.

4.3. Design Iterations

The overall applied process is best described by three main stages which constitute a design cycle. Note that the latter is generally a subset of more extended engineering cycles with at least 2 more stages: implementation in real-world situations and evaluation of those results. Design cycle performed in the project is described herein with.

1) The first stage covers the problem investigation and definition (see chapter 1 and 2), based on stakeholder needs, project goals, civil and naval literature, and the navy in-house inventory.
2) The second stage is the actual design phase, which involves the definition of requirements (see chapter 3), exploration of a wide range of available and a more limited range of proper treatments (chapter 5, 6 and 7). The last part is the careful selection of treatment options relying on the value engineering approach and supported by consensus of the project members.
3) The third and last stage of the process requires theoretical and experimental validation of first the preliminary, then the detailed design solutions. This can be achieved by using a minor set of scenarios for analysis, literature on theoretical methods and experimentation with representative test samples. For the latter, a reduced set and range of variables could be utilised allowing the comparison of expectation limits and obtained results. Then, an effective feedback initiates possibly the next design cycle for another iteration for further improvement.

Although sensor development in this project included a mocking example of real-life implementation and test (in reference to samples immersed into seawater for around 10 years in a work-bench laboratory at Endures BV), such sensor test condition was not iterated and extended to similar samples and use cases and so the last move of sensor testing cannot be regarded as a valid extension of the design cycle to an engineering cycle with all of its implications. Thus, this sensor development is not regarded as a result of fully compliant engineering design procedure with an aim to present a real market ready product. However, until reaching the prototype stage, the three mentioned design steps are followed in each iteration.

4.4. Technology Selection

Technology selection was performed by the following principle and steps. First, all potential inspection technologies were reviewed in the international literature and the actual state of the art was briefly listed. Categories for prioritisation of wide selection of techniques were set based on main informative features, performance metrics, practical usability, economic aspects and personal training requirements. In general, maritime compatibility is a plausibly overruling factor. After that in priority, absolute condition assessment capability of the techniques was viewed and chosen priority over instantaneous rate evaluation means, regardless of surface and bulk deterioration processes tested by the methods. Then, free public availability, key performance indicators featured one main category for technology ranking. Possible transition from inspection to monitoring use case of the sensor technologies was also main

factor in consideration. Geometric peculiarities of the test methods, spatial requirements and complexity of the tested materials and structures were the second. Further key feature in the decision making was the types of tested deterioration, integrity loss and corrosion processes, i.e., coatings and steel structures, uniform corrosion, localised types crevice and pitting corrosion, stress corrosion cracking and corrosion fatigue. Test parameters and materials were moderate in important for categorisation, similar to specific features assigned as strengths and shortcomings or limitations. All these factors were added and further weighed with economic factors. In a general value engineering viewpoint, this is simplified to divide all main features used in numerator with the denominator, i.e., economics, cost factors. As a result, any technologies with high score such as the short range ultrasonic, eddy current and magnetic memory methods, electrical resistance and electrochemical techniques (from those only impedance considered) were selected for further analysis and comparison. After identification of the most severe integrity issues, this list was shortened to the most appropriate techniques which offered representative assessment of condition of maritime coatings. Thus, the list was shortened to two main categories such as the electrical/electrochemical and eddy current techniques. The former is closely related to each other in real-life maritime field applications, so segregation of these in this context would not be advantages and practical. The eddy current techniques as a still large group of diverse methods were retained to the aerospace engineering, so electrical/electrochemical methods were chosen to development for maritime implementation. In the evaluation procedure, the value engineering approach [250,251] was followed to select proper treatments via several iterative steps and helped a lot in providing guidance to the right direction and ensure validity of all selection steps.

5. DESIGN CYCLE I – PRELIMINARY STAGE

5.1. Motivation to Initial Sensors

Owing to the fact that ballast tanks of naval ships contain sea water at least 25% of the cruising period which means for over that time coatings experience immersion type of exposure. Sea water is a good ionic conductor electrolyte regardless of the actual temperature, varying typically between ~5 and 12.5°C. Thus, this period was exploited for wet phase testing via *electrochemical sensing*, using metallic (primary) electrodes for electrical testing, which is a proven method in a classical sense. This approach is supported by industrial routines and international standards, wide adoption in scientific [252−254] and in engineering aspects [255−259] to evaluate coatings in the presence of electrolyte and the use of EIS for electric testing. In addition, experts at Endures BV, also utilizes this technique in a variety of ways for inspection both in the laboratory and at field.

Selecting electrochemical sensing is a chance and limitation in itself at the same time. It is a chance because the unavoidable presence of seawater allows this type of characterization, whereas limitation as coating condition assessment cannot be performed over periods when seawater is not available. As an additional reasoning, wire-based electrodes are thought to represent practical advantage over monolith alternatives in application universality and operation reliability in cases of varying water level and diverse substrate geometry, which would certainly not easily be addressed by monolith electrodes. In this chapter, part of the results obtained with some wire-based electrodes are presented and discussed.

5.2. Approach

Electrochemical testing of materials, in this case coatings, works exactly the similar way as general impedance testing works. It includes the steps of starting with the impression of a voltage over a specific surface, interface and volume range of materials for electrification, then measuring the intensity decay or increase of an output signal and appropriate estimation of the phase signal (distortion) compared to input signal. Overall, it means evaluation of electrical transmission lines in regard with impact of the tested materials on propagation of the electrical signals. The complexity of such an evaluation when applied to coatings increases by at least two factors.

The Faraday impedance involves interfacial charge transfer resistance and double layer capacitance in a minimum case, from which none of them behave linearly in response to perturbation voltage and current signals. This is overcome by applying low input voltages and/or currents for excitation which primarily arise linear system response. Thus, magnitude of the input signals must be carefully matched with resistance of the material, kinetic reaction rate of the investigated system. Another aspect is the emerge of Warburg impedance with increasing electrolyte infiltration into coatings over extended immersion exposure. Usually, accurate segregation of all components in the impedance spectra can be very difficult and its validity always matter debate between experts.

With regards to the electrodes, in the ideal situation the work and counter electrodes are located moderately close to test materials close enough to yield a homogeneous and proper degree of electrification but not too close to avoid capacitive noise in the output signal. Individual electrodes are expected to have the same activation for sensing all over surface of tested specimens. A further level of complication arises by the fact that closely located electrodes and test materials feature high cell capacitance and long distant arrangement features high resistance, strong electrical concealment for detailed sensing by the electrolyte, obvious shortcomings of test configurations in the presence of electrolyte. This means electrodes must have perfect fitting surface morphology with, as a negative of surface morphology of the investigated structures. In addition, no resistance variation along the macroscopic surface is allowed to happen to preclude any involvement of constant phase elements for modelling description of phase dispersions. Thus, such criteria are almost impossible to comply with in real-life situations and diverse, complex surface structures. Therefore, often a very good approximation of homogeneous surface activation is assumed and accepted. All in all, these underline the importance of an appropriate choice of electrode selection or configuration, electrical test modes and parameters. Optimisation of the former is focused on and discussed in this thesis work, while the latter is generally addressed according to actual circumstances and given as details of experimental parameters without any special statement.

Wire based electrodes, electrolyte, substrates and coatings are introduced and described in the first three subsequent experimental sections. This is followed by description on instrumentation as integrated electrometer and frequency analyser and the applied method for data analysis. In the final subsection, 5.3.6, the motivation for the test matrix is stated. After that, section 5.4 presents the experimental results, along with evaluation and discussion with all implications leading to the next iteration stage of the design process.

5.3. Experimental

5.3.1. Electrodes

The preliminary sensor electrodes were created in many shapes and sizes from tin coated copper wires with two diameters. All electrodes were hand-made majority prepared in pairs nominally the same for the sake of joint assessment of the electrodes via applying on the same coatings over different macroscopic sections with an assumption of equal condition, while electrically coupled with the steel substrates. The electrodes of major interests were formulated in spiral and meander shapes in 3 different sizes, but due to brevity of time only two larger in size were tested. The spiral and meander shapes were aimed at investigation because similar configuration of the former utilised for eddy current testing of steel substrates under coatings, whereas the latter provides effective sensing of coating properties, i.e., conductivity and permittivity with sufficient sensitivity and without marked inductive response in the impedance response signal. It must be noted single-wire spiral electrodes are not expected to model inductivity of wire-loops (used for inductive sensing) due to lack of forward and backward leads (or

'up' & 'down' turns of loops) but served as surrogates to analyse impedance responses from dielectrics. In fact, terminal spirals are not directly comparable to pancake coils genuinely suited for eddy current testing of conducting, e.g., aerospace alloys, as taken to further development in the DTP. The meander shape is regarded as linear alternative of the spiral, both featuring transition between the ideal monolith planar (fill factor of 1) electrode and the highly distributed spatial configurations (with fill factor of ~0.5). Then, results were compared to the outcome obtained with the 'reference' type electrodes.

Table 3. Main properties of the hand-made preliminary sensor electrodes

Electrode types	Wire & geometrical diameter (mm)	Complete length (immersed zone, mm)	Number of wire arms	Surface (cm^2)	Surface ratio (m^2/m^2) to		Estimated geometrical cell capacitance [ii] (F)	Estimated electrical double-layer capacitance [iii] ($\mu F\ cm^{-2}$)
					Coating area	Pt gauze		
Investigated configurations								
Double meander (DM)	0.5	490	2	7.7	0.78	0.14	4.03×10^{-10}	154
Extended meander (EM)	0.5	1500	2	23.6	2.38	0.43	1.23×10^{-9}	471
Extended spiral (ES)	0.5	245	2	3.9 (7.7 [i])	0.39 (0.78)	0.14 (0.07)	5.53×10^{-11}	77
Large spiral (LS)	0.5	1700	1	26.7	2.70	0.49	3.83×10^{-9}	534
Reference configurations								
Pt gauze (cylinder)	35	50	-	55	5.55	1.00		1100
Carbon (planar) plate	35.5	Complete	-	9.9	1.0	0.18	1.71×10^{-11}	198
Carbon (planar) plate	80 [vi]	Complete	-	50.3	0.64	-	8.67×10^{-11}	1005

[i] Native geometrical surface is also given although effective surface was lower due to close reeling of wire pairs, so double-wire data given in parentheses.

[ii] Cell capacitance was estimated based on permittivity of sea water (ε_r=78) at room temperature and using reference engineering formulas for calculations [260]

[iii] Pseudo capacitive character of the electrodes were calculated based on double-layer capacitance of carbon electrodes immersed in sea water [261]

[vi] Coating surface area tested with the large PMMA-CE electrode was 78.5 cm^2 with inner diameter of 100 mm and the cell capacitance derived at electrode-coating distance of 40 mm.
All electrodes were fixed at a distance of ≈30 mm off the coating surface, except for the platinum gauze with its closest perimeter located at a distance of ~5 mm.

There were two types of counter electrodes for reference testing. The one platinum gauze was used for laboratory testing, and another PMMA housed planar carbon electrode primarily utilised for coating inspection at fields. Comparison between and the scale of departing test results obtained with the wire-based electrodes and the 'reference' ones led to conclusions to dismiss the concept or accept and take it for further development. Although many other electrodes were created but these in numbers combined with independent variables for testing resulted in an extensive test matrix which could not be fully explored over the short timeframe. Hence, detailed analysis of those electrodes is omitted in the subsequent section. In an electrochemistry viewpoint, tin plating of copper wires is protecting from major corrosion issues in fresh water but somewhat in sea water. Therefore, electrodes were rinsed with tap and distilled water after short-term use for impedance and small vertex potential DC scanning. In another standpoint, the validity of estimation of coating resistance is ensured by the fact polarisation resistance and charge-transfer resistance of tin-plated copper remained orders of magnitude below (~10^3 ohm cm^2) resistance of the coatings. Geometrical details and derived parameters of the electrodes are given in Table 3.

As it is shown in, the ratio of geometrical electrode surface and the investigated coating areas were closely matched except for the extended spiral (ES) while the double meander (DM) was exceeded by the EM and LS electrodes. Compared to the platinum reference, LS was closest in surface area. Small differences in geometrical surface translate into large cell and double-layer capacitance of the test configurations due to spatial alignment of the electrodes and the presence of sea water. The EM and LS featured high cell and pseudo-capacitance over the DM, ES and standard electrode configurations. Despite the large lateral size, low and moderate contribution to such parameters by the monolith planar reference electrode is a definite advantage. These properties mean incapability of representative assessment of coating capacitive characteristics with wire electrodes. On the other hand, increased size and/or lower charge-transfer resistance of counter electrodes can offer a more representative estimation of coating resistance via two electrodes test setup, owing to the decreasing additional resistance measured in series with the coating in the test circuit. Therefore, wire-based electrodes are regarded as alternative means of assessment of coating properties, pore resistance but not recommended to use for evaluation of capacitive character. To support this view, coating resistance is always referred to as a more sensitive parameter / indicator of coating condition rather than capacitive properties. This owes to the several orders of magnitudes of difference between scaling of coating resistance (10^6–10^{12} ohm cm^2) along with capacitive character (10^{-9}–10^{-12} F cm^{-2}). Inner capacitance of the meander configuration was moderate with lower variation (based on length of the wire arms), closer to each other than the spiral electrodes, owing to the steady distance within arm segments almost independent of the covered

geometrical area. The LS with 25 turns at a diameter of 40 mm featured large cell and double-layer capacitance which is highly unfavourable due to the high base, own capacitive signal and so low degree of useful signal such as permittivity of the coatings. Although large cell capacitance would mean high rate of interacting surface between electrodes and coating surface, unfortunately this translates to high double-layer capacitance as well. This is partly the main reason for wire-based electrodes not in use for laboratory setups.

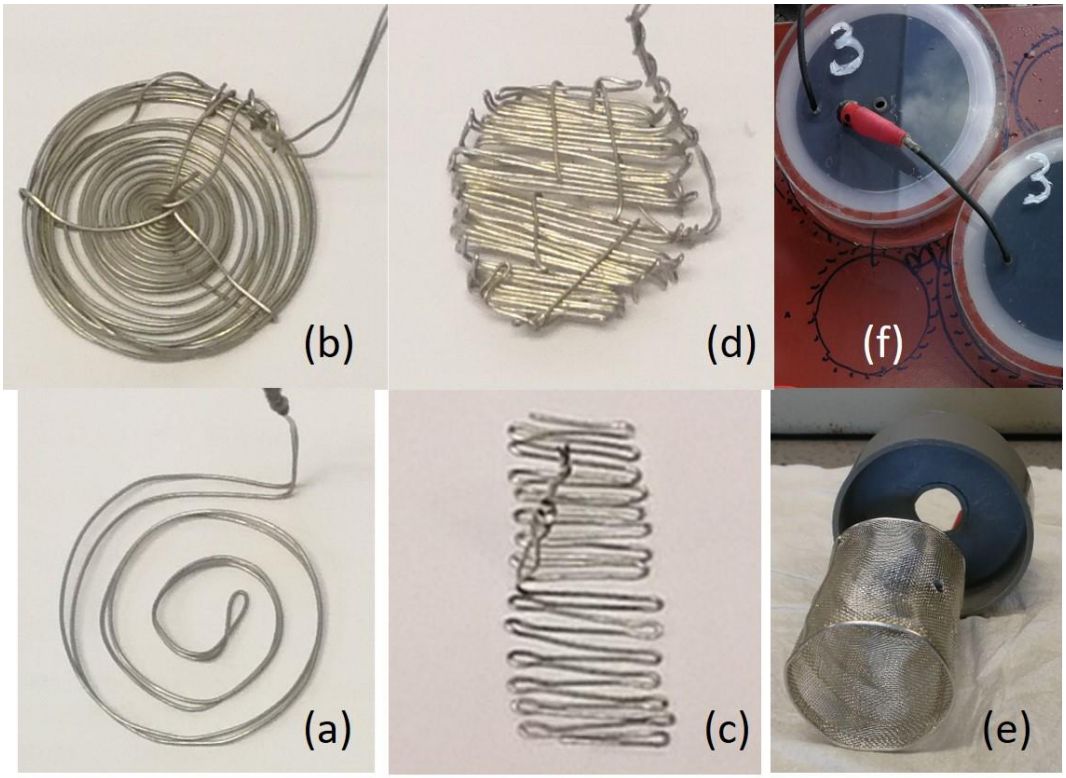

Figure 4. Images of the preliminary type electrodes along with the reference types: the extended spiral (a), the large spiral (b), double meander (c), extended meander (d), platinum gauze (e) and the planar carbon electrode (in PMMA housing, f).

5.3.2. Electrolyte

The sea water electrolyte was double filtered to remove micro-size suspended particles prone to sediment, and let slowly warm up to get rid of air bubbles before filling measure cells not to disturb measurement results (electrical field distribution perturbation and shielding effect by the high resistive bubbles). This choice is justified by representative modelling potential of real-life situations for immersion exposure and traditional electrochemical techniques to characterise coating/steel samples. The two chemical parameters, i.e., salinity or salt molar concentration and the hydrogen ion activity are important for corrosion testing, governing factors for coating deterioration. As it is shown in Table 4, these properties remained less than 10 relative percent with seasonal variations. Other parameters like oxygen concentration are manly depends on temperature which was constant in the laboratory.

Table 4. Properties of the sea water with refence to its seasonal variation

Seasons	Temperature (°C)	Salinity (g/L)	pH
Early Spring (03-04.2020)	11.9	28.20	8.26
Late Spring (05-06.2020)	14.1	30.20	8.09
Autumn (26.10.-06.11.2020)	13.6	31.95	8.31

5.3.3. Substrates and Coatings

Carbon steel panels in lateral size of 30×30 cm and 50×50 cm was first grit blasted to obtain metallic clean surface with the required roughness of SA2.5 (according to ISO 8503-1) and an average maximum peak to valley (Rz) of 55 µm. Three different surface conditions of steel specimens covered neat metallic state without treatment (reference), salted and pre-corroded ones. The 'salted' sample was treated with salt water featuring conductivity of 350 µS cm^{-1}, and the 'pre-corroded' was surface rusted by outdoor exposure for 48 hours. Self-prime pure epoxy coating (Hempadur Multi-Strength 45753) containing two components, i.e., the base 45755 and curing agent 98750 in overall solid volume of 80±2% was applied with heavy-duty airless spray (in compliance with EU Directive 2004/42/EC on VOC emission) on steel panels nominally in the same wet thickness and cured at ambient conditions. However, beyond the impact of pre-treatment, dry film thickness varied markedly within the same sample, several thicknesses of stripes found the same horizontally and varied vertically for all coating samples. This is partly due to none routine procedure at the supplier (Hempel A/S) in this low thickness range. For all coatings and panels, twenty-four sample points were collected. In order words, 24 different areas were gaged evenly distributed from each other as a 2D net over surface of the panels to asses average and variation of dry film thickness (DFT). For the measurement, eddy current tester (Elcometer 456/4 /LG03536/ thickness gage) was used in coupled with a probe (FNF1-LG04532) for measurements after two-point calibration spanning over the actual thickness range before every measure series. Results of the three coating/steel samples are summarised in Table 5.

Table 5. Average and STD of dry thickness of coatings on steel panels with three different surface states

Condition, type of treatment	Neat (reference)	Salted	Surface rusted
Sample areas used for assessment of sensing electrodes			
Average (µm)	171	320	222
STD (µm)	11	56	20
Sample areas under reference carbon electrodes			
Average (µm)	197	341	221
STD (µm)	20.9	23.2	16.1

The, samples were fitted with number of PMMA tubes and carbon electrode capped cylinders with diameters of 3.55 cm and 10 cm, providing cells on top of the coatings with geometrical surface areas

of 9.9 and 78.54 cm^2, respectively. Dry coating thickness under the carbon electrodes were somewhat different than the areas fitted with small diameter plastic tubes. Thus, these were measured and the measurement results were corrected in accordance. Immersion test was conducted for over 2184 and 816 hours on surface locations fitted with small diameter tubes and large diameter cylinders, respectively. Although none of these timeframes would mean any problem to high quality thick coatings like the reference one, the salt contaminated and pre-corroded steel substrates indicated substantial degradation over these times partly due to the low DFT. Thus, the immersion exposure was terminated and coating/steel samples were tightly sealed to preserve their state for later test.

5.3.4. Instrumentation

Immersion tests and the electrochemical measurements were carried out at 25±2°C. Electrical testing of the coating/steel samples was performed with an AMETEK PARSTAT 4000 potentiostat, galvanostat and frequency analyser. Electrical testing was carried out via both AC and DC modes, initiating measure sequences with impedance spectroscopy over the frequency from 40 kHz to 0.1 or 0.02 Hz (subjected to change occasionally), using voltage perturbations between 10 and 50 mV RMS depending on coating resistance and the magnitude of measured current. Nine points were recorded for a decade. The number of integration cycles was altered in the LF and HF ranges and measured signals were noise filtered by default setting. The LPR type DC technique was used in 2nd part of the measure sequences to obtain results and compare with outcome of the impedance assessment. The polarisation rate was 10 mV/min between vertex voltages of ±15 mV to obviate marked perturbation and precluding expedited deterioration of local areas. In part, owing to the high specific coating resistance in initial phase of the exposure, reference electrode was omitted to use for the measurements. This is partly due to the fact, minor potential shifts and slight drifts in the absolute potential do not invalidate results on high serial resistance. So, there was no concern on assessment of coating resistance (majority) coupled in series. The equipment was used in two electrode mode settings by STD pairing of four electrodes into WE-RE and CE-SE couples. In theoretical sense, this complied with the reduced test matrix. However, in practical viewpoint, this can be multiplied by a factor of two because measurements can be performed in technical sense by two distinct setups, i.e., one electrode pair contacted with electrolyte (ionic conductor in cells) and the other pair direct wire connected to steel substrates (electrical conductor), or both electrode pairs contacted with the electrolyte without direct wire connection to steel substrates (pure ionic connection). Although the latter may be more importance due to universal applicability at fields, the former is generally considered to be a standard for laboratory assessment. Therefore, effect of these measure setups was also investigated in the preliminary stage, then learnt facts and drawn inferences led to important technical terms on prototype sensor development. Further details are given in subsequent part of the thesis and representative images of the two configurations can be found in the appendix. During all measurements, coating/steel samples, electrodes and leads were kept in a closed Faraday cage which was connected to ground the same as the equipment. Sample panels fitted tightly in

inner width of the cage but the cage and the plate edges were covered with paint, so proper grounding was only achieved intentionally by direct wire connection to the steel substrates.

5.3.5. Data Evaluation

For data evaluation, the Zview and Cview software packages (supplied by Scribner Associates Inc) were used for fitting AC and DC results, respectively. Impedance data were fitted by using the Levenberg-Marquardt non-linear least squares fitting algorithm with calc-modulus data weight setting. In majority of the cases, the fitting procedure was assisted by the automated fitting algorithm. The complex and noise spectra could only be fitted manually and optimised for at least reaching error below 15%. In general, the nested or ladder type equivalent circuit (pictured in Figure 5) provided universal and adequate topology for fitting impedance data.

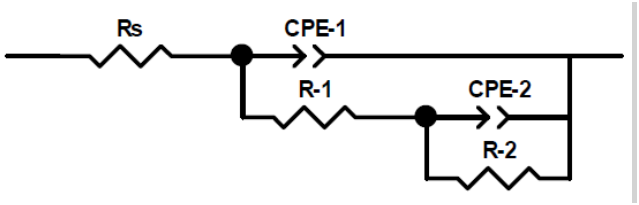

Figure 5. The nested or ladder type topology as the most suited equivalent circuit to model coatings.

For very few cases, the ladder topology was not sufficient for modelling and fitting due to altered deterioration stage of the coatings. Thus, other equivalent circuits were tested in an attempt to get well matching coating resistance between AC and DC methods in part of validation by complementary techniques on the same material property. Alternatives like the Kelvin-Voigt (full series couple of parallel lumped elements) and the Maxwell (fully parallel) topologies [262] were utilised for comparison. In general, ladder topology was well descriptive of deterioration process of the coatings with moderate thickness in intact and initial stage of deterioration (only the most outer part infiltrated), whereas the full parallel Maxwell topology describe coatings from moderate deterioration to complete breakdown. In rest cases, the Kelvin-Voigt afforded appropriate topology for fitting in line with coatings state at initial stage of immersion tests. Minor mismatch between fitting results based on ladder and the Kelvin-Voigt circuits was neglectable. As for the LPR results, strictly linear range of the data was fitted with line. If there were more than one specific slope in the dataset, then linear range of the anodic branch was fitted. Inverse of the slope is good estimator of coating resistance. All resistance and constant phase element (a capacitance substitute) results were normalised to geometrical surface area and coating thickness. In case of two-cell type measurement coupled in series nearby on top of coatings (genuinely used for non-destructive inspection purposes), resistance was normalised with a multiplication factor of half, whereas CPE normalised via multiplication factor of two for the sake of straight comparison with one-cell results.

5.3.6. Motivation of Test Matrix

The four preliminary electrodes were intended to test on three types of coating/steel samples featuring pristine and two deteriorated states, i.e., salt contaminated and pre-corroded. With a full factorial, this parameter set would lead to a minimum of 24 measurements without any repetition and parallels. The reasons for this test matrix are threefold. In comparison with the two reference electrodes, sensing ability of the wire electrodes was to assess as a function of structural extent with intact and deteriorated coatings, corroded steel substrates as well as combination of these cases. A reduced test matrix was created to decrease number of tests, and accepted by supervisory project leaders for validation of concept while complying with LEAN engineering aspects [263,264]. The investigated independent variables are summarised in Table 6.

Table 6. Test matrix to investigation of preliminary electrodes using test samples with salt contamination (III), pre-corroded steel substrate (V) and neat, reference coating/steel (XI) panels.

Electrode types	Type and state of coatings	
	Pristine (deteriorated)	Deteriorated (immersed into filtered sea water)
Extended spiral	III, V, XI	III, V, XI
Large spiral	III, V, XI	III, V, XI
Double meander	III, V, XI	III, V, XI
Extended meander	III, V, XI	III, V, XI

5.4. Results and Discussion

5.4.1. Electrochemical Tests

After measurements in the five cells, the least scattering results stemming from three cells were averaged for comparison. Pore resistance of the coating/steel samples obtained with the various electrodes by both AC and DC testing modes are summarised in Figure 6.

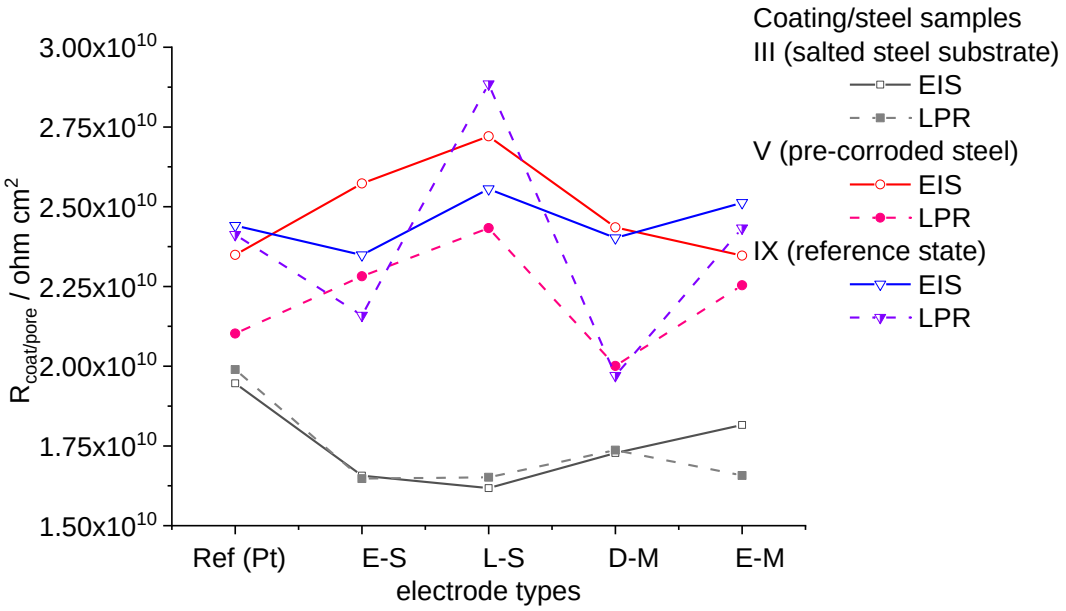

Figure 6. Pore resistance of all three types of coating/steel samples derived from impedance and LPR data (at 240 hours exposure of 'thick' coatings).

Major conclusion is on impact of the electrode geometries. The meander type electrodes led to lower pore resistance compared to the results obtained with spiral alternatives, although the variations were not remarkable. As for the former parameter, it is important for the validity of sensor data on absolute range of coating/pore resistance. In aspects of techniques, the DC (LPR) and AC (EIS) test results indicated moderately varying results with coating-steel samples similarly to the outcome obtained with the various electrodes with the same technique. With mild degree of hydration of the coatings in first 240 hours of immersion, majority of the impedance results showed higher pore resistance with greater STD than DC (LPR) data except for the salted sample (III), regardless of the electrodes. This is interpreted as lower sensitivity of the EIS method to pore resistance variation in comparison with the DC type LPR technique in early deterioration stage. Explanation for this phenomenon is partly related to the fact, time constant of micro-pores assessed >1 Hz, above the threshold of full penetration of oscillating electrical field into the pores of mildly hydrated coatings ($\leq 10^{-3}$ Hz) which is known as frequency dependent penetration depth [265−269]. In addition, large distance of working/reference and counter/sensing electrodes coupled via the electrically strongly shielding electrolyte leads to low sensitivity of detection of pore resistance. This is interpreted as effective screening of details of material

properties in a distance, acting against detection sensitivity. Surface area and charge-transfer resistance of the electrodes plays only inferior role in measure of pore resistances. Direction of deviations was the same from the reference nearly in all cases, as pore resistance was always overestimated in comparison with the reference setup. In general, sensitivity of the wire-electrodes was in line with the expectation not departing markedly from each other and from the reference. Nonetheless, deviations arising by the various electrodes were larger than scale of the coating-specimen samples, which is unacceptable for an accurate and reliable assessment of coating condition. This is despite the fact that the impact of surface treatment cannot be evaluated sensitively by the wet chemistry technique in the initial immersion stage. Referring to the difference between the AC and DC techniques, pore resistance varied the largest with the LS and DM electrodes as shown in Figure 7.

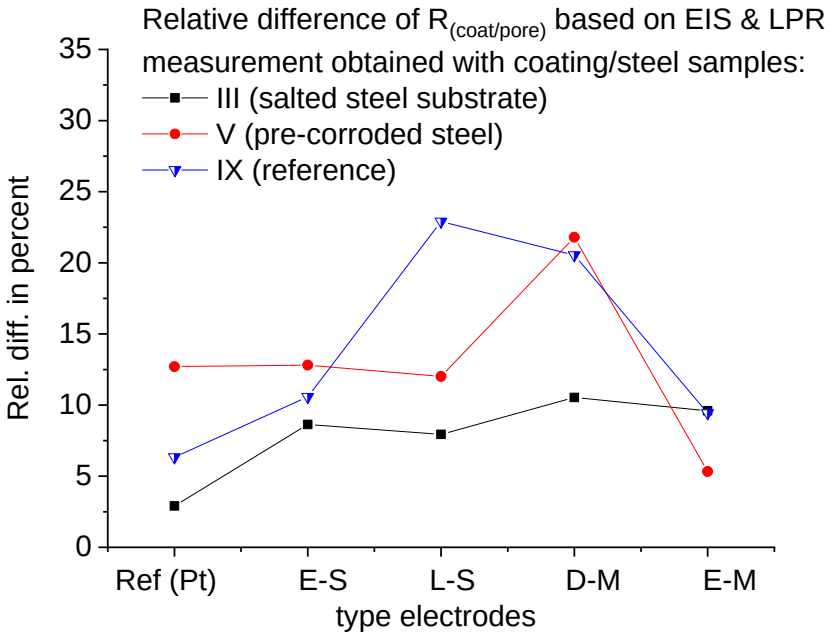

Figure 7. Relative percentage of difference between pore resistance of coatings obtained with impedance and LPR techniques.

Aside from outcome with the reference sample, relative difference by the ES and LS electrodes was similar and moderate with the pre-treated samples. Overall, the extended meander (EM) led to the lowest deviation from the reference case along with the least variation of the results. Other geometrical configurations proved to be less favourable than the EM.

Figure 8 depicts relative differences driven by the various types of electrodes in compared to the reference. Pore resistance measured with the ES and LS were generally much greater in difference by both AC and DC testing modes, than data obtained with the meander electrodes. The EM performed clearly better than the DM.

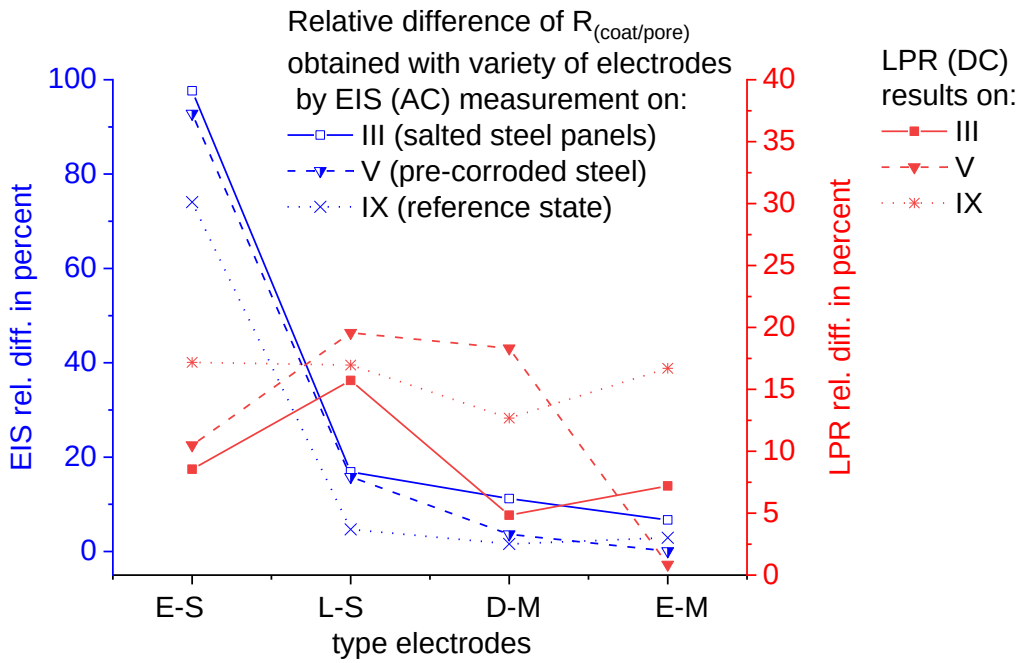

Figure 8. Percentage of relative difference of pore resistance of coatings obtained with impedance testing mode compared to the results obtained with the reference Pt gauze electrode.

Overall, the extended meander electrode provided the lowest differences in EIS (AC) mode and performed well in LPR (DC) mode. The plausible inference, electrode geometry is highly influential on sensitivity and accuracy of pore resistance, beyond variation of material properties even in early deterioration phase, good condition of the coatings. In another viewpoint, impedance testing is far more sensitive to electrode geometry on sensing performance than DC techniques. Hence, owing to the preferential application of impedance testing of coatings at the field, definition of proper electrode geometry is pivotal for proper sensor application.

Relative differences of the constant phase element (CPE) one and two components compared to the reference electrode results are summarised in Figure 9. When description of coating capacitive character is in focus by the CPE(1) parameter, then meander electrodes performed better than spiral ones, from which the EM indicated the best results. Nonetheless, evaluation of the CPE(2) led to more deviating, less accurate assessment than CPE(1) with the wire electrodes. This probably means less accurate assessment of double layer capacitance at the steel surface, and as a consequence no accurate and reliable delamination sensing with such type of electrodes.

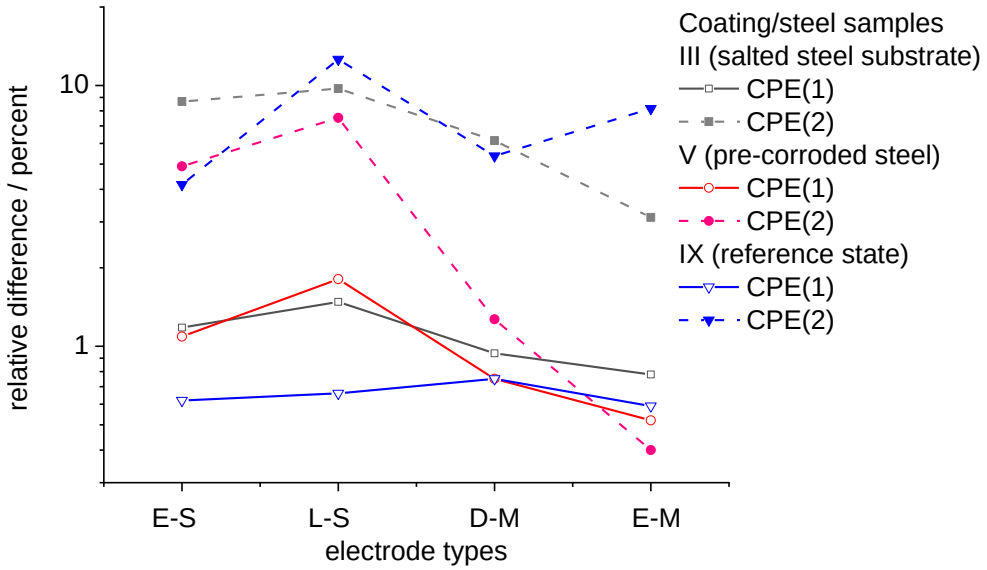

Figure 9. Relative differences of the capacitive property of the coatings decomposed into CPE(1) and CPE(2) obtained with the sensing electrodes in comparison with the reference type platinum gauze electrode.

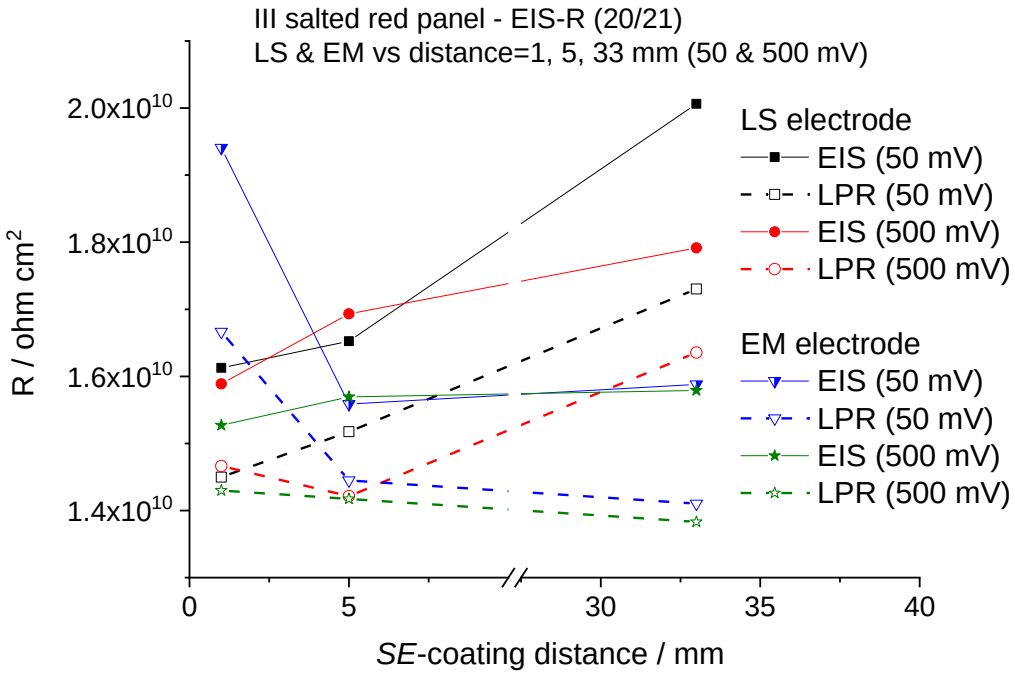

Figure 10. Pore resistance of the coating/salted steel sample (III) characterized with the large spiral (LS) and the extended meander (EM) electrodes with two scanning voltages as a function of various distance.

In Figure 10, pore resistance of the coating/salted steel sample (III) characterized with the LS and EM with two scanning voltages are depicted as a function of varied electrode distance. According to the

theoretical expectation, increased test voltage resulted in moderate drop in pore resistance in all cases. Lower dependence by the testing voltage means less arousal of non-linear Faraday type electrochemical, interfacial charge-transfer processes. On the other hand, increasing distance between the coating and the sense electrodes lead to definition of higher pore resistance more than theoretically expected based on the electrolyte resistance (around 0.4, 2, 13 ohm) coupled in series between the coating and electrodes. So, detection accuracy of the LS seemed to more dependent on and heavily affected by the increasing electrode distance than the EM featuring entirely different characteristic. The latter has implication for field application by non-expert personals. Different behaviour and perturbation of sensing ability of these electrodes is clearly reflected in Figure 11 in which pore resistance presented as a function of scanning voltage at fixed electrode distances. Above a moderate distance (5 mm), the EM sensing of pore resistance was almost independent of testing voltage than the LS, similarly to the impact of electrode distance as aforementioned (Figure 10).

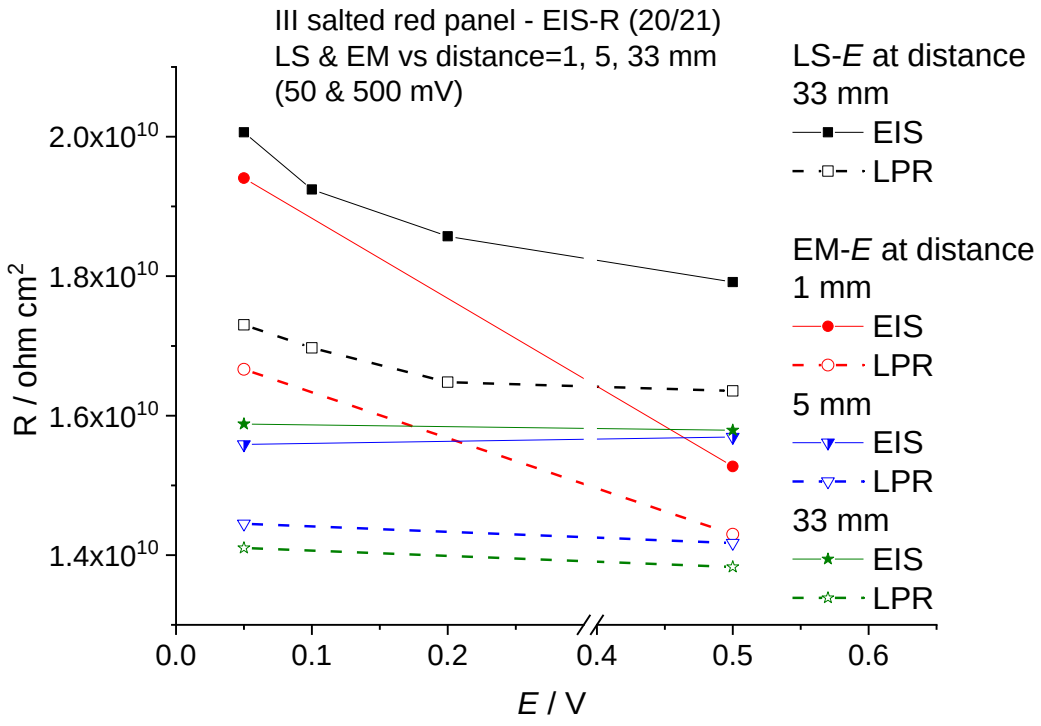

Figure 11. Pore resistance of the coating/salted steel sample (III) characterized with the large spiral (LS) and the extended meander (EM) electrodes fixed at various distances as a function of scanning voltage.

The variation of CPE(1) and CPE(2) by the LS and EM electrodes are depicted in Figure 12 and Figure 13, respectively. Weakening sensing performance of the LS is reflected by decreasing CPE(1) and CPE(2) quantities with the increasing electrode distance, which corresponds to decreasing capacitive property of the coating and the interface, respectively. What is more, testing voltage increase only lead to further deterioration of sensing function. Spectra and the fitting results are summarised in the appendix.

In this respect, neglectable effect of the EM was observed when CPE(2) derived and almost ideal behaviour manifested to CPE(1) evaluation regardless of the applied voltage. Voltage dependent representation of the same results can be found in the Appendix.

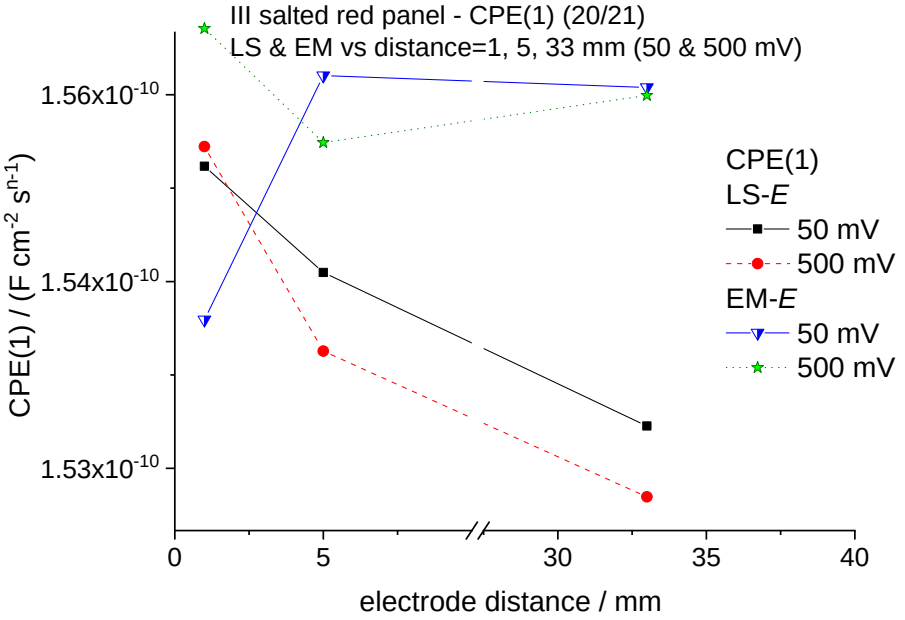

Figure 12. CPE(1) of the coating/salted steel sample assessed with large spiral (LS) and extended meander (EM) electrodes with two scanning voltages as a function of various distance.

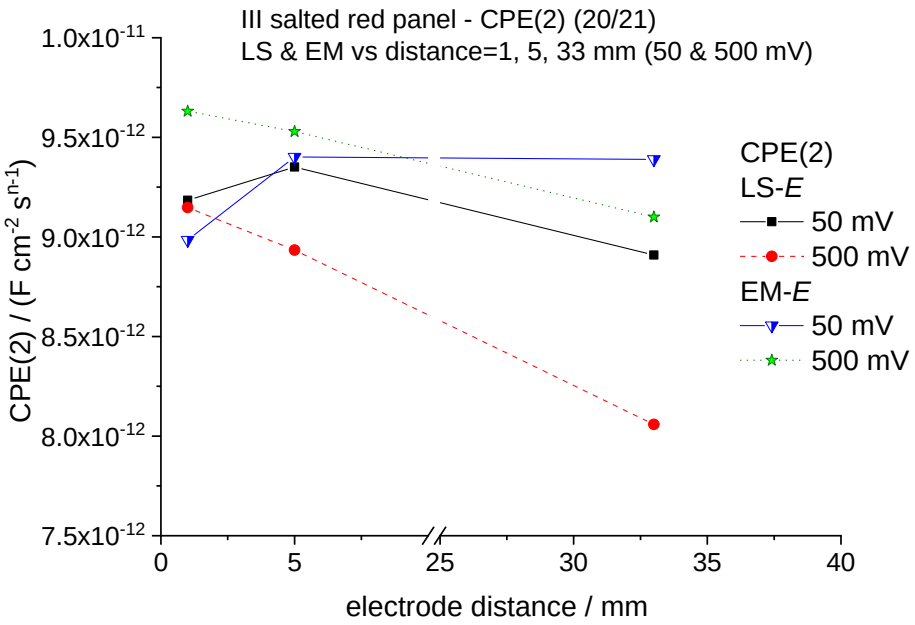

Figure 13. CPE(2) of the coating/salted steel sample assessed with large spiral (LS) and extended meander (EM) electrodes with two scanning voltages as a function of various distance.

5.4.2. Evaluation of Test Results

Aa a summary, both in terms of pore resistance and capacitive character of the coatings, meander electrodes, especially the extended meander indicated lower variations, less impacted electrical sensing ability by, e.g., distance between electrodes and coating surface as well as the applied testing voltage.

Nevertheless, limited credibility of the wet phase testing of coatings arises by the varied assessment results based on the coating and substrate condition, depending on the applied measurement technique, i.e., AC and DC test modes. This is exemplified in a small dataset presented in Figure 14 and Figure 15 summarising coating properties derived from data measured with the extended meander electrodes with wire connected (laboratory) and no connection to substrate (used in practice for inspection) modes. Highly varied estimation of the coating resistance was experienced with the AC and DC techniques (Figure 14) despite the fact, these results must provide closely matched results. Aside from shortcomings by the electrical testing modes applied in the wet phase setup, the practically important 2 cells configuration (without electrical connection to the substrates) provides different results from the single electrode configuration (Figure 15), not only by the averaging effect of the two macroscopic areas but probably some contribution from double layer capacitance to the coating capacitive character. These differences are still experienced despite normalisation of the raw sensor data.

For first, it can be difficult to interpret as the 2C config includes resistance twice from the coating, electrolyte and the interface (charge-transfer resistance) while neglecting resistance of the substrate, then direct wire connection (DWC) configuration includes each from all of those factors. Thus, lower coating resistance with 2C setup can be interpreted as exchange current contribution from uncoated electrodes and so estimating lower the coating resistance.

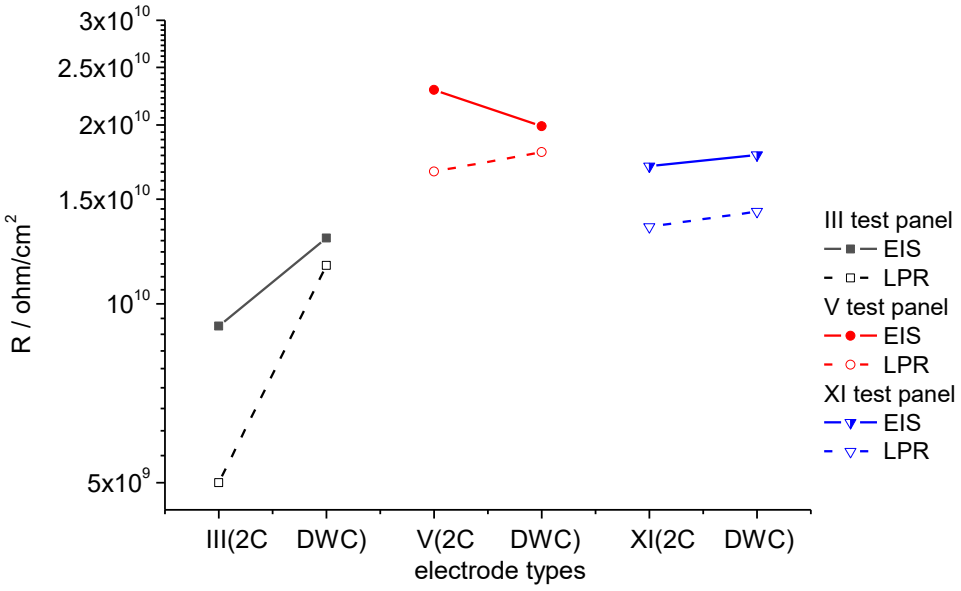

Figure 14. Coating resistance of all three types derived from data obtained with the extended meander electrode, measured with 2 cells (2C) and direct wire connection setups.

There could two separate ways for correction. The one is to make correction, extrapolation based on the difference between results of the two setups for a somewhat increased coating resistance. The other way is to define the exact solution and charge-transfer resistance as well as, or exchange current density of the electrodes in the electrolyte. The former needs at least two measurements with two distinct configurations from which one might not be feasible at field, while the latter requires laboratory tests for validation type correction. This would only apply for the reference condition but the situation becomes more complex for contingent correction when coating and steel substrate deteriorate over time as it is seen on varied difference of data obtained with samples III and V (Figure 14). Usually, the two-cell configuration provides lower estimated coating resistance than the direct wire connected one, but it is subjected to change with electrical test modes, parameters and condition of the coating-steel specimens. The lower resistance expectedly means lower resistance in series as a consequence of absence or a partial contribution from the electrode-electrolyte interface, but the ideal case obtained with the reference panel (XI) clearly does not apply for the salt contaminated and corroded interface featured test samples. When the coating and substrate is deteriorated, both the range and slope shift with test modes and measure parameters. Sensitivity of AC and DC test modes are also affected by the measure configurations. The one counter electrode laboratory test is known to include some distortion in the assessment but such scale does not disturb corrosion engineers in evaluation of corrosion resistance, protection or rate of processes. For rapid field test and inspection assessment, this is acceptable as data with estimation of condition of assets varies within a low multiplication factor.

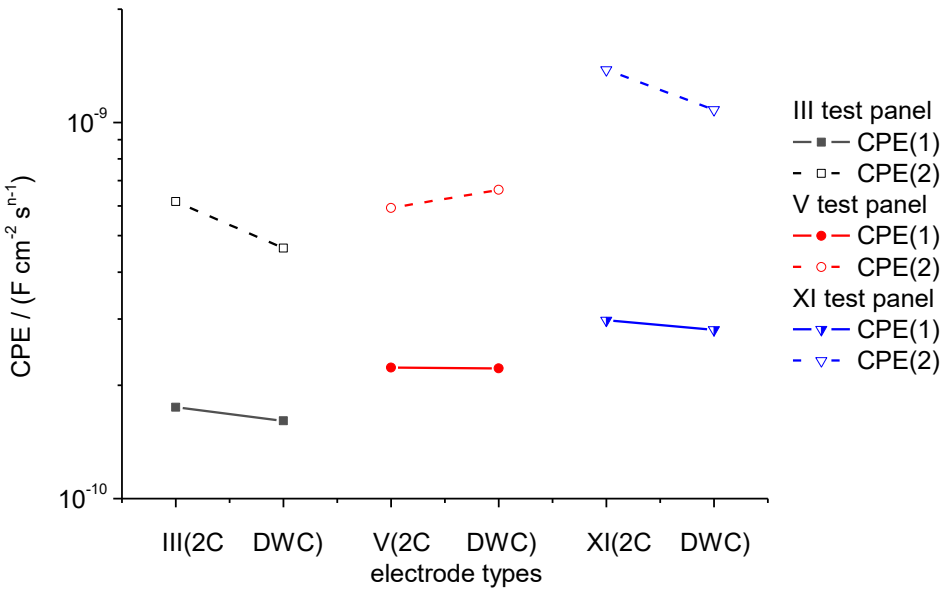

Figure 15. Constant phase elements of all three panels derived from data obtained with the extended meander electrode, measured with 2 cells (2C) and direct wire connection setups. All data evaluation was performed with the same topology featuring electrical circuit, so parameters of the main passive components are presented herewith.

Differential capacitance related CPE results are presented in Figure 15. Difference between 2C and DWC results is obvious for all three conditions of the coating-steel samples. Both the CPE(1) and CPE(2) are slightly overestimated by the 2-cell setup in 2 out of the three samples. This provides clue on the possibly less accurate, signal of early coating deterioration and presence of corrosion by high double-layer capacitance similarly to the tendency of coating resistance in majority of the tests. Regardless of the tendency of changes, the CPE(2) turned out to vary more than the CPE(1) in all cases. This means the critical corrosion and delamination related processes are less accurately assessed by the 2-cell setup, which can be explained by the more complex impedance spectra as a result of superposition of two distinctive spectra, more difficult fitting and extrapolation to the LF and DC range. Electrochemical factors like the high double layer capacitance with its low impedance on graphite (CE) [270] does not seem to take a marked role. Altogether the 2-cell setup with nominally equal interfaces carries plausible advantages compared to the DWC one besides acceptable compromise on assessment of coatings condition.

In comparison with the results obtained at 24 days of immersion with the reference PMMA-housed planar carbon electrodes representing ideal geometry for testing flat substrates, the extended meander type wire electrode provided similar coating, pore resistance results with the pre-corroded (V) and reference (XI) samples at overall specific resistance of ~2×10^{10} ohm cm^2. Exception of the salted (III) sample with orders of magnitude lower pore resistance between 10^6 and 10^8 ohm cm^2, instead of the ~5×10^9 ohm cm^2 derived after the EM, can only be interpreted with the size and more representative location effect of test samples well-known in engineering. Thus, the smaller coating surface area located at outer region of test panel coupled with the highly uneven distribution of fine salt under the coating led to such a high difference in the estimated pore resistance. The larger the cell and so the surface area for testing is, the higher probability of representative assessment can be obtained. An order of magnitude difference in pore resistance with the highly varied cell sizes could most probably be hard to avoid with the salted (III) sample. As for capacitive character of the coatings expressed in CPE parameter, planar monolith carbon electrodes led to estimation of orders of magnitude wider range between ~2×10^{-9} and 1×10^{-11} F cm^{-2} s^{n-1} than that was obtained with the less sensitive all wire electrodes, in accordance with the theoretical expectations. Hence, major shortage of wire type electrodes and unfeasibility for accurate condition assessment became obvious. There were more results and evidence in this subject but extent of this chapter on findings coupled with interpretation preferably restrained to serve clarity, coherence of the presented material and the ease of interpretation and comprehension of the readers.

The aforementioned limitations and inferences on wet phase sensing performance, credibility and reliability of results lead to conclude on the preference of dry phase testing of coatings via at least two separate physical embodiments, which is discussed in the subsequent two stages of design cycles.

6. DESIGN CYCLE II – COMMERCIAL MODEL ELECTRODES

6.1. Motivation for Generation II Sensors

Based on the experimental results presented in Chapter 5 (Design Cycle I), accurate detection of coating condition and corrosion of steel substrates by the means of wet-phase testing with certain types of electrode and test setups is considered as not accurate. Varied electrode geometries lead to moderate deviations in sensor readings and derived data depending on type of test setups, besides the impact of macroscopic distinct tested surface areas. Resistance and capacitive character assessment are opposite affected. Difference in outcome by direct wire coupling to substrate and two-cell setups may generally be acceptable. Although solutions to these problems is manifold, our choice was restrained to physical embodiment of scientifically proven concept such as to test in-plane open-ended strip-line electrode configuration for sensing with bending electrical fields. Although accurate solution to bending electrical fields and estimation of interaction with materials can be difficult to complex electrode geometries and material arrangements [271], the concept and its application was well established and wide-spread in use [272−278]. At the same time, this concept is in compliance with maritime programmatic design requirements. Therefore, testing this concept was decided to perform by laboratory experimentation and answer the question of 'can technical requirements be met by microstrip-line electrodes?'. The main goal of this experimentation campaign was to ascertain credibility of such electrode configuration and sensing mode for dry-phase testing of solid-state materials, which is otherwise not plausible based on the international literature. The latter statement owes to the fact, coplanar microstrip-line electrodes are widely used for electrochemistry and liquid-gas phase sensing, but sensing high resistance solid-state materials was not widely proven demonstrated to our best knowledge. Further important considerations are shared in the following subsections.

6.2. Sensing with Coplanar Electrodes and Bent Electric Fields

Among open electrode geometries, coplanar alignment is the most favourable for planar structures, coating testing under real-life conditions. Majority of the applications prefer coplanar configuration with numerous in-plane electrode geometries. The reasons are twofold. The coplanar electrode alignment allows high interaction of electrical fields with materials, which translates to high detection sensitivity, and universal applicability on various geometries and morphologies [279]. In general, bending electrical field develops between differently impressed electrodes, e.g., positively polarised driver electrode and the zero potential sense electrode (compensated to ground by the electrometer) in normal direction to the electrode planes. This bent electrical field concentrates between open-ended electrode edges and the voltage decays steeply in-plane inner electrode areas and with distance from electrodes in normal direction. Thus, this field is also referred to as the fringing one. Electrode width and gap, height of materials has primary impact on impedance in sensor conductors (transmission lines) [280]. Decreasing electrode width and gap leads to increasing detection sensitivity at the expense of decreasing penetration

depth. The former allows assessment of material properties close to reference, while the latter means restrained penetration depth, volumetric range of material testing and reduced robustness against lift-off variations, which the design hardware is mandatory to optimise for. Overall, these result in advantage as customisable concentration of fringing electric field in the tested materials and so detection sensitivity. In this regard, interdigitated configurations feature superior performance over traditional planar disk-disk and ring configurations [281−283]. Moreover, IDEs also provide high SNR and accuracy for material characterization, which could not be achieved by macroscopic electrodes. Therefore, such electrode configuration was selected for investigation at this design cycle.

In the following subsections, motivation to test matrix is described first. Then experimental relating to this design cycle is concisely given, followed with presentation and discussion of test results.

6.3. Motivation of Test Matrix

Due to time constraints, a reduced test matrix was accepted for experimentation. The matrix contained target independent variables such as condition of coatings (2) and steel substrates (3), characterised with the planar monolith carbon electrode (reference) and 3 sensors as mono-, quad- and hexa-arrays made of the IDE(0.2). Thus, the number of experiments led to 24 measurements without repetitions. Although this number would seem to be excessive to achieve over a relatively short time because of the necessary additional preparations and preliminary tests of the electrodes, in the end all configurations were managed to test. The reduced test matrix is summarized in Table 7. Feasible solution to decrease number of measurements was to omit using the IDE(0.1) and investigation of coating thickness variation due to its minor importance and expected contribution to knowledge.

Table 7. Test matrix to experimentation with the four different electrodes: the planar reference and the strip-line interdigitated electrode mono- and array configurations

Coating condition	State of steel substrates	Electrical sensing with electrodes	
Pristine	Intact	1 planar	IDE(0.2) in 3 sizes
Mildly deteriorated			
Pristine	Salt contaminated	1 planar	IDE(0.2) in 3 sizes
Mildly deteriorated			
Pristine	Pre-rusted	1 planar	IDE(0.2) in 3 sizes
Mildly deteriorated			

6.4. Experimental

6.4.1. Electrodes and Fabrication of Electrode Arrays

Two types of interdigitated electrodes were purchased from the supplier Metrohm Nederland BV (manufactured by the MicruX Technologies) to support and validate the concept of dry phase testing of materials. The one featured nominal electrode width and gap of 200 μm so herewith referred to as

IDE(0.2), and another with the same parameters of 100 µm hereby referenced as IDE(0.1). These geometrical arrangements are aimed at varying penetration depth into the coatings. The IDE(0.2) was manufactured on rigid ceramic substrate while metallisation of the IDE(0.1) was carried on flexible thin polymer platform. Both types of electrodes contained gold surface finishing for chemical inertisation. In fact, real geometry of the electrodes indicated different picture. The IDE(0.2) was manufactured by large tolerance (with less governed lateral deposition technique) and so indicated high variation of electrode width and gap over entire length of the electrodes. Although the IDE(0.1) showed undisputed improvement in regard with geometrical uniformity, this sample did not feature exact geometry as stated by the manufacturer. Nevertheless, these deviations are not expected lead to markedly effects in sensing performance aside from moderate frequency dispersion of impedance spectra measured with the IDE(0.2). Microscopy images of microstrip-line IDEs are given in the Figure 16 and geometrical data summarised in Table 8. The main concern by using these electrodes for coating testing was the insufficient penetration depth, the shallow main sensitivity range for detection and so the effective current range to detect with the equipment.

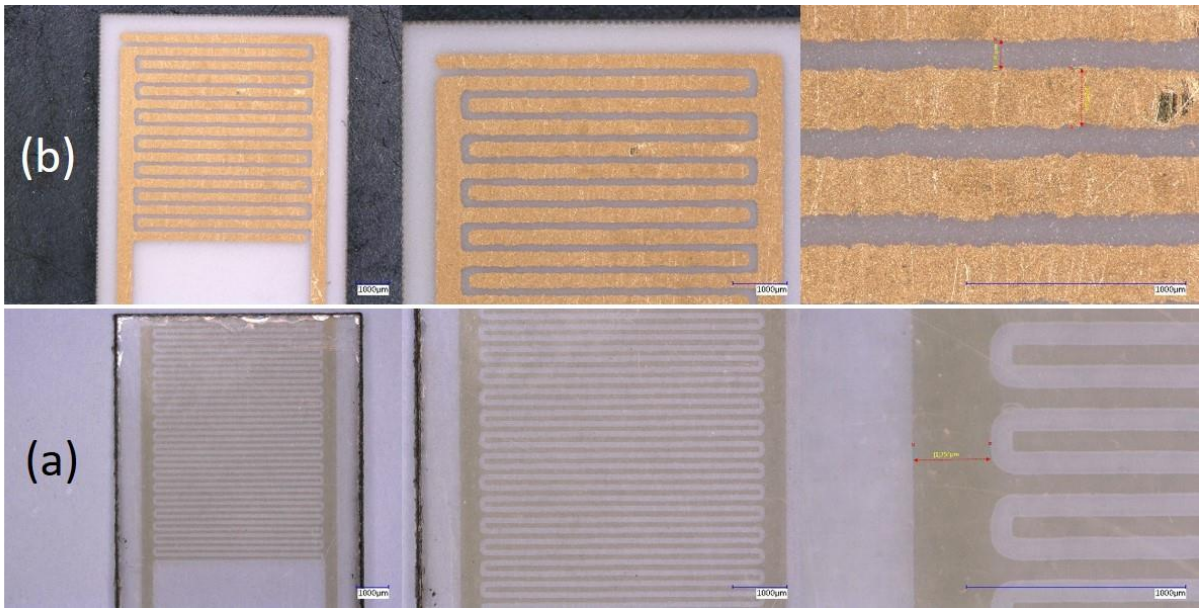

Figure 16. Microscopy images of the IDE(0.1) (a) and the IDE(0.2) (b) single monolith type electrodes in increasing magnification from left to right.

Table 8. Geometrical details of the IDE(0.2) and IDE(0.1) samples

Electrode type	Electrode width (µm)	Electrode spacing (µm)	Electrode (single) length (mm)	Number of electrodes	Overall size of the electrode area (cm^2)
IDE(0.2)	270	140	5.21	16	0.344
IDE(0.1)	90	100	5.11	36	0.371

By using the manufacturer provided shielded electrodes, only a single electrode could be coupled to the equipment, which was a major difficulty due to the very low current range for detection by the small size electrodes, large resistance and low permittivity coatings. In an attempt to overcome this, individual electrodes were soldered and connected with wires of quality cable (cat5e) first, then quality of those was assessed by impedance testing. If soldered individual electrodes reached resistance magnitudes of 10^{12} and 10^{10} ohm with the manufacturer cable, those were accepted as appropriate for electrode array formation. Owing to the quantity limitation, electrode arrays were formed by side-by-side alignment of single blocks fitted with back sides in numbers of four and six on thin sticky tapes then mono-blocks coupled parallel with each other. To connect with the test equipment, IDE arrays and later mono-blocks were equipped with female banana connectors (with diameter size of 4 mm). Images of the IDE arrays are given in appropriate results subsections.

6.4.2. Preparation of Coating-Steel Substrate Samples

The same type of paint coatings (Hempadur Multi-Strength 45753) was applied in low thickness onto the same type of steel substrates as used for Design Cycle I. Standard deviation of the DFT was significant in comparison with thicker the coatings in the first experimental series (Chapter 5) indicating major variations in length and minor variations in width of the substrates. This was caused by application of the spray gun at varied rates over width sections of steel panels. Therefore, thickness of the coatings was measured over several areas (32) equally distanced from each other, then thickness and STD were derived for each sample. Informative evaluation results are summarised in Table 9.

Table 9. Average and STD of dry thickness and after initiation of immersion exposure (24 hours) of the coatings on steel panels with three different surface states

Condition, type of treatment	Neat (reference)	Salted	Surface rusted
Sample areas used for assessment of sensing electrodes			
Average (μm)	157	163	123
STD (μm)	25.7	29.5	61.2
Sample areas under reference carbon electrodes			
Average (μm)	152	153	126
STD (μm)	19.5	19.8	53.0

In general, the 984 hours of immersion test of thick coatings with sea water leads to no or mild deterioration at room temperature but at the end of Design Cycle II experimentation, thin coatings indicated severe damages over majority of coating surface, especially in progress of corrosion of steel substrates. This is why after a relatively short time; immersion test was terminated and coating/steel samples were foiled tightly to preserve condition for subsequent further testing.

6.4.3. Electrical Test Mode

Compared to the wet phase testing with traditional macro-size electrodes, test sequence was changed according to technical feasibility of measure modes to high resistance materials at low test voltages. For standard measurements, impedance tests were conducted with voltage perturbation of 0.1 V rms and in cases with 0.2 and 0.4 V rms as referred to. All other impedance test settings used for the series of coating characterisation was the same as mentioned in the previous section (Chapter 5).

6.5. Test Results and Discussion

6.5.1. Mono-block Interdigitated Electrodes

Pore resistance was derived from impedance spectra measured with the mono-IDE in initial and exposed state of the coatings (I, IV, V) summarised as a function of thickness mean in Figure 17.

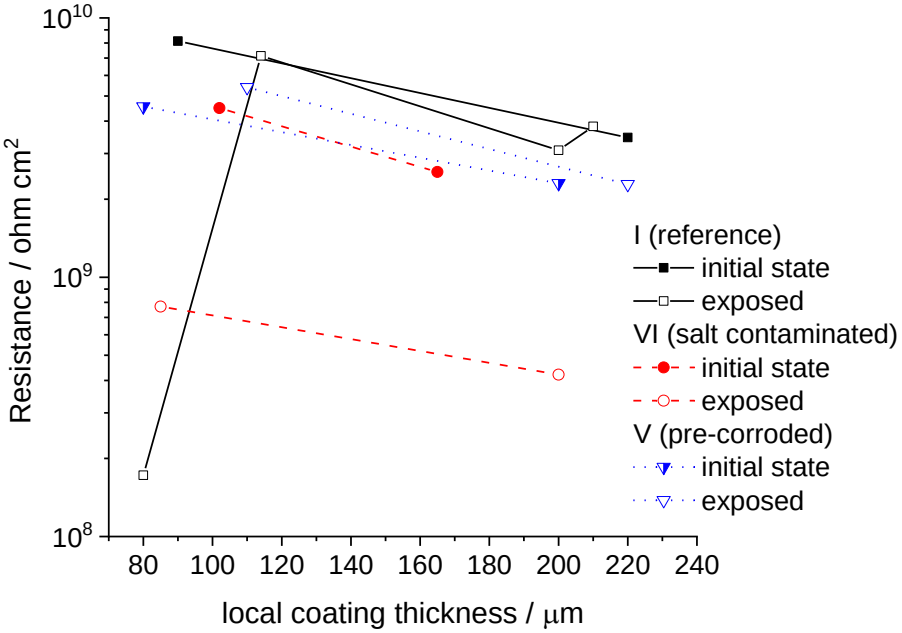

Figure 17. Normalised coating resistance assessed in initial and exposed (after 984 hours) states of the test panels with the mono-IDE(0.2).

The first impression is the generally decreasing coating resistance with increasing thickness with around the same slope. This is contradictory with the expectation of property of dielectric layers. Referring to the findings by the planar carbon electrode, coating resistance of the reference (I) was similar to the reference data (~5.5×10^9 ohm cm^2). Contaminated (IV) and pre-corroded (V) samples were reference assessed to feature specific resistance between 2 and 7×10^7 ohm cm^2 which was far overestimated by using the mono-IDE(0.2) with derived results of 4×10^9 and 6×10^8 ohm cm^2. Relative order also changed to the reference in case of deteriorated condition, similar resistance of samples I and V (Figure 17) instead of sample IV and V by the refence. Despite the low depth penetration of IDE(0.2), comparable relative resistance reductions could be obtained with the reference case over the immersion

exposure. This is manifested by the resistance changes: slight to sample I and almost 10 times to sample IV. In another aspect, in initial phase of the exposure, difference in coating resistance between the samples I, IV and V did not reflect 16% department in local dry thickness. Aside from reference results, the mono-IDE indicated higher resistance of intact sample (I) compared to the contaminated (IV) and pre-corroded (V) ones. This must be valid over limited penetration depth. In addition, resistance drop of ~10 times by sample IV from initial to exposed state was in qualitative agreement with reference results.

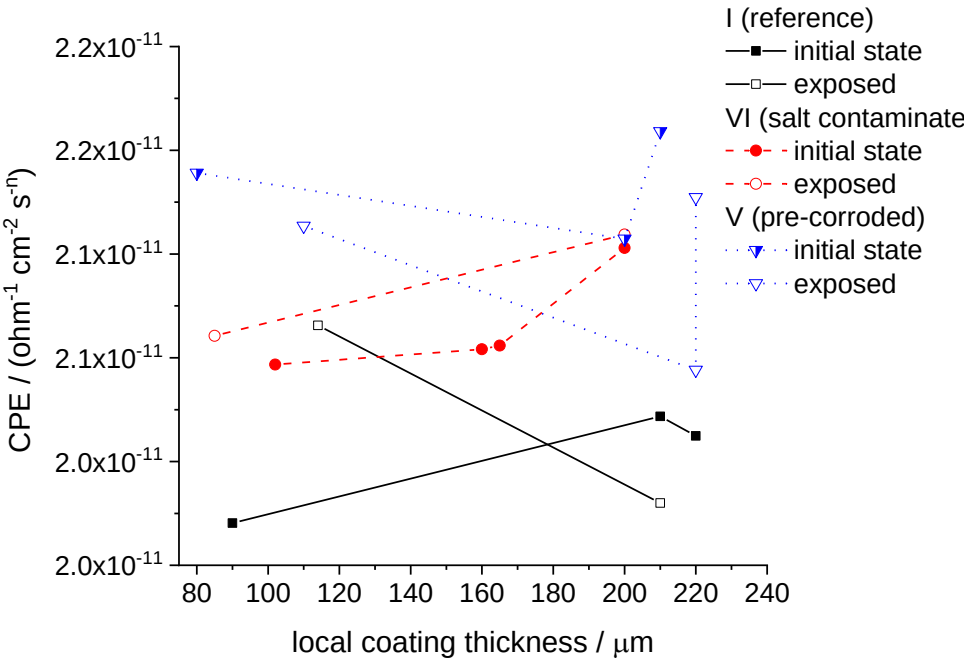

Figure 18. CPE assessed in initial and exposed (after 984 hours) states of the test panels with the mono-IDE.

Single constant phase element data are presented in Figure 18. At absolute scale of the data, this dataset was one and two orders of magnitudes inferior to that obtained with the reference setup. It is in accordance with the theoretical expectation on difference between dry and wet phase testing of dielectrics. This is partly parallel with an order of magnitude difference between data measured with 2C and DWC setups of wet phase testing. Relative order of the CPE data seemed scaling well with material properties, i.e., increasing permittivity of coatings with contaminants, from sample I, via IV and to V. What is more, this assessment reflected acceptable parallel scaling with coating thickness. Capacitive character of coatings was increasing to sample I and IV, roughly stable with sample V, which for the latter two was in line with outcome by the refence setup. Overall, this result reflects sensitive detection at low IDE feature size and testing voltage. In addition, positive experience with the mono-IDE was the relative difference and changes of capacitive character of coatings over time exposure, matching the tendency ascertained by the reference setup.

General findings, only one-time constant could be observed and assigned in impedance spectra measured with IDEs for fitting and evaluation. Therefore, single CPE exponent is discussed in the

following for all IDE configurations. Thus, CPE components to the samples with two states assessed with the mono-IDE are summarised in the Appendix. The very high exponents for coatings departed from the reference outcome. The high exponents hint on almost homogeneous coating resistance and 2D flat surface, which suggests limited penetration depth. Variation of this parameter by immersion exposure of the salt contaminated (IV) and pre-corroded (v) samples fits the impact of diffusion process, increasing and decreasing uneven local coating thickness from pristine to exposed states, respectively. Thus, only limited effect of thickness variation, lower exponents were defined to greater thicknesses. Nonetheless, these data are to be carefully considered as lower exponent defined only to the intact and exposed sample I.

Referring to the reference results, high CPE exponents were close to unity similar to CPE(1) results by IDE(0.2), but CPE changes over time were similar to variation of the CPE(2). As a promising result, the relative differences between CPE data derived to samples with thinner (I, IV, V) and thicker (III, V, XI) coatings indicated greater capacitive character in absolute value along with increasing mean thickness. Overall, results by the mono-IDE(0.2) was convincing. Thus, it was decided to take this configuration to further design development.

6.5.2. Quad-Array Interdigitated Electrodes

Parallel configuration of the single interdigitated electrode within few numbers, i.e., four and six would have expectedly to result in increasing current and so proportionally higher sensitivity of detection. After performing series of experiments by the same way as with the mono-IDE, results derived to the quad-array configuration are presented in Figure 19 and 20. Coating resistance of the reference (I) was inferior by around 6 times, while resistance of samples (IV) and (V) was overestimated by around 10 times to 2 and 4×10^8 ohm cm^2 (Figure 19). Resistance decreases from intact to exposed condition of the pre-corroded sample (V) was in agreement with the reference outcome, whereas deterioration and relative stability of samples I and IV were not match with expected by the reference. This must plausibly be consequence of sensing artefact, i.e., lower resistance without electrolyte ingress and decreasing coating resistance with larger local thickness in deteriorated state.

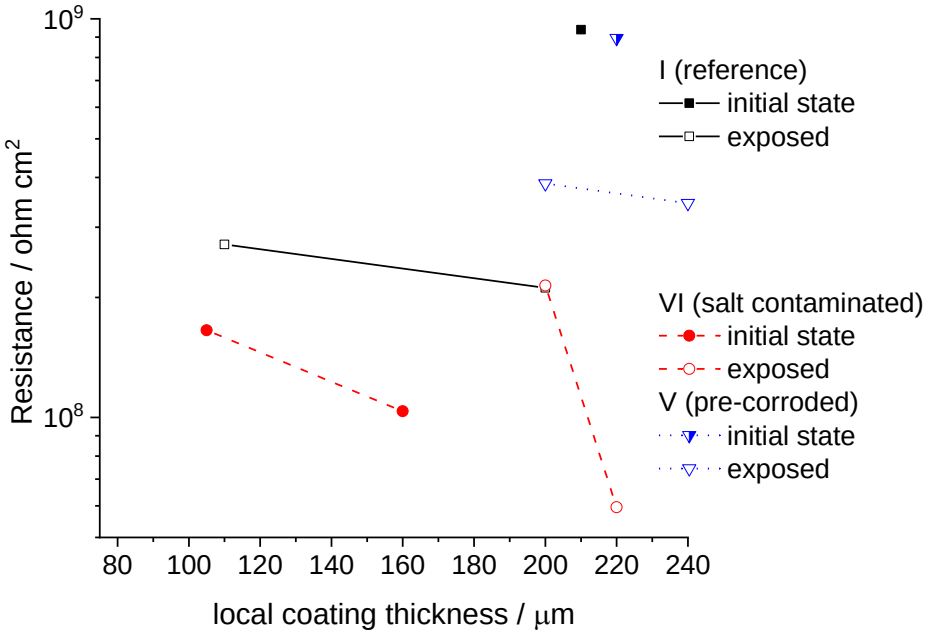

Figure 19. Normalised coating resistance assessed in initial and exposed (after 984 hours) states of the test panels with the quad-array IDE(0.2).

In terms of scaling and dynamics with the number of IDE mono-blocks, somewhat restrained detection sensitivity was manifested over resistance range of the samples with less than two orders of magnitude, in comparison with the mono-block IDE. A possible explanation for this sensitivity drop is the interaction of individual electrodes, main conductors around block edges and alternate polarity coupling of individual electrodes in tight array formations. So, the D-S,D-S, etc coupling configuration is probably less effective than the paired polarity, coupling configuration, D-S,S-D,D, etc. Although the latter probably leads to better results in case of multiple combination of small mono-IDEs, there was not time to test this hypothesis in laboratory practice.

At an absolute scale, CPE results (Figure 20) remained hundred times lower in magnitude compared to outcome by the reference setup. Dynamic range of detection improved from the CPE range of $2–2.2\times10^{-11}$ by the mono-IDE to $2.3–2.8\times10^{-11}$ ohm^{-1} cm^{-2} s^{n} (Figure 18). As an obvious inference by comparison of the means of detected ranges, sensing scaling by the quad-array IDE configuration also showed enhancement. In terms of relative order of the CPE data, immersion exposed results were greater than derived pristine conditions of the samples and the relative extent of changes remained in the acceptance range.

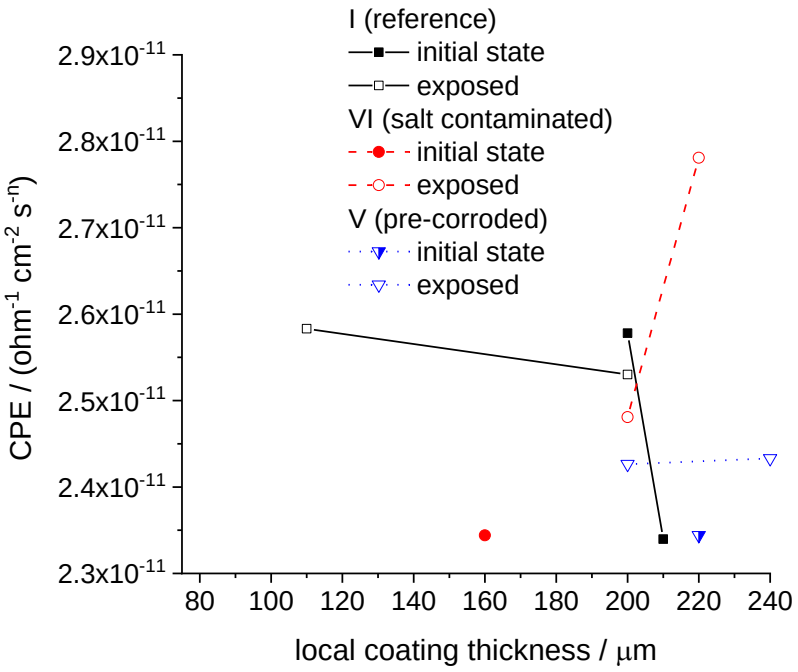

Figure 20. CPE of the test panels assessed in initial and exposed (after 984 hours) states of the test panels with the quad-array IDE.

In general validity of this dataset and so the electrode configuration was not confirmed by repeated measurements. So, capacitive character changing in reverse manner with the increasing local thickness could have caused by the presence of air-gap between IDEs and samples. In reality, this was unavoidable due to the lack of any feasible solution to technical issues, electrical connection of the mono-block IDEs in array configurations. No other explanation could be arisen. In this CPE series, sample V results were clearly exceptional because larger contribution must have been assessed after immersion exposure to this sample compared to the other two. As for the CPE exponents (Appendix), relative order of data was in line with outcome of the reference setup, and matched well with the tendency of sample V assessed in CPE(2) variation by the reference and mono-IDE results (Appendix). As a general impression, lower CPE exponents were assessed with electrode configuration between 0.775 and 0.965 with the quad-array than mono-IDE (0.9975−0.9650). This is related to imperfect geometrical alignment of blocks in the array and the herewith encountered inhomogeneous thickness of coatings. The latter is clearly more subjected to experience with arrays than a mono-block. Increasing exponents with the greater local thickness was in agreement with results provided by other IDE and reference setups.

As a summary, no accurate and partly credible results were gathered by using the 2nd sample series and modified (resoldered) quad-array IDE configuration. Further peculiar results are delineated in last section of this chapter.

6.5.3. Hexa-Array Interdigitated Electrodes

Coating resistance evaluation by the hexa-array is summarised in Figure 21. Similar to other IDE configurations, coating resistance was between 10^9 and 10^8 ohm cm^2, around 5 times above ascertained by the reference setup. Dynamic range seemed to shrink somewhat further from the mono- and quad-array IDEs to the scale of between 10^8 and 3×10^9 ohm cm^2 in regard with the samples. Although relative order of resistance was not perfect match with the reference, showing larger value to sample IV than sample I both with the same local thickness (and markedly higher to sample V), exposed condition of coatings was assessed with increasing capacitive character compared to initial states. Nevertheless, resistance scaling with the local coating thickness was not unanimous with this configuration either. Absolute range of the CPE results (Figure 22) was similar to the data obtained with other IDE configurations. Further improvement in the sensing dynamic range was manifested by the CPE results varying between 2.4×10^{-11} and 3.2×10^{-11} ohm^{-1} cm^{-2} s^n over quad and mono-IDEs. Hence, some scaling enhancement by increased mean of the CPE results was found while knowing the lower CPE character of the quad-array than the hexa-array under air case measure (blind sensing for background correction). Relative order of initial (pristine) and exposed states of the coatings was not in agreement with outcome of the reference since capacitive character of sample IV showed neglectable increment by the immersion exposure (not supported by the reference). In addition, sample I must have been below the actual assessed absolute range and less increased by the immersion testing.

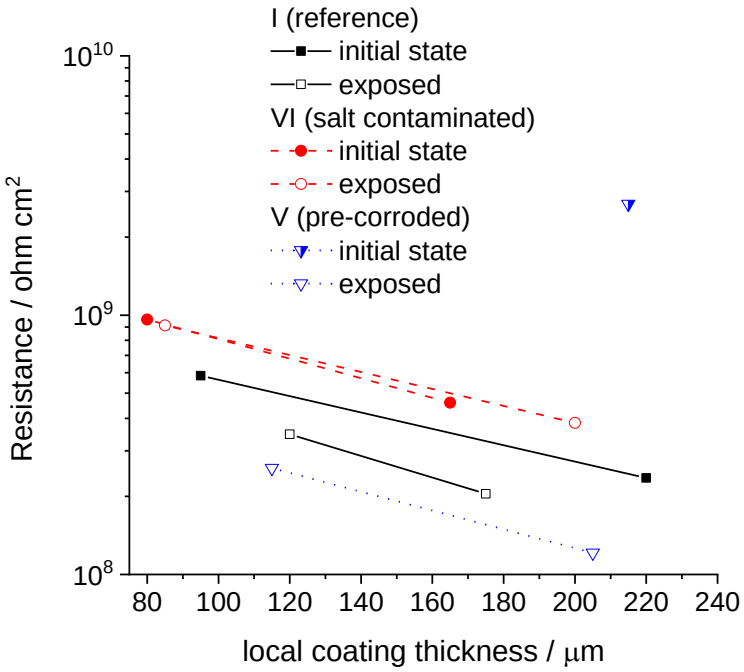

Figure 21. Normalised coating resistance assessed in initial and exposed (after 984 hours) states of the test panels with the hexa-array IDE(0.2).

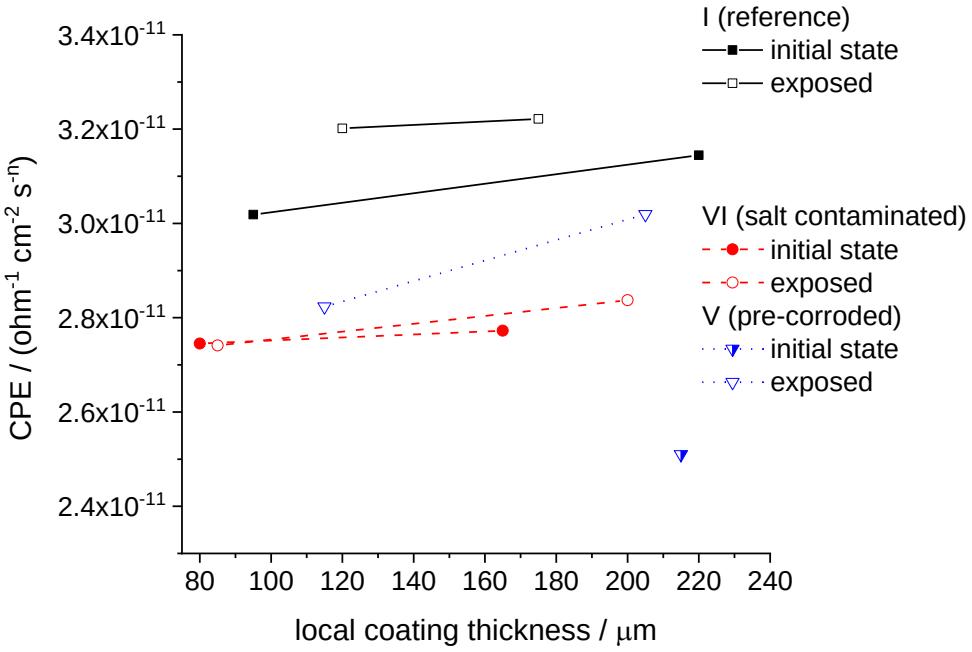

Figure 22. Constant phase element of the test panels assessed in initial and exposed (after 984 hours) states of the test panels with the hexa-array IDE(0.2).

Absolute range of CPE exponents (appendix) was similar to CPE(1) results, whereas variation of this parameter was similar to changes of the CPE(2) parameter and its exponent by the reference setup. Overall, both the former and the latter would expectedly mean increasing homogeneity of coatings by electrolyte infiltration, which could not be confirmed by condition of steel substrates. This is due to the fact; interface was not in the main penetration depth range. In general, CPE exponents indicated further decrease compared to mono- and quad-array IDE results 0.9975−0.9875 and 0.9975−0.9650, respectively. This is accepted by technical consequence of increasing uneven surface character of arrays with growing number of mono-blocks (minor impact) and a much greater effect of thickness variation of the coatings. Impedance data and fitting results of design cycle II data are presented in the appendix.

There are remarks on part of the experimental findings. Absolute range of the CPE data was greater measuring under air without test samples (blind sensing mode for background signal assessment). No any plausible explanation was found to this phenomenon. Based on physics fundamentals, difficult interpretation owes to contradiction of greater capacitive character of the low permittivity environment (air) compared to test materials. According to the expectation, CPE results would have been at least doubled with all pristine samples compared to measure under air. This must have been valid based on low volumetric penetration depth of IDEs and equal relative permittivity of the sensor ceramic platforms with initial condition of the epoxy coatings. This behaviour seemed to correlate opposite and translate into apparent estimation of decreasing capacitive characteristic at increasing coating thickness.

The results were obtained with indirect, long and split wire connections with the same array-IDE configurations, i.e., double-wire node-connected quad-array IDE and split-arms double-wire through-

node connected hexa-array IDE led to useless detection sensitivity and inconclusive results under air and with test samples (in absence of air gap). Thus, double-node wire connection must have been rearranged to shortened direct wire-connection. Then, sensitivity of detection to resistance of materials, e.g., air and test samples decreased by more than three orders of magnitude while detection of capacitive character was minor affected. Regardless of absence of air between electrodes and samples, no credible data were obtained with long-wire connected configurations. On top of that, grounding of the aluminium foil back-plate shielding lead to an order of magnitude change in electrode resistance only for the array electrodes but for the mono-IDE. Thus, as an expected behaviour was found by shunted mode detection with the array type IDEs under air, while the mono configuration seemed to be insensitive for this. Good scaling and improved dynamics of the array electrodes could also be noticed by the increasing capacitive character of the bare electrodes. This hints on enhanced sensing of inner capacitive character of array electrodes, which is clearly unfavourable for detection sensitivity. The CPE exponents close to unity suggested the same conclusion which underscores the importance of proper designed wiring of sensor in compliance with electrical engineering. This picture changed a lot when long-wire lead connection was reconfigured to short-wire connections without junctions and nodes. Then, resistance of the quad- and hexa-array decreased by more two orders of magnitude and the CPE data showed unequivocally increased sensitivity of detection at moderated exponents. Acceptable configuration of array electrodes with direct wiring connection was far less sensitive to the presence of back-plate shielding and grounding than long-wire, split lead connected configurations. Explanation for minor detection sensitivity in those cases and vice versa the greater sensitivity in target volume range (materials under test) is due to the grounding back-plate shielding, called the shunted mode, but this did not affect markedly sensitivity of proper IDE configurations with short leads.

Additional experimental findings helped disclose probable origin of these artifacts and shortfalls and so became beneficial for our understanding on complexity and delicate nature of design of IDE sensors. These utmost results are reviewed as follows. The short and direct wire-connected quad-array IDE was used first for impedance testing under air, polycarbonate and poly-methyl methacrylate test samples. Then, impedance data were evaluated with equivalent circuit of a resistance coupled in series with a parallel connected resistance and CPE (schematic: R(R/CPE)). Resistance showed the expected relative order, high resistance under air and decreasing with PMMA and further with PC. The absolute scale was between 7.5×10^{9} and 10^{10} ohm cm^2. Single CPE results varied between $1.72-1.9\times10^{-11}$ F cm^{-2} s^{n-1} from air, to PC and PMMA materials. Nonetheless, a seemingly contradictory behaviour was found as the PMMA did not respond with monotonously decreasing resistance and increasing CPE with the increasing testing voltage. These results were also assessed with an extended equivalent circuit which contained the same core circuit as aforementioned and one more CPE component coupled parallel with the main R/CPE lumped elements (schematic: R((R/CPE)/CPE)). This was attempted to test due to the reason of moderate frequency dispersion of impedance data which could not be fit plausibly with one CPE. Thus, derived resistance data increased up to between 8×10^{10} and 2.5×10^{11} ohm cm^2. The

CPE(1) results were between 4.1−5.6×10^{-12} F cm^{-2} s^{n-1} to PMMA, to air and PC. Due to erroneous relative scaling, CPE(1) could not be a representative parameter to describe material properties. On the other hand, the CPE(2) results varied between 1.65 and 2.3×10^{-11} F cm^{-2} s^{n-1} exhibited proper relative scaling from air to PC and PMMA test pieces. Hence, the CPE changed monotonously with the AC testing voltage so this part of the response signal stemmed from genuine interaction and so representative material properties. Then, the same IDE configuration was used to test 'thick coatings'. Pristine state of coatings was aimed to test around edge of samples, obviating the error source of air gap in the main sensing range. Thus, resistance estimation of intact part of the coatings were between 8×10^{10} and 5.2×10^{11} ohm cm^2 close to the refence results between 9×10^{10} and 2.2×10^{11} ohm cm^2 right after immersion of coatings (not presented). Moreover, the CPE(1) results varying between 3.6−9.5×10^{-12} F cm^{-2} s^{n-1} was close to the refence CPE(2) data of ~2.5×10^{-12} F cm^{-2} s^{n-1} (without thickness normalisation). The CPE(2) results were ~1.6×10^{-11} F cm^2 s^{n-1} one fourth of the reference CPE(1) results (~5×10^{-11} F cm^{-2} s^{n-1}). So, based on this comparison it became clear such material assessment results do not transfer directly into wet condition results but the former can still be descriptive directly on condition of the coatings. After series of further experiments with long and split-wire connected quad-array IDE, loss of detection sensitivity was experienced in the forms of greater resistance and low capacitance character of coatings without depending on electrical testing parameters.

6.6. Evaluation of Design Cycle II Results

Based on all experimental results, presented partly and discussed in this chapter, the following conclusions were drawn.

- Microstrip-lines and the interdigitated configuration of edge-coupled electrodes were accepted for further investigation and development with some important proviso. Stipulations cover increased electrode width and gap for deeper penetration depth and longer electrode strip-lines for increased detection sensitivity. The former must be comparable with coating thickness.
- Single coherent large electrode blocks are always preferred to arrays due to the reason for unnecessary parallel connection coupling between blocks and so avoid suppression of sensitivity and reliability of detection.
- Short and proper wiring of sensor electrodes are preferred for all array formations.

Thus, next generation type sensors are expected to demonstrate proper sensitivity and reliability over full cross-section of the coatings without any major shortcomings and compromise manifested during the former two design cycles. Furthermore, project members supported taking this concept further to next stage of design cycle and test at least two, genuinely different hardware solutions to ensure satisfying outcome to the stakeholder. These details are described in the next chapter entitled as Design Cycle Three – The Prototypes.

7. DESIGN CYCLE III – PROTOTYPES

7.1. Motivation for and Description of Generation I Sensors

7.1.1. Interdigitated Sensors

After learning from the outcome of design cycle I and II, all strip-line configuration prototypes must feature sufficiently large surface area based on the combination of increased electrode length, width and gap so that increased sensitivity, greater penetration depth and robustness against variation of air gap ensured. Beyond user related limitations, moderate air gap tolerance is genuinely required due to uneven and slightly curved vessel geometries and surface morphology of the coatings. IDE type sensor would not contain parallel connected subunits to avoid unfavourable interaction of those and the related loss of sensitivity. Furthermore, monolithic IDE sensor contains favourably two electrodes. No three and four electrode configurations are needed for non-contact sensing mode operation (usage profile) and so the lack of possible shunting surface currents as well as good ionic conductors (sea water). Reliability of capacitive material testing is further assured by keeping constant clearance from the substrate. Thus, guard electrode application between driver and sensing electrodes can be omitted. If these trade-offs would not lead to a proper solution, then other electrode geometries must be considered for further development. Although the IDE 3 was thought to offer proper balance between sensitivity and air gap toleration, a smaller version was designed coded as the IDE 4 with an aim to offer increased sensitivity at the cost of lower penetration depth and air gap tolerance. Except for the main features (electrode width and gap), design parameters of the IDE 4 prototype were the same as for the IDE 3. Geometrical details of the IDE 3 and IDE 4 prototypes are summarised in Table 10.

Table 10. Geometrical details of the IDE 3 and IDE 4 prototypes

IDE 3	Dimensions (mm)	IDE 4	Dimensions (mm)
Width	1.1	Width	0.55
Electrode gap (spacing)	1.1	Electrode gap (spacing)	0.55
Length of single electrode	50	Length of single electrode	50
Number of sensing electrodes	52		
Length of all electrodes (driver or sensing)	5200	Length of all electrodes (driver or sensing)	5200

7.1.2. Concentric Array Sensors I and II

Aside from the intention to test viability of capacitive imaging, there was a strong motivation to implement one traditional design approach. This would work best at providing fully credible or at least complementary results on material properties besides the IDE prototypes. As the latter ones estimate

permittivity of the coatings affected by the sea water via electrically excitation and measure of capacitive characteristics, a dry state test mode is to assess resistance of the coatings. Thus, standard guidelines on surface resistivity measurements [284] were followed to develop design solution which is described in the following. The concentric array I prototype was designed to contain an outer grounded copper frame film (red coloured in Figure 24) locating on the material surface for shielding and stabilisation of the active inner electrode section. Inner section captures an array of ring and disk electrodes featuring driver (positive impressed voltage) and sensing functions (compensated to ground for sensing), respectively. Electrodes are arranged in couples in-plane along with two lateral axes. The size of ring and disk electrodes was optimised for targeted material properties, surface resistance range of the coatings (10^6–10^{11} ohm cm^2) for the thickness of 1 mm. This was matched with maximum allowed excitation voltage with mobile electric testers in AC−DC modes in compliance with international standard [284] on performing surface resistance characterisation of materials. This electrode alignment is regarded as a reference partly based on its unique cell constant. Any interdigitated type concentric electrode alignments are not standard compliant due to varied (distributed) cell constants and so not considered for implementation by the DTP. Geometrical data of concentric array I and II sensors are in Table 11.

Table 11. Geometrical details of the concentric array I and II prototypes.

Concentric array I prototype	Dimensions (mm)		Dimensions (mm)
Diameter of inner disk electrode	4.0		
Electrode gap	1.0		
Inner diameter of outer ring electrode	6.0	Surface ratio of disk & ring electrodes	0.64
Outer diameter of outer ring electrode	7.6		
Width of outer ring electrode	0.8	Probe geometrical constant	15.5
Concentric array II prototype			
Diameter of inner ring electrode	2.0	Outer diameter of inner ring	4.0
Inner diameter of middle ring electrode	4.8	Outer diameter of middle ring electrode	5.2
Electrode gap between mid-ring & inner disk & outer ring electrodes			0.4
Width of middle ring electrode	0.2		
Inner diameter of outer ring electrode	6.0	Outer diameter of outer ring electrode	7.6

Development of the single probe unit in prototype I to prototype II covered two major modifications. The inner disk electrode was redesigned to a moderate wide inner ring electrode, and a narrow ring electrode was added between the inner and outer ring electrodes in prototype II. The inner ring electrode with increased flexibility of the sensor laminate is intended to improve conformal coverage, air-gap free

deployment on coatings of varied geometry. The mid ring electrode is grounded to sink surface currents between the driver and sense electrodes, so to increase the rate of measured useful current through the tested material.

7.2. Derivation of Cell Constants

Derivation of resistance and permittivity of materials can be performed by various methods for DC and stationer AC results. To arrive for proper closed formulas to define physical parameters require more eloquent mathematical knowledge and skills than described in simple closed formulas [285−287]. In case of simple geometries, exact analytical solution is obtained by solving Poisson and Laplace equations with Dirichlet boundary condition [288,289], while complex structures FEM solvers provide accurate estimations [290−293]. To perform rapid and sufficiently accurate assessment, closed expressions are also available in the literature. In the following, two mathematical methods are referred to calculate response of interdigitated electrodes and the results compared to each other. Material resistivity and capacitive character is calculated using cell constant (K_{cell}) as given in the Equations 1 and 2. In addition, resistance derivation from measurement results is given in Equation 3.

$$R = \frac{K_{cell}}{R_{coat}} \qquad \textit{Equation 1}$$

$$C_{cell} = \frac{\epsilon_o \times \epsilon_r}{K_{cell}} \qquad \textit{Equation 2}$$

$$R = \rho \times k \qquad \textit{Equation } 3$$

The proportionality factor, cell constant (m^{-1} or cm^{-1}) expresses ratio between sensor active surface area and penetration depth of electrical field, effective cross-section of tested materials. Thus, specific resistance (ρ, ohm m) multiplied with the cell constant returns measured resistance (*R*, ohm) and in turn measured resistance divided by cell constant returns specific resistance of the coating. According to the literature, there are number of ways to define cell constant of interdigitated electrodes for variety of materials and test conditions. In part of the solution, majority of capacitive assessment includes elliptical integrals to calculate normal component and charge accumulation by the electrical field. Capacitance was estimated for the IDE-0.55 and IDE-1.1 prototypes based on a recent literature example [294]. Using multiplication factor of 4.3 as relative permittivity of polyimide sensor substrate material, 1.154×10^{-10} F capacitance is expected to measure with both sensors due to the same geometrical ratio of width of and gap between strip-line electrodes. This normalised to unit length (1 m) of the sensor electrodes becomes equal with 2.912×10^{-11} F m^{-1}. Estimated cell constants were around 0.251 for both sensor electrodes. Experimental results showed acceptable match especially in regard with thin blocking layer of polyimide cover on both sides of the prototypes over active electrode areas in the closest, the

most sensitive sensor volume range. Theoretical, experimental and derived results are summarised in Table 12.

When IDE type sensors are used for detection of insulators, then the lowest cell constant maximises sensitivity. In other words, larger active electrode surface is by greater electrode length is to formulate over unit surface area. Such sensors with a length of 5.2 m compared to the small electrode width and gap (0.55 and 1.1 mm) is unique in the literature. This means if such probes may fail at sensitivity with testing high resistive maritime coatings, then most probably there must be no point in making any further attempt to accommodate IDE type sensors for development in the DTP.

Table 12. Theoretical, experimental and derived material properties of the IDE sensors

Derived material properties	Sensor electrode types	
Theoretical	IDE-0.55	IDE-1.1
Capacitance (F)	1.154×10^{-10}	1.154×10^{-10}
Cell constant (m^{-1})	0.251	0.251
Experimental (under air)		
Capacitance (F)	2.52×10^{-10}	2.13×10^{-10}
Cell constant (m^{-1})	0.151	0.179

Other recent capacitance calculation-based cell constant estimation of IDE strip lines [295] lead to similar results (Table 13). In conclusion, simple expressions lead to minor overestimation of material capacitive characteristic but differentiation obtained with varying geometry of IDEs. Thus, if estimation by closed expression is to optimise geometry of IDE sensors in early design stage, then experimental validation is certainly advised and highly recommended.

Table 13. Theoretical, experimental and derived properties of the IDE sensors

Estimated material properties	Sensor electrode types	
	IDE-0.55	IDE-1.1
Capacitance under air (F)	1.4×10^{-10}	1.12×10^{-10}
Capacitance with tested material (ε_r = 5, F)	1.63×10^{-10}	1.30×10^{-10}
Sum of capacitance (F)	3.04×10^{-10}	2.41×10^{-10}
Cell constant (m^{-1})	0.271	0.341

In comparison with the concentric array, I hardware, resistance of the IDE sensors is markedly low and capacitive base signals were high in similar proportion. These are in agreement with larger length of edge-coupled electrodes and equal or around half of the electrode gap with the IDE-0.55 sensor.

To counteract shortcomings of open-ended strip-line sensors, concentric electrode configuration was introduced. Similarly to the aforementioned, calculation of accurate trans-capacitance response

signal of sensors require dedicated mathematical approach or detailed FEM. As for the latter, calculation results provide potential amplitude variation in-plane over the sensor surface between and around the concentric electrodes for both cases when outer ring electrified and inner disk excited for sensing [296]. The impact of edge coupling is obvious for the disk-ring electrode configurations. It is plausible, voltage perturbation with the outer ring is generally more sensitive for material testing than using smaller inner disk electrode for electrification, while providing effective shielding from EMI noise to nested disk, sense electrode. Although these simulation results can be very descriptive, these are still rudimentary modelling of full aspects of AC testing of materials, due to missing validated capacitive response signal as a function of material properties and extensive solution space to describe expected impedance test results. Skin-effect leads to shrinking tested volume range with increasing frequency of voltage signals while frequency distortion of current signals directly informative on system, material properties.

To use concentric electrode configuration in the DTP was also motivated by literature data on sensitivity of concentric and semi-concentric probes superior to strip-line configurations [297]. In addition, assessment of insulators is strongly advised to perform with concentric probes and disk−ring electrodes by international standards [284,298−303]. Industrial examples offer surface/volume concentric ring probes in the resistivity range of 103 and 1013 ohm with test voltage of 10−100 V while measuring current at 13 and 1.7 mA, respectively [304]. Special electrode configurations are still in compliance with the ASTM D257, ANSI/ESD STM11.11 [305] and STM11.12 [306] standards. The concentric array of spring-loaded pin probes with various pin-head configurations, e.g., the 'ETS Model 8' series resistance/resistivity probes' by Electro-tech Systems, Inc offer chance for continuous monitoring rather than operation in inspection use case [307]. As a further step in customisation, miniaturised concentric pin-arrays, i.e., the PRF-912B Miniature E12 Micro Probe Set by Prostat® Corporation [308] are constructed to offer accurate surface resistance assessment over small areas in wide resistance range ($1-10^{12}$ ohm). The latter corresponds to upper limit of maritime coatings in good condition.

Surface resistivity (ρ) and capacitive character (*CPE*) of paint coatings with thickness of up to 1 mm, is derived from DC and AC measurement results of surface resistance (R) as given in the following. First, the cell constant (k) and the single probe solution is expressed. Then, it is extended to arrays with arbitrary number of probes via using calculated normalising correction factors given subsequently. The cell constant k is calculated as expressed in Equation 4:

$$k = \frac{2\pi}{ln\left(\frac{r_2}{r_1}\right)} \qquad \textit{Equation 4}$$

where r_2 and r_1 are the inner and outer radius of ring and disk electrodes in a single probe, respectively. As a 2-dimensional segment of cylindrical structure, this factor expresses the ratio of length and distance between inner and outer sensor electrodes. Although this simplification means pure 2-dimensional conduction mechanism and neglects any marked conductivity contribution from 'bulk'

phase, 3-dimensional of coatings, the expression provides generally good estimation. Explicit derivation of overall surface resistance (*R*) requires multiplication with the cell constant (k) and the sum of surface (A) confined with the ring-disk electrodes (Equation 5).

$$\rho = R \times k \times A \qquad Equation\ 5$$

Thus, array extension related correction is given by sum of the electrodes covered surface area and so surface resistivity of coatings (ρ) equals with DC extrapolated resistance extraction from impedance spectra or ratio of testing voltage and measured current (according to the Ohm's law) obtained from chrono-amperometry, chronopotentiometry and potentiostatic measurement results. The sum of surface area of tested materials, paint coating is given in Equation 6.

$$A = \pi \times (r_2^2 - r_1^2) \times n \qquad Equation\ 6$$

Advantage of this resistance derivation, condition assessment becomes easy to understand and interpretate sensor readings by maintenance experts, technicians and crew members. This warrants the chance to perform justified trouble-shooting relating to surface installation of the sensors based on possibly erroneous measurement results which can be noticed and rectified by less trained personals. In the aspects of sensor optimisation, the cell constant is a key factor to ensure close surface area of the driver and sense electrodes while keeping lateral size of a single cell low to assure moderate extent for arrays. The electrode gap is required to be comparable with coating thickness to ascertain sufficient penetration depth and to gain full cross-sectional assessment. The concentric array prototypes were designed to feature the same cell constant of 15.5 (recommended for wide-range resistivity assessment) with overall surface area of 141.4 and 45.2 cm^2 (between the electrodes) by utilising 900 and 288 probes. After correction, dimension of the surface resistance becomes conform with general standard of ohm cm^2. The number of probes at low testing voltage of 1 V ensures reliable detection of current over 3 times above the minimum threshold of majority of mobile and laboratory test equipment (0.1 nA) applicable to naval coatings with specific resistance of up to 2.5×10^{14} ohm m. The latter may seem to be excessive as this range corresponds to excellent coating condition which can obviously be the case within the initial two years of service after paint-shop work. In another viewpoint, this resistance range is not interested by experts to facilitate organisation of maintenance actions. Therefore, this means redundancy in the prototype for current detection offering the chance to reduce the number of probes and decrease lateral size of the sensor laminate (322×272 cm). Normalisation of the CPE component is to be performed by the set of same correction factors but in this case, division must be applied (instead of multiplication) as stated in Equation 7.

$$CPE_{norm} = \frac{CPE_{meas}}{k \times A} \qquad \textit{Equation 6}$$

Thus, dimension of data can be expressed as ohm^{-1} cm^{-2} s^{n} or F cm^{-2} s^{n-1}. Further transformation to data featuring idealised theoretical capacitive property in dimension of F cm^{2} needs further correction based on frequency of data extraction from spectra as stated in Equation 5 in which *C* stands for absolute capacitance of an ideal capacitive element (valid without resistance at certain frequency) and Z_{CPE} stands for impedance of a real capacitor vs angular frequency range. The maximum featuring frequency is the normalising frequency for data to be normalised over the frequency range (Equation 8).

$$Z_C = \frac{1}{C} \times \frac{1}{\omega} = \frac{1}{Y_o} \times \frac{1}{\omega^n} = Z_{CPE} \qquad \textit{Equation 7}$$

Combination of the Cole-Cole impedance [309,310] with parallel coupled resistive and capacitive elements leads to angular frequency independent expression as stated in Equations 9 and 10.

$$Y_o = R^{n-1} C^n \qquad \textit{Equation 8}$$

$$C = R^{\frac{1-n}{n}} \times Y_o^{\frac{1}{n}} \qquad \textit{Equation 10}$$

The latter DeBrug formula [311] offers capacity assessment based on parallel combination of resistive and capacitive elements. Capacity evaluation by the Randle's arrangement may also result in the same outcome [312−314]. Generally, using the CPE data at a frequency of 1/(2×π) can be a good approximation for capacity assessment of coatings, although time constant of some coatings ('black coatings') were usually far below the lowest scanned frequency limit (0.05 Hz).

7.3. Motivation for a Subset Test Matrix

At this stage of the project (before two months of completion), the main priority shifted towards validation of repeatability and reliability of sensing. This was accompanied with a strong expectation of directly transferable material/coating properties assessed by the prototype sensors with the outcome evaluated with the traditional wet phase setup. Due to time constraints, the number of experiments in the test matrix was radically cut to proceed first with prototypes measuring at least 3 times to ascertain repeatability, and the traditional setup (one measure) with an intact and deteriorated states of substrates. Outcome of the eight measurements leading to dataset of specific material and condition must have been confirmed at least by another testing stage. Thus, sixteen datapoint must have been gathered over two full days of experimentation. In case of repeatable outcome, further coating/steel samples could have been characterised by the same test procedure. Further experimentation with salt contaminated and pre-corroded coating/steel samples was performed on the case when aforementioned results were in agreement with our expectation. Type and the number of measurements is summarised in Table 14.

Table 14. Number of experiments to evaluate generation I prototype sensors, referring to reduced test matrix

	Number of measurements	
	Prototypes (3)	Traditional setup (1)
Reference coating*		
Pristine state	3×2	2
Deteriorated state	3×2	2
Coating/salt contaminated steel substrate**		
Pristine state	3×2	2
Deteriorated state	3×2	2
Coating/pre-corroded steel substrate**		
Pristine state	3×2	2
Deteriorated state	3×2	2

*High priority experimentation

**Low priority experimentation

7.4. Experimental

7.4.1. Prototype Electrodes

The IDE 3 and IDE 4 prototypes were manufactured as 2−layer boards (no internal tracks) made of FR4 Laminate - TG150, with 3 Oz copper on bottom and upper layers (track thickness of 105 μm).

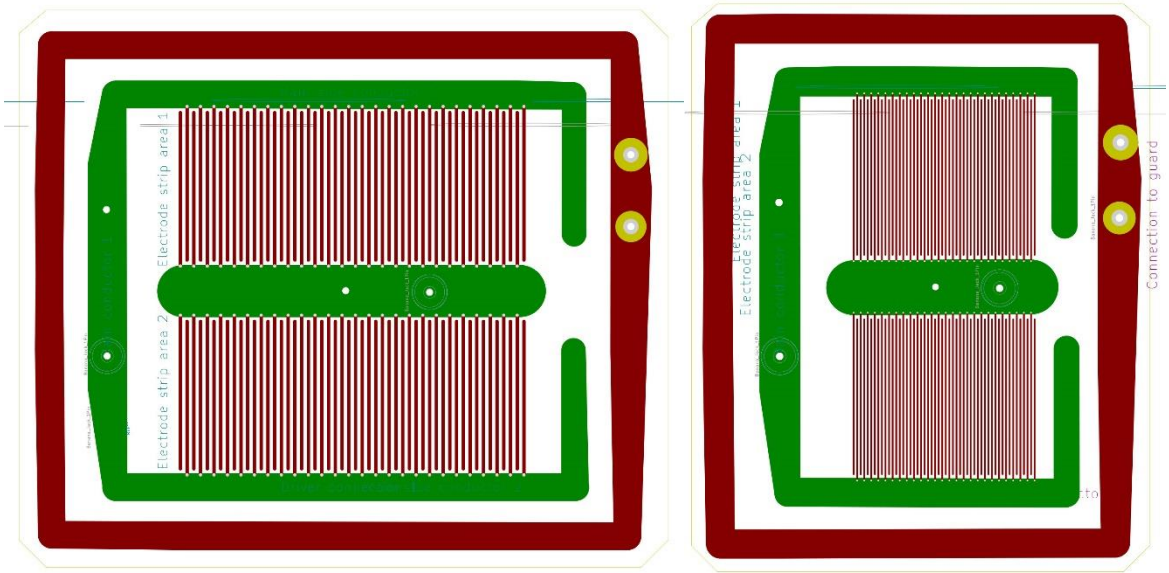

Figure 23. Front side view of the IDE 3 (left) and IDE 4 (right) protypes by the 'PCB layout editor' with vias and pads, connecting the 2 outer layers on top (green coloured) and bottom (red coloured, the active sensing area) parts of the sensor.

Surface finish was HAL standard – ROHS compliant. Lateral size of the IDE 3 and 4 prototypes were 212 mm (x) and 181,6 mm (y), 142 mm (x) and 176 mm (y), respectively, both with the same overall

thickness of 1.6 mm. Both IDEs were fitted with green solder mask on top of the bottom and upper surface. The IDE 3 and 4 prototypes are presented in Figure 23 in front side views. Both sensors are designed to contain an outer, perimeter type copper frame-layer (at the sensing surface) fitted with two pads to fit with surface mounted connectors (preferable with female banana type in diameter of 4 mm) for electrical connection. Function of this frame-layer is twofold. The one is to electrically shield inner electrodes from outer capacitive noise and to afford extra mechanical stability in lateral dimension of the sensor. The second copper frame-layer is top surface located (opposite side of sensing surface) a used as the driver electrode. This provides additional shielding to the inner sensing electrode and further mechanical stability to the platform. The third top surface located inner layer electrode is the sensing electrode. This was designed to have low ratio of direct in-plane edge-coupling between driver and sensing electrodes so as to keep the ratio of high percentage line couple of inner IDE area and preclude sensitivity loss by direct coupling between main conductors of the driver and sensing electrodes. The edge-coupled sensing electrode area includes twice 52 electrodes, each within length of 50 mm. Electrode width and spacing is doubled to IDE 3 compared to IDE 4 (1.1 mm and 0.55 mm). All main conductors are equipped with two pads for surface mounting connection on top, back sides of the prototypes. Optimisation of the sensing electrode section was based on the international literature and calculations results. Raw earlier versions of the IDE 3 included the same electrode geometry and some amendments like accommodating an outer in-plane shielding electrode but the entire structure was way too large in lateral size, so unacceptable for further development due to incapacitated field application.

The concentric array I sensor was manufactured as a 4−layer laminate with one internal layer for copper tracks to connect array of sensing electrodes (3 layers overall). This was made of FR4 Laminate - TG150, with 2 Oz copper (track thickness of 70 μm) for internal and external layers to ensure optimal flexibility. Surface finish was chemical gold (ENIG) due to chemically stable characteristic (corrosion resistance), accuracy and reliability of detection, blocking nature of the electrodes in salty environment over long-term use. This owes to the fact, the sensor expected to use in directly connected mode. Lateral size of the concentric prototype II was 322 mm (x) and 274 mm (y), in overall thickness of 0.4 mm. PCB layout editor type front-side view of the sensor is presented in Figure 24.

The concentric array II sensor was manufactured also as a 4−layer laminate with one internal layer to separate 2 layers of copper tracks (3 polymer layers overall). The inner layer was composed of FR4 Laminate, which carried two copper layers on its both sides in thickness of 63 μm (approx. 2 Oz copper for each track). Polymer film was deposited on both sides in thickness of 130 μm. Front and back plate copper tracks on top of separator films were coated in thickness of 63 μm. Thus, neat thickness of the sensor laminate was 780 μm. Surface finish of exposed copper tracks was chemical gold (ENIG) type. Relative permittivity of the sensor laminate is estimated as ~4.5. Dimension of the concentric prototype III was cubic with length of 184 mm in x and 183 mm in y direction. PCB layout editor type front-side view of prototype II is in Figure 24.

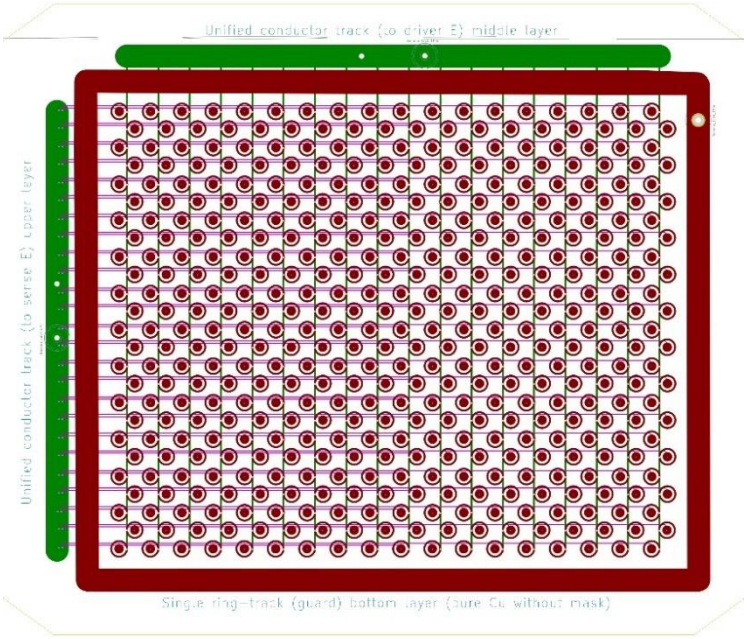

Figure 24. Front side view of the concentric array I protype by ‘PCB layout editor’ with vias and micro-vias (connecting inner layer copper tracks), pads, connecting 2 outer layers on top (green) and bottom (red coloured, active sensing area) parts of the sensor, inner layer tracks connect (purple) disk sensing electrodes between micro-vias and outer main tracks.

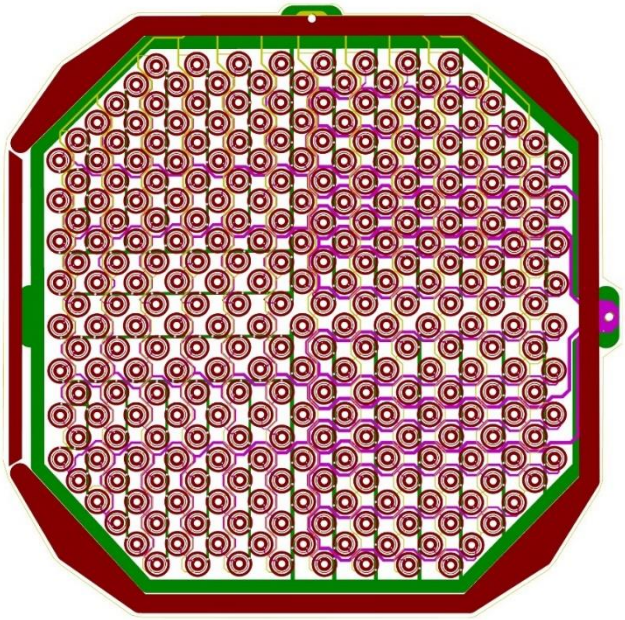

Figure 25. Front side view of the concentric array II protype by ‘PCB layout editor’ back-plate copper tracks (green) for driver electrode connection, front-side copper tracks (red) with array of sensor probes and shielding bracket, 2 inner layer copper tracks to connect sensor and sink electrodes separately via micro-vias. Driver and sensor electrode connections located at copper pads on both left and right-hand sides of the laminate. Upper located pad serves as sink electrode connection (ground).

For surface resistivity assessment, direct implementation of standard geometries [284] would not have led to proper design solution because large single unit probes are low electrode covered surface area for sensing and so require high testing voltage. In addition, these are optimised for dedicated resistance ranges within 4 orders of magnitude ranges between two, i.e., 10^{15}–10^{11} ohm and 10^{7}–10^{3} ohm. For the DTP, maintenance and asset management targeted resistance range is in 5 decades between 2.5×10^{11} and 2.5×10^{6} ohm cm^2 for epoxy coatings with thickness of ~1 mm. The concentric array II sensor was optimised to test materials of large resistance without compromised sensing. Details of the material properties, electrical testing parameters and minimum number of probes are given in Table 15. The highest number of probes served as a reference to obviate detection bottleneck in the useful current range by the testing electrometer. As it is denoted in Table 15, a minimum of 840 piece of concentric electrode pairs must be combined into an array to reach sufficient current limit detectable reliably by a mobile equipment as it was described in the previous section. Thus, rounded number of probes (900) were aligned into array (design parameter) in the concentric array I sensor.

Table 15. Material characterization and electrical testing parameters when using the concentric array I prototype. Minimum detectable current by the AC/DC tester estimated as 1.3×10^{-10} A.

Max. AC-DC testing voltage (V)	Effective perimeter (cm)	Surface resistance (ohm per square)	Volume resistance (ohm cm)	Number of probes	
	1.26	1.61×10^{12}	8.84×10^{11}	Surface sensing mode	Volume sensing mode
		Measured current			
0.25 (AC)		1.55×10^{-13}	2.83×10^{-13}	839	460
10.0 (DC)		6.20×10^{-12}	1.13×10^{-11}	21	12

For easy real-life use of the concentric array II sensor, lateral size of the patch sensor was rationalised by decreasing the number of probes to around one third of the prototype I. Regarding the octagon type lateral shape optimisation of the laminate, this led to array coupling of probes in total number of 288. This revision in the prototype II is also considered as proper match with moderate coating resistance range which is most interested by coating inspectors, maintenance experts and asset management.

7.4.2. Coatings for Prototype Assessment

Carbon black pigmented epoxy coatings were deposited in wet thickness leading to DFT of around 1 mm on carbon steel substrates with lateral size 50×50 cm. Instead of accelerated aging, three types of coating-specimen samples were prepared, i.e., the neat reference, salt contaminated and pre-corroded ones similarly as used for previous two design cycles. A month-long immersion exposure was applied to the samples in filtered sea water leading to initial degree of hydration, non-diffusive water uptake. All other parameters of the coatings and specimens were identical with statements of previous sections.

Sensitivity assessment of the prototypes were performed via 'dry state' measurements. Right before experimentation, coatings were cleaned and dried at room temperature to remove contaminants, possible electrically conductive shunting pollutants and permittivity contributor substances. The former is priority to perform validated measurement with the concentric array sensor and the latter is important for credible sensing with the IDE_3 and IDE_4 prototypes. The concentric array was applied in contact mode, pressed onto coating surface by backside application of elastic laminate and ~20 N load distributed evenly on the backplate. Some volume was left empty (removed) from the laminate to route connecting wires out of the sensor backside to test equipment. As part of possible troubleshooting, the quality of electrical connection between the sensor and coating surface must be checked by repeated measurements at various backplate loads and increased test voltage. If detected signals are noiseless, stable and do not change remarkably for magnitude and phase data then the results can be accepted as valid test results. After impedance test was performed, IDE prototypes were used for assessment of coatings condition in non-contact mode. In majority, no macroscopic air gap was between the sensor and substrate. In some case, well-controlled minimal clearance was kept at 0.02 mm at all four corners of the boards. When testing with the prototypes was finished then traditional impedance procedure with wet phase and planar electrodes was carried out over the same area as the prototypes mounted. Electrical test setup was the same as discussed in Design Cycle II.

7.5. Test Results

The prototypes were first tested under air to define base sensor signal (resistance and capacitive character). Blind measurement offers estimation of physical parameters of the sensors, then derivation of properties of the tested materials. Constant phase element data derived from the impedance spectra were normalised with vacuum permittivity (8.854×10^{-14} F cm^{-1}) and average of those are summarised in Table 16.

Table 16. Estimated permittivity of sensors derived from impedance data measured under air, reference permittivity of polyimide (3.5), polyimide glass-flake composite (4.2), FR4 epoxy of PCBs (4.7)

Sensors	Estimated rel. permittivity
IDE-0.55	<22
IDE-1.1	<17
CA	4.1

Overestimated relative permittivity of the polymer (polyimide) sensor platform was obtained to both IDE sensors. This is interpreted as a consequence of additional and longer segments for capacitive interaction of conductor tracks (in front-side and coplanar configurations) via both homogeneous and fringing fields. Possibly, short volume-range concentrating fringing fields by the IDE-0.55 contributed

markedly to such overassessment (increased over the IDE-1.1) as its volume range of high sensitivity is more overlapped with the thin polymer blocking layer on the sensors.

Nevertheless, very good permittivity estimation was obtained with the gen. I type concentric array (CA) sensor, corresponding with the expected range of polyimide at low frequencies (between 4.1 and 4.5). Such sensor accuracy would be acceptable translating to on-site condition assessment of maritime coatings. Results on condition assessment of short-term exposed ('black') panels with prototype sensors in comparison with traditional wet phase test mode are presented in the following. First, outcome of the coating and neat steel substrate sample is discussed. Coating resistance ranges measured and derived to the IDE-1.1 and IDE-0.55 sensors were an and two orders of magnitude greater compared to the CA results, respectively, regardless of the applied test voltage (Figure 26). In comparison with the traditional wet phase testing, similar results to the CA were assessed with the lowest test voltage (0.1 V) in single cell configuration, while double cells setup led to around ten times lower result (unfortunately this data could not be extended to higher voltages). All other increased test voltages led to two orders of magnitude difference with the single cell setup compared to the reference CA sensor.

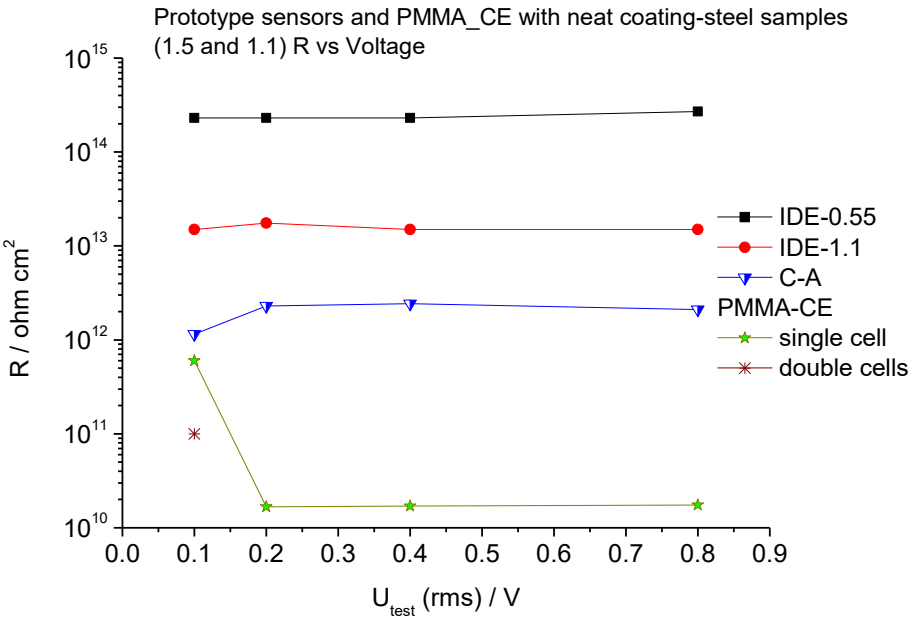

Figure 26. Coating resistance of short term exposed, hydrated coatings on neat metallic steel substrates, derived from impedance data obtained with the IDE and CA prototypes, PMMA-CE planar electrodes.

In comparison with sensors resistance, blind signals measured under air (appendix), the CA sensor manifested three orders of magnitude drop of overall resistance as a response to the pristine and thick epoxy coating insulator. The IDE-1.1 sensor indicated ten times drop in resistance magnitude, whereas the IDE-0.55 showed almost unchanged response. Bering in mind the similar insulator character of the sensor polymer platforms comparable to the epoxy and shorter distance between conductor tracks in some sensor sections than DFT of the coating, this result reflects on markedly varying sensitivity of the

prototypes in contact and non-contact modes to the high resistive insulator coating. CPE character of coatings assessed with the sensors showed a different picture, the results are summarised in Figure 27.

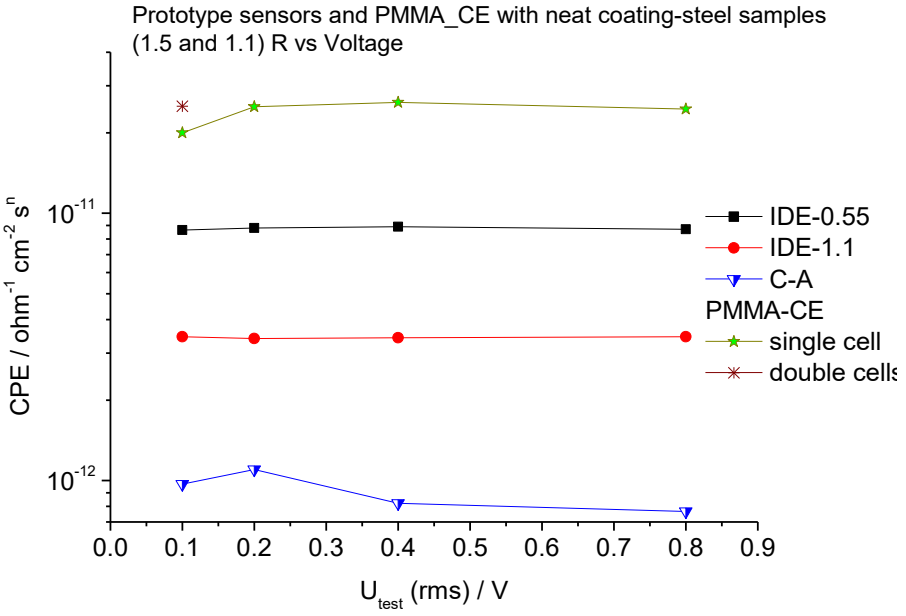

Figure 27. Constant phase element of short term exposed, hydrated coatings on neat metallic steel substrates, derived from impedance data obtained with the IDE and CA prototypes, PMMA-CE planar electrodes.

The CA provided capacitive response around 10^{-12} ohm^{-1} cm^{-2} s^{n}, more than doubled than its base signal. Similarly, the IDE-0.55 and IDE-1.1 indicated detection of capacitive character within almost ten times increase compared to base signals whilst falling far from range of the wet phase test results both with the single and double-cells setups. Compared to base signals, the IDE-0.55 and IDE-1.1 manifested high and moderate sensitivity to assess capacitive character. These results are regarded excellent as both epoxy coating and sensor platform polymer feature roughly the same permittivity while useful volumetric range for sensing shrunk compared to base sensor signals. Thus, such increases agree with the theoretical expectation. Traditional wet phase sensing indicated considerably higher CPE results with the single cell setup, compared to double-cell test configuration, which is mainly caused by distortion of the high-capacity electrical double layer on bare counter electrode. On the other hand, no match of data by the IDE sensors suggests inaccurate estimation of coating capacitive character, while the CA seemed to work to resistivity characterisation in an acceptable way. Complementary physical parameters by the sensors (resistivity by IDEs and capacitance by CA) may not fully valid to assess such high resistance solid materials.

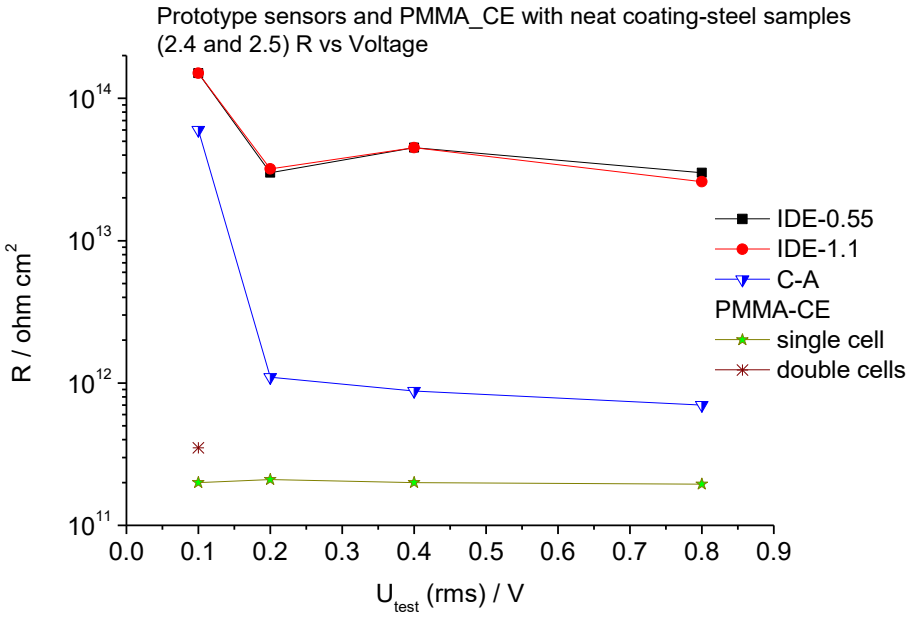

Figure 28. Coating resistance of short term exposed, hydrated coatings on pre-corroded steel substrates, derived from impedance data obtained with the IDE and CA prototypes, PMMA-CE planar electrodes.

In case of the panel sample with pre-corroded steel substrate, the results presented in Figure 28 and Figure 29 indicated pronounced differentiations in sensitivity of the prototypes. Resistance characterised with the CA decreased beyond two orders of magnitude as a function of test voltage increase. Measurement performed at 0.1 V rms did not provide valid resistance assessment (Figure 28), while dropping resistance with the increasing test voltage is connected to the presence of semi-conductor corrosion products under coating. Such negative differential resistance phenomenon can only be assigned to semiconductors. To confirm this interpretation, no such effect has been recorded at this scale to non-corroded and uncontaminated samples. Furthermore, this effect could also be experienced with the otherwise non-sensitive IDE probes with around order of magnitude decreases over the test voltage range. These results were entirely different to what was indicated by the wet phase setup, showing no marked resistance variation over entire test voltage range, overall, around ten times lower than that was manifested by the reference CA sensor. This outcome is explained by missing effective sensing by wet phase setup without the impact of electrolyte infiltration. In other words, the volume range of electrolyte ingress limits detection range of wet phase test. So, no valuable information is obtained on interface materials as long as no electrolyte penetration and hydration occur. This leads to strict condition of EC testing with the wet phase setups and possibly inferior reliability of assessment. Therefore, it is not advised to use for rapid quality testing of freshly prepared and partly dried coatings along with steel substrates, since no valuable information on quality of the manufacturer and contractors can be obtained.

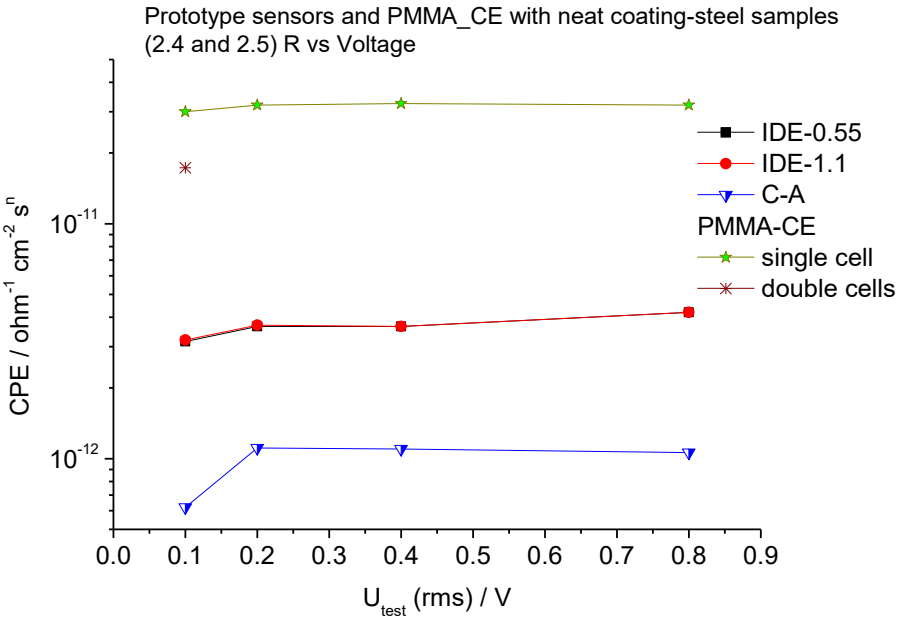

Figure 29. Constant phase element of short term exposed, hydrated coatings on pre-corroded steel substrates, derived from impedance data obtained with the IDE and CA prototypes, PMMA-CE planar electrodes.

The CPE results did not scale and vary in the range (Figure 29) as found to the panel with neat steel substrate. Sensitivity to capacitive response by the IDE sensors were altered and so provided almost the same results over the test voltage. Test results with the IDE-1.1 indicated somewhat higher sensitivity compared to neat coating, while the IDE-0.55 drop markedly in sensitivity. In fact, based on previously shown and these results, it would suggest the IDE-1.1 reached full cross-sectional sensing of the coating to the interface. The CA sensor responded with similar increment in coating capacitive character as a function of test voltage, to signals from neat steel substate (Figure 27). The wet phase setup with double cell configuration provided similar results to the IDE sensors with moderate overestimation, while the single cell setup led to obviously erroneous ten times of over-estimation. This suggests condition assessment of coating and steel substrates by wet phase setups would be far less accurate and credible than attainable with dry phase test setups both via contact and non-contact modes. Coating resistance of the salt contaminated panel indicated restrained scaling of sensor responses with test voltage (Figure 30), to outcome of the pre-corroded substrate (Figure 28). Almost the same resistance was assessed with the CA to the salt contaminated and pre-corroded samples. Unlike in previous cases, these were similar to outcome by the wet phase setup. This means full cross-sectional sensitivity of the CA sensor to assess the impact of chemical agent at the surface. The ten times difference was noticed between the single and double cells setups in the wet phase mode. In this case, IDE sensors returned resistance data similar to the neat substrate sample, which the lack of sensing functionality in depth of 1 mm at the steel interface. Nevertheless, as for the CPE results, both IDE sensors manifested credible results by the extent of

relative shifts in magnitude of the capacitive character leading to almost perfect match with double cells setup of the wet test (Figure 31).

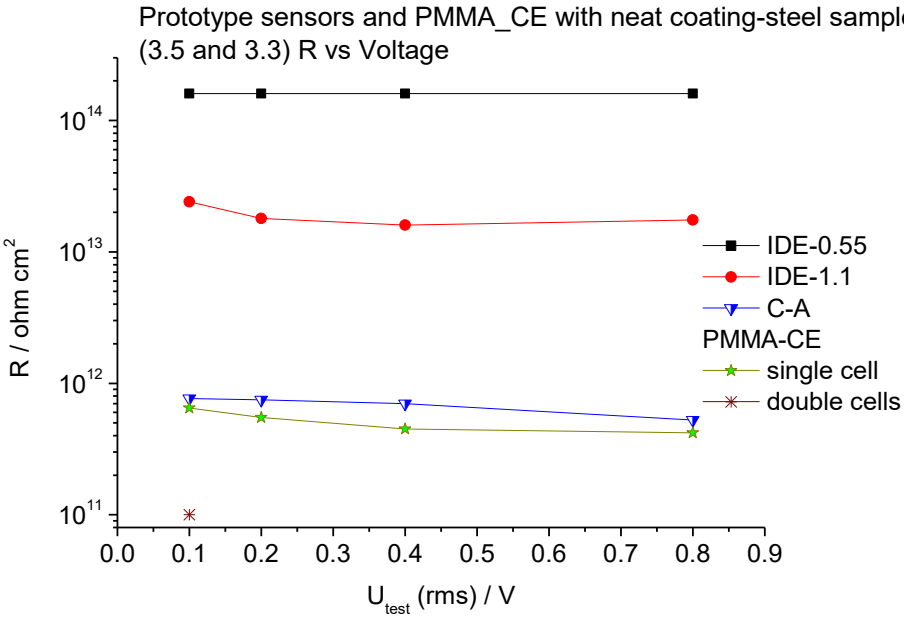

Figure 30. Coating resistance of short term exposed, hydrated coatings on salt contaminated steel substrates, derived from impedance data obtained with the IDE and CA prototypes, PMMA-CE planar electrodes.

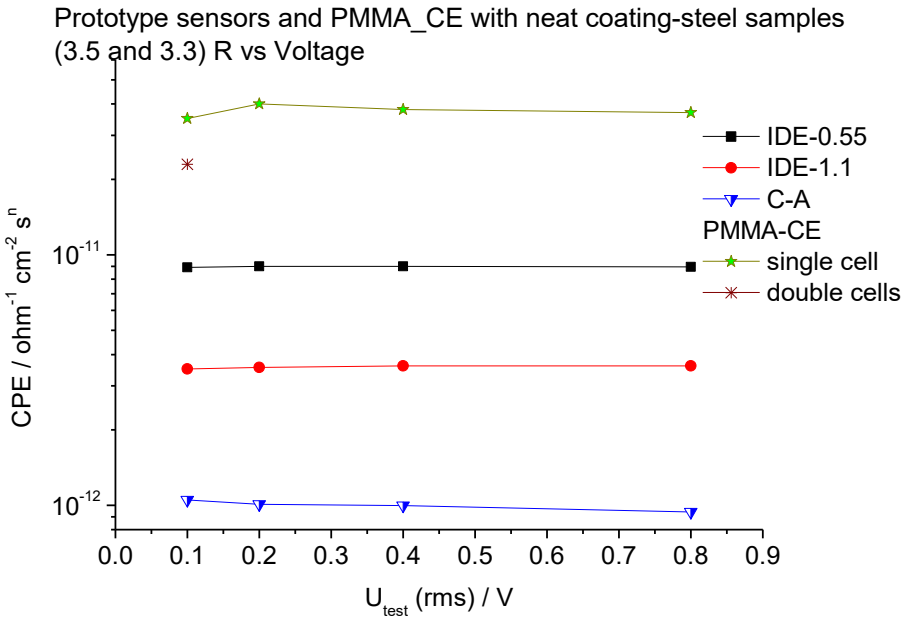

Figure 31. Constant phase element of short term exposed, hydrated coatings on salt contaminated steel substrates, derived from impedance data obtained with the IDE and CA prototypes, PMMA-CE planar electrodes.

This underlines validity of measurement and parameter estimation. Compared to the IDE-0.55, sensitivity of the IDE-1.1 and CA to capacitive material characteristic remained inferior. Furthermore, strong effect of the electrochemical double-layer capacitance arising on the uncoated (counter) measure electrode led to around 10 times of range in outcome by the single cell over the double cells. In the viewpoint of resistance variation with test voltage, CA sensor results correlated with wet phase testing. Alignment of cells with test electrodes and fitting of the CA I sensor on real life modelling maritime coating is depicted in Figure 32.

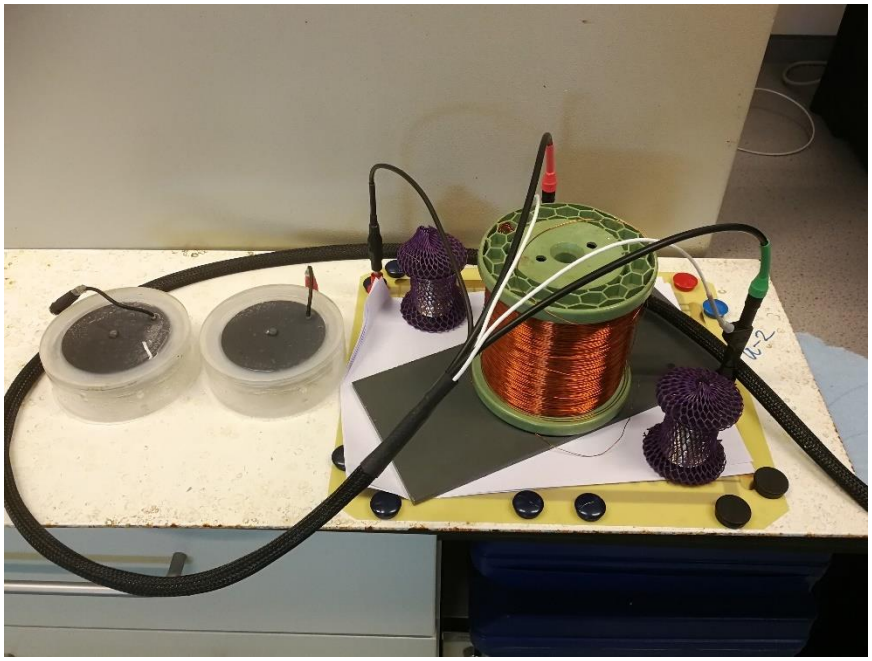

Figure 32. Image of electrical test of long-term exposed maritime model 'white coating' for resistance and capacitive characteristics, tested with PMMA-CE planar electrodes (left) and CA I prototype (right, loaded with several weights (coils) to reduce the air gap between sensor and coating surface).

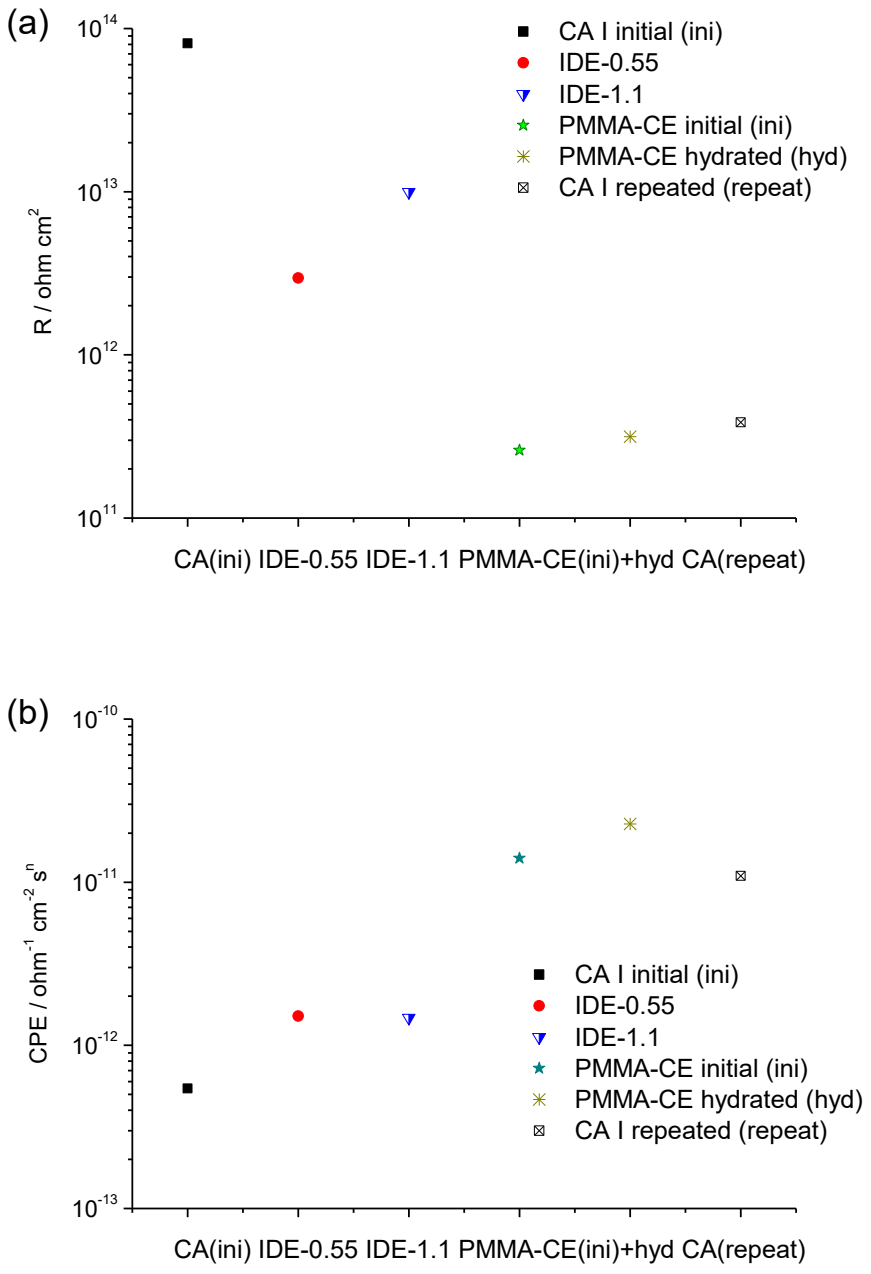

Figure 33. Coating resistance (a) and capacitive characteristic (b) of long-term exposed real 'white coating', derived from impedance data obtained with the IDE and CA prototypes, PMMA-CE planar electrodes. Repeated measurement with the CA sensor refers to remeasure on the same location with modified, closer attaching configuration between the sensor and coating.

In general, the CA and wet phase setups were only reliably to test long-exposed high resistance 'white' coating (without grounding the steel substrate). Based on some measurements, results could be obtained with the IDEs but these regarded as mainly informative. Thus, coating resistance was evaluated as around the same with CA and wet phase setups (Figure 33a), while the IDE-0.55 and IDE-1.1 sensors indicated responses with order of magnitude higher and above. Capacitive responses of the prototypes

were very similar around 1.6×10^{-12} ohm^{-1} cm^{-2} s^n (Figure 33b). As always, the carbon electrode led to 10 times higher estimation of coating capacitive character, at 2×10^{-11} ohm^{-1} cm^{-2} s^n.

After extraction and normalisation of data taken from the raw sensor readings, pure material properties solely related to the coatings were defined based on parallel circuit coupling of resistive and capacitive elements. Initial and derived data are summarised in Table 17. To quantitative assessment of the sensors results, it is advisable to remind about literature reference on resistance of epoxy. DC bulk phase and surface resistance is around 10^{13-14} ohm cm^2 [315] and 10^{11-12} ohm cm^2, respectively [316,317]. Thus, sensor derived data to the neat substrate samples (1.5 & 1.1), the IDE-0.55 proved to be out of range for both volume and surface resistivity, whilst IDE-1.1 and the CA provided results in line with effective volume resistance of epoxy. Nevertheless, the CPE derived data indicated high and moderate sensitivity of the IDE-0.55 and IDE-1.1 sensors based on good match with the expected one. Only the CA result fell short with around half of the expected level. In case of the pre-corroded sample (2.4 & 2.5), coating resistance estimation was found excessive with both IDE sensors, but the CA sensor data were at the boundary of volume and surface resistance. As for the assessment of capacitive characteristic, both IDE sensors indicated moderate sensitivity at around half of the expected maximum, exceeding the CA provided and derived data by about three times. With the salt contaminated sample (3.5 & 3.3), estimations with all prototypes were in the range of volume resistance.

Capacitive data underscored high and moderate sensitivity of the IDE-0.55 and -1.1 sensors besides the mediocre performance of the CA with somewhat greater indication compared to results of the neat and pre-corroded test panels. Aside from the model coatings, the long-term exposed real-life ‘white’ coating panel led to manifestation of annihilating sensitivity of the IDE sensors and increased sensitivity of the CA for both capacitance (around one third of the theoretically expected level) and resistance assessment (the latter related to the boundary of surface and volume ranges). Interestingly, due to several orders of magnitude difference between capacitive character of epoxy coatings and electrochemical double layer, no marked contribution of the latter translates into overall capacitance as it cannot be straight calculated via series coupling of capacitive elements into increment over space-charge estimation. Nevertheless, all measurement results indicated such a tendency and by knowing direction of changes by the electrolyte ingress, these results are generally considered to be informative rather than reference data.

Table 17. Derived coating resistance and CPE based capacitance estimations vs sensors base signals, in comparison with literature reference (on epoxy resistance) and informative space charge-based capacitance estimation of coating surface unit (F cm^{-2}) with ε_r = 4.1. Coating resistance and capacitance data were expressed and calculated with parallel coupling of resistive ($1/R_{meas} = 1/R_{sens}+1/R_{coat}$) and capacitance ($C_{meas} = C_{sens}+C_{coat}$) elements.

	Epoxy resistance		Coating capacitive character ($F = 3.63\times10^{-12}$) over surface area (1 cm^2) and DFT (1 mm)	
	Sensor resistance (ohm cm^2)		Sensor capacitive response (F)	
IDE-0.55	$3-6\times10^{14}$		2×10^{-12}	
IDE-1.1	$1.5-3\times10^{14}$		1.5×10^{-12}	
CA	$2-4\times10^{15}$		4×10^{-13}	
	Base signal	Coating	Base signal	Coating
'Black' coating-neat steel substrate (1.5 & 1.1)				
IDE-0.55	2×10^{14}	6.0×10^{14}	8.5×10^{-12}	6.5×10^{-12}
IDE-1.1	1.5×10^{13}	1.6×10^{13}	3.3×10^{-12}	1.8×10^{-12}
CA	2×10^{12}	2.0×10^{12}	$8\times10^{-13} - 10^{-12}$	5.0×10^{-13}
PMMA-CE	$10^{11} - 6\times10^{11}$		$9\times10^{-12} - 2.5\times10^{-11}$	
'Black' coating-pre-corroded steel substrate (2.4 & 2.5)				
IDE-0.55	1.5×10^{14}–3×10^{13}	9.1×10^{13}	$3-4\times10^{-12}$	1.5×10^{-12}
IDE-1.1		1.1×10^{14}		2.0×10^{-12}
CA	$10^{12} - 8\times10^{11}$	9.0×10^{11}	$6\times10^{-13} - 10^{-12}$	4.0×10^{-13}
PMMA-CE	$2-3.5\times10^{11}$		$6\times10^{-12} - 3\times10^{-11}$	
'Black' coating-salt contaminated steel substrate (3.5 & 3.3)				
IDE-0.55	1.5×10^{14}	3.0×10^{14}	9×10^{-12}	7.0×10^{-12}
IDE-1.1	1.9×10^{13}	2.1×10^{13}	3.5×10^{-12}	2.0×10^{-12}
CA	$6-8\times10^{11}$	8.0×10^{11}	10^{-12}	6.0×10^{-13}
PMMA-CE	$10^{11} - 6\times10^{11}$		4×10^{-11}	
Long-term exposed 'white' coating steel substrate				
IDE-0.55	3×10^{12}	3.0×10^{12}	2×10^{-12}	0
IDE-1.1	10^{13}	1.1×10^{13}	2×10^{-12}	5.0×10^{-13}
CA	4×10^{11}	4.0×10^{11}	1.8×10^{-12}	1.4×10^{-12}
PMMA-CE	3×10^{11}		$1.5-2\times10^{-11}$	

Due to the representative assessment by the CA sensor working in contact mode and the fact material resistance can also be assessed by DC methods, the CA was involved in a series of electrical testing modes for comparison. For such purpose, the AC type impedance investigation and several DC type characterisations such as chrono-amperometry at different voltages, chrono-potentiometry and potentiostatic scanning were applied for some minutes on the real modelling 'white' coating. The raw measurement data are presented in the appendix and derived results are summarised in Table 18.

Table 18. Resistance results of the long-exposed 'white' coating-panel sample from AC and DC data measured with the concentric array (CA) sensor

Measurement mode	**Estimated coating resistance ohm cm^2**
Chrono-amperometry (at 0.1V)	5.1×10^{11}
Chrono-amperometry (at 1V)	4.8×10^{11}
Chrono-potentiometry (at 5nA)	3.9×10^{11}
Potentiostatic (at 1V)	3.6×10^{11}
Impedance test (at 1V rms)	
R(coat)	3.9×10^{11}
CPE(coat)	1.1×10^{-11} (ohm^{-1} cm^{-2} s^{n})

As it clearly seen in the data, the CA provided very similar coating resistance based on all three DC methods and the impedance derived one. This is to aside from minor distortions in the data arising from the increasing voltage and elapsing time with number of electrifications for measurements, leading to somewhat lower resistance by increasing number of excitation stresses. Lower resistance by impedance results in the measurement series is related to altered material properties and increased conduction by the skin-effect. To compare required time for material testing or throughput in number of tests to perform over unit time, DC techniques clearly outperform impedance test mode by a factor of at least 8. Only the capacitive characteristic cannot be assessed by DC approaches but marked difference in throughput of the methods is more than a simple advantage.

Thus, from the three prototypes, the gen. I type concentric array sensor proved to be universal (versatile for test techniques), acceptably accurate and reliable for evaluation, if technical issue like non-contacting all probes of the array on the surface is not counted. Therefore, this sensor was selected for condition assessment of a true maritime coating exposed to almost real-life environmental conditions for around a decade at Endures BV. Such a coating located on lower part of a mono-pylon, modelling foundation of an off-shore wind turbine, was selected for validation in real-life modelling circumstance. Then, the coating was fitted with two cells filled with sea water and containing electrodes for wet phase testing. The CA provided evaluable results immediately after fitting the sensor tightly on the surface,

whereas wet phase setup led to poor quality data (low quality spectra with full-scale capacitive noise) even after some time of hydration conditioning.

Fitting of the CA I sensor on the mono-pylon to test immersion exposed part of a heavy-duty maritime coating is presented in Figure 34.

Figure 34. Image of the CA I prototype on the mono-pylon to test sea water immersion exposed part of a heavy-duty maritime coating. The sensor was fitted with stripes and thick leader laminate on back plate of the sensor.

Outcome of the electrical test on monopile coating is summarised in Table 19.

Table 19. Resistance and CPE data derived from spectra measured with the CA and the traditional wet phase setup on yellow coating (heavy duty epoxy with glass flake) of the mono-pylon

Sensor, configuration & measure mode	**Estimated coatings resistance ohm cm^2**	**CPE component ohm^{-1} cm^{-2} s^n**
Concentric array (CA) sensor	7.14×10^{10}	9.51×10^{-12}
Magnet fitted PMMA-CE with 2 electrodes (2 in series)	8.04×10^{10}	1.43×10^{-11}

In this case of the coating sample, fast fitted cells and the not enough hydrated coating led to some over-estimation of coating resistance, although the two derived results are in good agreement. For different reasons, the CPE parameter also reflected some overestimation by wet phase testing but both derived data are fairly close to each other and so can generally be acceptable. Nevertheless, the exceptionally poor data obtained with the wet phase testing with abundant noise in the spectra (proper fitting is rather

miraculous than straight and well established) is clearly no match and not competitive at all either with the impedance and DC based sensor reading derived data obtained with the concentric array prototype.

7.6. Evaluation of Design Cycle III Prototypes

To summarise findings on the gen. I prototype sensors, interdigitated electrodes working in non-contact mode proved to be moderately sensitive to evaluate the capacitive character of high resistance coatings in response to application of fringing fields. On the other hand, these sensors did not provide valuable estimation of the coating resistance, although derived results were in the range of specific volume resistivity of epoxy in accordance with the literature. Furthermore, in general aspects on practical usability, these sensors cannot work properly and do not provide useful data without backplate shielding and grounding of substrate of the tested panels. Thus, the use of such sensors in real-life situations is unfeasible.

The concentric array sensor was found applicable and reliable to characterise the range of coating resistance and versatile to work in variety of AC and DC test modes. In addition, working in contact mode with moderate effective penetration depth, it was found to reveal the presence of corroded phase under coatings. What is more, this sensor provided data to approximate material permittivity. These are all without any extra backplate shielding on and around the sensor. In comparison with the traditional type wet phase test setup, the concentric array sensor is superior in almost all aspects, which is in line with the expectations based on international standards and recommendations [308]. So, CA is recommended for laboratory and field applications with much higher preference than traditional wet phase setups.

8. Validation of Concentric Array Sensors in Open-Sea Environment

8.1. Generation I Type Concentric Array Sensor

After completion of my laboratory investigation at Endures BV, test series with the traditional wet phase setups with various electrode sizes and the concentric-array sensor was continued further by using model and real-life coating samples. Experimental setups and results obtained in 2020 and presented at the DTP meeting on 14 February 2021 are shown in Figure 35, 36 and 37 discussed herewith.

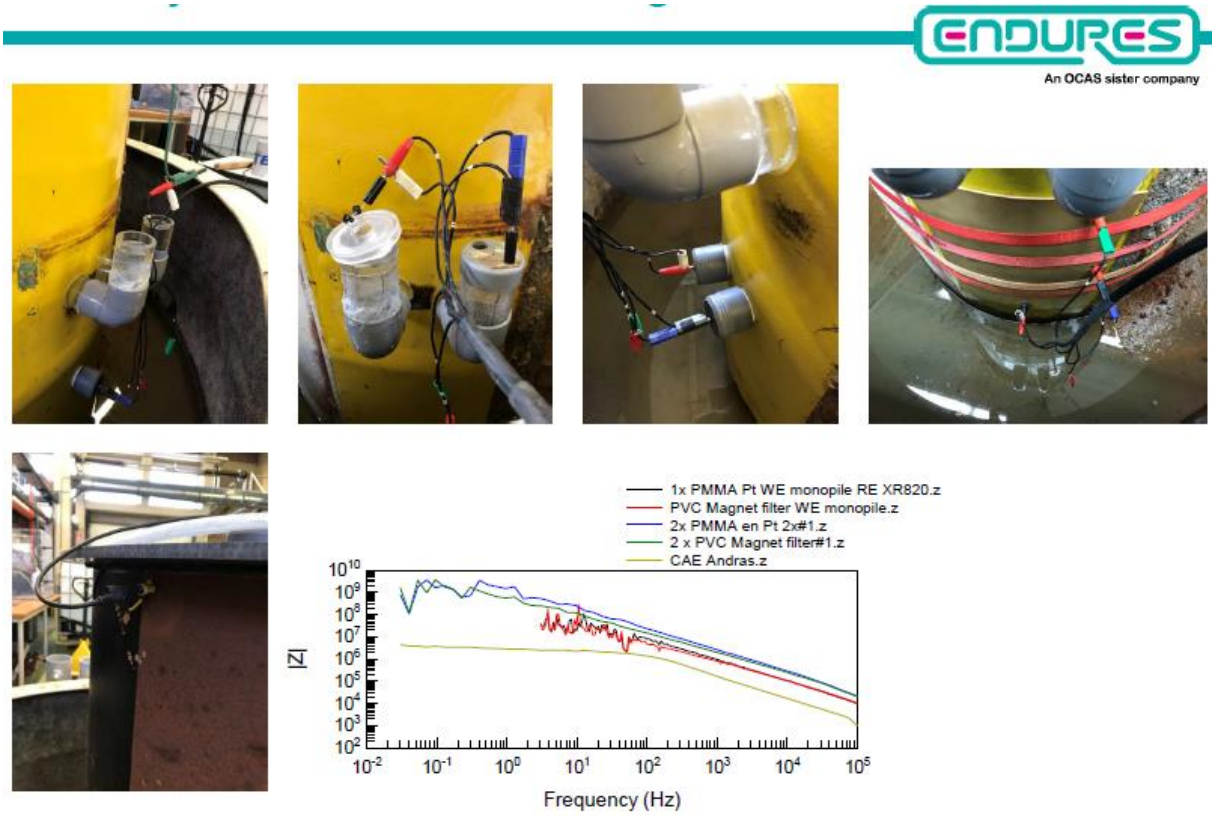

Figure 35. The long-term filtered sea water exposed coating (on the model offshore pylon) was tested with a set of traditional wet cells-electrodes configurations (top-left) and the concentric array sensor (top-right). Results: amplitude parts of measured impedance spectra (middle in bottom), data without any correction and derivation (source: Endures BV).

Various forms of the wet phase cell installation setups (upper 3 from left) were applied along with the single installation configuration of the CA (upper right) as in seen in Figure 35. As obvious benefits of the latter configuration compared to traditional electrochemical method, measured impedance spectra were almost completely free of noise in the medium and LF range. Besides this fact, practical advantage of the CA sensor is the immediate applicability of the prototype sensor on all sorts of coatings in comparison with the wet phase test mode which usually requires days of hydration, conditioning (highly

impractical with naval vessels) before characterisation while still not compete-able with the CA sensor. The smooth spectra of the CA sensor are related to macroscopic gap-free electrical contact on the coating surface, the absence of higher order harmonics in and so distortion of the spectra. This clearly was not the case with the wet phase test methods, showing lots of noise in the medium and LF ranges. This noise stems from ineffective penetration of the LF electric field in coating cross-section and electrification of the test coating area. This not only makes the fitting estimation questionable but even validity of the LF spectrum can be questionable to use for representative characterisation. Location of the modulus spectrum in the lower magnitude range is directly connected to the superposition effect of the cell constant and the redundant large surface (mainly 2D conduction path between the electrodes) of the CA sensor. The latter is one of the main factors for the robust sensing. Thus, high quality sensing performance of the CA prototype combined with the rapid installation and high-throughput test-ability in practicality means superior value in characterisation of coatings compared to all wet phase test setups.

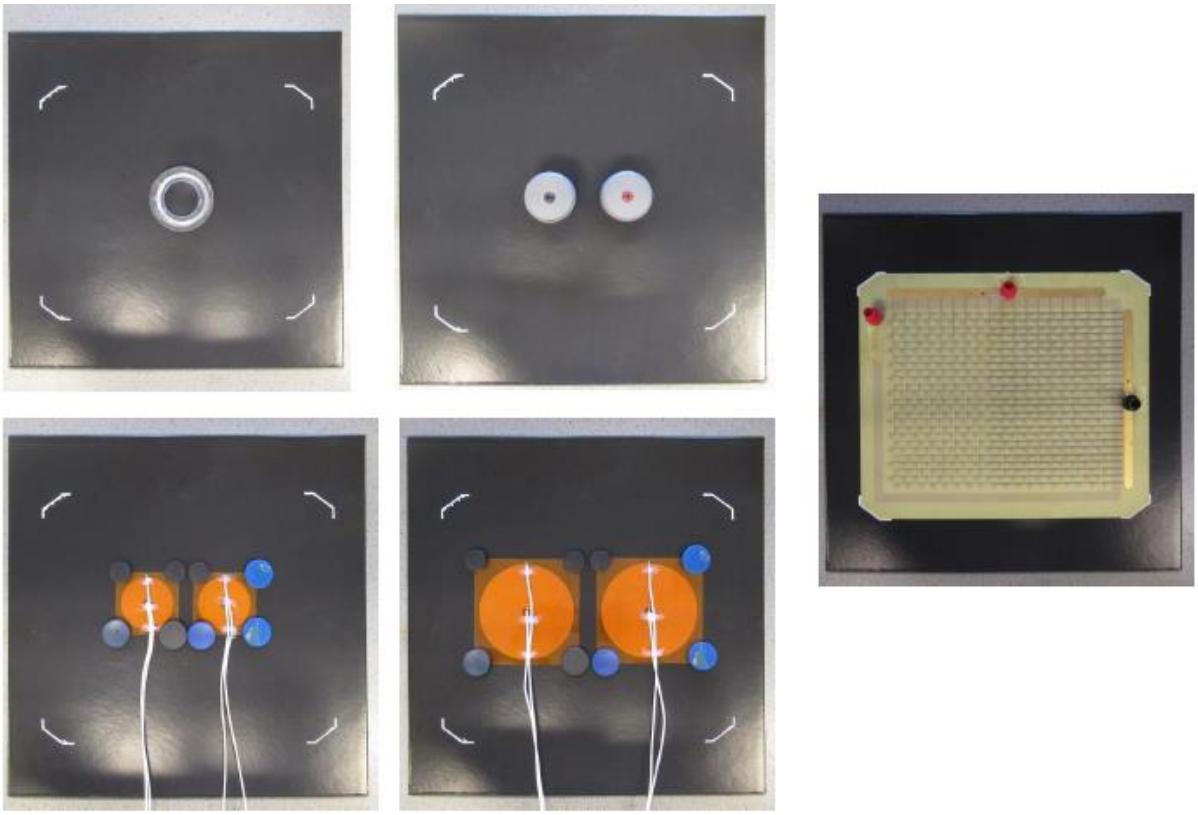

Figure 36. Newly applied, pristine real maritime modelling coating fitted with small planar electrodes (upper left), smaller and larger coils (bottom left) and the concentric array sensor (right) over area of the same centre location (source: Endures BV).

Direct comparison of the various types of sensors developed in the DTP project is important for the main stakeholder (MoD). All of the sensors were tested over the same area of pristine type coatings. From these tests, one example is presented in Figure 36. Difference in size of the planar electrodes, coils coils (developed in the DTP project for Eddy Current testing) and the prototype CA sensor are clearly noticed on these front-side views. The test results are summarised in Figure 37. At first sight, the major

difference is clearly found in shifted impedance modulus and phase of the impedance spectra of the CA sensor. The somewhat more than three orders of magnitude lower resistance of the CA is by the cell constant (15.5) and the overall large coating surface (141.4 cm^2) directly tested within gaps of ring-disk electrodes of the CA sensor. The HF shift of the inflection point in the phase spectra is explained physically by the several orders of magnitude lower, only the coating capacitive character sensed by the CA in comparisons with the wet phase setups sensing always the interface effect by the double layer capacitance which is orders of magnitude higher than that can be measured to low voltage perturbed dielectrics (coatings).

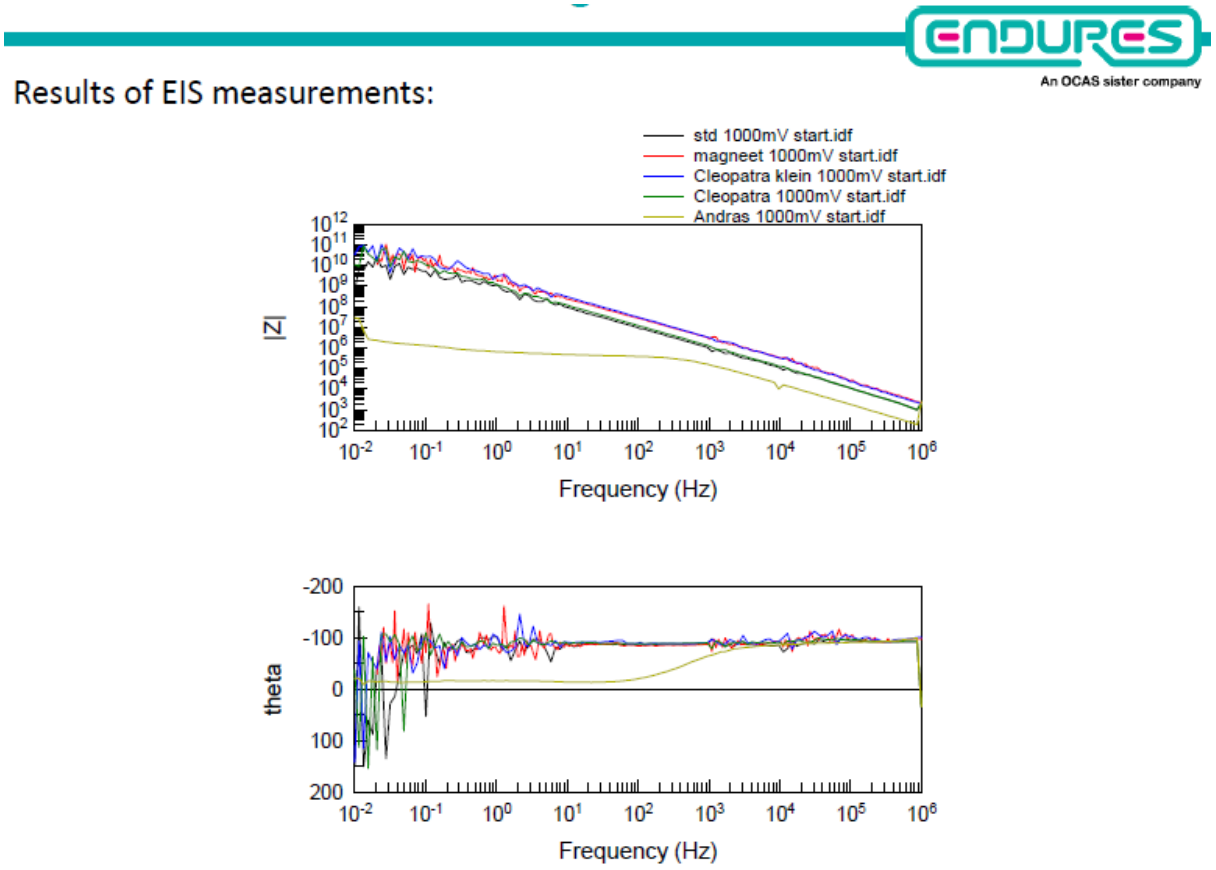

Figure 37. Impedance test results obtained on the newly applied, pristine real maritime modelling coating fitted with variety of electrodes (given in Figure 36) presented in Bode plots (source: Endures BV).

Lower capacitance in electrical circuits always causes a decreasing time constant which in turn leads to HF shift of the inflection point in the detected impedance spectra. So, the measured outcome is in perfect agreement with the theoretical expectation.

8.2. Generation II Type Concentric Array Sensor

After testing and analysing performance of the concentric array sensor, further development of the generation I type prototype was requested. Revision of the sensor in an additional design cycle resulted in the generation II type concentric array sensor hardware which featured multiple modifications as

proposed in 6.3.4. Validation of the hardware was carried out via both laboratory and real-life modelling samples by Endures B.V. between summer and late autumn 2021. Application of the traditional wet phase test setup for characterization of a model maritime coating applied on a model offshore pylon above and below the water line is shown in Figure 38. Derived data by the wet phase test setup served as a comparison with the sensor readings obtained with the generation II type concentric array hardware applied above and below water line as shown in Figure 39.

Figure 38. Application of traditional wet phase test setup for characterization of coating applied on model offshore pylon above and below water line. The one cell setup with direct wire connection to the substrate (left) and the two cells setup without direct wire connection to substrate (middle) located on coating surface below water line, one cell setup with direct wire connection to substrate above water line (right).

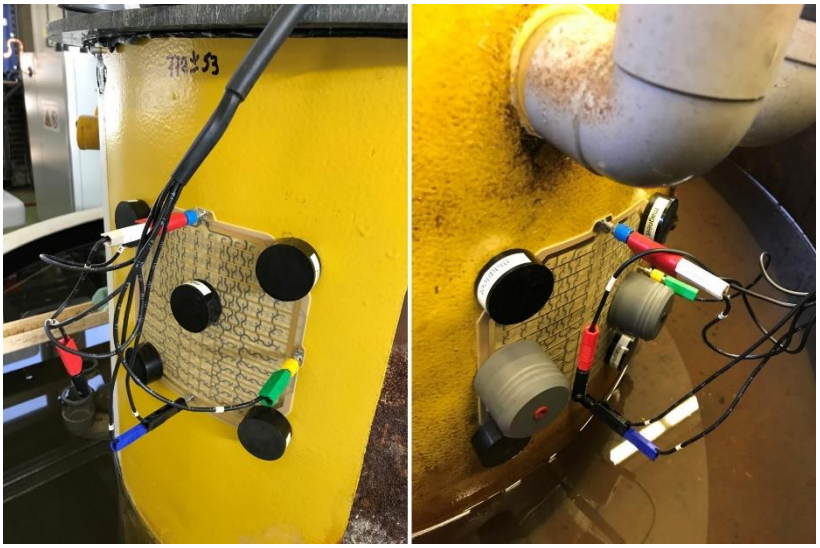

Figure 39. Application of generation II type concentric array sensor for characterization of coating applied on model offshore pylon above (left) and below water line (right). The sensor

was tightly fitted with magnets rather than stripes as was done with the generation I type concentric array prototype.

Coating resistance derived from impedance data are presented in Figure 40. By the traditional wet phase setup, coating resistance was estimated as changing at few times of 10^9 ohm cm^2 and remain well below 10^{12} ohm cm^2 to the immersion and air exposed regions, respectively. The variation of data derived from impedance results obtained with the two different wet phase cell setups may not seem first as high by reminding few times of data variations often experienced with EC techniques to corrosion affected processes. Nevertheless, this variation seems markedly excessive when compared to results obtained with the gen. II CA sensor which returned almost the same results twice in a measure series. There was an order of magnitude of difference in absolute range of the data obtained by the two test methods in both states of the coating. The gen. II CA returned more than three orders of magnitude difference in resistance of the coating areas exposed to air and sea water. This translated into around 6 times of difference in immersion and air exposed state of the coating, compared to the scale of wet phase setup derived data. If a possible straight rectification of the CA derived data would be considered to achieve by revision of the normalisation factor, e.g., eight, then single state of the coating, i.e., intact pristine or immersion aged state could only be selectively matched but both at the same time. This impression can only be confirmed by the outcome of estimation of the coating capacitive character.

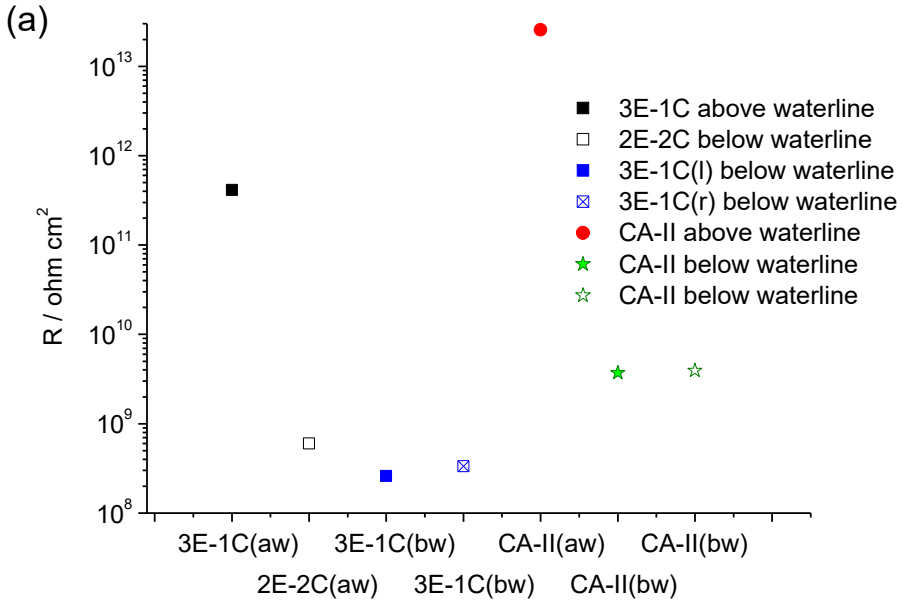

Figure 40. Resistance of coating applied on model offshore pylon and immersion tested for 11 years at Endures BV. Measurements performed via both wet type electrochemical (EC) and solid setups. The EC setup was carried out in two distinct cell configurations with three electrodes in one cell and with two electrodes in two cells, while generation II type concentric array (CA) or prototype II used for the solid setup without any additional electrode.

Estimation of the coating capacitive character by the sensors are summarised via normalised constant phase element data in Figure 41. In this assessment, CPE character of the immersed coating tested with the wet phase setup indicted 10 times difference by the one and two cells' setups. In addition, air exposed state of the coating was assessed with similar an order of magnitude difference compared to the sea water immersed region. Credibility of sensor readings becomes questionable when estimated state of the materials varies at a scale directly comparable with material properties.

In comparison, the gen II CA sensor assessed an order of magnitude lower capacitive character of the coating in air exposed state. This shifted more than two orders of magnitude with the sea water immersed part of coating assessed in markedly increased capacitive nature, infiltrated state, which lied in between the wet phase test results data. In absolute range of derived data, sea water exposed coating assessed with the two cells wet phase setup and the CA sensor is close to theoretical expectations but validity of rest of data is rather questionable. In case of the CA sensor provided 100 times increase of CPE coating character between air and sea water exposed state. This seems to be excessive by around 5 times based on expected relative permittivity changes of the coating between air and sea water exposed condition.

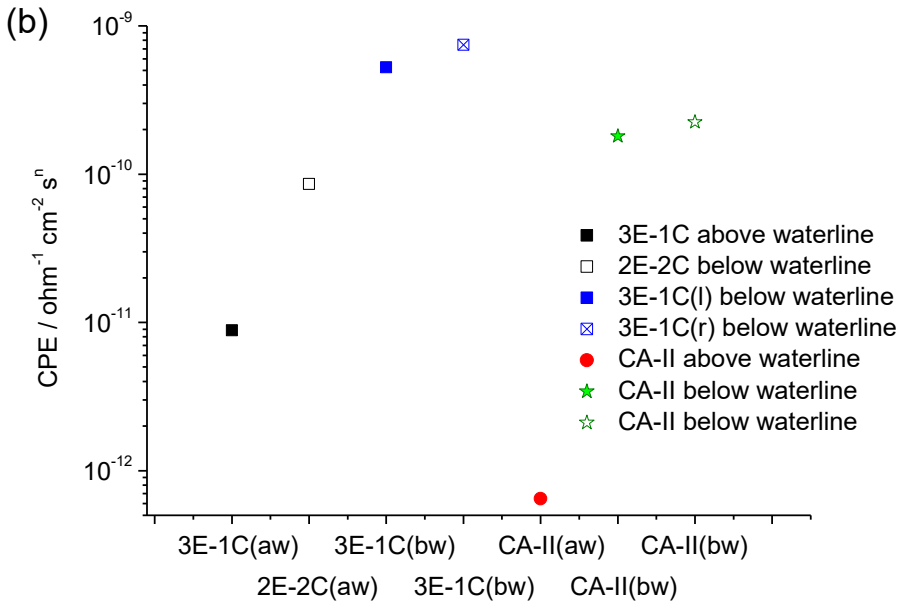

Figure 41. Constant phase element of coating applied on model offshore pylon and immersion tested for 11 years at Endures BV. Measurements performed via both wet type electrochemical (EC) and solid setups. The EC setup was carried out in two distinct cell configurations with three electrodes in one cell and with two electrodes in two cells, while generation II type concentric array (CA) or prototype II used for the solid setup without any additional electrode.

In a physical sense, no CPE normalisation to pure capacitive character, neither accounting detection of corrosion products would justify such a range of difference. Therefore, derivation of large resistance along with very low capacitive character of the coating in air exposed state is related to experimental

artefact, although most of the material properties are in line with the ones referenced in the literature. This artefact probably stems from lower effective electrode surface area of the sensor due to physically unattached part of the electrodes and the low transmission, electrification yield of the high resistance coating in the presence of air gap between the sensor electrodes and coating surface especially in dry state (restrained susceptibility to pick up excitation).

9. DISCUSSION of FINAL RESULTS

9.1. Performance of Generation I & II type Sensors

As it was delineated in the previous chapter, interdigitated electrode-based sensors working in non-contact mode are not recommended to characterise high resistance coatings in real-life use cases despite the fact these can be appropriate in some cases to asses permittivity of coatings with good sensitivity. This advice is closely related to the fact, coating resistance is always more sensitive material property for condition assessment than permittivity based capacitive characteristics probed even with fringing fields. Furthermore, not recommending IDE type sensors for maritime applications relates to the high sensitivity to absence of electrical shielding and grounding of coating substrates, so as to disturbance by capacitive electrical noises. Useful signals are often too low in intensity which can be entirely disrupted by superposition of EMI noise and strain currents. Thus, although the concept for such a sensing mode might be justified, the real value and feasibility of this technical approach seems to be more than vague.

In exchange, the concentric array prototypes are well applicable to test high resistive paint coatings featuring different dry film thicknesses and condition related specific resistance. In addition, while these are insensitive to electrical noises stemming from the environment and working robustly during sensing, this sensor type offers versatile work function for material testing by both AC and DC modes. None of these advantages are featured by IDE sensors. The option to explore CUI is clearly a general industrial interest and so increases the value of the hardware. This picture is completed with a further possible feature of approximation of permittivity of probed materials. In the viewpoint of applicability, sensing performance and reliability of sensing, the concentric array sensor outperforms traditional type wet phase setups in all aspects, whilst it stays compliant with international standards and recommendations [308]. Therefore, the concentric array is generally recommended for laboratory and field applications regardless of types of real-life situations.

9.2. Design Requirements Met

Most of the technical requirements of design objectives (Chapter 3) were straight and some proven to meet. Although some of the requirements such as the rate of detection or sensor availability and reliability of sensor data (mentioned in points 12^{th} and 13^{th}) are difficult to prove at this stage, the concentric array sensor is considered to meet the majority of the project delineated requirements. Programmatic or implementation related design requirements are believed to be addressed by the prototypes. Nevertheless, technical requirements are always in priority for the selection of condition monitoring sensors. Hence, only the concentric array prototype was accepted as feasible hardware solution.

9.3. Design Requirements Unmet

The only requirement that was truly not met, is the development of a genuine inspection device rather than the expected monitoring equipment. The inability to obtain such a device reverts to many aspects. To remind about the chapter on careful design considerations, this shortfall may not be solved by any conventional means. Bearing in mind, there are many aspects and few contradictory requirements on testing low permittivity thin-layer materials in the presence of high relative humidity and high permittivity fluid or moisture, as well as metallic conductor substrates acting as strongly inductors in response and very good absorbers to high frequency electrical field radiations. To segregate electrical and inductive parts in the sensor data stemming from corrosion effected substrate and inhomogeneously deteriorating coating may depart far from the role of maintenance technicians and experts at the field, working on rapid condition assessment. Special customisation of electrode geometries and electrical test parameters may be addressed in part of the shortage, but maritime application certainly presents more difficulties for a real value-based sensor implementation, complicating much more the overall situation.

9.4. Critical Assessment of Project and Thesis Work

My contribution to the DTP was severely limited by many factors. Commence of the project work was delayed with around two and half months without completion of academic terms at the UT due to unfavourable timing. In addition, overall pace of the project was slow and not governed into a clear and right foreseen direction from the concept to detailed design until three quarter of time of the DTP progressed after my involvement. There were not too many good experiences earned at the UT either in an attempt to comply with academic requirements and specially to facilitate progress of the project work. In addition, fundamental project goals were not officially and effectively assisted by modelling and simulation, although this approach could have been arguably the most beneficial part leading to a firm DTP outcome. Furthermore, the strong Covid-19 related restrictions all through the 2020 calendar year restrained the pace of progress and achievements.

10. APPLICATION of the SENSORS in PRACTICE

The concentric array prototype designed in this PDEng program is, and well feasible, for inspection, owing to its direct contact mode sensing, and material characterisation. Although IDE prototypes work for sensing in non-contact mode, due to the short distance sensing range of fringing fields, the large lateral size and hardly well controllable small clearance between sensor laminates and tested surfaces, these sensors are also regarded as inspection devices rather than for continuous monitoring, despite strong expectation of the stakeholders at the beginning of the project. Nevertheless, this does not mean the herewith presented sensors cannot be used in continuous monitoring mode, rather not recommended to apply in this mode to avoid blocking effect of the sensors against mass transport of the environmental species and so to preclude invalid to condition assessment over certain locations. Note that, the

mechanism changing effect by continuous installation of the sensors can have both decreasing and increasing impact of the environment via additional barrier function and deposition-based activation. In another aspect, intelligent industrial automated solutions are available for numerous mounting options (outside of the current design space) which can certainly lead to monitoring equipment applicable over critical areas. To enable work of the ship crew, maintenance experts end users with extended capabilities for condition assessment, proper hardware/software solutions can be readily integrated with the proposed hardware prototypes. In the following subsections, electrical parameters for material characterisation and the critical asset areas for regular inspection are discussed.

10.1. Electrical Testing Parameters for Condition Assessment of Coatings

Coating assessment with IDE sensors require and allow exclusively impedance testing, due to effective AC coupling between sensor probes and coatings. Although solder mask based electrical insulation of the large conductor tracks is solved in regard with the active sensing area (bottom surface), no warranty can ever be obtained on credible (reliable) use of such sensors because of the low probability of perfect fitting to the often-uneven surfaces (investigated samples) with the long and thin electrode arrays. What is more, electrical shunting of closely located driver and sensing electrode pars or strong signal by the moderately humid, sea water on the coating surface in sensitive part of the fringing field can be real source of measure artefact at field application, while implementation of grounded guard electrode between sensor electrode pairs at low feature size like 0.55 mm of the IDE 4 can be difficult to overcome technologically. Accommodating a shield electrode at width size of 0.15 mm while keeping 0.2 mm distance from driver and sensing electrodes could have been a solution, but so prototypes would have been more complicated to manufacture (one additional layer). When electrical testing of coatings performed with IDE prototypes, parameters involve minimum (and for the equipment maximum too) excitation voltage of 1 V (in rms) between the frequency range of 40 kHz and 0.1 Hz. The investigated coating surface must be clean, free of contamination which could provide contribution to the detected capacitive coupling signal based on permittivity of substances. Clearance between the IDE sensor boards and substrates must be constant, kept with insulating spacers at a distance of no more than 0.1 mm. If detected current signal is weak (no valuable response spectra obtained) or coatings feature high resistance (out of detection range from half of the semicircle) then measurement can be repeated at higher perturbation voltage (up to 10 V) to gain sufficient current signal intensity and decrease clearance to at least half a distance from 0.05 down to 0.025 mm. The latter may not be recommended due to difficult controllability of clearance at field application, or combination of both may offer full remedy to increase detection sensitivity but increasing test voltage to 10 and 100 V can get out of range, obvious limitation by the test equipment and damage the coating.

In comparison with capacitive imaging, electrical testing modes and parameters by using the concentric array prototype represents universality in practice. Coating characterisation can be carried out by both AC and DC modes which offer numerous advantages. Thus, DC test mode is part of standard

compliant reference technique, originally used for resistance assessment, but it may be sensitive for electrochemical deposition of chemical substances during field use. On the other hand, AC technique is mainly used to define breakdown strength of dielectric materials [318,319]. Many equipment does not offer the required large amplitude voltages in AC mode, but this technique is less sensitive for electrochemical deposition of chemical species. To the latter, the same settings were applied for impedance testing of coating samples as utilised for the IDE prototypes, but in this case contact mode sensing, whereas to the former on testing parameters and procedure are delineated as follows. Standard procedure recommends an equipment capable of impressing 500 V in DC mode to materials with resistivity of 10^{11}–10^{15} ohm [284]. Testing voltage can be lowered by reference to 100 V when resistivity of materials falls between 10^{10} and 10^{7} ohm. These thresholds are required to use to remain in the reliably detectable current range (0.1 nA) by moderate size concentric probes without array pattern-based extension to sensing current enhancement. Therefore, the concentric array prototypes are designed to measure sufficient response current (at least 0.1 nA) with a testing voltage of around 1 V. This is pivotal to avoid deposition of chemical species at the field at the gold finished surface of the electrodes deactivating, decreasing catalytic activity of electrodes for charge-transfer and so blocking Faradaic reactions and deposition of elements like hydrogen, etc. The sensor must be mounted on physically and chemically clean surface and under low humidity. Sufficient force (~20 N) must be applied at back-panel of the sensor via moderate thick elastic laminates, to stick the sensor tightly to coating surface (after removal depositions). Electrification of the dielectric materials, coatings must be attained by potentiostatic measurement for at least one or two minutes to avoid capacitive estimation errors (underestimation of resistance and over of capacitive character), until current response becomes stable over time. Then, the voltage and current ratio multiplied by the unique cell constant (design parameter I) and surface by the number of array segments must provide accurate estimation of coating resistivity. The first factor is known as input parameter, the second measured and rest two design parameters are also known. Derivation of the actual coating resistance and so barrier protection character must be easily defined by the crew members and maintenance experts (satisfied technical and programmatic terms).

10.2. Corrosion Affected Areas for Monitoring and Inspection

In general sense, the recent trend [320] of substandard manufacturing and low-quality construction work [321] would certainly justify utilisation of corrosion sensors for monitoring and/or frequent inspection of critical areas such as stress concentration zones [322] around notches, weld butts and toes along heat affected zones, biaxial type high dimensional joint sections. Nevertheless, these types of areas are so abundant at a moderate ship size, that it would not be effective to monitor by large number of sensors. Instead, only the most critical locations must be targeted. Based on the literature and in-house expert advice by Endure BV, the worst affected and high-risk locations were selected as sea, fresh and sewage

water tanks bordered with double-shell hulls and biaxial joint segments of girders and stiffener web systems which are susceptible for rapid integrity loss of coatings and subsequently steel structures [15].

High performance and reliable protection can be afforded by good condition of the paint coatings, based on a firm barrier function to separate corrosive environment from the ship steel structures by blocking mass transport of components through coatings [16]. In some cases, deterioration may develop without coating breakdown as uniform and/or local corrosion of substrates [17]. Locations with tags and fasteners with crevices, welded areas and pin holes are hot-spots for initiation of corrosion and rapid spread to other structural elements [323−326]. Mechanical damage of coatings often leads to fast localized integrity loss in steel plates in short term and deposition of muds, slurry and sea crustaceans on coatings long-term. Coating failure may occur via delamination and buckle at a macro-scale (≥7.5 mm) [327]. In regard with fatigue, not only steel structures are affected over service life [328−330], but brittle fracture, rupture and increasing opening of disintegrated coating areas are also main areas for sea water to access steel plates. This process is inevitable over the long-term due to shrinkage, decreasing ductility, increasing brittleness and fatigue cracking of coatings [331,332]. In this respect, the largest strain impacted locations pose the highest integrity risk and so primarily subjected to sensor application. Besides aging related loss of physical protection, low-quality maintenance would indirectly increase severity of environment induced issues by allowing progress of bio-fouling. The latter enables formation of differential aeration galvanic cells (driven by concentration gradient of depolarisator species) then activation of surface processes by corrosive species like chlorides and sulphides. This makes the situation more difficult even on short term. Top of all, environmental condition of the coatings is not uniform over entire surface, which leads to differentiation of states of the same coating. In later phase of the processes, localised events like pitting and crevice corrosion extends further into micro- and macro-cracking from the surface region into bulk phase of the steel plates [333]. Therefore, all these factors must be carefully considered when target locations and critical areas are selected for sensor application regardless of type of the operation mode, i.e., continuous monitoring or inspection.

10.3. Guideline to Use the Prototype Sensor

On time application of the sensor for coating inspection, the concentric array is advised to use over coating surface areas on critical locations subjected to frequent small amplitude oscillatory and large one directional magnitude straining. Further hot-spot locations for coating testing are inner and outer range of stagnant and low-stream rate areas with abiogenic and biogenic depositions. After deterioration of the coating and short induction time, these areas become primary targets of accelerated uniform, activated crevice and pitting corrosion. In case of proper maintenance, these depositions are removed regularly and so no activation and acceleration may take place, only initial stage of differentiation in the coating state. Depending on local temperature experienced by structures during service below and above 10°C, occurrence for inspection is recommended to occur at every and half a year of service life, respectively. Thermal and chemical effects are worsened by mechanical effects on integrity of coatings.

In this respect, vessels and locations primarily subjected to frequent and large extent of straining must be inspected over every half a year or even more frequently depending on the number of extreme environmental events experienced by vessels during service.

In inspection mode, a single concentric array sensor allows to perform more than fifty measurements over eight hours in DC mode and at least eight tests in AC mode per day when handled by experienced crew personnel and maintenance expert. When two additional parallel measurements are required to ensure reliability and credibility of results, then these numbers translate to a minimum of seventeen and three separate hot-spot locations with DC and AC test modes. Thus, for a frigate twenty separate locations to investigate with the sensor can probably be enough in bottom and up parts of the aft, mid and aft sections on both ship sides. For a large and complex supply ship, this number can increase to doubled and tripled to allow assessment of the largely different locations and effects of the local environments. As for confined areas, ballast tanks are strongly advised to inspect vertically at least three different locations such as bottom, frequent summer, seawater level (most critical section) and the mainly non-immersed section. The former two are generally more affected than the last. Therefore, quality assessment at those two locations can be utmost informative on general condition of asset state and maintenance need. Although the most accurate condition assessment can only be attained by comparison of states characterised at initial and certain stages of lifetime, maintenance experts are always entitled to follow the easier and a universally more applicable way such as to perform instantaneous condition assessment of coatings at any locations. Then, as a next step of evaluation, derived data must be rated in accordance with general engineering recommendations on maritime and heavy-duty coatings. This scale includes four quality classes with certain specific resistance ranges as summarised in Table 20.

Table 20. Absolute scale of quality rating of maritime and heavy-duty coatings based on specific resistance (ohm cm^2)

Coating specific resistance (ohm cm^2)	Quality level	Recommendation
10^{10}–10^{13}	Excellent	No action required
10^{8}–10^{10}	Good	Inspection once a year
10^{6}–10^{8}	Moderate	More than twice a year (PM)
$<10^{6}$	Poor	CoM

To make a comparison with the data listed in Table 20 and to conclude on the condition of asset locations offers a straight and rapid evaluation for effective maintenance service.

As for applicability of the prototypes in real-life situations, the concentric array sensor in its present form as a first stage prototype is readily applicable for condition assessment of maritime coatings. Nevertheless, there are many ways to improve this preliminary prototype design, which is discussed in previous section of the thesis.

11. SUMMARY, CONCLUSIONS and RECOMMENDATIONS

- Three major design cycles were performed in a sequential manner and an additional one was devoted to a comprehensive revision of one selected generation I prototype.
    - In the three sequential design cycles, various types of wire-based and interdigitated electrodes were tested for coating assessment. Only a few of the wire-based electrodes provided acceptable sensor readings and featured the possibility to work in a monitoring use case, hence another hardware solution was sought.
    - Non-contact mode sensing with interdigitated electrodes applied to characterise high resistance coatings proved to be inadequate for many reasons. Nonetheless, concentric array type sensors proved to be well performing and robust even in field modelling environment.
    - Revision of the concentric array sensor in a subsequent design cycle yielded lots of improvements to the 1st generation sensor, becoming more reliable for coating testing and easier applicable on coatings with typical geometries and surface morphologies.
    - Traditional wet phase setups implemented with 1 and 2 cells configurations provided a standard for evaluation of all developed sensors.
    - The overall performance advantage and reliability of test results obtained with the concentric array sensors is superior to the traditional type wet phase setup.
    - The generation II type concentric array sensor sufficiently addresses all major requirements: Corrosion affected ship structures, critical areas affected by local environment, application of the sensors along with evaluation of sensor readings, and the importance of regular high-quality maintenance were delineated in subsequent sections.
- As a conclusion, concentric array type sensors represent a mature design, and are strongly recommended for condition assessment of coatings on maritime structures while used in inspection mode. The variety of electrical test modes, sensing performance, accuracy and robust nature against capacitive transient noises and nearby radiations speak for themselves, and so it may not be improved far by any other electrode alignment and probe configuration.
- Recommendations are mainly related to the need for improvement of mechanical flexibility of the sensor laminate. Inclusion of fitting areas by certain types of fixation means on coating surfaces are also advisable in the sensor laminate to make the hardware more easily applicable.

REFERENCES

[1] Y. Sumi, Structural safety of ships developed by lessons learned from the 100-year history of break-in-two accidents. Mar Struct 64 (2019) 481–491. https://doi.org/10.1016/j.marstruc.2018.12.003

[2] G.H. Hoffmann, Analysis of Sir John Biles's experiments on H.M.S. Wolf, in the light of Pietzker's theory. Trans Royal Inst Nav Archit A: Int J Mar Eng 67 (1925) 41–65.

[3] C. Kell, Investigation of structural characteristics of destroyers 'Preston' and "Bruce" Part 2 - analysis of data and results. Trans - Soc Nav Archit Mar Eng 48 (1940) 125–172.

[4] E. DeCola, A review of double hull tanker oil spill prevention considerations. Report to Prince William Sound RCAC, December 2009.

[5] J. Kozak, Z. Górski, Fatigue strength determination of ship structural joints. Polish Marit Res 18 2(69) (2011) 28-36. doi: 10.2478/v10012-011-0009-8

[6] Corrosion of metals and alloys - Corrosivity of atmospheres - Classification, determination and estimation. Standard EVS-EN ISO 9223:2012. https://www.evs.ee/products/evs-en-iso-9223-2012

[7] EN ISO 12944-2: 2017, Paints and varnishes – Corrosion protection of steel structures by protective paint systems – Part 2: Classification of environments.

[8] Corrosion protection of ships a recommended practice by the Det Norske Veritas, Veritasveien 1, N-1322 Hovik, Norway, 2000.

[9] M. Natesan, S. Selvaraj, T. Manickam, G. Venkatachari, Corrosion behavior of metals and alloys in marine-industrial environment. Sci. Technol. Adv. Mater. 9 (2008) 045002.

[10] B. Chico, D. de la Fuente, I. Díaz, J. Simancas, M. Morcillo, Annual atmospheric corrosion of carbon steel worldwide. An Integration of ISOCORRAG, ICP/UNECE and MICAT Databases. Materials 10 (2017) 601 (1-26). doi:10.3390/ma10060601

[11] Y.M. Panchenko, A.I. Marshakov, L.A. Nikolaeva, V.V. Kovtanyuk, Prediction of first-year corrosion losses of copper and aluminum in continental regions. AIMS Mater Sci 5(4) (2018) 624–649.

[12] EN ISO 12944-5: 2018, Paints and varnishes, Corrosion protection of steel structures by protective paint systems, Protective paint systems.

[13] EN ISO 8501-1: 2007, Preparation of steel substrates before application of paints and related products. Visual assessment of surface cleanliness. Rust grades and preparation grades of uncoated steel substrates and of substrates after overall removal of previous coatings.

[14] H.-Q. Yang, Q. Zhang, S.-S. Tu, Y. Wang, Y.-M. Li, Y. Huang, A study on time-variant corrosion model for immersed steel plate elements considering the effect of mechanical stress. Ocean Eng 125 (2016) 134–146.

[15] M.T. Gudze, R.E. Melchers, Operational based corrosion analysis in naval ships. Corros Sci 50 (2008) 3296–3307. doi: 10.1016/j.corsci.2008.08.048

[16] R.E. Melchers, Mathematical modelling of the diffusion-controlled phase in marine immersion corrosion of mild steel. Corros Sci 45 (2003) 923–940. doi: 10.1016/S0010-938X(02)00208-1

[17] J.K. Paik, A.K. Thayamballi, Ultimate strength of ageing ships. Proc Instn Mech Engrs 216 Part M: J Eng Marit Envir 216 (2002) 57–77. doi: 10.1243/147509002320382149

[18] S. Qin, W. Cui, Effect of corrosion models on the time-dependent reliability of steel plated elements. Mar Struct 16 (2003) 15–34. doi: 10.1016/S0951-8339(02)00028-X

[19] J.K. Paik, A.K. Thayamballi, Y.I. Park, J.S. Hwang, A time-dependent corrosion wastage model for seawater ballast tank structures of ships. Corros Sci 46 (2004) 471–486.

[20] R.E. Melchers, Modeling of marine immersion corrosion for mild and low-alloy steels—Part 1: phenomenological model. Corros 59(4) (2003) 319–334.

[21] S. Ivosevic, R. Mestrovic, N. Kova, Probabilistic estimates of corrosion rate of fuel tank structures of aging bulk carriers. International Journal of Naval Architecture and Ocean Eng 11 (2019) 165–177.

[22] U.O. Akpana, T.S. Kokoa, B. Ayyubb, T.E. Dunbar, Risk assessment of aging ship hull structures in the presence of corrosion and fatigue. Mar Struct 15 (2002) 211–231.

[23] K. de Baere, H. Verstraelen, L. Lemmens, S. Lenaerts, R. Dewil, Y. van Ingelgem, G. Potters, A field study of the effectiveness of sacrificial anodes in ballast tanks of merchant ships. J Mar Sci Technol 2013, doi: 10.1007/s00773-013-0232-3
[24] K. de Baere, Corrosion in ballast tanks on board of merchant vessels, In situ study of the significant parameters. Associatiefaculteit Nautische Wetenschappen, Faculteit Wetenschappen, Departement Bio-ingenieurswetenschappen at the Univerity of Antwerpen, Antwerpen, 2011.
[25] Structural design. NORSOK N-001, Oslo: Norwegian Technology Standards, 2012.
[26] G.L. Cooper, Sensing probes and instruments for electrochemical and electrical resistance corrosion monitoring. ASTM Special Technical Publication 908 (1986) 237-250.
[27] D. Gilboe, Direct resistance measurement corrosion probe. Patent No.: US 7,034,553 B2, 2006.
[28] Y. Tan, Experimental methods designed for measuring corrosion in highly resistive and inhomogeneous media. Corros Sci 53 (2011) 1145–1155. doi: 10.1016/j.corsci.2011.01.018
[29] K. Wold, G. Sirnes, FSM Technology - 16 Years of field history-experience, status and further developments. NACE International, Corrosion 2007, 11-15 March, Nashville, Tennessee, 2007, 1-17.
[30] R.D. Strommen, H. Horn, K.R. Wold, New technique monitors pipeline corrosion, cracking. United States: N. p., 1993. Web.
[31] F. Varela, M.Y. Tan, M. Forsyth, An overview of major methods for inspecting and monitoring external corrosion of on-shore transportation pipelines. Corros Eng Sci Technol Intern J Corros Proc Corros Control 50(3) (2015) 226-235. https://doi.org/10.1179/1743278215Y.0000000013
[32] R.F. Wright, P. Lu, J. Devkota, F. Lu, M. Ziomek-Moroz, P.R. Ohodnicki, Corrosion sensors for structural health monitoring of oil and natural gas infrastructure: a review. Sensors 19 (2019) 3964. doi:10.3390/s19183964
[33] T.L. Skovhus, R.B. Eckert, E. Rodrigues, Management and control of microbiologically influenced corrosion (MIC) in the oil and gas industry—Overview and a North Sea case study. J Biotechnol 256 (2017) 31-45. http://dx.doi.org/10.1016/j.jbiotec.2017.07.003
[34] R.F. Wright, P. Lu, J. Devkota, F. Lu, M. Ziomek-Moroz, P.R. Ohodnicki, Review on corrosion sensors for structural health monitoring of oil and natural gas infrastructure. Proc. SPIE 10973, Smart Struct NDE Energy Sys Ind 4.0, 109730N. https://doi.org/10.1117/12.2514398
[35] C. Andrade, W. Baptista, N. Domingues, L.A. Correa, Corrosion monitoring and control of seawater injection systems using an expert system approach. NACE Internaional, Corrosion (2001) 11-16.
[36] T. Kosec, V. Kuhar, A. Kranjc, V. Malnarič, B. Belingar, A. Legat, Development of an electrical resistance sensor from high strength steel for automotive applications. Sensors 19 (2019) 1956. doi:10.3390/s19081956
[37] R.B. Figueira, Electrochemical sensors for monitoring the corrosion conditions of reinforced concrete structures: a review. Appl Sci 7 (2017) 1157. doi:10.3390/app7111157
[38] B. Carkhuff, R. Cain, Corrosion sensors for concrete bridges. IEEE Xplore, IEEE Instrum Meas Mag 6(2) (2003) 19-24. doi: 10.1109/MIM.2003.1200279
[39] D. Su, Y. Xia, R. Yuan, Self-powered wireless sensor network for automated corrosion prediction of steel reinforcement. Hindawi J Sensors 2018, Article ID 4125752, 10 pages. https://doi.org/10.1155/2018/4125752
[40] J. Peng, Corrosion detection of reinforcement of building materials with piezoelectric sensors. J Chem Chem Engin 66(5-6):261-265. doi: 10.15255/KUI.2017.010
[41] K. Kumar, S. Muralidharan, T. Manjula, M.S. Karthikeyan, N. Palaniswamy, Sensor systems for corrosion monitoring in concrete structures. Sens Transducers 67(5) (2006) 553-560.
[42] B. Valdez, J. Ramirez, A. Eliezer, M. Schorr, R. Ramos, R. Salinas, Corrosion assessment of infrastructure assets in coastal seas. J Mar Eng Technol 15:3 (2016) 124-134. doi: 10.1080/20464177.2016.1247635
[43] F.W. Schremp, Corrosion prevention for offshore platforms. J Pet Technol 36(4) (1984). https://doi.org/10.2118/9986-PA
[44] High temperature on-line monitoring of water chemistry and corrosion control in water cooled power reactors. Report of a co-ordinated research project. IAEA-TECDOC-1303, 2002.

[45] G. Rinaldi, T. Huber, H. McIntosh, L. Lebrun, H. Ding, J. Weber, Corrosion sensor development for condition-based maintenance of aircraft. Int J Aerosp Eng 2012, Article ID 684024, 11 pages. doi:10.1155/2012/684024
[46] S. Benavides, Corrosion control in the aerospace industry. Aircr Eng Aerosp Technol 81(3) (2009). https://doi.org/10.1108/aeat.2009.12781cae.001
[47] S.J. Harris, M. Hebbron, M. Mishon, Corrosion sensors to reduce aircraft maintenance. In RTO-MPAVT-144 workshop on enhanced aircraft platform availability through advanced maintenance concepts and technologies. Vilnius, Lithuania, 2006.
[48] A.-D. Nguyen, V. Godinez, 7 - Integrated health and corrosion monitoring systems in the aerospace industry. Corrosion Control in the Aerospace Industry, Woodhead Publishing Series, Met Surf Eng (2009) 151-171. https://doi.org/10.1533/9781845695538.2.151
[49] A.S. Trivedi, S.S. Bhadauria, R.S. Sengar, Analytical study of influence of pH and weight loss on steel corrosion embedded in reinforced concrete: a review paper. Int J Adv Sci Technol 91 (2016) 59-70. http://dx.doi.org/10.14257/ijast.2016.91.06
[50] A.K. Hamzat, I.A. Adediran, L.M. Alhems, M. Riaz, Investigation of corrosion rate of mild steel in fruit juice environment using factorial experimental design. Hindawi Int J Corros 2020, Article ID 5060817, 10 pages https://doi.org/10.1155/2020/5060817
[51] G. Karthik, M. Sundaravadivelu, Studies on the inhibition of mild steel corrosion in hydrochloric acid solution by atenolol drug. Egypt J Pet 25(2) (2016) 183-191. https://doi.org/10.1016/j.ejpe.2015.04.003
[52] A.D. Usman, L.N. Okoro, A review: weight loss studies on the corrosion behavior of some metals in various media. Chem Sci Rev Lett 4(13) (2015) 17-24. Article CS18204512
[53] U.O. Akpan, T.S. Koko, B. Ayyub, T.E. Dunbar, Reliability assessment of corroding ship hull structure. Nav Eng J (Technical Paper) Fall (2003) 37–48.
[54] D.W. Temple, M.D. Collette, Minimizing lifetime structural costs: Optimizing for production and maintenance under service life uncertainty. Mar Struct 40 (2015) 60–72.
[55] J.K. Paik, A.K. Thayamballi, J.M. Lee, Y.I. Park, Time-dependent risk assessment of aging ships accounting for general/pit corrosion, fatigue cracking and local denting damage. For presentation at the 2003 SNAME Annual Meeting in San Francisco, ABS Technical Papers 2003, pp. 219–255.
[56] F. Guo-Qing, H. Bing-Nan, R. Hui-Long, Reliability of the ultimate strength of ship stiffened panel subjected to random corrosion degradation. China Ocean Eng 31(1) (2017) 11–18.
[57] A. Zayed, Y. Garbatov, C.G. Soares, Reliability of ship hulls subjected to corrosion and maintenance. Struct Saf 43 (2013) 1–11.
[58] Risk-based life cycle management of ship structures, SSC-416 Prediction of structural response in grounding application to structural design, Ship Structure Committee, 2000.
[59] N. Yamamoto, K. Ikegami, A study on the degradation of coating and corrosion of ship's hull based on the probabilistic approach. J Offshore Mech Arct Eng 120 (1998) 121–128.
[60] J. Lampe, R. Hamann, Probabilistic model for corrosion degradation of tanker and bulk carrier. Mar Struct 61 (2018) 309–325.
[61] Y. Garbatov, C.G. Soares, Structural maintenance planning based on historical data of corroded deck plates of tankers. Reliab Eng Syst Saf 94 (2009) 1806–1817.
[62] Y. Garbatov, C.G. Soares, G. Wang, Non-linear time dependent corrosion wastage of deck plates of ballast and cargo tanks of tankers. Abs technical papers 2005, Proceedings of OMAE05, 24th International Conference on Offshore Mechanics and Arctic Engineering. June 12-17, 2005, Halkidiki, Greece. pp. 67–75.
[63] Y. Garbatov, C.G. Soares, G. Wang, Nonlinear time dependent corrosion wastage of deck plates of ballast and cargo tanks of tankers. Transactions of the ASME 129 (2007) 48–55.
[64] A. Zayed, Y. Garbatov, C.G. Soares, Corrosion degradation of ship hull steel plates accounting for local environmental conditions. Ocean Eng 163 (2018) 299–306.
[65] Y. Garbatov, C.G. Soares, G. Wang, Nonlinear time-dependent corrosion wastage of deck plates of ballast and cargo tanks of tankers. J. Offshore Mech. Arctic Eng. 129 (1) (2007) 48–55.
[66] C.G. Soares, Y. Garbatov, A. Zayed, G. Wang, Corrosion wastage model for ship crude oil tanks. Corros Sci 50(11) (2008) 3095–3106.
[67] C.G. Soares, Y. Garbatov, Reliability of maintained, corrosion protected plates subjected to non-linear corrosion and compressive loads. Mar Struct 12(6) (1999) 425–445.

[68] P.J. Kee, L. Myung, H.J. Sung, P.I. Young. A time-dependent corrosion wastage model for the structures of single-and double hull tankers FSOs and FPSOs. Marit Technol 40(3) (2003) 201−217.
[69] G.M. Ferrari, J.W. Klijnstra, Controlling costs for corrosion protection. Presentation at the 12th International Naval Engineering Conference and Exhibition “Innovative solutions to global trends”, Amsterdam, 21 May 2014.
[70] E. Delory, D.M. Toma, J. del Rio Fernandez, P. Cervantes, P. Ruiz, S. Memè, Ocean in situ sensors crosscutting innovations. Chapter. 4.1 A new generation of interoperable oceanic passive acoustics sensors with embedded processing. Challenges and Innovations in Ocean in Situ Sensors. (2019) 117-171. https://doi.org/10.1016/B978-0-12-809886-8.00004-1
[71] W. Hoppe, J. Pierce, O. Scott, Automated corrosion detection program. AFRL-ML-WP-TR-2001-4162, Final Report for 07 APRIL 1997–06 October 2001.
[72] F. Zou, F.B. Cegla, On quantitative corrosion rate monitoring with ultrasound. J Electroanal Chem 812 (2018) 115–121. https://doi.org/10.1016/j.jelechem.2018.02.005
[73] F. Cegla, J. Allin, Wireless ultrasonic thickness monitoring at elevated temperatures. Mater Eval 69(5) (2011) A26–A31.
[74] F. Honarvar, F. Salehi, V. Safavi, A. Mokhtari, A.N. Sinclair, Ultrasonic monitoring of erosion/corrosion thinning rates in industrial piping systems. Ultrasonics 53 (2013) 1251–1258. doi: 10.1016/j.ultras.2013.03.007
[75] M.-T. Thai, H. Ahmed, S.-C. Hong, J.-R. Lee, J.-B. Ihn, Broadband laser ultrasonic excitation and multi-band sensing for hierarchical automatic damage visualization. Int J Aeronaut Space Sci (2019) https://doi.org/10.1007/s42405-019-00210-4
[76] A.J. Manzo, S. Kenderian, H. Helvajian Application of laser ultrasonic non-destructive evaluation technique to additive manufacturing. Proc. SPIE 9738, Laser 3D Manufacturing III, 973810 (6 April 2016); https://doi.org/10.1117/12.2219866
[77] V.A. Deason, J.A. Johnson, K.L. Telschow, Nondestructive material characterization. Patent number: 4995260, 1991.
[78] Recommended practice Non-intrusive inspection — DNVGL-RP-G103. Edition May 2017.
[79] P. Khalili, P. Cawley, The choice of ultrasonic inspection method for the detection of corrosion at inaccessible locations. NDT&E Int 99 (2018) 80–92. https://doi.org/10.1016/j.ndteint.2018.06.003
[80] N.N. Nakamura, H. Ogi, M. Hirao, K. Nakahata, Mode conversion behavior of SH guided wave in a tapered plate. NDT&E Int 45 (2012) 156–161.
[81] F.B. Cegla, P. Cawley, P. Cawley, J. Allin J. Davies, High-temperature (>500°c) wall thickness monitoring using dry-coupled ultrasonic waveguide transducers. IEEE Trans Ultrason Ferroelectr Freq Control 58(1) (2011) 156-167. doi: 10.1109/TUFFC.2011.1782
[82] R. Howard, F. Cegla, Detectability of corrosion damage with circumferential guided waves in reflection and transmission. NDT and E Int 91 (2017) 108–119. http://dx.doi.org/10.1016/j.ndteint.2017.07.004
[83] P.B. Nagy, F. Simonetti, G. Instanes, Corrosion and erosion monitoring in plates and pipes using constant group velocity lamb wave inspection. Ultrasonics 54 (2014) 1832–1841. https://doi.org/10.1016/j.ultras.2014.01.017
[84] Ref.: http://www.advancedultrasonics.com/equipment-sales/isonic-3505/ Mistras Group BV, https://www.ndt.net/article/ecndt98/chemical/103/103.htm
[85] Chapter 5 - Eddy current testing in the NDE Handbook, Non-destructive examination methods for condition monitoring. (1989) 42-59. https://doi.org/10.1016/B978-0-408-04392-2.50011-4
[86] J. García-Martín, J. Gómez-Gil, E. Vázquez-Sánchez, Non-destructive techniques based on eddy current testing. Sensors 11 (2011) 2525-2565. doi:10.3390/s110302525
[87] A.N. AbdAlla, M.A. Faraj, F. Samsuri, D. Rifai, K. Ali, Y. Al-Douri, Challenges in improving the performance of eddy current testing: Review. Meas Control 52(1-2) (2019) 46–64. doi: 10.1177/0020294018801382
[88] K.B. Ali, A.N. Abdalla, D. Rifai, M.A. Faraj, Review on system development in eddy current testing and technique for defect classification and characterization. IET Circuits Devices Syst 11(4) (2017) 330-343. doi: 10.1049/iet-cds.2016.0327
[89] S. She, Y. Chen, Y. He, Z. Zhou, X. Zou, Optimal design of remote field eddy current testing probe for ferromagnetic pipeline inspection. Measurement 168 (2021) 108306. https://doi.org/10.1016/j.measurement.2020.108306

[90] J.H. Rose, C.-C. Tai, J.C. Moulder, Extreme sensitivity of eddy-currents to the surface conditions of nickel. Rev Prog Quant Nondestr Eval 16 (1997) 249-255.
[91] M. Blodgett, P.B. Nagy, Eddy current evaluation of electrical anisotropy in polycrystalline TI-6AL-4V. Rev Prog Quant Nondestr Eval 18 (1999) 1709-1716.
[92] V. Manoel A. Silva, C.G. Camerini, J.M. Pardal, J.C.G. de Blás, G.R. Pereira, Eddy current characterization of cold-worked AISI 321 stainless steel. J Mater Res Technol 7(3) (2018) 395–401. https://doi.org/10.1016/j.jmrt.2018.07.002
[93] C.-C. Tai, J.H. Rose, J.C. Moulder, Thickness and conductivity of metallic layers from pulsed eddy current measurements. Rev Prog Quant Nondestr Eval 15 (1996) 409-416.
[94] E. Gros, L. Udpa, J.A. Smith, K. Wachs, Determining confounding sensitivities in eddy current thin film measurements. AIP Conference Proc 1806 (2017) 110002. doi: 10.1063/1.4974680
[95] A.Y. Tetero, V.I. Hutnyk, Dependence of the magnetic field of eddy currents on the parameters of a crack in aluminum alloys. Mater Sci 44(2) (2008) 268-273. https://doi.org/10.1007/s11003-008-9071-5
[96] Y.N. Butusova, V.V. Mishakin, M. Kachanov, On monitoring the incubation stage of stress corrosion cracking in steel by the eddy current method. Int J Eng Sci 148 (2020) 103212. https://doi.org/10.1016/j.ijengsci.2019.103212
[97] W. Du, Q. Bai, Y. Wang, B. Zhang, Eddy current detection of subsurface defects for additive/subtractive hybrid manufacturing. Int J Adv Manuf Tech 95 (2018) 3185–3195. https://doi.org/10.1007/s00170-017-1354-2
[98] M. Grosso, C.J. Pacheco, M.P. Arenas, A.H.M. Lima, I.C.P. Margarit-Mattos, S.D. Soaresc, G.R. Pereira, Eddy current and inspection of coatings for storage tanks. J Mater Res Technol 7(3) (2018) 356–360. https://doi.org/10.1016/j.jmrt.2018.05.006
[99] A. Sophian, G. Tian, M. Fan, Pulsed eddy current non-destructive testing and evaluation: a review. Chin. J. Mech. Eng. 30 (2017) 500–514. doi: 10.1007/s10033-017-0122-4
[100] Y. Wang, M. Fan, B. Cao, B. Ye, D. Wen, Measurement of coating thickness using lift-off point of intersection features from pulsed eddy current signals. NDT&E Int 116 (2020) 102333. https://doi.org/10.1016/j.ndteint.2020.102333
[101] Y. He, G. Tian, H. Zhang, M. Alamin, A. Simm, P. Jackson, Steel corrosion characterization using pulsed eddy current systems. IEEE Sensors J 12(6) (2012) 2113-2120. doi: 10.1109/JSEN.2012.2184280
[102] G. Vértesy, Pulse-position type fluxgate sensors. in the Encyclopedia of Sensors Edited by C. A. Grimes, E.C. Dickey, M.V. Pishko Volume X: Pages (1–27), American Scientific Publishers (2006).
[103] Y. Li, Z. Liu, B. Yan, Y. Wang, I. Mukriz Z. Abidin, Z. Chen, A funnel-shaped probe for sensitivity enhancement in pulse-modulation eddy current inspection of subsurface flaws in conductors. Sensors Actuat A 307 (2020) 111991. https://doi.org/10.1016/j.sna.2020.111991
[104] Y. He, F. Luo, M. Pan, X. Hu, B. Liu, J. Gao, Defect edge identification with rectangular pulsed eddy current sensor based on transient response signals. NDT&E Int 43 (2010) 409–415. doi:10.1016/j.ndteint.2010.03.007
[105] M.A. Machado, L. Rosadob, N. Pedrosa, A. Vostner, R.M. Miranda, M. Piedade, T.G. Santos, Novel eddy current probes for pipes: Application in austenitic round-in-square profiles of ITER. NDT&E Int 87 (2017) 111–118. http://dx.doi.org/10.1016/j.ndteint.2017.02.001
[106] L.S. Rosadoa, J.C. Gonzalezd, T.G. Santos, P.M. Ramosa, M. Piedade, Geometric optimization of a differential planar eddy currents probe for non-destructive testing. Sensor Actuat A 197 (2013) 96– 105. http://dx.doi.org/10.1016/j.sna.2013.04.010
[107] L.S. Rosado, T.G. Santos, P.M. Ramos, P.Vilaca, M. Piedade, A differential planar eddy currents probe: Fundamentals, modeling and experimental evaluation. NDT&E Int 51 (2012) 85–93. http://dx.doi.org/10.1016/j.ndteint.2012.06.010
[108] P. Li, L. Cheng, Y. He, S. Jiao, J. Du, H. Ding, J. Gao, Sensitivity boost of rosette eddy current array sensor for quantitative monitoring crack. Sensor Actuat A 246 (2016) 129–139. http://dx.doi.org/10.1016/j.sna.2016.05.023
[109] S. Xie, Z. Duan, J. Li, Z. Tong, M. Tian, Z. Chen, A novel magnetic force transmission eddy current array probe and itsapplication for nondestructive testing of defects in pipeline structures. Sensor Actuat A 309 (2020) 112030. https://doi.org/10.1016/j.sna.2020.112030

[110] N. Yusa, H. Hashizume, R. Urayama, T. Uchimoto, T. Takagi, K. Sato, An arrayed uniform eddy current probe design for crack monitoring and sizing of surface breaking cracks with the aid of a computational inversion technique. NDT&E Int 61 (2014) 29–34. http://dx.doi.org/10.1016/j.ndteint.2013.09.004
[111] R.F. Abrantes, L.S. Rosado, M. Piedade, P.M. Ramos, Pulsed eddy currents testing using a planar matrix probe. Measurement 77 (2016) 351–361. http://dx.doi.org/10.1016/j.measurement.2015.09.026
[112] G. Chen, W. Zhang, Z. Zhang, X. Jin, W. Pang, A new rosette-like eddy current array sensor with high sensitivity for fatigue defect around bolt hole in SHM. NDT&E Int 94 (2018) 70–78. https://doi.org/10.1016/j.ndteint.2017.12.001
[113] W. Zhang, C. Wang, F. Xie, H. Zhang, Defect imaging curved surface based on flexible eddy current array sensor. Measurement 151 (2020) 107280. https://doi.org/10.1016/j.measurement.2019.107280
[114] Q. Ma, B. Gao, G.Y. Tian, C. Yang, L. Xie, K. Chen, High sensitivity flexible double square winding eddy current array for surface micro-defects inspection. Sensor Actuat A 309 (2020) 111844. https://doi.org/10.1016/j.sna.2020.111844
[115] Z. Sun, D. Cai, C. Zou, W. Zhang, Q. Chen, Design and optimization of a flexible arrayed eddy current sensor. Meas Sci Technol 28 (2017) 045105. doi: 10.1088/1361-6501/aa5b76
[116] S. Xie, L. Zhang, Y. Zhao, X. Wang, Y. Kong, Q. Ma, Z. Chen, T. Uchimoto, T. Takagi, Features extraction and discussion in a novel frequency-band-selecting pulsed eddy current testing method for the detection of a certain depth range of defects. NDT&E Int 111 (2020) 102211. https://doi.org/10.1016/j.ndteint.2019.102211
[117] C. Ye, Y. Wang, M. Wang, L. Udpa, S.S. Udpa, Frequency domain analysis of magnetic field images obtained using TMR array sensors for subsurface defect detection and quantification. NDT&E Int 116 (2020) 102284. https://doi.org/10.1016/j.ndteint.2020.102284
[118] Z.A. Ansari, B.A. Abu-Nabah, M. Alkhader, A. Muhammed, Experimental evaluation of nonmagnetic metal clad thicknesses over nonmagnetic metals using apparent eddy current conductivity spectroscopy. Measurement 164 (2020) 108053. https://doi.org/10.1016/j.measurement.2020.108053
[119] K. Mizukami, T. Ishibashi, K. Ogi, Non-contact strain monitoring of carbon fiber composites using spatial frequency domain eddy current imaging data. 2020, https://doi.org/10.1016/j.measurement.2020.108589
[120] S. Zhang, B. Ducharne, T. Uchimoto, A. Kita, Y.A.T. Deffo, Simulation tool for the Eddy current magnetic signature (EC-MS) nondestructive method. J Magn Magn Mater 513 (2020) 167221. https://doi.org/10.1016/j.jmmm.2020.167221
[121] A. Aoukili, A. Khamlichi, Modeling an eddy-curretn probe for detection of surface cracks inmetallic parts. Procedia Technol 22 (2016) 527-534. https://doi.org/10.1016/j.protcy.2016.01.112
[122] X.B. Qiu, L.L. Liu, C.L. Li, J.L. Wei, Y.F. Wu, X.C. Cui, Defect classification by pulsed eddy-current technique based on power spectral density analysis combined with wavelet transform. IEEE Trans Magn 50(9) (2014) 6200708. doi: 10.1109/TMAG.2014.2320882
[123] Z.D. Wang, K. Yao, B. Deng, K.Q. Ding, Theoretical studies of metal magnetic memory technique on magnetic flux leakage signals. NDT&E Int 43 (2010) 354–359. https://doi.org/10.1016/j.ndteint.2009.12.006
[124] H. Chen, C. Wang, X. Zuo, Research on methods of defect classification based on metal magnetic memory. NDT&E Int 92 (2017) 82–87. http://dx.doi.org/10.1016/j.ndteint.2017.08.002
[125] K. Xu, X. Qiu, X. Tian, Theoretical investigation of metal magnetic memory testing technique for detection of magnetic flux leakage signals from buried defect. NDT&E Int 33(1) (2018) 45-55. doi: 10.1080/10589759.2017.1293050
[126] Z.D. Wang, K. Yao, B. Deng, K.Q. Ding, Quantitative study of metal magnetic memory signal versus local stress concentration. NDT&E Int 43 (2010) 513–518. doi:10.1016/j.ndteint.2010.05.007
[127] H. Huang, G. Han, Z. Qian, Z. Liu, Characterizing the magnetic memory signals on the surface of plasma transferred arc cladding coating under fatigue loads. J Magn Magn Mater 443 (2017) 281–286. http://dx.doi.org/10.1016/j.jmmm.2017.07.067

[128] N. Venkatachalapathi, S.M.D.J. Basha, G.J. Raju, P. Raghavulu, Characterization of fatigued steel states with metal magnetic memory method. Mater Today: P 5 (2018) 8645–8654. doi:10.3390/met8020119
[129] Z. Hu, J. Fan, S. Wu, H. Dai, S. Liu, Characteristics of metal magnetic memory testing of 35CrMo steel during fatigue loading. Metals 8 (2018) 119. doi:10.3390/met8020119
[130] M. Roskosz, A. Rusin, J. Kotowicz, The metal magnetic memory method in the diagnostics of power machinery component. JAMME 43(1) (2010) 362-370.
[131] G. Wang, P. Yan, L. Wei, Z. Deng, The magnetic memory effect of ferromagnetic materials in the process of stress-magnetism coupling. Adv Mater Sci Eng (2017) Article ID 1284560. https://doi.org/10.1155/2017/1284560
[132] L.J. Yang, B. Liu, L.J. Chen, S.W. Gao, The quantitative interpretation by measurement using the magnetic memory method (MMM)-based on density functional theory. NDT&E Int 55 (2013) 15-20. https://doi.org/10.1016/j.ndteint.2013.01.002
[133] A. Dubov, S. Kolokolnikov, Assessment of the material state of oil and gas pipelines based on the metal magnetic memory method. Weld World 56(3-4) (2012) 11-19. doi: https://doi.org/10.1007/BF03321331
[134] M. Kouril, T. Prosek, B. Scheffel, Y. Degres, Corrosion monitoring in archives by the electrical resistance technique. J Cult Herit 15 (2014) 99–103. doi: 10.1016/j.culher.2013.04.002
[135] A.J. Perkins, D.K. Waterman, S. Fe Springs, A. Silverman, L. Cheser, Monitoring of corrosion induced loss of material by means of a plurality of electrical resistance measurements (field signature method, electrical resistance tomography), Patent No.: US 6,982,563 B2, 2006.
[136] Y. Si, J.P. Rouse, C.J. Hyde, Potential difference methods for measuring crack growth: A review. Int J Fatigue 136 (2020) 105624. https://doi.org/10.1016/j.ijfatigue.2020.105624
[137] Y. Li, F. Gan, Z. Wan, J. Liao, W. Li, Novel method for sizing metallic bottom crack depth using multi-frequency alternating current potential drop technique. Meas Sci Rev 15(5) (2015) 268-273. doi: 10.1515/msr-2015-0037
[138] R.E. Elmquist, M.E. Cage, Y.-H. Tang, A.-M. Jeffery, J.R. Kinard, R.F. Dziuba, N.M. Oldham, E.R. Williams, The ampere and electrical standards. J Res Nat Inst Stand Technol 106 (2001) 65–103. doi: 10.6028/jres.106.005
[139] ASTM B193-19, Standard test method for resistivity of electrical conductor materials. ASTM International, West Conshohocken, PA, 2019, www.astm.org doi: 10.1520/B0193-19
[140] ISO 16392:2017(en)Tyres — Electrical resistance — Test method for measuring electrical resistance of tyres on a test rig.
[141] N. Bowler, Four-point potential drop measurements for materials characterization. IOP Pub Meas Sci Technol 22 (2011) 012001 (11pp).
[142] L.J. Swartzendruber, Calculations for comparing two-point and four-point probe resistivity measurements on rectangular bar-shaped semiconductor samples. NBA Technical Note, 241, by The U. S. Department of Commerce National Bureau of Standards, 1964.
[143] S.P. Kikken, Measuring film resistivity understanding and refining the four-point probe set-up. B.Sc Thesis at the Department of Applied Physics Plasma & Materials Processing (PMP), Eindhoven University of Technology, 2018.
[144] https://www.mdc-europe.com/
[145] I. Miccoli, F. Edler, H. Pfnur C. Tegenkamp, The 100th anniversary of the four-point probe technique: the role of probe geometries in isotropic and anisotropic systems. J Phys: Cond Mater 27 (2015) 223201 (29pp).
[146] L. Yang, N. Sridhar, C.S. Brossia, D.S. Dunn, Evaluation of the coupled multielectrode array sensor as a real-time corrosion monitor. Corros Sci 47 (2005) 1794–1809. doi: 10.1016/j.corsci.2004.08.002
[147] J.P. Cai, S.B. Lyon, A mechanistic study of initial atmospheric corrosion kinetics using electrical resistance sensors. Corros Sci 47 (2005) 2956–2973. doi: 10.1016/j.corsci.2005.04.011
[148] S.Y. Li, Y.G. Kim, S. Jung, H.S. Song, S.M. Lee, Application of steel thin film electrical resistance sensor for in situ corrosion monitoring. Sens Act B: Chem 120 (2007) 368–377. doi: 10.1016/j.snb.2006.02.029

[149] T. Prosek, M. Kouril, L. R. Hilbert, Y. Degres, V. Blazek, D. Thierry, M. Ø. Hansen, Real time corrosion monitoring in atmosphere using automated battery driven corrosion loggers. Corros Eng Sci Technol 43(2) (2008) 129−133. doi: 10.1179/174327808X286374
[150] T. Prosek, M. Kouril, M. Dubus, M. Taube, V. Hubert, B. Scheffel, Y. Degres, M. Jouannic, D. Thierry, Real-time monitoring of indoor air corrosivity in cultural heritage institutions with metallic electrical resistance sensors. Stud Conserv 58(2) (2013) 117−128. doi: 10.1179/2047058412Y.0000000080
[151] M.A. Hicks A.C Pickard, A comparison of theoretical and experimental methods of calibrating the electrical potential drop technique for crack length determination. Int J Fract 20 (1982) 91–101. https://doi.org/10.1007/BF01141259
[152] N. Bowler, Y. Huang, Model-based characterization of homogeneous metal plates by four-point alternating current potential drop measurements. IEEE Trans Magn 41 (2005) 2102–2110. doi: 10.1109/TMAG.2005.847625
[153] J.R. Bowler, N. Bowler, Theory of four-point alternating current potential drop measurements on conductive plates. Proc R Soc A 463 (2007) 817–836. doi: 10.1098/rspa.2006.1791
[154] N. Bowler, Theory of four-point alternating current potential drop measurements on a metal half-space. J Phys D Appl Phys 39 (2006) 584–589. doi: 10.1088/0022-3727/39/3/024
[155] G. Sposito, P. Cawley, P.B. Nagy, An approximate model for three-dimensional alternating current potential drop analyses using a commercial finite element code. NDT&E Int 43 (2010) 134–140. doi: 10.1016/j.ndteint.2009.10.002
[156] J Liu, P. Bowen, DC potential drop calibration in matrix-cladded Ti MMC specimens with a corner notch. Int J Fatigue 25 (2003) 671–676. doi: 10.1016/S0142-1123(02)00089-0
[157] L. Shen, J. Li, B.M. Liaw, F. Delale, J.H. Chung, Modeling and analysis of the electrical resistance measurement of carbon fiber polymer–matrix composites. Compos Sci Technol 67 (2007) 2513–2520. doi: 10.1016/j.compscitech.2006.12.020
[158] D. Smyl, M. Pour-Ghaz, A. Seppänen, Detection and reconstruction of complex structural cracking patterns with electrical imaging. NDT&E Int 99 (2018) 123–133. https://doi.org/10.1016/j.ndteint.2018.06.004
[159] S. Yu, D.M. Petranovic, S. Krishnan, K. Lee, C.Y. Yang, Resistance matrix in crosstalk modelling for multiconductor systems. P 5th ISQED (2004) 122–125. doi: 10.1109/ISQED.2004.1283661
[160] P.O. Gartland, H. Horn, K.R. Wold, T. Hallan, FSM—developments for monitoring of stress corrosion cracking in storage tanks. NACE Int Corros Conf (Orlando, FL), OSTI Identifier: 128718, Report Number(s): CONF-950304-TRN: IM9550-103, 1995.
[161] A.M. Pritchard, P. Webb, H. Horn, Use of the FSM technique in the laboratory to measure corrosion inhibitor performance in multiphase flow NACE Int Corros Conf (San Diego, CA), 1998.
[162] K.A. Esaklul, A.L. Ballard, Challenges in the design of corrosion and erosion monitoring for deepwater subsea equipment—stretching the limits of technology. NACE Int Corros Conf (Nashville, TN), 2007.
[163] Y. Kawakam, H. Kanaji, K. Oku, Study on application of field signature method (FSM) to fatigue crack monitoring on steel bridges. Procedia Eng 14 (2011) 1059–1064. doi: 10.1016/j.proeng.2011.07.133
[164] https://nke-instrumentation.com/produit/aircorr-corrosion/
[165] https://www.institut-corrosion.fr/activities/aircorr-loggers-aircorr/?lang=en https://www.cosasco.com/er-corrosion-monitoring-data-loggers.html
[166] http://mp-innovation-awards.webflow.io/2017-winners
[167] A. Khan, A. Qurashi, W. Badeghaish, M.N. Noui-Mehidi, Md.A. Aziz, Frontiers and challenges in electrochemical corrosion monitoring; surface and downhole applications. Sensors 20 (2020) 6583; doi:10.3390/s20226583
[168] S.K. Verma, S.S. Bhadauria, S. Akhtar, Monitoring corrosion of steel bars in reinforced concrete structures. Hindawi Publishing Corporation The Scientific World Journal (2014) Article ID 957904, 9 pages. http://dx.doi.org/10.1155/2014/957904
[169] B.N. Nelson, P. Slebodnick, J. Wegand, D. Lysogorski, E.J. Lemieux, Corrosion sensors and ISIS; a condition-based approach to the inspection and preservation of tanks and voids on US navy ships. Intended to offer this paper to the ASM Fleet Maintenance and Modernization Symposium, (2011) 1-19.

[170] SSC-348 Corrosion Experience Data Requirements by the Ship Structure Committee, 1991.
[171] I. MacLeod, P. Morrison, V. Richards, N. West, Corrosion monitoring and the environmental impact of decommissioned naval vessels as artificial reefs. Procedia Met 2004, National Museum of Australia Canberra ACT, 4-8 October (2004) 53-74.
[172] T.W. Horn, Determining seasonal corrosion rates in ferrous-hulled shipwrecks: a case study of the USS Huron. M.Sc. Thesis at the Faculty of the Department of History East Carolina University, October, 2014.
[173] A. Guibert, O. Chadebec, J.-L. Coulomb, C. Ra, Ship hull corrosion diagnosis from close measurements of electric potential in the water. IEEE Trans Magn 45(3) (2009) 1828-1831. doi: 10.1109/TMAG.2009.2012796
[174] Navy Ships Corrosion Project Implementation. DoD Maintenance Conference, Fort Worth, Texas November 15, 2011.
[175] G.S. Duffóa, S.B. Farina, C.M. Giordano, Characterization of solid embeddable reference electrodes for corrosion monitoring in reinforced concrete structures. Electrochim Acta 54 (2009) 1010–1020. doi:10.1016/j.electacta.2008.08.025
[176] G. Duffo, S.B. Farina, C.M. Giordano, Embeddable reference electrodes for corrosion monitoring of reinforced concrete structures. Mater Corros 61(6) (2009) 480–489. doi: 10.1002/maco.200905346
[177] G. Qiao, G. Sun, Y. Hong, Y. Qiu, J. Ou, Remote corrosion monitoring of the RC structures using the electrochemical wireless energy-harvesting sensors and networks. NDT&E Int 44 (2011) 583–588. doi: 10.1016/j.ndteint.2011.06.007
[178] V. Maruthapandian, V. Saraswathy, S. Muralidharan, Development of solid-state embeddable reference electrode for corrosion monitoring of steel in reinforced concrete structures. Cem Concr Comp 74 (2016) 100-108. https://doi.org/10.1016/j.cemconcomp.2016.09.001
[179] B.E. Merten, D. Battocchi, D.E. Tallman, G.P. Bierwagen, Embedded reference electrode for potential-monitoring of cathodic protective systems. J Electrochem Soc 157(7) (2010) C244-C247. doi: 10.1149/1.3421793
[180] B.J.E. Merten, Embedded reference electrodes for corrosion potential monitoring, electrochemical characterization, and controlled-potential cathodic protection. PhD Thesis at the North Dakota State University of Agriculture and Applied Science, Major Department: Coatings and Polymeric Material, Fargo, North Dakota, December 2011.
[181] G.P. Bierwagen, X. Wang, D.E. Tallman, In situ study of coatings using embedded electrodes for ENM measurements. Prog Org Coat 46 (2003) 163–175. doi: 10.1016/S0300-9440(02)00186-8
[182] M. Sophocleous, J.K. Atkinson, A review of screen-printed silver/silver chloride (Ag/AgCl) reference electrodes potentially suitable for environmental potentiometric sensors. Sensor Actuat A 267 (2017) 106–120. https://doi.org/10.1016/j.sna.2017.10.013
[183] S. Papamatthaiou, U. Zupancic, C. Kalha, A. Regoutz, P. Estrela, D. Moschou, Ultra stable, inkjet-printed pseudo reference electrodes for lab-on-chip integrated electrochemical biosensors. Sci Rep 10 (2020) 17152. https://doi.org/10.1038/s41598-020-74340-1
[184] Z. Zhao, H. Tu, E.G.R. Kim, B.F. Sloane, Y. Xu, A flexible Ag/AgCl micro reference electrode based on a parylene tube structure. Sens Actuators B Chem 247 (2017) 92–97. doi:10.1016/j.snb.2017.02.135
[185] J. Tafel, Über die Polarisation bei kathodischer Wasserstoffentwicklung. Z Phys Chem 50 (1905) 641-712.
[186] G.T. Burstein, A hundred years of Tafel's equation: 1905–2005. A Commemorative Issue of Corrosion Science. Corros Sci 47 (2005) 2858–2870. doi:10.1016/j.corsci.2005.07.002
[187] M. Stern, A.L. Geary, Electrochemical polarization: I. A theoretical analysis of the shape of polarization curves. J Electrochem Soc 104(1) (1957) 56-63.
[188] M. Stern, A method for determining corrosion rates from linear polarization data. Corrosion 14(9) (1958) 440t-444t.
[189] T.G.E. Niblock, Micro-fabricated sensor. Patent number: Pub. No.: US 2006/0006137 A1, 2006.
[190] T. Taylor, A. Hagensen, TANK 241-AN-102 Multi-probe corrosion monitoring system project lessons learned. ARES Corporation, 2008. RPP-RPT-37508, Rev. 0 (A-6002-767 (REV 1))
[191] F. Zahiri, Applications of aerospace-developed corrosion health monitoring system (CHMS). Analatom Inc, https://analatom.com/products-AN110.html

[192] M.H. Nazir, A. Saeed, Z.A. Khan, Electrochemical corrosion failure analysis of large complex engineering structures by using micro-LPR sensors. Sensors Actuat B 268 (2018) 232–244. https://doi.org/10.1016/j.snb.2018.02.191
[193] R.J. Connolly, D. Brown, D. Darr, J. Morse, B. Laskowski, Corrosion detection on buried transmission pipelines with micro-linear polarization resistance sensors. In: P. Tse, J. Mathew, K. Wong, R. Lam, C. Ko, (eds) Engineering Asset Management - Systems, Professional Practices and Certification. Lecture Notes in Mechanical Engineering. Springer, Cham, 2015. https://doi.org/10.1007/978-3-319-09507-3_58
[194] M.H. Nazir, Z.A. Khan, A. Saeed, K. Stokes, Modeling the effect of residual and diffusion-induced stresses on corrosion at the interface of coating and substrate. Corros 72(4) (2016) 500-517. doi: 10.5006/1804
[195] D. Darr, B. Laskowski, In situ corrosion monitoring and assessment with diagnostic and prognostic capabilities for condition-based maintenance. STO-MP-AVT-303, 13 (2012) 1-22.
[196] D. Brown, D. Darr, J. Morse, B. Laskowski, Theoretical and experimental evaluation of a real-time corrosion monitoring system for measuring pitting in aircraft structures. European Conf Prog Health Manag Soc 3 (2012) 1-9.
[197] D.W. Brown, R.J. Connolly, B. Laskowski, M. Garvan, H. Li, V.S. Agarwala, G. Vachtsevanos, A novel linear polarization resistance corrosion sensing methodology for aircraft structure. Annual Conference Prog Health Manag Soc (2014) 298-308.
[198] D.W. Brown, J.R. Connolly, D.R. Darr, V.S. Agarwala, Linear polarization resistance flex sensors and methods that involve structure as working electrode(s). Patent number: WO 2015/200899, 1-56.
[199] D.W. Brown, R.J. Connolly, D.R. Darr, B. Laskowski, Linear polarization resistance sensor using the structure as a working electrode. European Conference Prog Health Manag Soc (2014) 1-7.
[200] http://electrawatch.com/
[201] A. Amirudin, D. Thierry, Application of electrochemical impedance spectroscopy to study the degradation of polymer-coated metals. Progress in Organic Coatings 26 (1995) 1-28.
[202] F. Mansfeld, Use of electrochemical impedance spectroscopy for the study of corrosion protection by polymer coatings. Rev Appl Electrochem 39, J Appl Electrochem 25 (1995) 187-202.
[203] J.N. Murray, Electrochemical test methods for evaluating organic coatings on metals: an update. Part I. Introduction and generalities regarding electrochemical testing of organic coatings. Prog Org Coat 30 (1997) 225-233.
[204] J.N. Murray, Electrochemical test methods for evaluating organic coatings on metals: an update. Part II: Single test parameter measurements. Prog Org Coat 31 (1997) 255–264.
[205] J.N. Murray, Electrochemical test methods for evaluating organic coatings on metals: an update. Part III: Multiple test parameter measurements. Prog Org Coat 31 (1997) 375–391.
[206] N.K. Volmajer, M. Steinbücher, P. Berce, P. Venturini, M. Gaberšček, Electrochemical impedance spectroscopy study of waterborne epoxy coating film formation. Coatings 9 (2019) 254. doi:10.3390/coatings9040254
[207] S. Permeh, K. Lau, M. Duncan, Characterization of biofilm formation and coating degradation by electrochemical impedance spectroscopy. Coatings 9 (2019) 518. doi:10.3390/coatings9080518
[208] C.G. Oliveira, M.G.S. Ferreira, Ranking high-quality paint systems using EIS. Part I: intact coatings. Corros Sci 45 (2003) 123–138. https://doi.org/10.1016/S0010-938X(02)00088-4
[209] G. Bouvet, D.D. Nguyen, S. Mallarino, S. Touzain, Analysis of the non-ideal capacitive behaviour for high impedance organic coatings. Prog Org Coat 77 (2014) 2045–2053. https://doi.org/10.1016/j.porgcoat.2014.02.008
[210] M. Musiani, M.E. Orazem, N. Pébère, B. Tribollet, V. Vivier, Determination of resistivity profiles in anti-corrosion coatings from constant-phase-element parameters. Prog Org Coat 77 (2014) 2076–2083. http://dx.doi.org/10.1016/j.porgcoat.2013.12.013
[211] Z.S. Sahir, J.M. Sykes, Effect of temperature on the impedance response of coated metals. Prog Org Coat 77 (2014) 2039–2044. http://dx.doi.org/10.1016/j.porgcoat.2014.02.009 0300-944
[212] C.N. Coniglio, K. Nguyen, R. Kurji, E. Gamboa, Characterizing water sorption in 100% solids epoxy coatings. Prog Org Coat 76 (2013) 1168–1177. http://dx.doi.org/10.1016/j.porgcoat.2013.03.011

[213] E. van Gheema, J. Vereecken, J. Schoukens, R. Pintelon, P. Guillaume, P. Verboven, L. Pauwels, Instantaneous impedance measurements on aluminium using a Schroeder multisine excitation signal. Electrochim Acta 49 (2004) 2919–2925. doi:10.1016/j.electacta.2004.01.050
[214] S. Ramanathan, R. Vimala, S. Sruthi, Multi-sine EIS-drift, non-linearity and solution resistance effects. ECS Trans 45 (13) (2013) 37-50. doi: 10.1149/04513.0037ecst
[215] D. Koster, G. Du, A. Battistel, F. La Mantia, Dynamic impedance spectroscopy using dynamic multi-frequency analysis: A theoretical and experimental investigation. Electrochim Acta 246 (2017) 553–563 http://dx.doi.org/10.1016/j.electacta.2017.06.060
[216] M. Dinu, T. Hauffman, C. Cordioli, A. Vladescu, M. Braic, A. Hubin, C.M. Cotrut, Protective performance of Zr and Cr based silico-oxynitrides used for dental applications by means of potentiodynamic polarization and odd random phase multisine electrochemical impedance spectroscopy. Corros Sci 115 (2017) 118–128. http://dx.doi.org/10.1016/j.corsci.2016.11.018
[217] T. Breugelmans, E. Tourwé, J.-B. Jorcin, A. Alvarez-Pampliega, B. G., H. Terryn, A. Hubin, Odd random phase multisine EIS for organic coating analysis. Prog Org Coat 69 (2010) 215–218. doi:10.1016/j.porgcoat.2010.04.008
[218] T. Breugelmans, E. Tourwé, Y. van Ingelgem, J. Wielant, T. Hauffman, R. Hausbrand, R. Pintelon, A. Hubin, Odd random phase multisine EIS as a detection method for the onset of corrosion of coated steel. Electrochem Commun 12 (2010) 2–5. doi:10.1016/j.elecom.2009.10.008
[219] G. Ji, L.F. Macıa, B. Allaert, A. Hubin, H. Terryn, Odd random phase electrochemical impedance spectroscopy to study the corrosion behavior of hot dip Zn and Zn-alloy coated steel wires in sodium chloride solution. J Electrochem Soc 165(5) (2018) C246-C257. doi: 10.1149/2.0741805jes
[220] R.W. Bosch, J. Hubrecht, W.F. Bogaerts, B.C. Syrett, Electrochemical frequency modulation: a new electrochemical technique for online corrosion monitoring. Corros 57(1) (2001) 60-70. doi: 10.5006/1.3290331
[221] A. Rauf, E. Mahdi, Reliability and usefulness of causality factors of electrochemical frequency modulation. Int J Electrochem Sci 7 (2012) 10108–10120.
[222] F. Fathima, S. Ramanathan, Review—nonlinear electrochemical impedance spectroscopy. J Electrochem Soc 164 (7) (2017) H443-H455. doi: 10.1149/2.0391707jes
[223] P. Rajesh, S. Ramanathan, Non–linear electrochemical impedance spectroscopic analysis of instabilities in electrochemical systems. Electrochem Soc Trans 85 (13) (2018) 1145-1153. doi: 10.1149/08513.1145ecst
[224] J. Yin, M. Lu, J.P. de Gyvez, Full-signature real-time corrosion detection of underground casing pipes. IEEE Trans Instrum Meas 49(1) (2000) 120-128. https://doi.org/10.1109/19.836321
[225] R.G. Kelly, J. Yuan, S.H. Jones, W. Blanke, J.H. Aylor, W. Wan, A.P. Batson, A. Wintenberg, G.G. Clemefia, Embeddable microinstruments for corrosion monitoring. Corrosion 1997, paper number: 294, 1-12.
[226] J. Gu, H. Yao, K. Wang, B. Parviz, B. Otis, A 10μA on-chip electrochemical impedance spectroscopy system for wearables/implantables. 2014 IEEE Asian Solid-State Circuits Conference (A-SSCC), IEEE Xplore 2015, doi: 10.1109/ASSCC.2014.7008922
[227] F. Meng, L. Liu, Y. Cui, T. Zhang, Y. Li, F. Wang, A novel design of electrochemical noise configuration based on embedded electrodes for in-situ evaluation of epoxy coating under marine alternating hydrostatic pressure. Prog Org Coat 131 (2019) 346–356. https://doi.org/10.1016/j.porgcoat.2019.03.005
[228] C.S. Brossia, D.S. Dunn, Apparatus and method for detecting the degradation of a coating using embedded sensors. Patent Number: US 6,911,828 B1, 2005.
[229] B. Zajec, M.B. Leban, T. Kosec, V. Kuhar, A. Legat, S. Lenart, K.F. Bizjak, K. Gavin, Corrosion monitoring of steel structure coating degradation. Tehnicki Vjesnik 25(5) (2018) 1348-1355. https://doi.org/10.17559/TV-20170206004112
[230] K.N. Allahar, V. Upadhyay, G.P. Bierwagen, V.J. Gelling, Monitoring of a military vehicle coating under Prohesion exposure by embedded sensors. Prog Org Coat 65 (2009) 142–151. doi:10.1016/j.porgcoat.2008.10.011
[231] K. Allahar, Q. Su, G. Bierwagen, Non-substrate EIS monitoring of organic coatings with embedded electrodes. Prog Org Coat 67 (2010) 180–187. doi:10.1016/j.porgcoat.2009.10.001
[232] Y. Shi, C. You, A sensor system designed for remote coating degradation detection. 2010 IEEE Sensors Applications Symposium (SAS), IEEE Xplore 2010, doi: 10.1109/SAS.2010.5439388

[233] F.R.M. Aguiar, R.C. Gomes, Remote inspection method for detecting operational conditions of coatings. Patent number: WO2016201530A1, 2016.
[234] F. Hermerschmidt, D. Burmeister, G. Ligorio, S.M. Pozov, R. Ward, S.A. Choulis, E.J.W. List-Kratochvil, Truly low temperature sintering of printed copper ink using formic acid. Adv Mater Technol (2018) 1800146. doi: 10.1002/admt.201800146
[235] Y. Zhang, N. Anderson, S. Bland, S. Nutt, G. Jursich, S. Joshi, All-printed strain sensors: building blocks of the aircraft structural health monitoring system. Sensor Actuat A 253 (2017) 165–172. http://dx.doi.org/10.1016/j.sna.2016.10.007
[236] P. Pasakon, J.P. Mensing, D. Phokaratkul, C. Karuwan, T. Lomas, A. Wisitsoraat, A. Tuantranont, A high-performance, disposable screen-printed carbon electrode modified with multi-walled carbon nanotubes/graphene for ultratrace level electrochemical sensors. J Appl Electrochem 49(2) (2019) 217–227. https://doi.org/10.1007/s10800-018-1268-1
[237] S.J. Rowley-Neale, D.A.C. Brownson, G. Smith, C.E. Bank, Graphene oxide bulk-modified screen-printed electrodes provide beneficial electroanalytical sensing capabilities. Biosensors 10 (2020) 27. doi:10.3390/bios1003002
[238] E.P. Randviir, D.A.C. Brownson, J.P. Metters, R.O. Kadara, C.E. Banks, The fabrication, characterisation and electrochemical investigation of screen-printed graphene electrodes. Phys Chem Chem Phys 16 (2014) 4598-4611. doi: 10.1039/c3cp55435j
[239] S. Cinti, F. Arduini, M. Carbone, L. Sansone, I. Cacciotti, D. Moscone, G. Palleschi, Screen-printed electrodes modified with carbon nanomaterials: a comparison among carbon black, carbon nanotubes and graphene. Electroanalysis 27(9) (2015) 1-10. doi: 10.1002/elan.201500168
[240] J.A. Smith, Integrated detector technology for corrosion inspection. Final Report, 6/01/99-2/28/00, NSN 7540-01-280-5500, 17.04.2000.
[241] http://www.electrawatch.com/Ships.html
[242] P.T. Anastas, J.B. Zimmerman, Design through the twelve principles of green engineering. Environmental Science & Technology 37(5) (2003) 94A-101A.
[243] R. Hesketh, Introduction to sustainable and green engineering: general principles and targets. in book: Reference Module in Earth Systems and Environmental Sciences, Encyclopaedia of Sustainable Technologies (2017) 497-507. doi: 10.1016/B978-0-12-409548-9.10530-5
[244] R.P. Hesketh, M.H. Gregg, C.S. Slater, Chapter 4 Green engineering education. Sustainability Science and Engineering 1 (2006) 47-87. https://doi.org/10.1016/S1871-2711(06)80011-5
[245] https://www.epa.gov/green-engineering
[246] "Green engineering is the design, commercialization, and use of processes and products in a way that reduces pollution, promotes sustainability, and minimizes risk to human health and the environment without sacrificing economic viability and efficiency. Green engineering embraces the concept that decisions to protect human health and the environment can have the greatest impact and cost-effectiveness when applied early, in the design and development phase of a process or product."
[247] Ivy Hooks, Writing good requirements. Proceedings of the Third International Symposium of the INCOSE – Vol. 2, 1993. Prepared by the requirements working group of the international council on systems engineering.
[248] Restriction of Hazardous Substances Directive 2002/95/EC (RoHS 1), Directive 2002/95/EC of the European Parliament and of the Council. Eur-lex.europa.eu. Retrieved 3 July 2015., https://certifications.thomasnet.com/certifications/glossary/other-certification_registration/european-commission/rohs-compliant/, https://www.rohsguide.com/rohs-faq.htm, https://www.rohsguide.com/ https://www.nist.gov/standardsgov/compliance-faqs-rohs
[249] INCOSE, Systems Engineering Handbook: A guide for system life cycle processes and activities, version 4.0. Hoboken, NJ, USA: John Wiley and Sons, Inc, 2015. ISBN: 978-1-118-99940-0
[250] R. Park, Value engineering: a plan for invention. CRC Press, 1998, ISBN 9781574442359.
[251] J. Mandelbaum, D.L. Reed, Value engineering handbook. Institute for defense analyses. September 2006, IDA Paper P-4114, Log: H 06-000611.
[252] M. Kendig, S. Jeanjaquet, R. Brown, F. Thomas, Rapid electrochemical assessment of paint. J Coat Technol 68 (863) 39-47.
[253] J.J. Suay, I.M.T. Rodriguez, R. Izquierdo, A.H. Kudama, J.J. Saura, Rapid assessment of automotive epoxy primers by electrochemical techniques. J Coat Technol 75(946) (2003) 103-111. doi: https://doi.org/10.1007/BF02720157

[254] J.M. McIntyre, H.Q. Pham, Electrochemical impedance spectroscopy; a coatings optimization. Prog Org Coat 27 (1996) 201-207.
[255] D. Loveday, P. Peterson, B. Rodgers—Gamry instruments, evaluation of organic coatings with electrochemical impedance spectroscopy. JCT Coatings Tech (2005) 22-27.
[256] L.G.S. Gray, B.R. Appleman, EIS: electrochemical impedance spectroscopy, A tool to predict remaining coating life? JPCL (2003) 66-74.
[257] https://www.gamry.com/assets/Application-Notes/REAP.pdf
[258] J.R. Scully, S.T. Hensley, Lifetime Prediction for organic coatings on steel and a magnesium alloy using electrochemical impedance methods. Corrosion 50(9) (1994) 705–716. https://doi.org/10.5006/1.3293547
[259] C.-T. Chen, B.S. Skerry, Assessing the corrosion resistance of painted steel by AC impedance and electrochemical noise techniques. Corrosion 47(8) (1991) 598–611. https://doi.org/10.5006/1.3585298
[260] https://www.emisoftware.com/calculator/wire-pair-capacitance/
[261] B.A. Fellman, Carbon-based electric double layer capacitors for water desalination. MSc Thesis in Mechanical Engineering at the Massachusetts Institute of Technology, Jun 2010.
[262] A. Todinova, L. Contreras-Bernal, M. Salado, S. Ahmad, N. Morillo, J. Idıgoras, J.A. Anta, Towards a universal approach for the analysis of impedance spectra of perovskite solar cells: Equivalent Circuits and Empirical Analysis. Chem Electro Chem 4 (2017) 2891–2901. doi: 10.1002/celc.201700498
[263] W.A. Levinson, Lean Management System LMS:2012, (2016): A Framework for Continual Lean Improvement. CRC Press. p. 11. ISBN 9781466505384. Retrieved 5 May 2019.
[264] U. Dombrowski, T. Mielke, Lean Leadership – 15 Rules for a Sustainable Lean Implementation. Procedia CIRP. 17 (2014) 565–570. doi:10.1016/j.procir.2014.01.146
[265] R. de Levie, On porous electrodes in electrolyte solutions. I. Capacitance effects. Electrochim Acta 8 (1963) 751–780. doi:10.1016/0013-4686(63)80042-0.
[266] R. de Levie, On porous electrodes in electrolyte solutions. Electrochim Acta 8 (1963) 751–780. doi:10.1016/0013-4686(63)80042-0
[267] M. Keddam, C. Rakotomavo, H. Takenouti, Impedance of a porous electrode with an axial gradient of concentration. J Appl Electrochem 14 (1984) 437-448.
[268] S.J. Cooper, A. Bertei, D.P. Finegan, N.P. Brandon, Simulated impedance of diffusion in porous media. Electrochim Acta 251 (2017) 681–689. https://doi.org/10.1016/j.electacta.2017.07.152
[269] J. Huang, Y. Gao, J. Luo, S. Wang, C. Li, Shengli Chen, J. Zhang, Editors' Choice—Review—Impedance response of porous electrodes: theoretical framework, physical models and applications. J Electrochem Soc 167 (2020) 166503. doi: 10.1149/1945-7111/abc655
[270] E.A. Stricker, X. Ke, J.S. Wainright, R.R. Unocic, R.F. Savinell, Current density distribution in electrochemical cells with small cell heights and coplanar thin electrodes as used in EC-S/TEM cell geometries. J Electrochem Soc 166(4) (2019) H126-H134. doi: 10.1149/2.0211904jes
[271] Z. Chen, R.C. Luo, Design and Implementation of capacitive proximity sensor using microelectromechanical systems technology. IEEE Trans Ind Electron 45(6) (1998) 886-894. doi: 10.1109/41.735332
[272] B. Timmer, W. Sparreboom, W. Olthuis, P. Bergveld, A. van den Berg, Optimization of an electrolyte conductivity detector for measuring low ion concentrations. Lab Chip 2 (2002) 121–124. DOI: 10.1039/b201225a
[273] A.V. Rukavina, Non-invasive liquid recognition based on interdigital capacitor. Sensors and Actuators A 228 (2015) 145–150. http://dx.doi.org/10.1016/j.sna.2015.03.019
[274] A. Guimerà, G. Gabriel, E. Prats-Alfonso, N. Abramova, A. Bratov, R. Villa, Effect of surface conductivity on the sensitivity of interdigitated impedimetric sensors and their design considerations. Sensors and Actuators B 207 (2015) 1010–1018. http://dx.doi.org/10.1016/j.snb.2014.10.134
[275] H. Sadeghian, Y. Hojjat, M. Soleimani, Interdigitated electrode design and optimization for dielectrophoresis cell separation actuators. Journal of Electrostatics 86 (2017) 41-49. http://dx.doi.org/10.1016/j.elstat.2017.01.012
[276] G.J.A.M. Brom-Verheijden, M.H. Goedbloed, M.A.G. Zevenbergen, A microfabricated 4-electrode conductivity sensor with enhanced range. Proceedings 2 (2018) 797. doi:10.3390/proceedings2130797

[277] A. Rivadeneyra, José F. Salmerón, M. Agudo-Acemel, L.F. Capitan-Vallvey, J.A. López-Villanuev, A.J. Palma, Asymmetric enhanced surface interdigitated electrode capacitor withtwo out-of-plane electrodes. Sensors and Actuators B 254 (2018) 588–596. http://dx.doi.org/10.1016/j.snb.2017.07.141
[278] N. Couniot, A. Afzalian, N. van Overstraeten-Schlögel, L.A. Francis, D. Flandre, Capacitive biosensing of bacterial cells: Analytical model and numerical simulations. Sensors and Actuators B 211 (2015) 428–438. http://dx.doi.org/10.1016/j.snb.2015.01.108
[279] T. Chen, J.R. Bowler, N. Bowler, Analytical solution for capacitance calculation of a curved patch capacitor that conforms to the curvature of a homogeneous cylindrical dielectric rod. Appl Phys Lett 104 (2014) 032901. doi: 10.1063/1.4862434
[280] I.J. Bahl, Stanislaw S. Stijchly, Analysis of a microstrip covered with a lossy dielectric. IEEE Trans Microw Theory Techn 28 (2) (1980) 104-109.
[281] V. Novickij, A. Tabasnikov, S. Smith, A. Grainys, J. Novickij, Analysis of planar circular interdigitated electrodes for electroporation. IETE Tech Rev (2015) 1-7. doi: 10.1080/02564602.2014.1000982
[282] T. Chen, N. Bowler, Design of interdigital spiral and concentric capacitive sensors for materials evaluation. AIP Conf Proc 1511 (2012): 1593–1600. http://dx.doi.org/10.1063/1.4789232.
[283] T. Chen, Capacitive sensors for measuring complex permittivity of planar and cylindrical structures. PhD Thesis at the Iowa State University, Ames, Iowa 12294, (2012). https://lib.dr.iastate.edu/etd/12294.
[284] ASTM D257-14, Standard test methods for DC resistance or conductance of insulating materials, ASTM International, West Conshohocken, PA, 2014, www.astm.org. doi: 10.1520/D0257-14
[285] T.-T. Ngo, A. Bourjilat, J. Claudel, D. Kourtiche, M. Nadi, Design and realization of a planar interdigital microsensor for biological medium characterization. pp. 23−54, chapter in S.C. Mukhopadhyay (ed.), Next Generation Sensors and Systems, Smart Sensors, Measurement and Instrumentation 16, ISBN: 978-3-319-21670-6, Springer International Publishing Switzerland 2016, doi: 10.1007/978-3-319-21671-3_2
[286] V. Shtrauss, A. Kalpinsh, U. Lomanovskis, J. Rotbahs, Tomographic imaging by electrical methods, Latvian J. Phys. Tech. Sci., 3 (1995) 23–47.
[287] C.-U. Kim, G. Li, J. Li, H. Jong, C. Ro, Y. Song, G. Pak, S. Im, Numerical analysis on effective electric field penetration depth for interdigital impedance sensor. 7th International Conference on Applied Electrostatics (ICAES-2012) IOP Publishing Journal of Physics: Conference Series 418 (2013) 012020. doi:10.1088/1742-6596/418/1/012020
[288] M. Jamil Amir, M. Yaseen, R. Iqbal, Exact solutions of Laplace equation by differential transform method. (2013) 8 pp. arXiv:1312.7277
[289] T. Fukuchi, High-order accurate and high-speed calculation system of 1D Laplace and Poisson equations using the interpolation finite difference method. AIP Advances 9 (2019) 055312. doi: 10.1063/1.5096395
[290] J. Oberländer, Z.B. Jildeh, P. Kirchner, L. Wendeler, A. Bromm, H. Iken, P. Wagner, M. Keusgen, M.J. Schöning, Study of interdigitated electrode arrays using experiments and finite element models for the evaluation of sterilization processes. Sensors 15 (2015) 26115−26127. doi:10.3390/s151026115
[291] M. Shenouda, D.R. Oliver, Fabrication of an interdigitated sample holder for dielectric spectroscopy of thin films. J Phys Conf Ser 619 (2015) 012028. doi:10.1088/1742-6596/619/1/012028
[292] M. Ibrahim, J. Claudel, D. Kourtiche, M. Nadi, F. Montaigne, G. Lengaigne, Optimization of planar interdigitated electrode array for bioimpedance spectroscopy restriction of the number of electrodes. Fifth Int Conf Sens Technol IEEE Xplore (2011) 612−616.
[293] S. Sathya, S. Muruganand, N. Manikandan, K. Karuppasamy, Design of capacitance based on interdigitated electrode for BioMEMS sensor application. Mater Sci Semicond Process 101 (2019) 206–213. https://doi.org/10.1016/j.mssp.2019.06.005
[294] F.R. Zypman. Mathematical expression for the capacitance of coplanar strips. J Electrostatics 101 (2019) 103371. https://doi.org/10.1016/j.elstat.2019.103371
[295] J. Hrisko, Capacitive soil moisture sensor theory, calibration, and testing. technical report. Maker Portal LLC, New York, NY, July 5 2020. doi: 10.13140/RG.2.2.36214.83522

[296] X. Yin, D.A. Hutchins, G. Chen, W. Li, Preliminary studies on the design principles of capacitive imaging probes for non-destructive evaluation. Int J Appl Electromagn Mech 42 (2013) 447–470. doi: 10.3233/JAE-131676
[297] R.S. Lima, M.H.D.O. Piazzetta, A.L. Gobbi, T.P. Segato, M.F. Cabral, S.A.S. Machado, E. Carrilho, Highly sensitive contactless conductivity microchips based on concentric electrodes for flow analysis. Chem Commun 49(97) (2013) 11382−11384. doi: 10.1039/C3CC45797D
[298] IEC 60093:1980: 'Methods of test for insulating materials for electrical purposes; volume resistivity and surface resistivity of solid electrical insulating materials', International Electrotechnical Commission Std.
[299] IEC 62631-3-1:2016: 'Dielectric and resistive properties of solid insulating materials – Part 3-1: determination of resistive properties (DC methods) – volume resistance and volume resistivity – general method', International Electrotechnical Commission Std.
[300] IEC 62631-3-2:2015: 'Dielectric and resistive properties of solid insulating materials – Part 3-2: determination of resistive properties (DC methods) – surface resistance and surface resistivity', International Electrotechnical Commission Std
[301] 'DIN IEC 60093:1993-12; VDE 0303-30:1993-12 Prüfverfahren für elektroisolierstoffe; spezifischer durchgangswiderstand und spezifischer oberflächenwiderstand von festen, elektrisch isolierenden Werkstoffen (IEC 60093:1980); Deutsche Fassung HD 429 S1:1983', Deutsche Institut für Normung e.V., Verband der Elektrotechnik Elektronik Informationstechnik e. V. Std.
[302] 'DIN EN 62631-3-1:2017-01; VDE 0307-3-1:2017-01 Dielektrische und resistive Eigenschaften fester Isolierstoffe – Teil 3-1: Bestimmung resistiver Eigenschaften (Gleichspannungsverfahren) – Durchgangswiderstand und spezifischer Durchgangswiderstand – Basisverfahren (IEC 62631-3-1:2016); Deutsche Fassung EN 62631-3-1:2016', Deutsche Institut für Normung e.V., Verband der Elektrotechnik Elektronik Informationstechnik e. V. Std
[303] 'DIN EN 62631-3-2:2016-10; VDE 0307-3-2:2016-10 Dielektrische und resistive Eigenschaften fester Isolierstoffe – Teil 3-2: Bestimmung resistiver Eigenschaften (Gleichspannungsverfahren) – Oberflächenwiderstand und spezifischer Oberflächenwiderstand (IEC 62631-3-2:2015); Deutsche Fassung EN 62631-3-2:2016', Deutsche Institut für Normung e.V., Verband der Elektrotechnik Elektronik Informationstechnik e. V. Std.
[304] www.trakinc.com
[305] ANSI/ESD - ANSI/ESD STM11.11-2015: Surface resistance measurement of static dissipative planar materials.
[306] ANSI/ESD STM11.12-2015: ESD association standard test method for protection of electrostatic discharge susceptible items - volume resistance measurement of static dissipative planar materials.
[307] https://www.electrotechsystems.com/
[308] www.prostatcorp.com
[309] K.S. Cole, R.H. Cole, Dispersion and absorption in dielectrics I. Alternating current characteristics. J Chem Phys 9 (1941) 341–352. https://doi.org/10.1063/1.1750906
[310] K.S. Cole, R.H. Cole, Dispersion and absorption in dielectrics II. Direct current characteristics. J Chem Phys 10 (1942) 98−105. https://doi.org/10.1063/1.1723677
[311] G.J. Brug, A.L.G. van den Eeden, M. Sluyters-Rehbach, J.H. Sluyters, The analysis of electrode impedances complicated by the presence of a constant phase element. J Electroanal Chem 176 (1984) 275−295. https://doi.org/10.1016/S0022-0728(84)80324-1
[312] C.H. Hsu, F. Mansfeld, Concerning the conversion of the constant phase element parameter Y0 into a capacitance. Corrosion 57/ No. 9 (2001) 747−748. https://doi.org/10.5006/1.3280607
[313] M.R. Shoar Abouzari, F. Berkemeier, G. Schmitz, D. Wilmer, On the physical interpretation of constant phase elements. Solid State Ionics 180 (2009) 922–927. https://doi.org/10.1016/j.ssi.2009.04.002
[314] B. Hirschorn, M. Orazem, B. Tribollet, V. Vivier, I. Frateur, M. Musiani, Determination of effective capacitance and film thickness from constant-phase-element parameters. Electrochim Acta 55 (2010) 6218–6227. doi:10.1016/j.electacta.2009.10.065
[315] W. Zhao, Y. Fan, H. Chen, Dielectric properties and corona resistance of Si-B/epoxy nano-composites. J Mater Sci Mater Electron 30 (2019) 16298–16307. https://doi.org/10.1007/s10854-019-02000-w

[316] J. Wang, Y. Jin, C. Wang, Y. Wang, Electrical conductivity, dielectric permittivity and dynamic mechanical properties of graphene/epoxy nanocomposites. Dig J Nanomater Biostructures 13(4) (2018) 959-967.
[317] C.F. Pitt, B.P. Barth, B.E. Godard, Electrical properties of epoxy resins. IRE Trans Comp Parts December (1957) 110-113.
[318] P. Gill, Electrical power equipment maintenance and testing. Second Edition, CRC Press, 1574446568, 2009.
[319] B. Sultan, J. Andersson, T. Hjertberg, Electrical breakdown testing of materials intended for use in PV modules. at the IEC Standard Development and Progress, 3rd Atlas/NIST Workshop on Photovoltaics Materials Durability Gaitherburg, Maryland December 8-9, 2015.
[320] T. Mizukami, I. Ishikawa, M. Yuasa, Trends of recent hull damage and counter-measures. Class NK Tech Bull 12 (1994) 25-45.
[321] Y. Satoshi, Shipyard experience in structural design of double hull tankers-past, present and future. – Tanker Structure Cooperative Forum (TSCF), Shipbuilders Meeting 2007.
[322] J. Yagi, I. Tomita, Definition of hot spot stress in welded plate type structure for fatigue assessment. IIW-XIII- 1414-91, 1991.
[323] Y. Sumi, Y. Chen, S. Hayashi, Morphological aspects of fatigue crack propagation. Part I. Computational procedure. Int J Fracture 82 (1996) 205–220.
[324] Y. Sumi, Y. Chen, Z.N. Wang, Morphological aspects of fatigue crack propagation. Part II. Effects of stress biaxiality and welding residual stress. Int J Fracture 82 (1996) 221–235.
[325] Y. Sumi, H. lyama, Z. Bozic, Y. Kawamura, Multiple fatigue cracks propagating in a stiffened panel. J Soc Nav Archit Jpn 179 (1996) 407–412.
[326] Y. Sumi, Fatigue crack propagation and computational remaining life assessment of ship structures. J Mar Sci Technol 3 (1998) 102-112. https://doi.org/10.1007/BF02492565
[327] S.C.G. de Sousa, Coating breakdown analysis of steel plates in marine structures. MSc Thesis at the Centre for Marine Technology and Ocean Eng (CENTEC), Instituto Superior Tecnico University of Lisbon, Portugal, July 2015.
[328] O.T. Vördal, T. Moan, Lessons learned from predicted versus observed fatigue of offshore steel structures in the North Sea. Proceedings of the 3rd Offshore Structural Reliability Conference OSRC, Stavanger, Norway, 2016.
[329] W. Fricke, Fatigue strength of ship structures, Part I. Germanischer Lloyd, Hamburg, 1997.
[330] Fatigue assessment of ship structures. Classification Notes No. 30.7, by DNV GL Det Norske Veritas, February 2003.
[331] D.G. Lee, B.C. Kim, Investigation of coating failure on the surface of a water ballast tank of an oil tanker. J Adhes Sci Technol 19(10) (2005) 879–908, doi: 10.1163/1568561054929946
[332] J.W. Ringsberg, A study on the influence of ageing of coatings on their mechanical properties and fracture in ballast tanks. Ships Offshore Structr 17(1) (2017) S268–S279. doi: 10.1080/17445302.2016.1247488
[333] H.M. Mahmoud, R.J. Dexter, Propagation rate of large cracks in stiffened panels under tension loading. Mar Struct 18(3) (2005) 265–288. doi. 10.1016/j.marstruc.2005.09.001

Appendix 1 Design Cycle I – Planar Electrodes

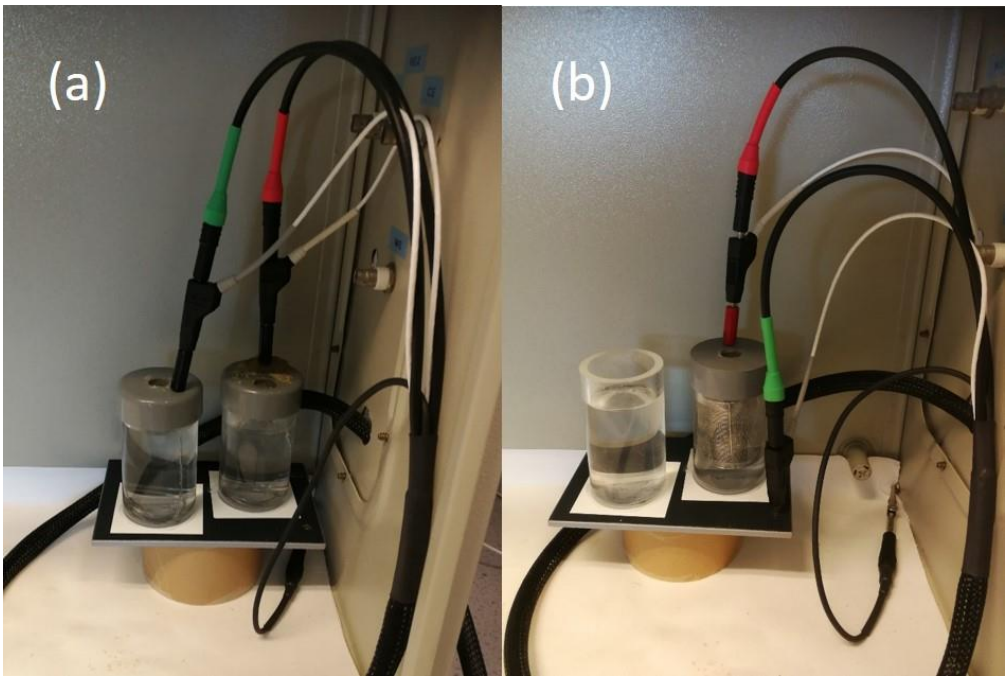

Figure A.42. Test configurations: 2 cells without wire connection to substrate (a), one cell with wire connected substrate (b).

Results obtained with planar carbon electrodes used for traditional type coating inspection are presented in this subsection to serve as a basis for comparison of the results gathered with wire-based electrodes. Pore resistance was derived to all three thin coatings/steel substrates measured with both wire-connected and no connection to substrate modes. In case of the reference coating/steel sample I (Figure A.43), comparison of the initial and later derived data, pore resistance of the coating remained unchanged at specific resistance $>10^{10}$ ohm cm^2 highlighting excellent condition over complete immersion period. The major difference was connected to altered sensing capability of the test setups. Thus, using two cells without wire connection to substrate provided hundred times lower pore resistance (at ~10^8 ohm cm^2) compared to the single-cell setup. The salt contaminated sample IV indicated high pore resistance comparable to the reference in the beginning, which reduced by around ten times to the end of exposure. Similarly, to the reference sample I, the electrical test setup weighted much more in altering the results than true condition of the coatings. Around two and a half orders of magnitude reduction of the pore resistance were manifested to measuring with the 2 cells setup than the single cell-direct wire connection mode but 10 times lower results were credibly derived at the end of exposure by the reference setup. The pre-corroded sample V showed lower resistance on average specific resistance between 10^9 and 10^6 ohm cm^2 compared to the aforementioned two samples, and the difference between results obtained via the two setups increased to 10^3 which is unacceptable by any standard and organisation. Nonetheless, sample V showed stable condition over the immersion period. This can be an example to reflect on

inevitable consequence of missing indication on low-quality surface preparation and paint ship work during coating application by the contractors, beyond the false positive, too early misleading detection beyond the organisation of earlier than necessary maintenance actions. The real reason for this failure is unavoidable by relying on wet phase test modes.

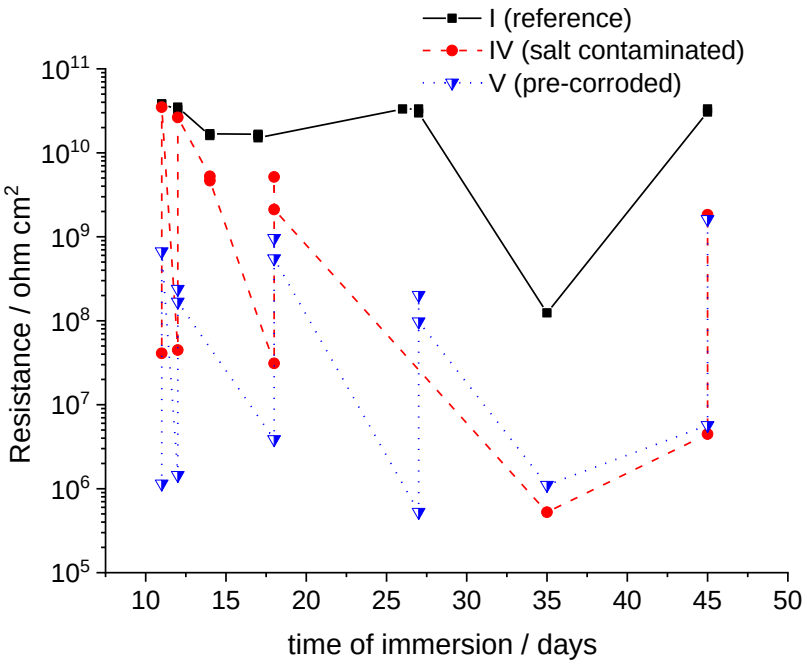

Figure A.43. Pore resistance of the coating/steel substrates obtained with planar carbon disk electrode (regarded as reference) used in 2C and dwc modes.

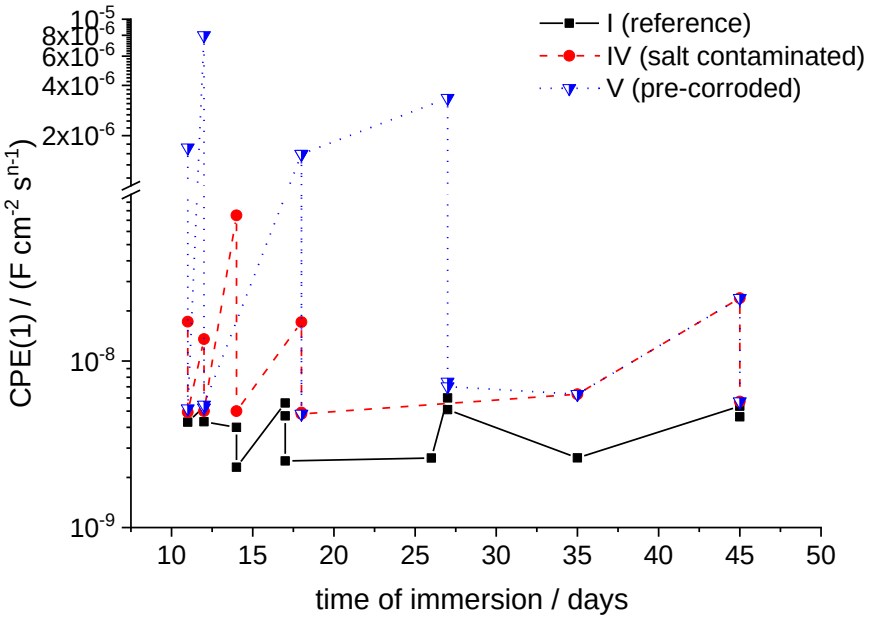

Figure A.44. CPE(1) of the coating/steel substrates obtained with planar carbon disk electrode (regarded as reference) used in 2C and dwc modes.

Faraday type shunting by electrochemical processes can lead to not entirely blocked electrode characteristic and so it would lead to complete screening, concealing of the high pore resistance coating (connected in series), or in other words overriding currents at the electrodes interface (coupled in parallel) besides the low current across surface areas of the coatings. Constant phase elements 1 and 2 of all coting/steel substrates derived from the same impedance results as aforementioned are depicted as a function of time in Figure A.44. In case of the CPE(1), the reference coating indicated the lowest and stable interfacial capacitive character in accordance with the exception. In addition, measure setup resulted in relatively minor deviation in the results. In comparison, the samples IV and V showed considerably higher capacitive nature along with more fluctuation over time. In these cases, the measure setup regardless of type of the electrodes (rather independent of geometrical factors) lead to several times and more than 100 times of deviations at the beginning and middle stage of the exposure which is the interested condition by naval maintenance entities.

The CPE(2) part of impedance spectra manifested some definite increments in magnitudes (Figure A.45) ~3 times to sample I and IV and ~30 times to sample V, over the CPE(1) counterparts (Figure A.44). In this case, validity of assessment of CPE(2) part of the impedance spectra proved to be critical owing to the almost four orders of magnitude difference between the data derived from results measured with the two setups as it is clearly seen in data points over the same exposure periods.

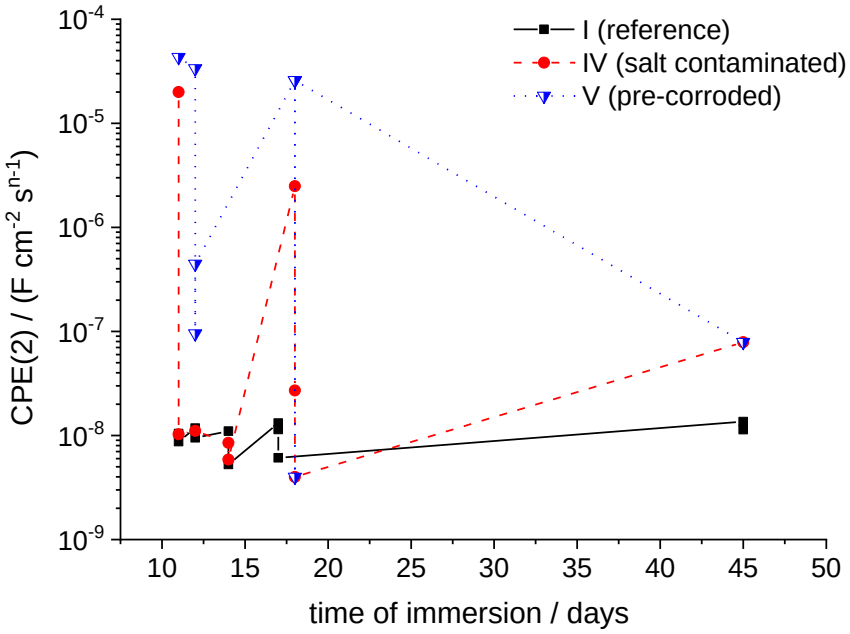

Figure A.45. CPE(2) of the coating/steel substrates obtained with planar carbon disk electrode (regarded as reference) in 2C and dwc modes.

As an inference, although shift of the impedance involves changes of the resistance then the capacitive elements is theoretically clear and well proven, this leads to highly questionable credibility of the sensor

data. In addition, reliability of detection comes into focus and may become critical when coating/steel substrates experience minor and moderate deterioration.

In Figure A.46(a) and (b), exponents of the constant phase elements (1) and (2) are summarised as a function of time exposure. This parameter is informative on homogeneous character of lateral distribution of resistance and geometry expressed in fractal state of the electrochemically active surface.

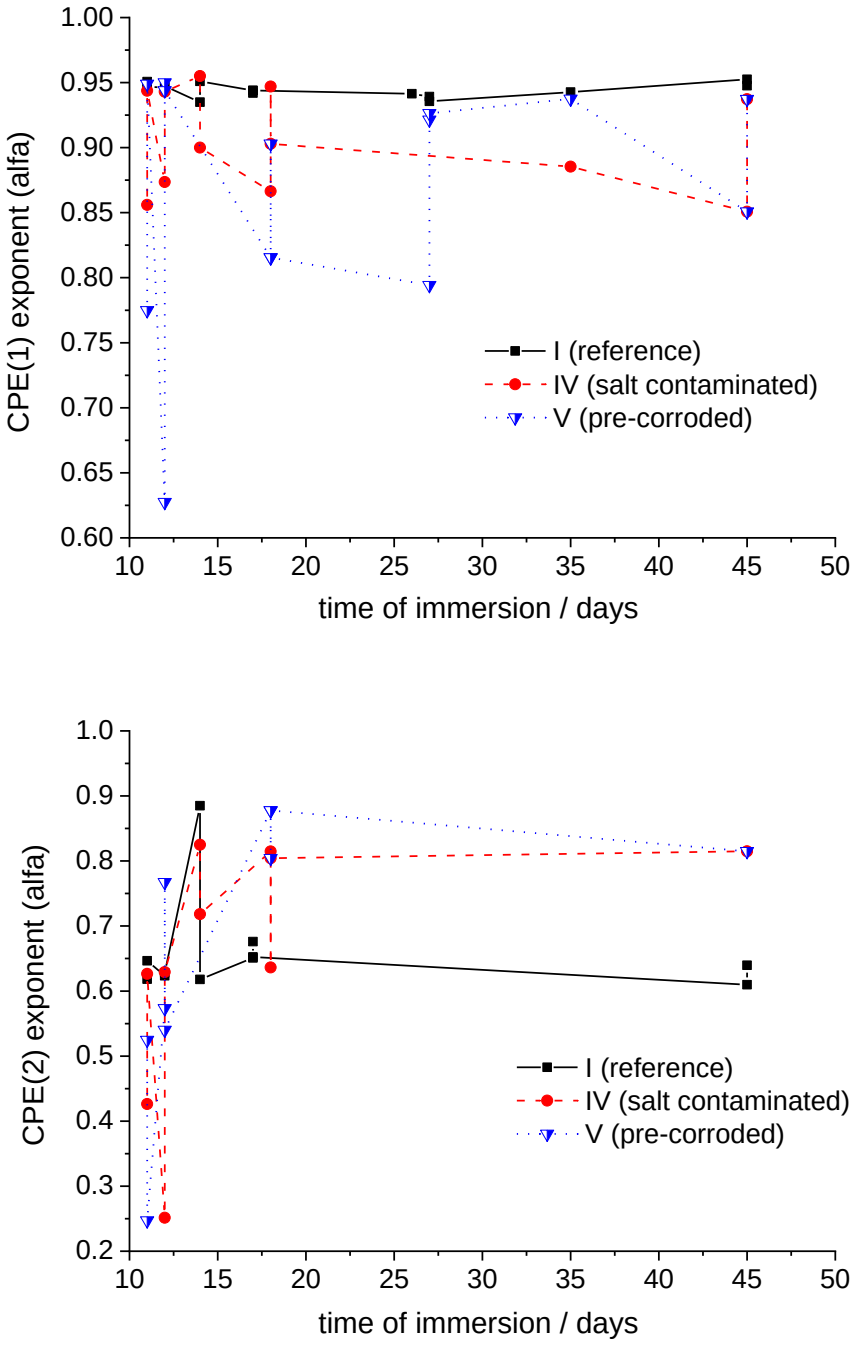

Figure A.46. Exponent of the constant phase elements 1 (a) and 2 (b) of the coating/steel substrates obtained with planar carbon disk electrode in 2C and dwc modes.

Thus, this offers quality assessment of electrode sensing capabilities along with the recorded variation of coating thickness at times of initial and exposed states. Stable CPE(1) and much lower, less varying, slightly decreasing CPE(2) factors were derived to the reference coating sample I. The former is connected to almost ideally flat surface and/or interface with uniform lateral resistivity, and the latter is associated with a partly resistive nature with getting into ideal mass transport regime described with the Warburg impedance (0.5). The former matches the low thickness variation (~12 rel. %) in initial stage of exposure but the latter may not entirely fit with greater variation of thickness mean (~30.5 rel. %) in later stage of exposure (swollen state via hydration). In this case, decreasing pore resistance coincided with increasing CPE and reduced CPE exponents, which was excessive by the two measure setups compared to properties variation of coating/steel samples.

Based on absolute and time variation of CPE and exponent data, the CPE(1) is assigned to more of the interfacial character of the samples and CPE(2) with the coating characteristics. Increased exponent of the CPE(2) reference sample (I) at 14, 17 and 45 days of exposure by the two cells setup means loss of detection sensitivity to the coatings, and this statement is also valid for rest of the samples (IV and V). Therefore, inferences suggest no representative sensing of coatings by the wet phase setups. Thus, IDE configuration was tested for sensing deterioration of coatings and the substrates with an intention to prove the concept of representative characterisation by a wide-range industry applicable solution.

Fitting results of the large spiral and the extended meander electrodes are summarised in the following.

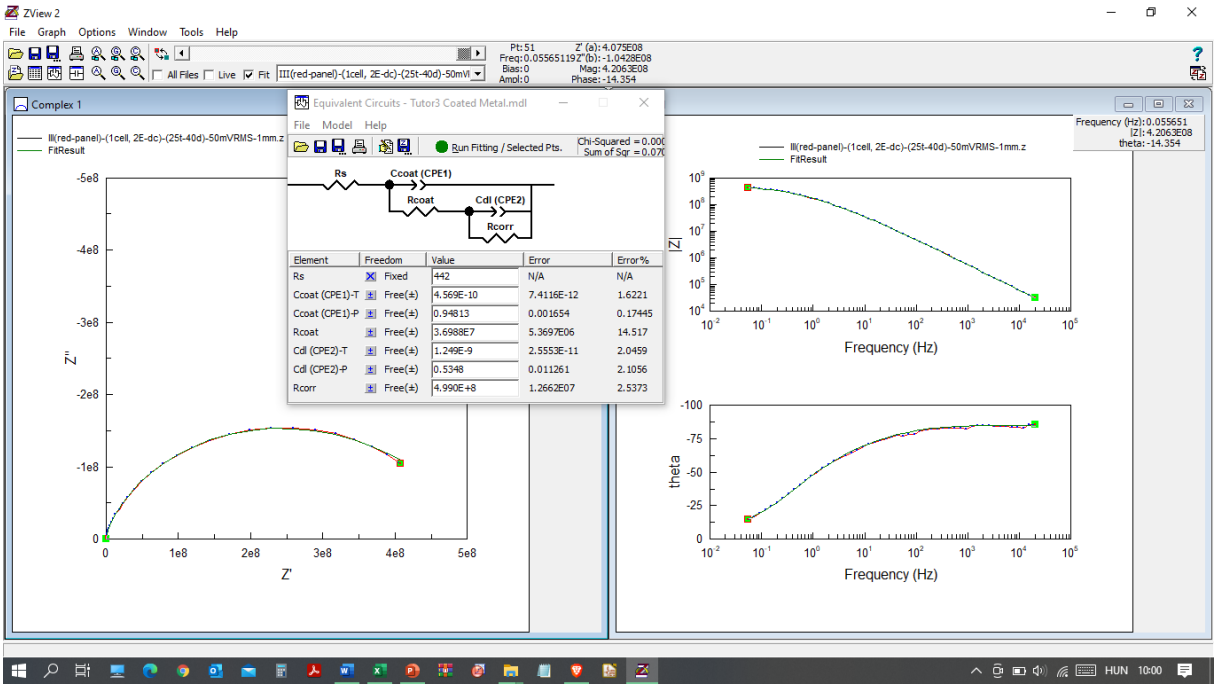

Figure A.47. Fitted impedance spectra measured with the large spiral wire electrode in a distance of 1 mm from the coating surface, at a test voltage of 50 mV.

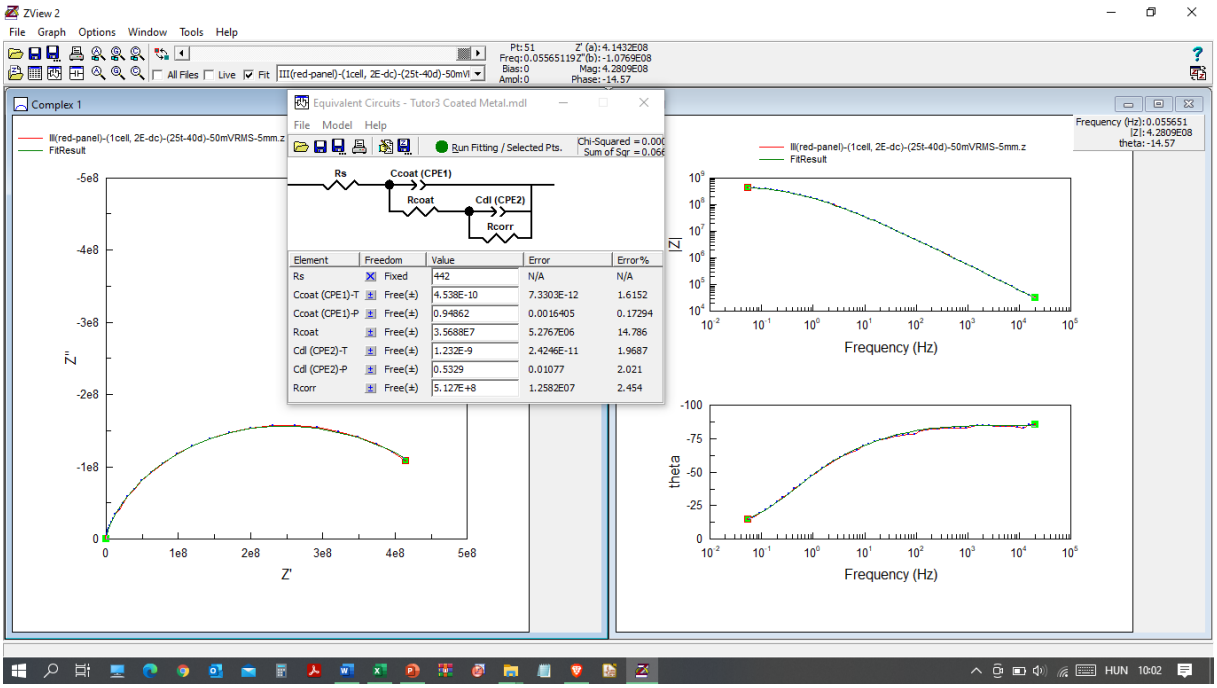

Figure A.48. Fitted impedance spectra measured with the large spiral wire electrode in a distance of 5 mm from the coating surface, at a test voltage of 50 mV.

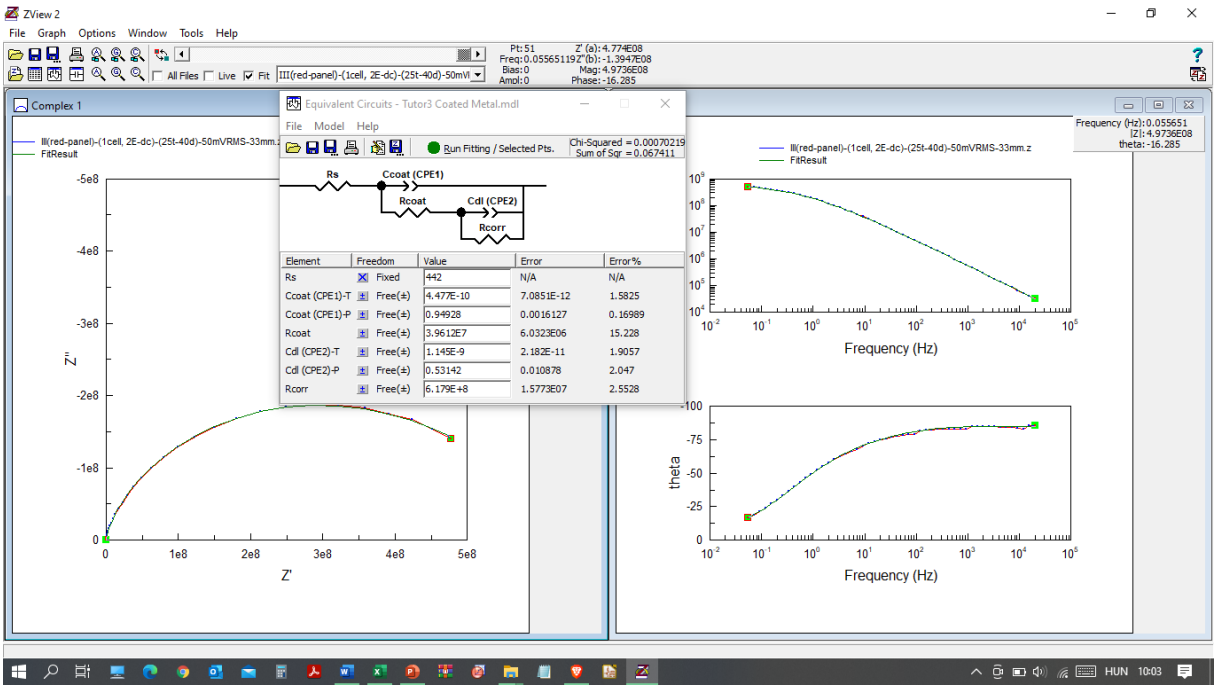

Figure A.49. Fitted impedance spectra measured with the large spiral wire electrode in a distance of 33 mm from the coating surface, at a test voltage of 50 mV.

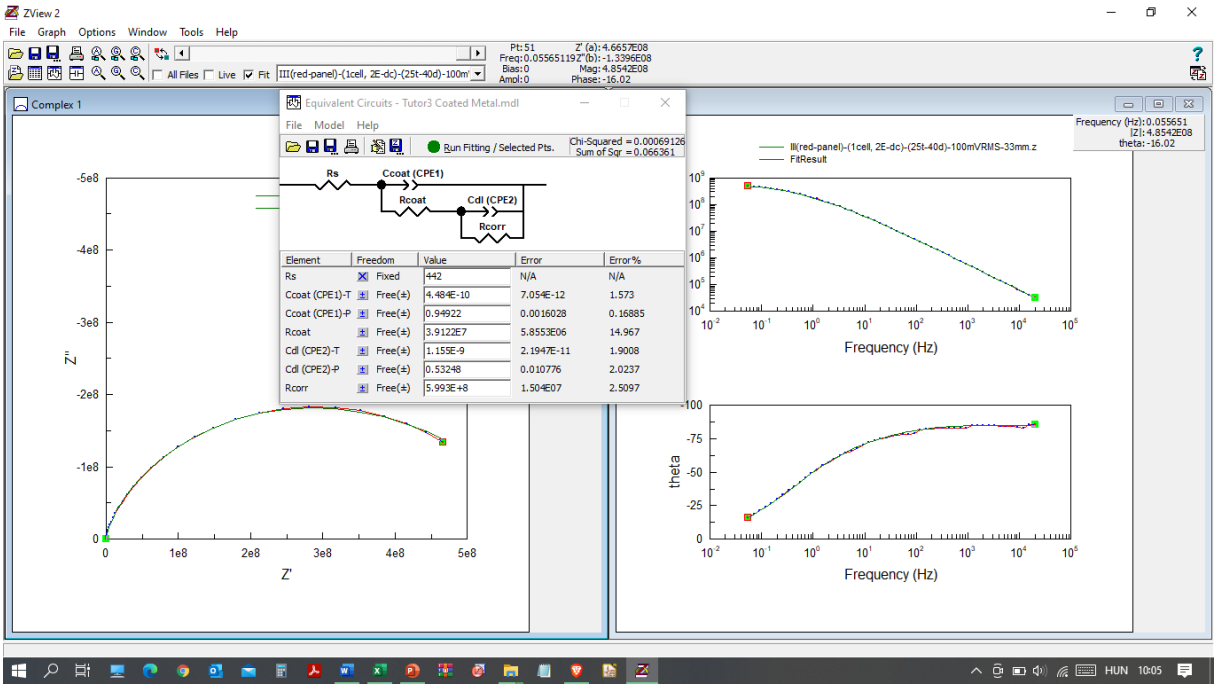

Figure A.50. Fitted impedance spectra measured with the large spiral wire electrode in a distance of 33 mm from the coating surface, at a test voltage of 100 mV.

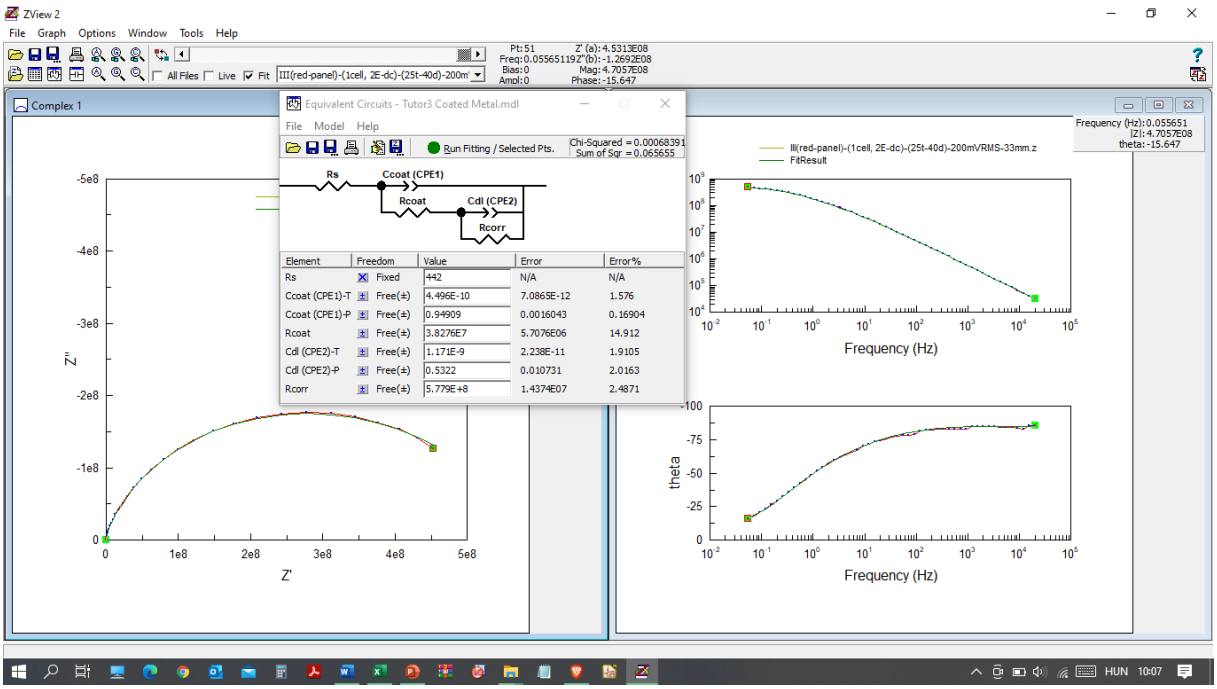

Figure A.51. Fitted impedance spectra measured with the large spiral wire electrode in a distance of 33 mm from the coating surface, at a test voltage of 200 mV.

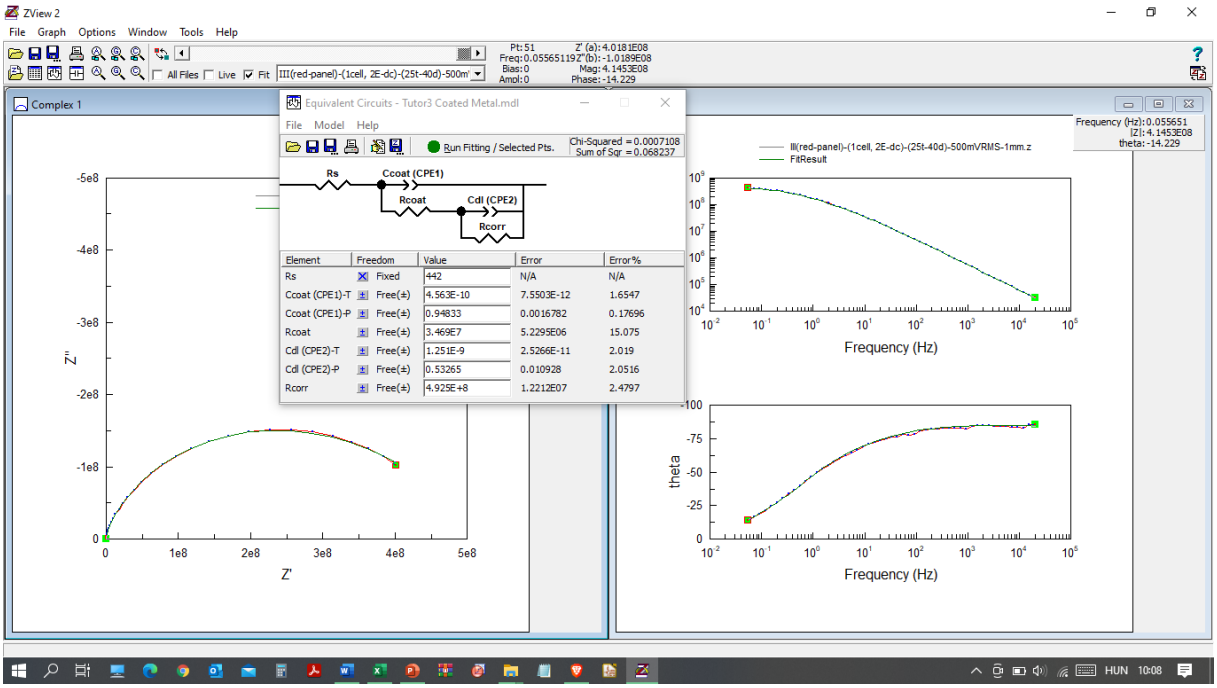

Figure A.52. Fitted impedance spectra measured with the large spiral wire electrode in a distance of 1 mm from the coating surface, at a test voltage of 500 mV.

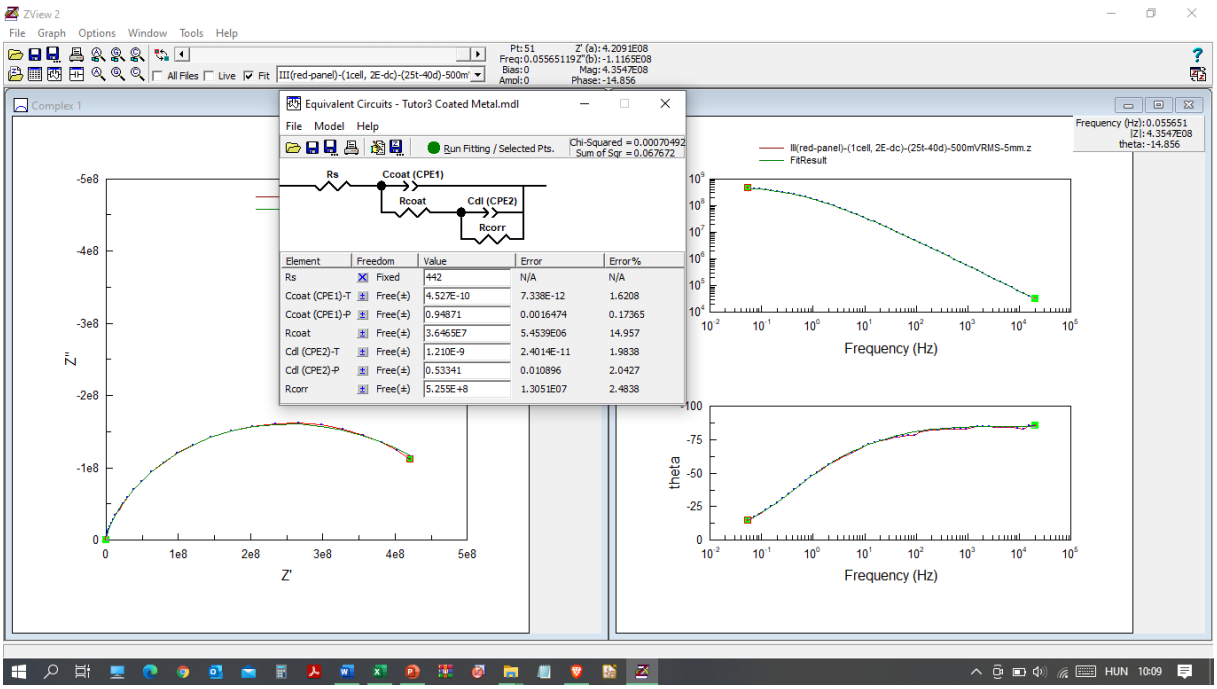

Figure A.53. Fitted impedance spectra measured with the large spiral wire electrode in a distance of 5 mm from the coating surface, at a test voltage of 500 mV.

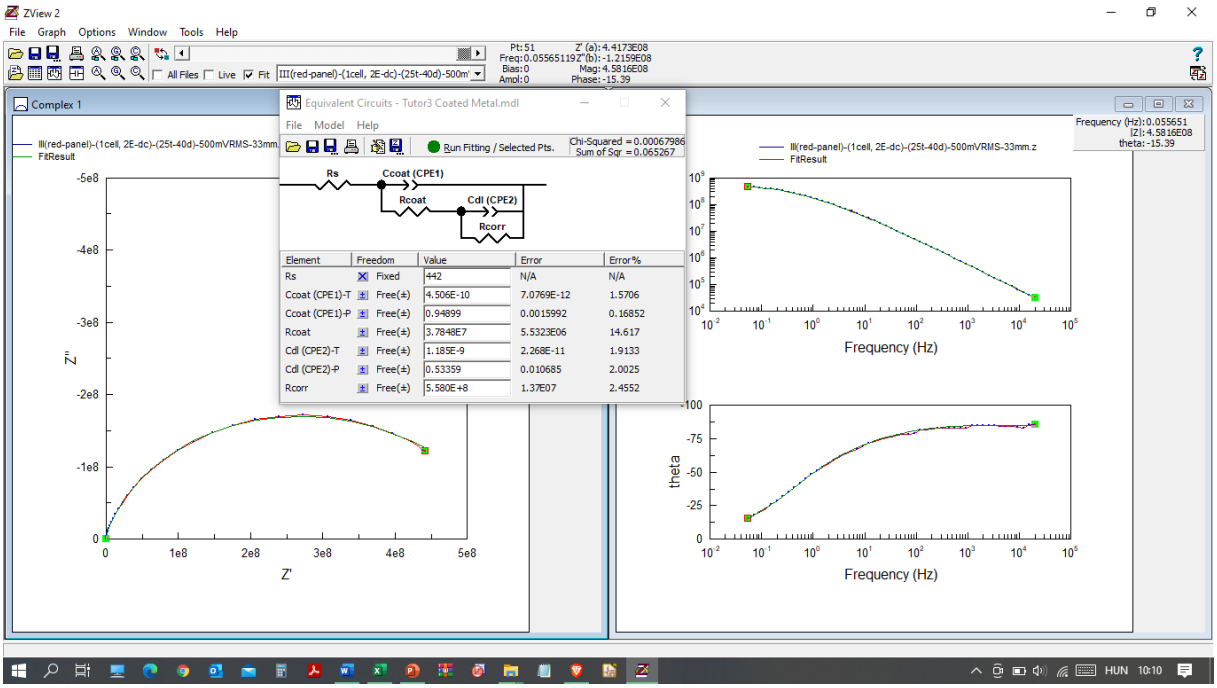

Figure A.54. Fitted impedance spectra measured with the large spiral wire electrode in a distance of 33 mm from the coating surface, at a test voltage of 500 mV.

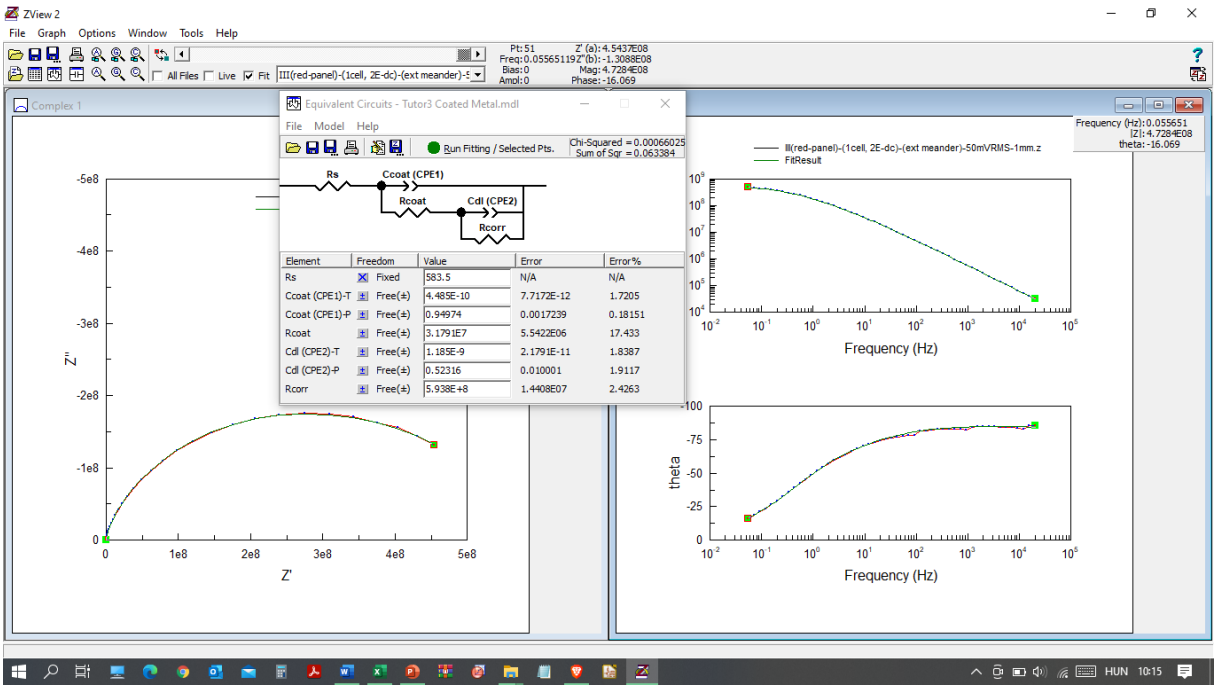

Figure A.55. Fitted impedance spectra measured with the extended meander wire electrode in a distance of 1 mm from the coating surface, at a test voltage of 50 mV.

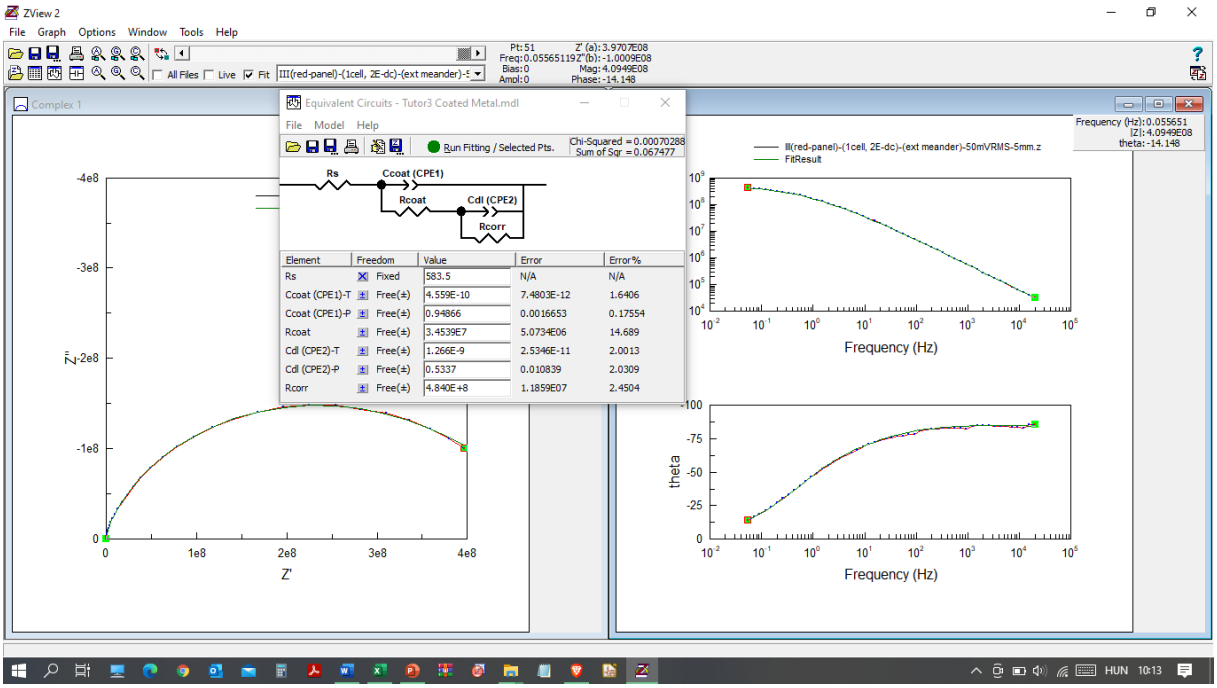

Figure A.56. Fitted impedance spectra measured with the extended meander wire electrode in a distance of 5 mm from the coating surface, at a test voltage of 50 mV.

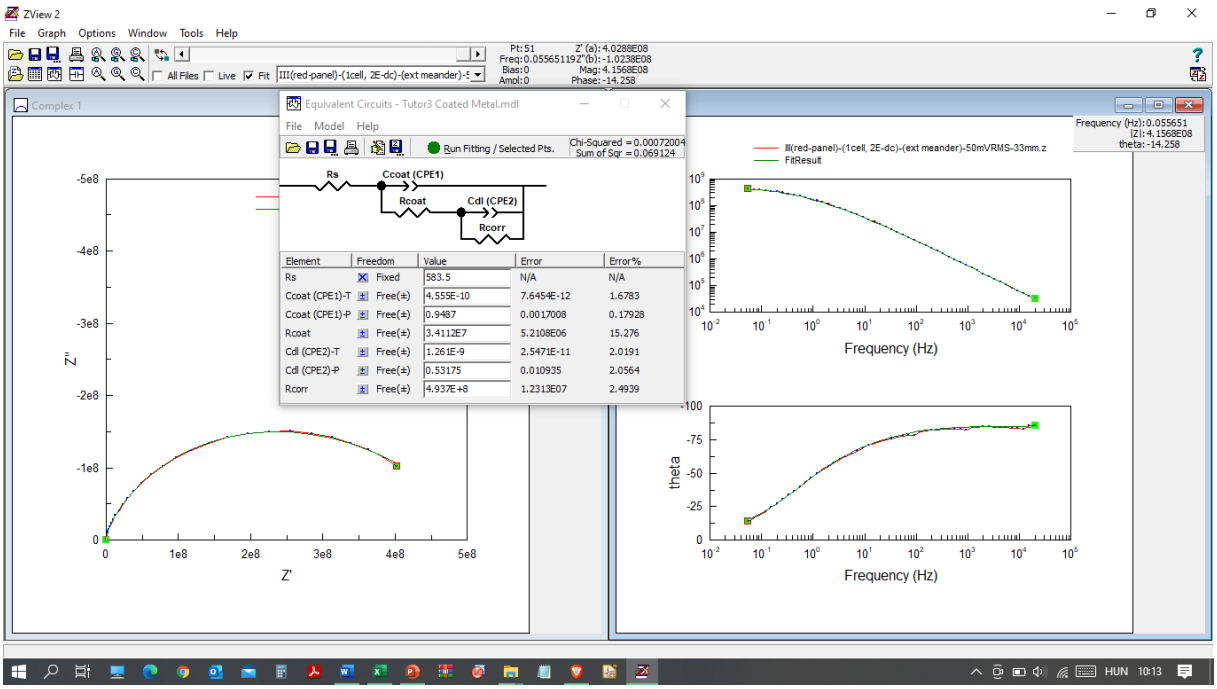

Figure A.57. Fitted impedance spectra measured with the extended meander wire electrode in a distance of 33 mm from the coating surface, at a test voltage of 50 mV.

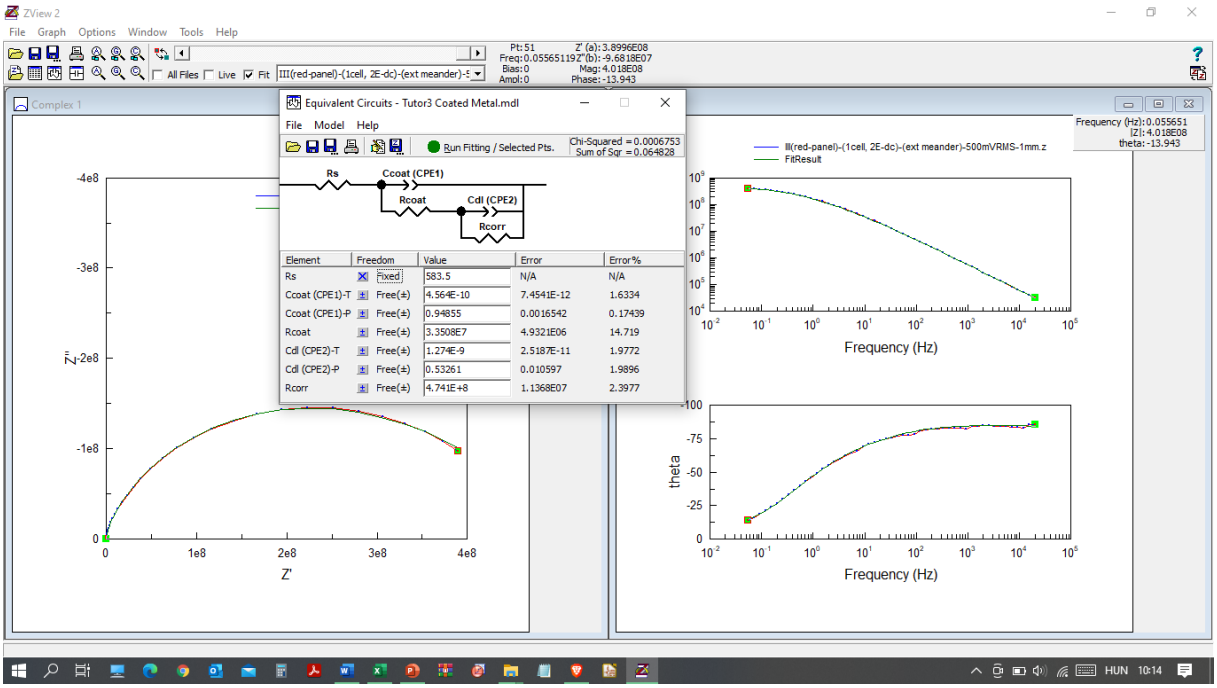

Figure A.58. Fitted impedance spectra measured with the extended meander wire electrode in a distance of 1 mm from the coating surface, at a test voltage of 500 mV.

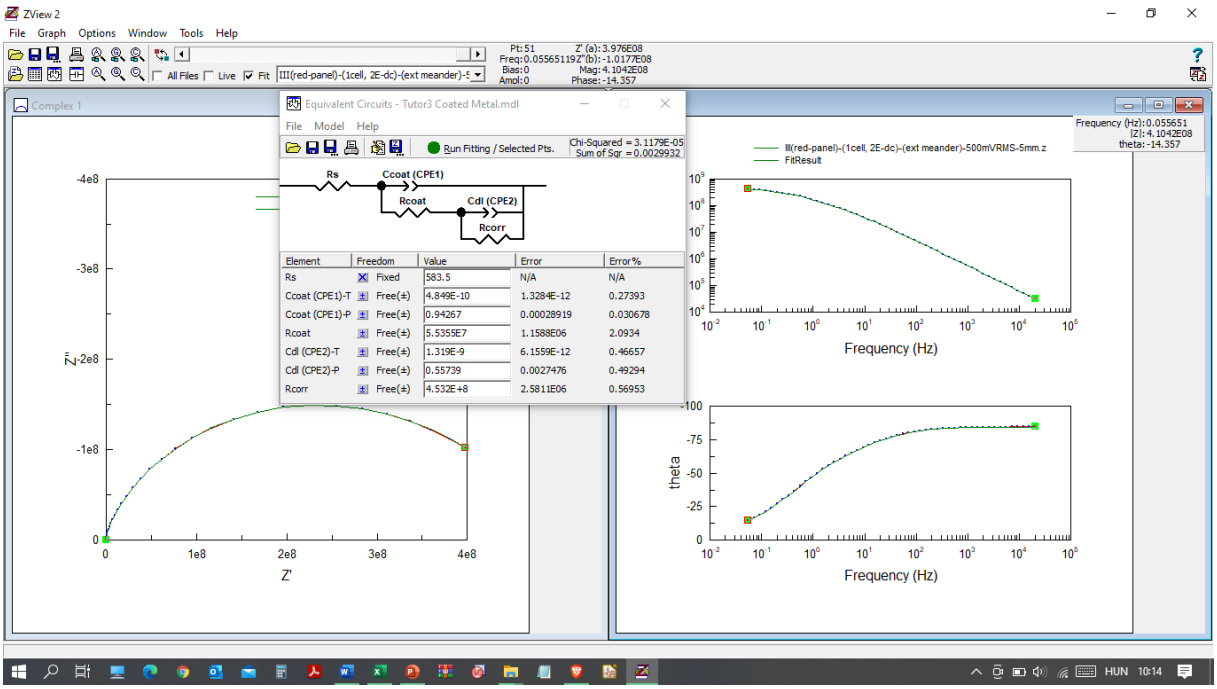

Figure A.59. Fitted impedance spectra measured with the extended meander wire electrode in a distance of 5 mm from the coating surface, at a test voltage of 500 mV.

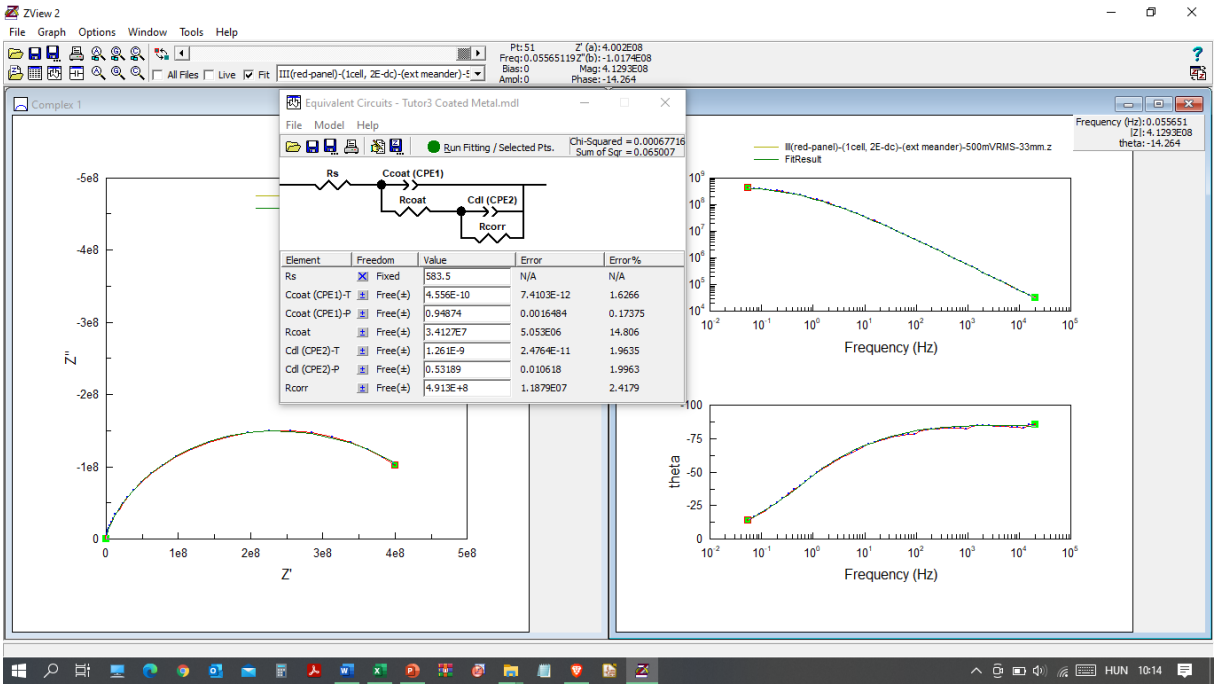

Figure A.60. Fitted impedance spectra measured with the extended meander wire electrode in a distance of 33 mm from the coating surface, at a test voltage of 500 mV.

Appendix 2 Design Cycle II – Interdigitated Electrodes

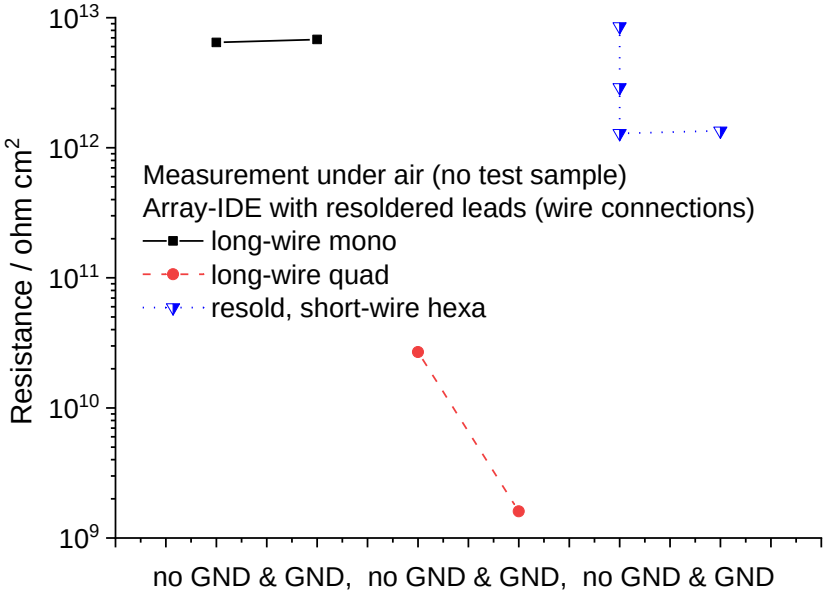

Figure A.61. Resistance to the sensor testing under air with back-plate shielding free or no ground (GND) and grounded (GND) shielding configurations of the mono-, quad- and hexa-array IDEs.

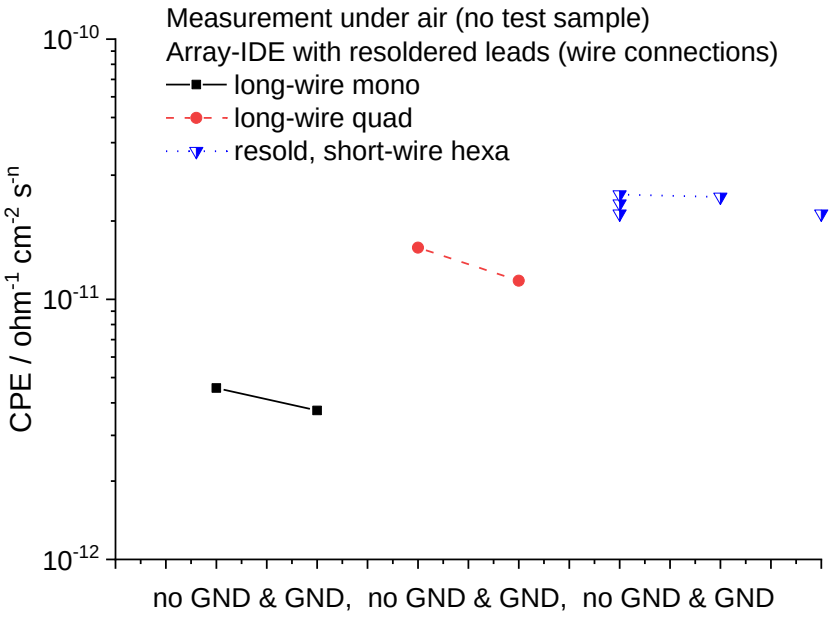

Figure A.62. CPE data to the sensor testing under air with back-plate shielding free or no ground (GND) and grounded (GND) shielding configurations of the mono-, quad- and hexa-array IDEs.

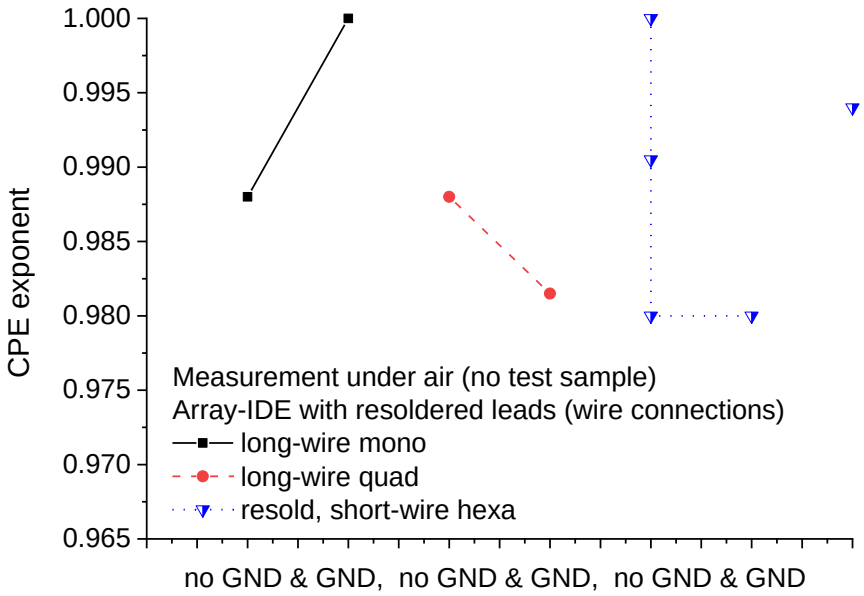

Figure A.63. CPE exponents to the sensor testing under air with back-plate shielding free or no ground (GND) and grounded (GND) shielding configurations of the mono-, quad- and hexa-array IDEs.

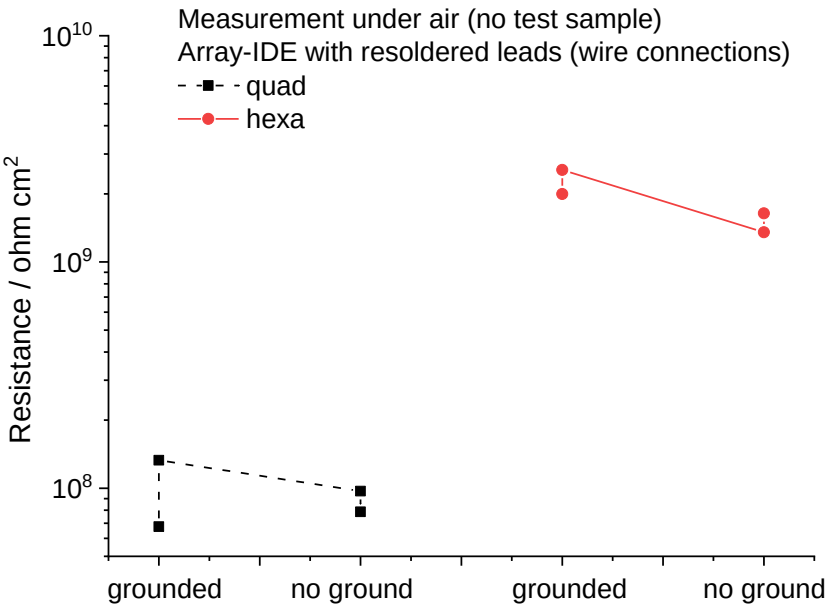

Figure A.64. Resistance of resoldered sensors tested under air with back-plate shielding free, no ground (GND) and grounded (GND) shielding configurations of the quad- and hexa-array IDEs.

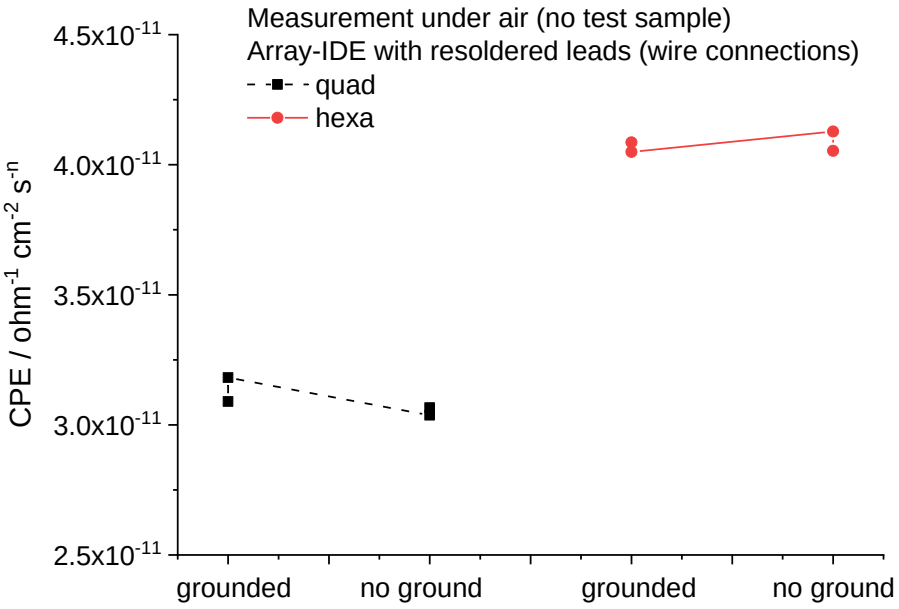

Figure A.65. CPE data of resoldered sensors tested under air with back-plate shielding free, no ground (GND) and grounded (GND) shielding configurations of the quad- and hexa-array IDEs.

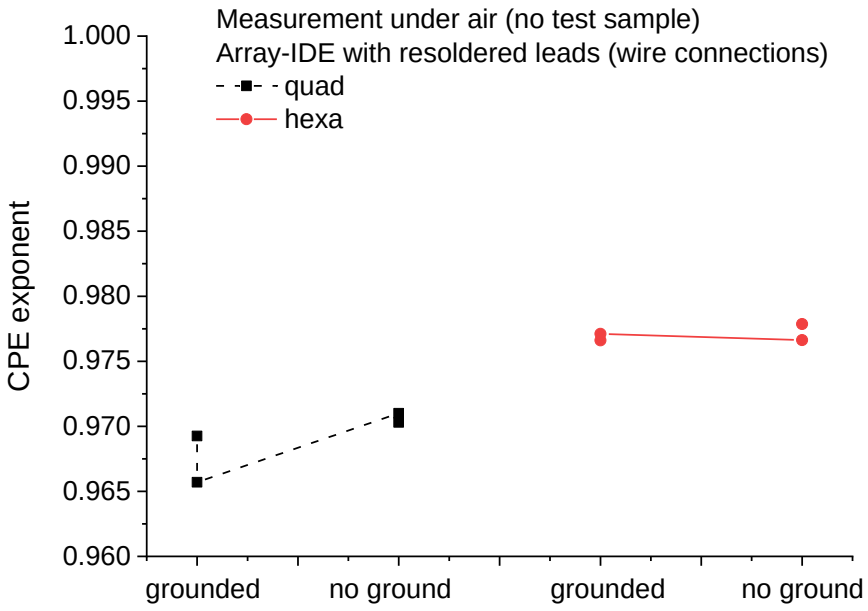

Figure A.66. CPE exponents to the resoldered sensors tested under air with back-plate shielding free, no ground (GND) and grounded (GND) shielding configurations of the quad- and hexa-array IDEs.

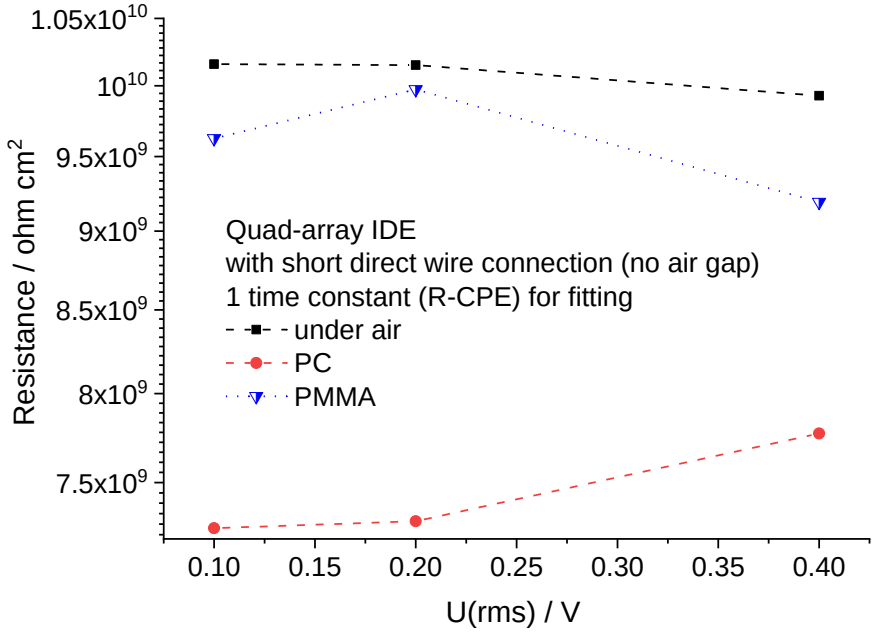

Figure A.67. Resistance measured with direct-wire connected quad-array IDE under air, polycarbonate and poly-methyl methacrylate materials at varied AC testing voltages. Spectra data derived with an equivalent circuit containing one parallel connected resistor and CPE, which coupled with a resistive element in series, schematic circuit logic: R(R/CPE).

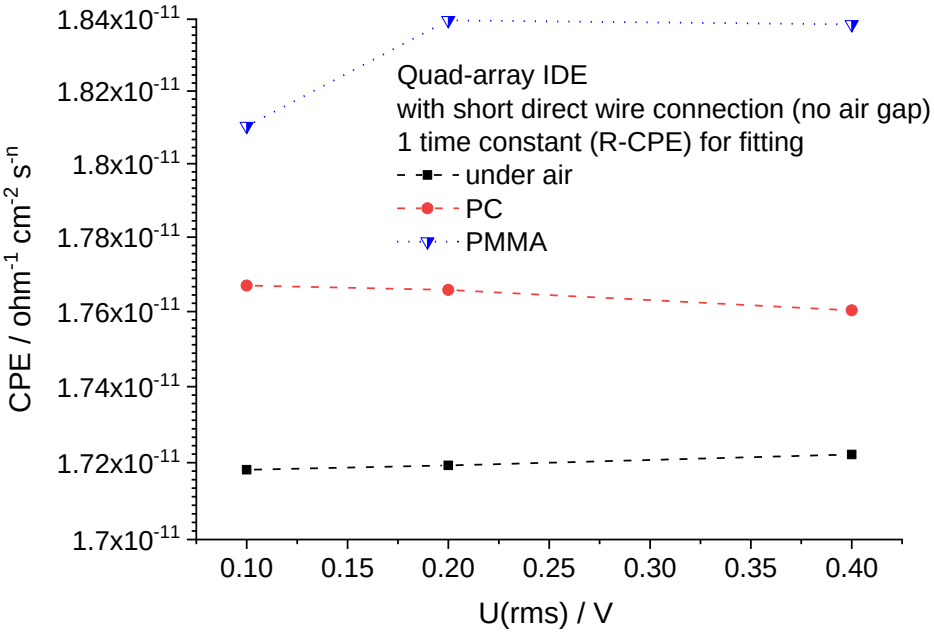

Figure A.68. CPE(single) results derived from impedance data obtained with direct-wire connected quad-array IDE under air, polycarbonate and poly-methyl methacrylate materials at varied AC testing voltages. Spectra fitting with the same model (circuit: R(R/CPE) as mentioned in caption of Figure A.67.

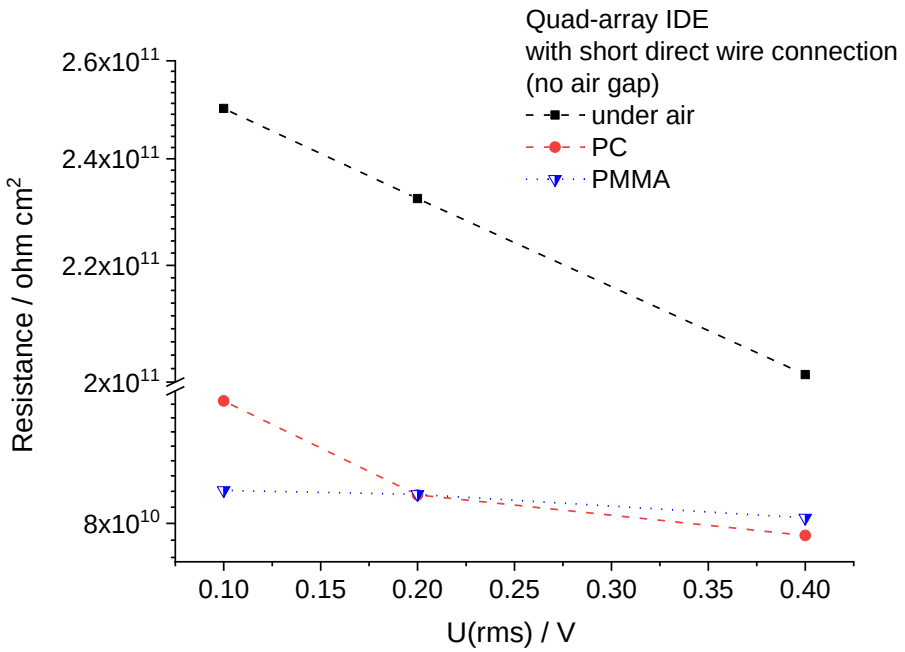

Figure A.69. Resistance measured with direct-wire connected quad-array IDE under air, polycarbonate and poly-methyl methacrylate materials at varied AC testing voltages. Spectra data derived with an equivalent circuit containing one parallel connected resistor and CPE(1), which coupled with another CPE(2) in parallel and a resistive element in series (circuit: R((R/CPE(1))/CPE(2))).

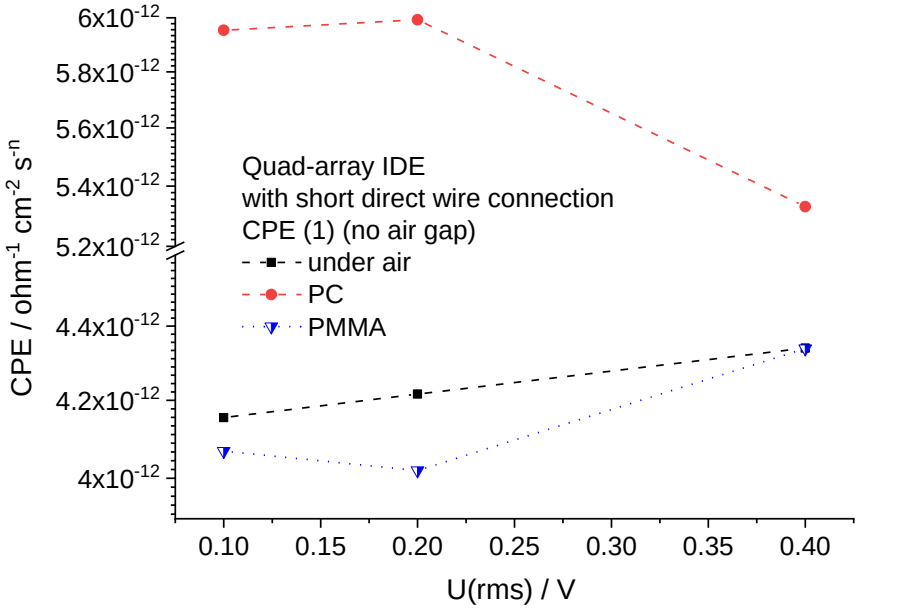

Figure A.70. CPE(1) results derived from impedance data obtained with direct-wire connected quad-array IDE under air, polycarbonate and poly-methyl methacrylate materials at varied AC testing voltages. Spectra data derived with an equivalent circuit (R((R/CPE(1))/CPE(2))) the same as given in Figure A.69.

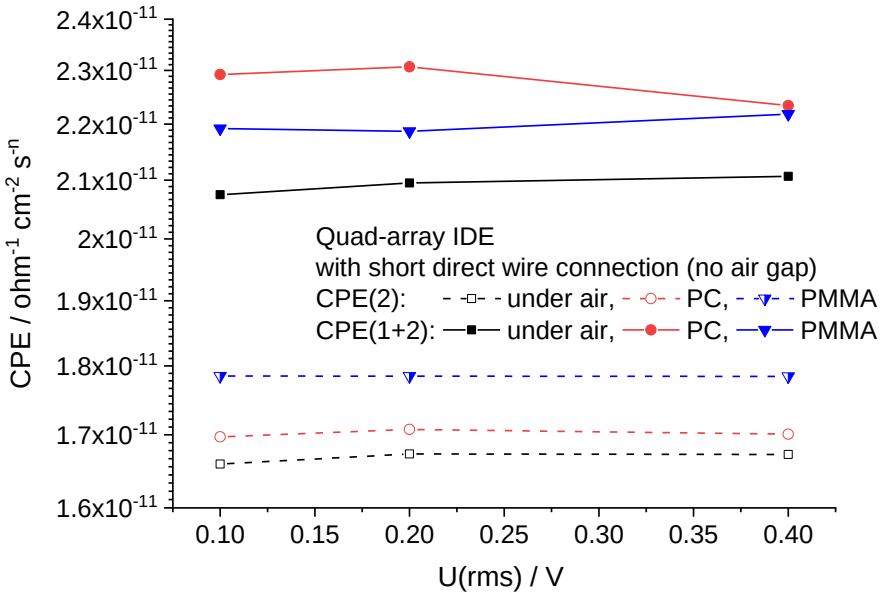

Figure A.71. CPE(2) and CPE(1+2) results derived from impedance data obtained with direct-wire connected quad-array IDE under air, polycarbonate and poly-methyl methacrylate materials at varied AC testing voltages. Spectra data derived with an equivalent circuit (R((R/CPE(1))/CPE(2))) the same as given in Figure A.69.

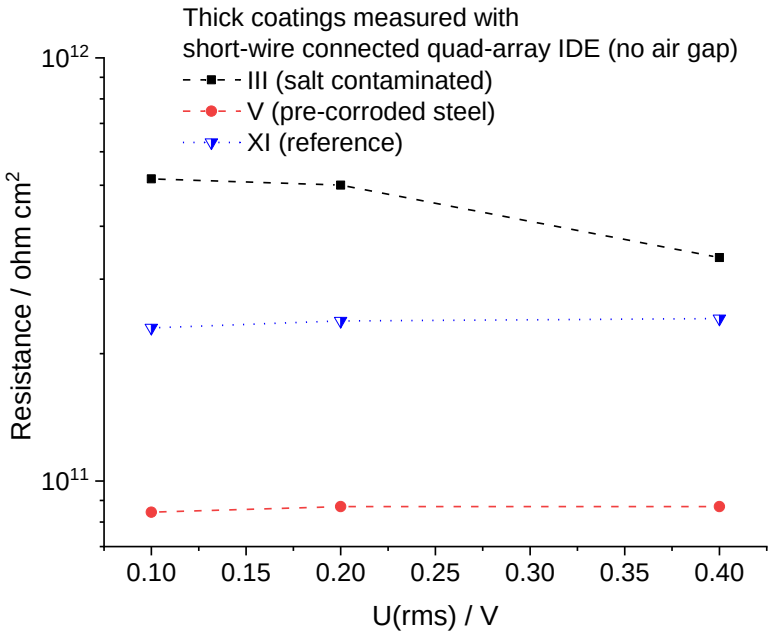

Figure A.72. Resistance measured with direct-wire connected quad-array IDE on thick epoxy coatings: salt contaminated (III), pre-corroded steel (V) and reference (XI) samples, at varied AC testing voltages. Spectra data derived with an equivalent circuit containing one parallel connected resistor and CPE(1), which coupled with another CPE(2) in parallel and a resistive element in series (circuit: R((R/CPE(1))/CPE(2))).

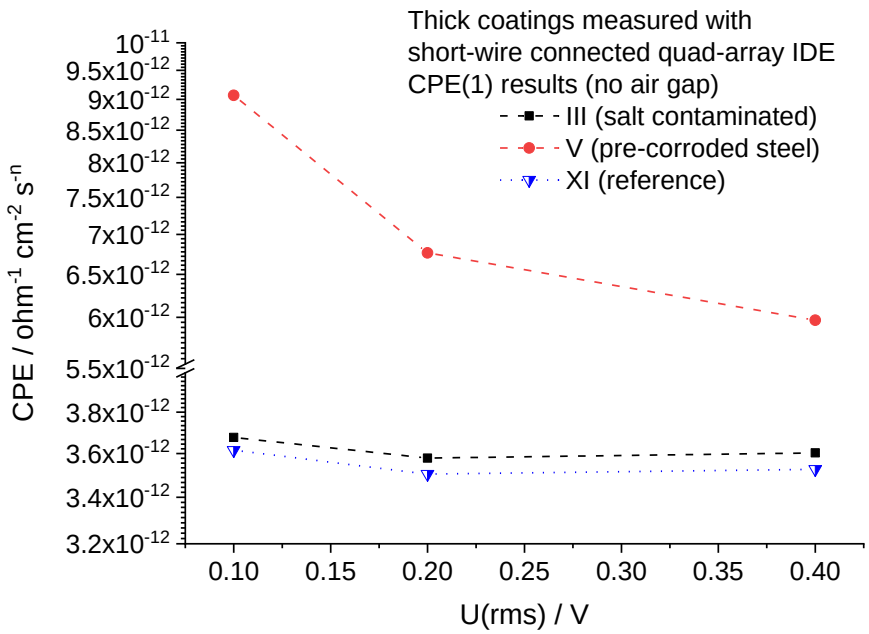

Figure A.73. CPE(1) results derived from impedance data obtained with direct-wire connected quad-array IDE on thick epoxy coatings: salt contaminated (III), pre-corroded steel (V) and reference (XI) samples at varied AC testing voltages. Spectra data derived with an equivalent circuit (R((R/CPE(1))/CPE(2))) the same as given in Figure A.72.

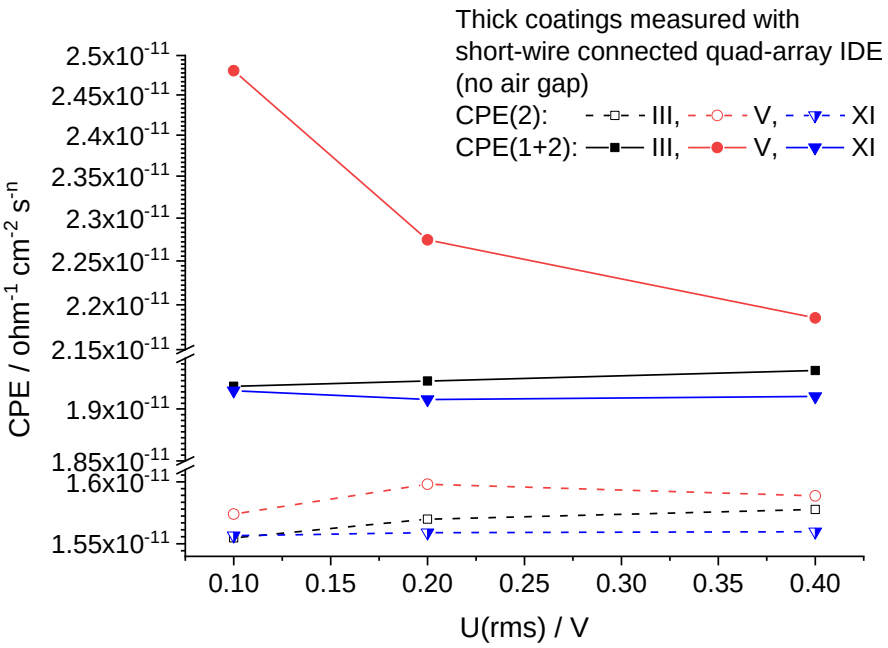

Figure A.74. CPE(2) and CPE(1+2) results derived from impedance data obtained with direct-wire connected quad-array IDE on thick epoxy coatings: salt contaminated (III), pre-corroded steel (V) and reference (XI) samples at varied AC testing voltages. Spectra data derived with an equivalent circuit (R((R/CPE(1))/CPE(2))) the same as given in Figure A.72.

Measured impedance data without any derivation along with topology of circuits of electrical circuits and fitting results are summarised in the following.

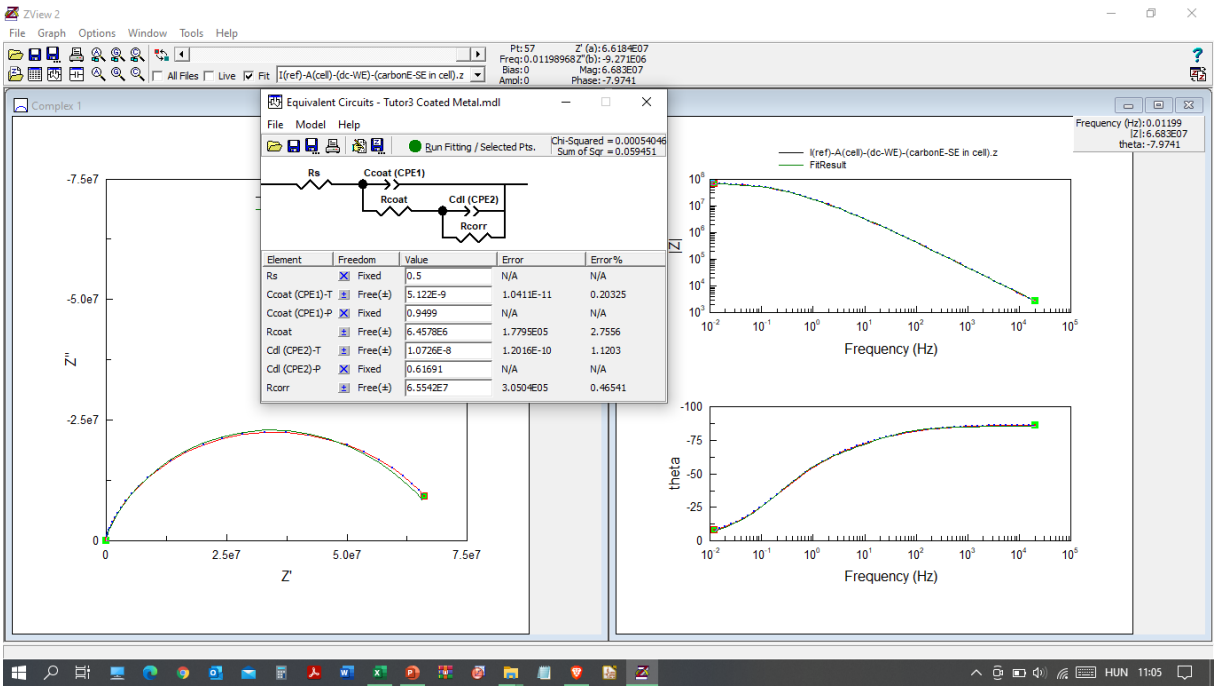

Figure A.75. The PMMA-CE characterised ‘A’ area of the reference (I) type ‘thin red’ coating sample in intact state, measured with direct wire connection to the substrate (one cell configuration).

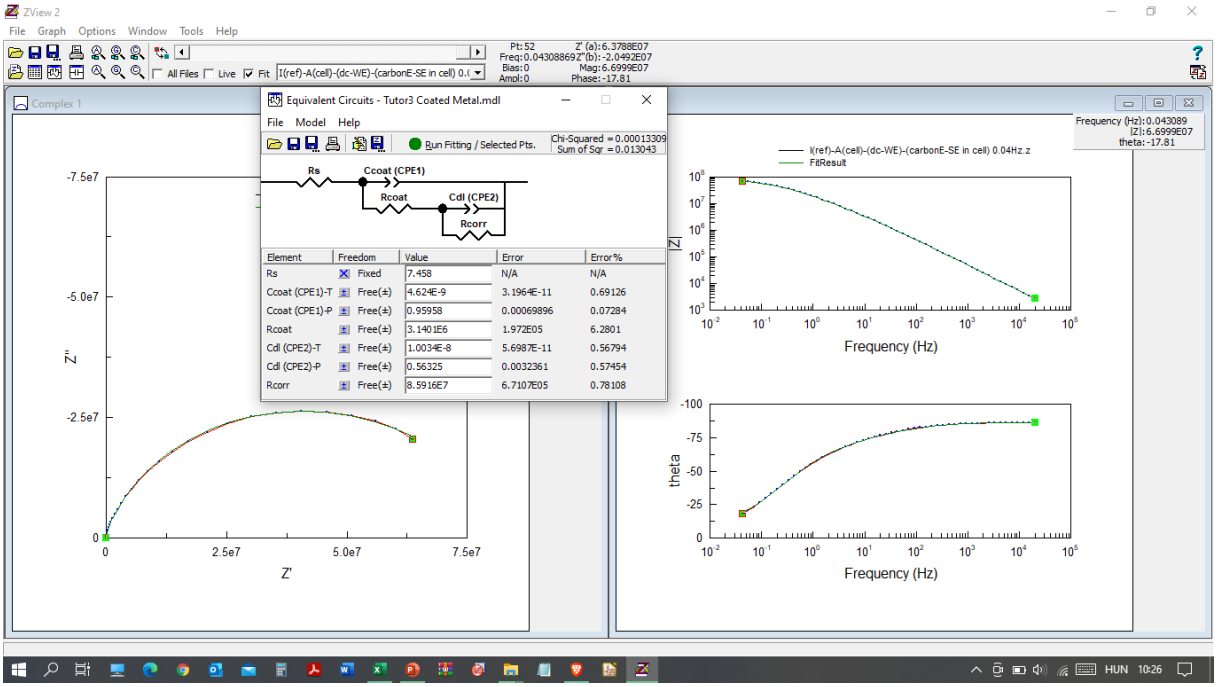

Figure A.76. The PMMA-CE characterised ‘A’ area of the reference (I) type ‘thin red’ coating sample in medium exposed state, measured with direct wire connection to the substrate (one cell configuration).

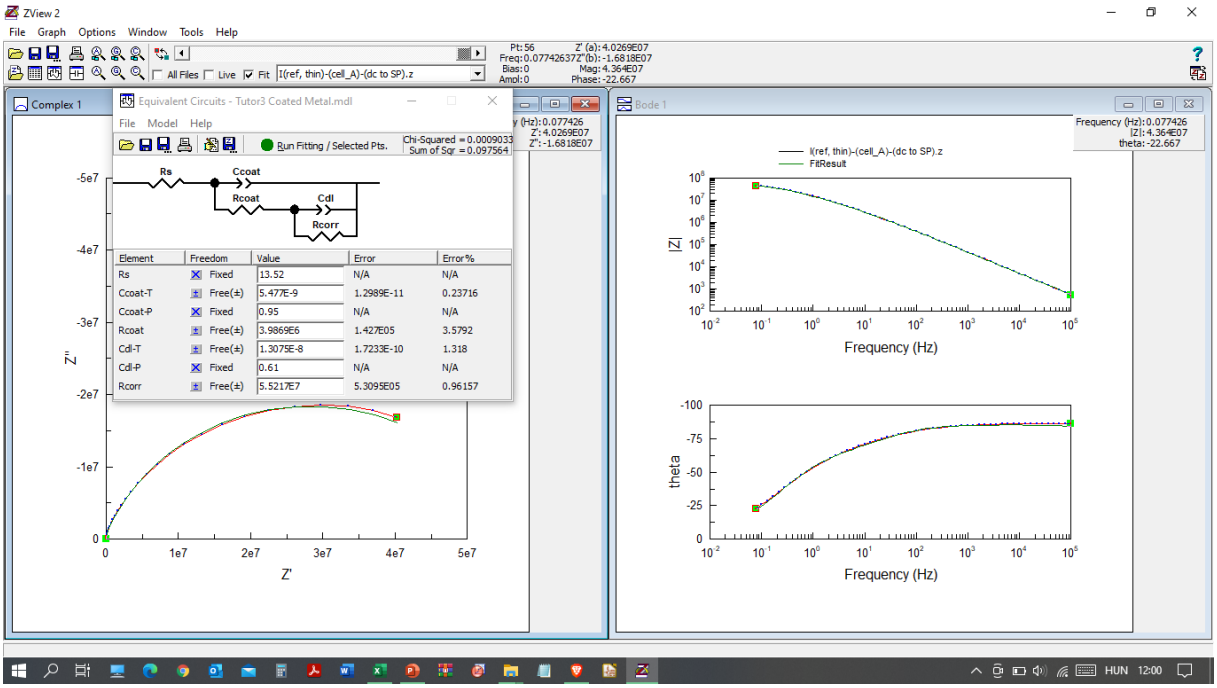

Figure A.77. The PMMA-CE characterised ‘A’ area of the reference (I) type ‘thin red’ coating sample in exposed state, measured with direct wire connection to the substrate (one cell configuration).

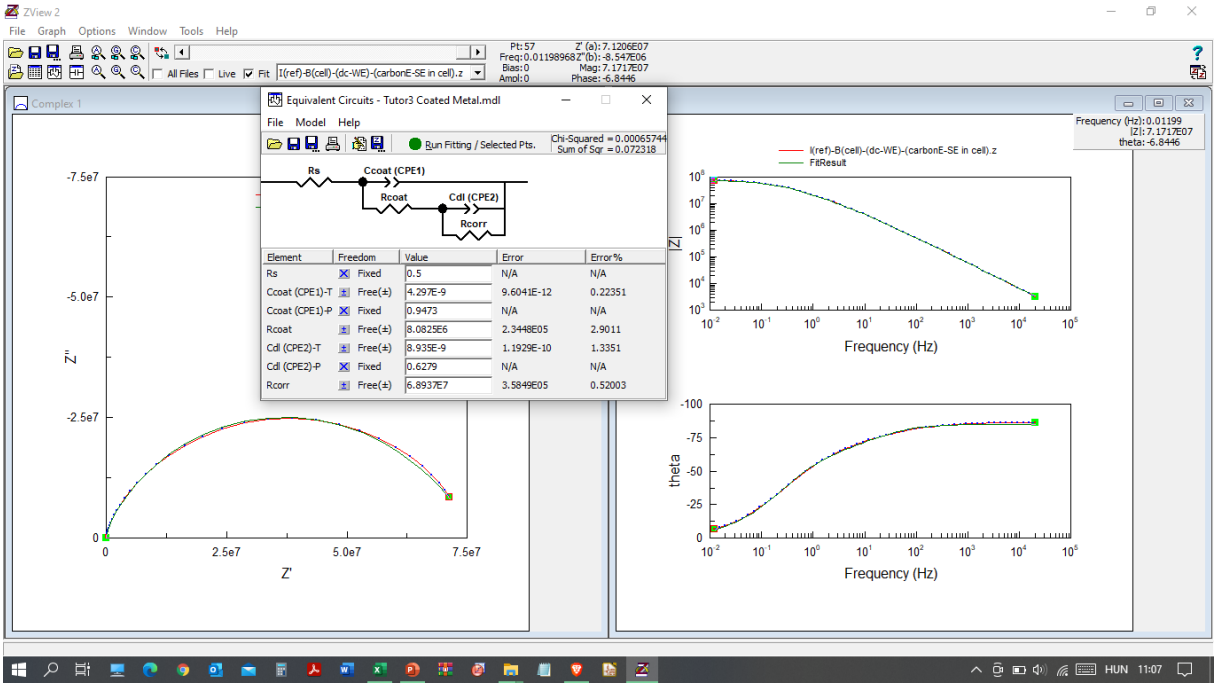

Figure A.78. The PMMA-CE characterised ‘B’ area of the reference (I) type ‘thin red’ coating sample in intact state, measured with direct wire connection to the substrate (one cell configuration).

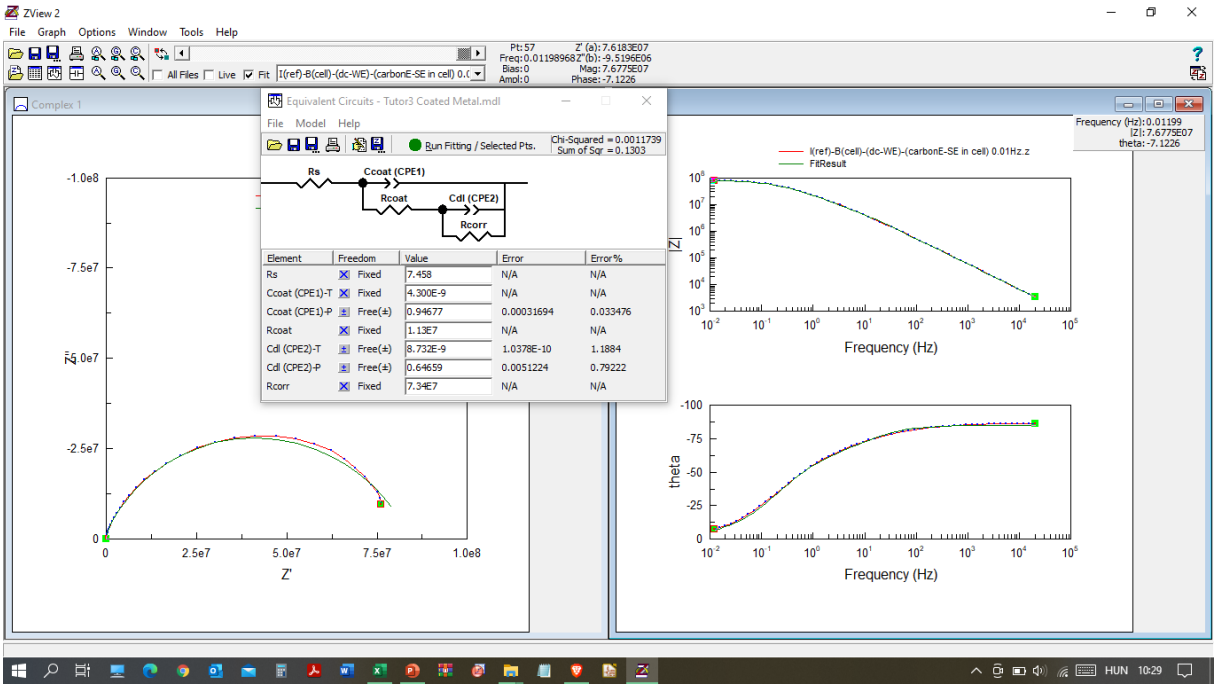

Figure A.79. The PMMA-CE characterised ‘B’ area of the reference (I) type ‘thin red’ coating sample in medium exposed state, measured with direct wire connection to the substrate (one cell configuration).

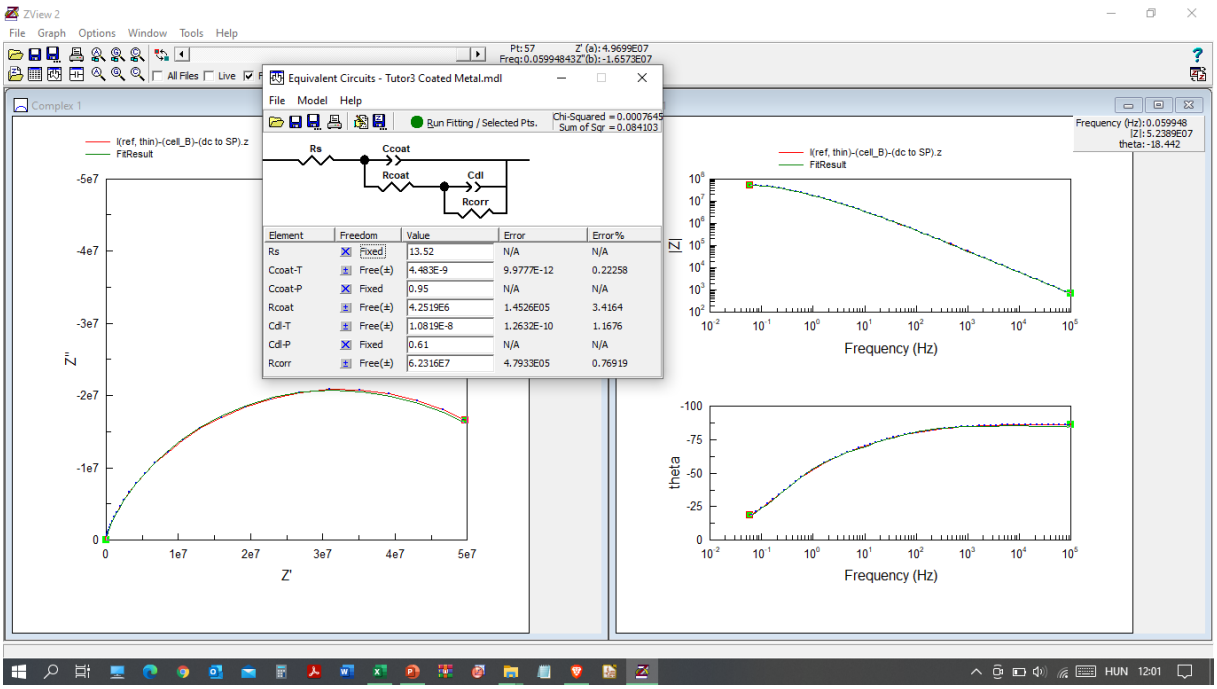

Figure A.80. The PMMA-CE characterised ‘B’ area of the reference (I) type ‘thin red’ coating sample in exposed state, measured with direct wire connection to the substrate (one cell configuration).

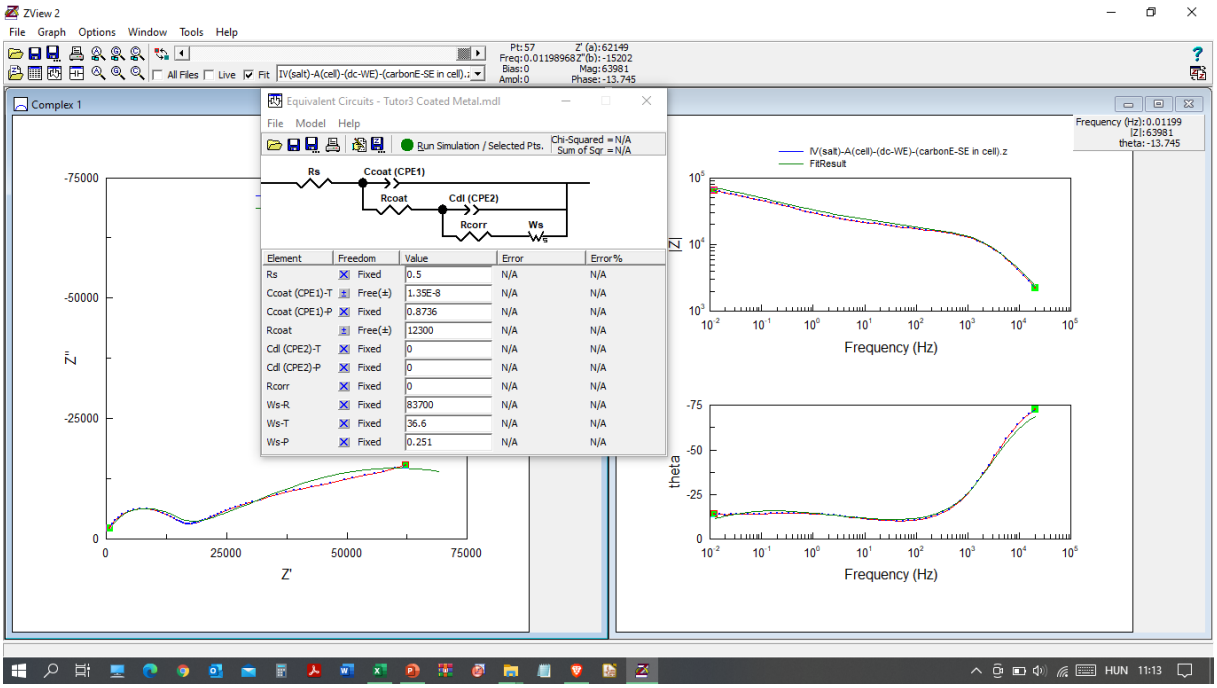

Figure A.81. The PMMA-CE characterised ‘A’ area of the salt contaminated (IV) type ‘thin red’ coating sample in intact state, measured with direct wire connection to the substrate (one cell configuration).

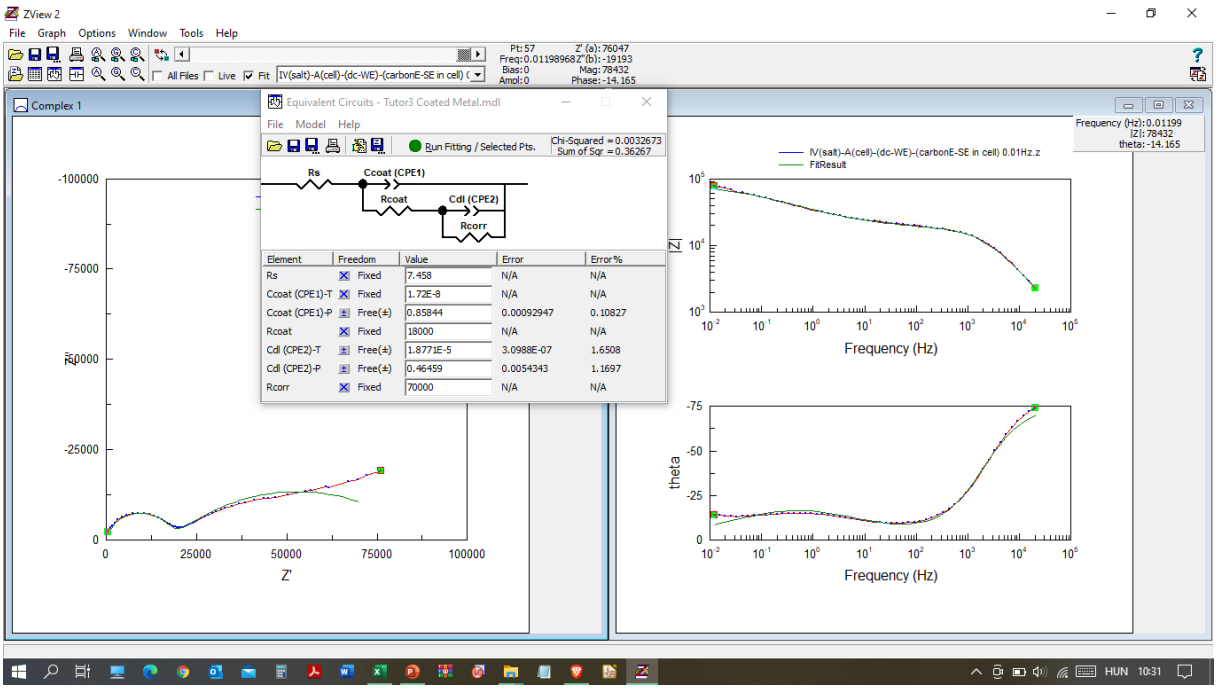

Figure A.82. The PMMA-CE characterised ‘A’ area of the salt contaminated (IV) type ‘thin red’ coating sample in medium exposed state, measured with direct wire connection to the substrate (one cell configuration).

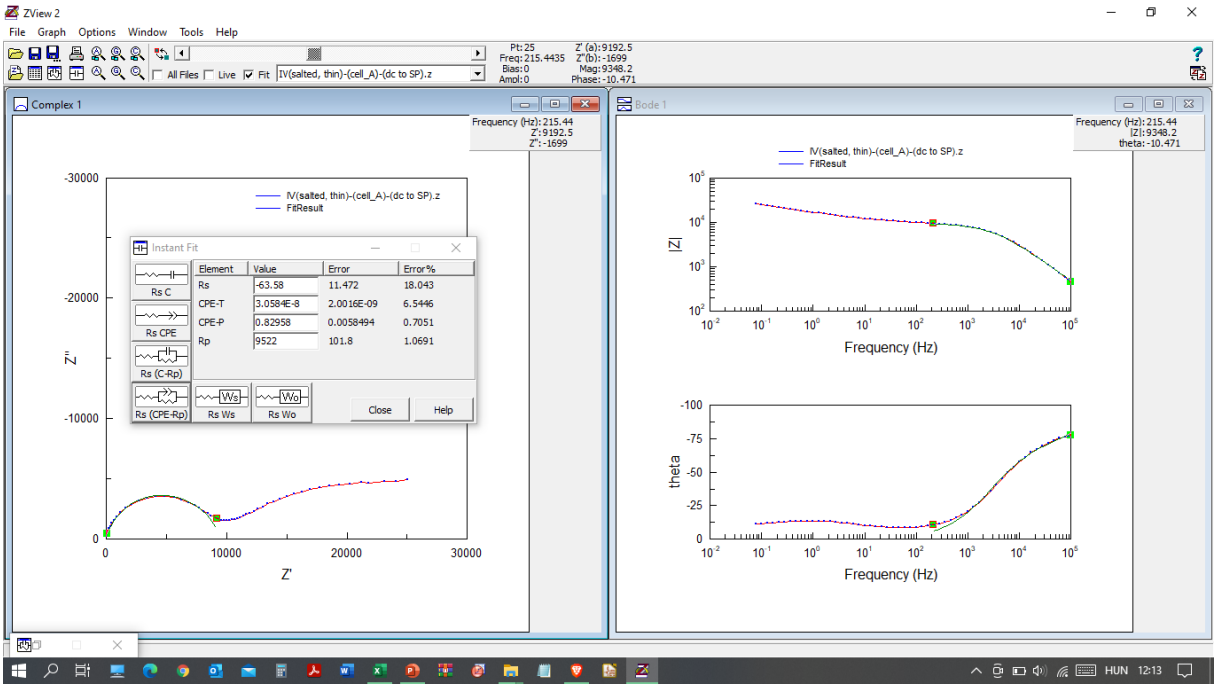

Figure A.83. The PMMA-CE characterised ‘A’ area of the salt contaminated (IV) type ‘thin red’ coating sample in exposed state, measured with direct wire connection to the substrate (one cell configuration).

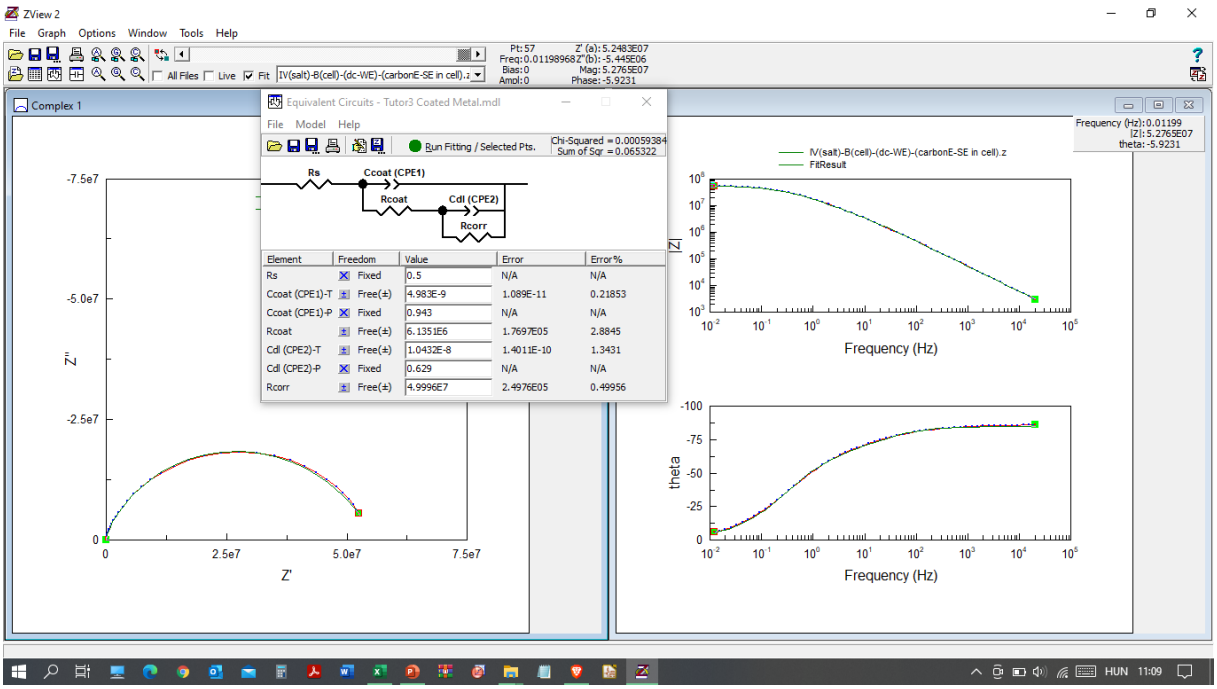

Figure A.84. The PMMA-CE characterised ‘B’ area of the salt contaminated (IV) type ‘thin red’ coating sample in intact state, measured with direct wire connection to the substrate (one cell configuration).

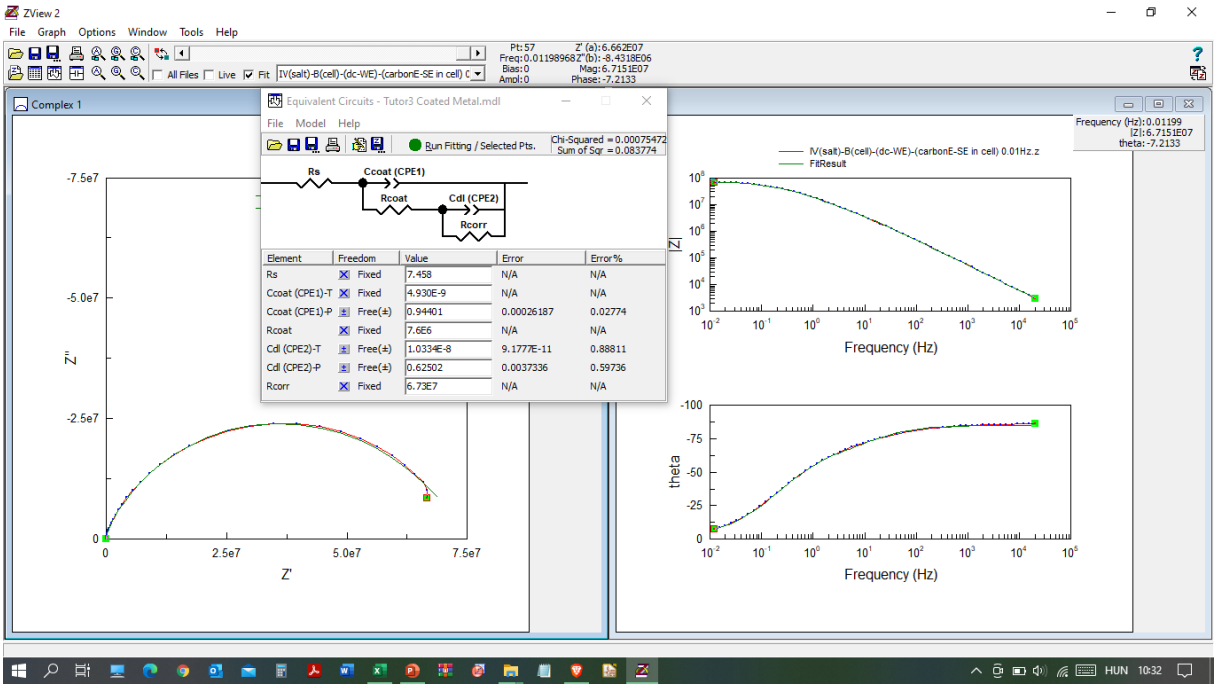

Figure A.85. The PMMA-CE characterised ‘B’ area of the salt contaminated (IV) type ‘thin red’ coating sample in medium exposed state, measured with direct wire connection to the substrate (one cell configuration).

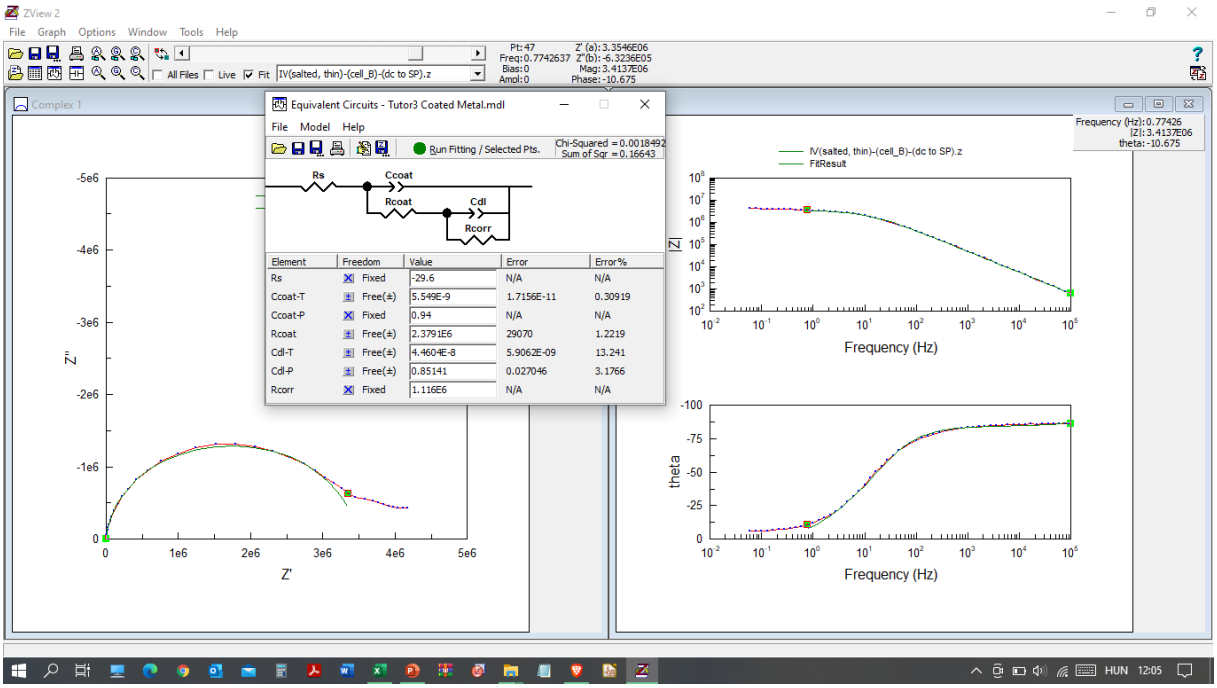

Figure A.86. The PMMA-CE characterised ‘B’ area of the salt contaminated (IV) type ‘thin red’ coating sample in exposed state, measured with direct wire connection to the substrate (one cell configuration).

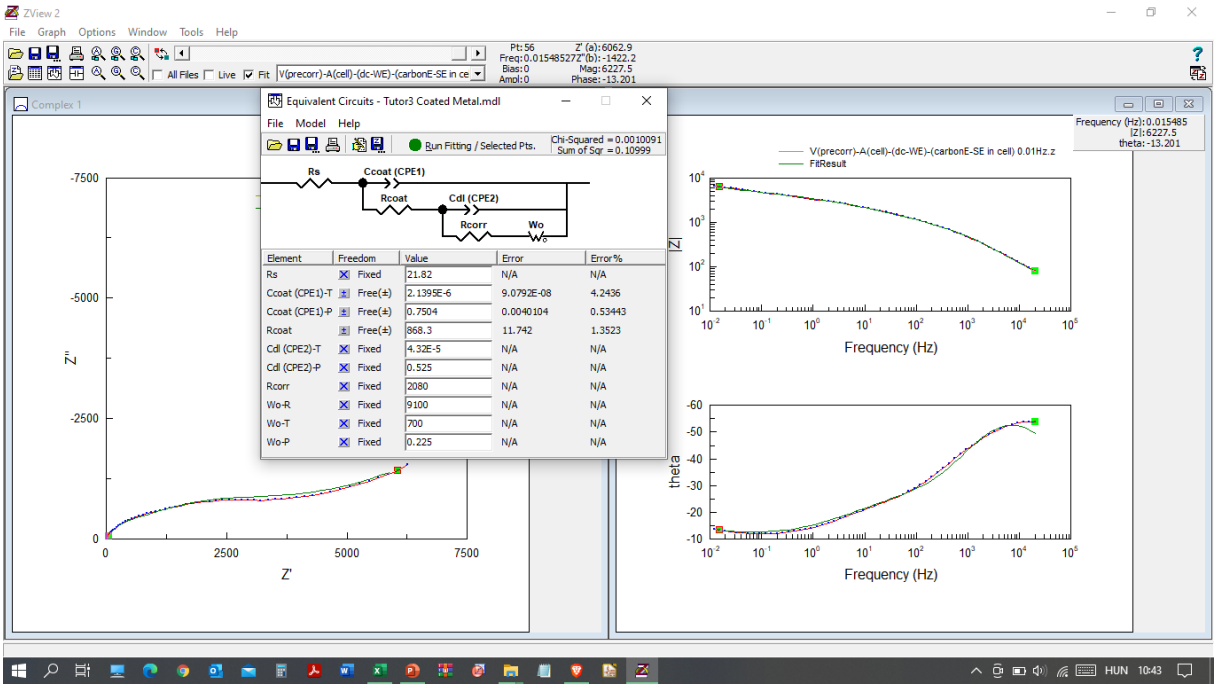

Figure A.87. The PMMA-CE characterised ‘A’ area of the pre-corroded (V) type ‘thin red’ coating sample in intact state, measured with direct wire connection to the substrate (one cell configuration).

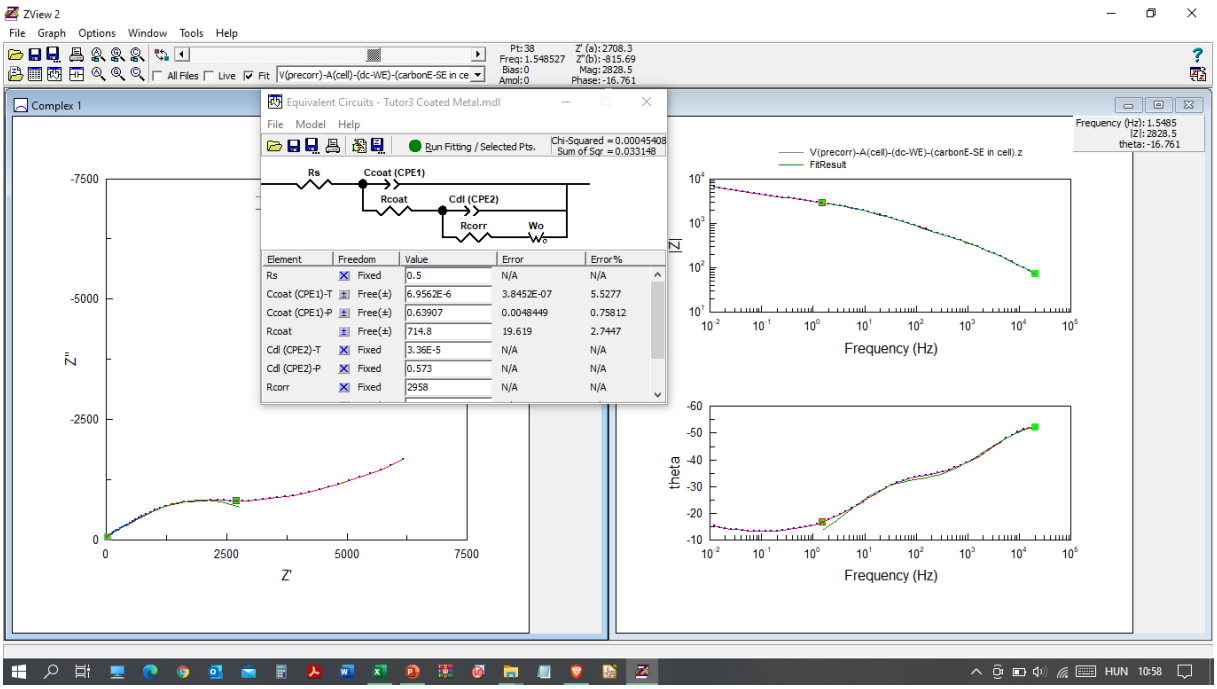

Figure A.88. The PMMA-CE characterised ‘A’ area of the pre-corroded (V) type ‘thin red’ coating sample in medium exposed state, measured with direct wire connection to the substrate (one cell configuration).

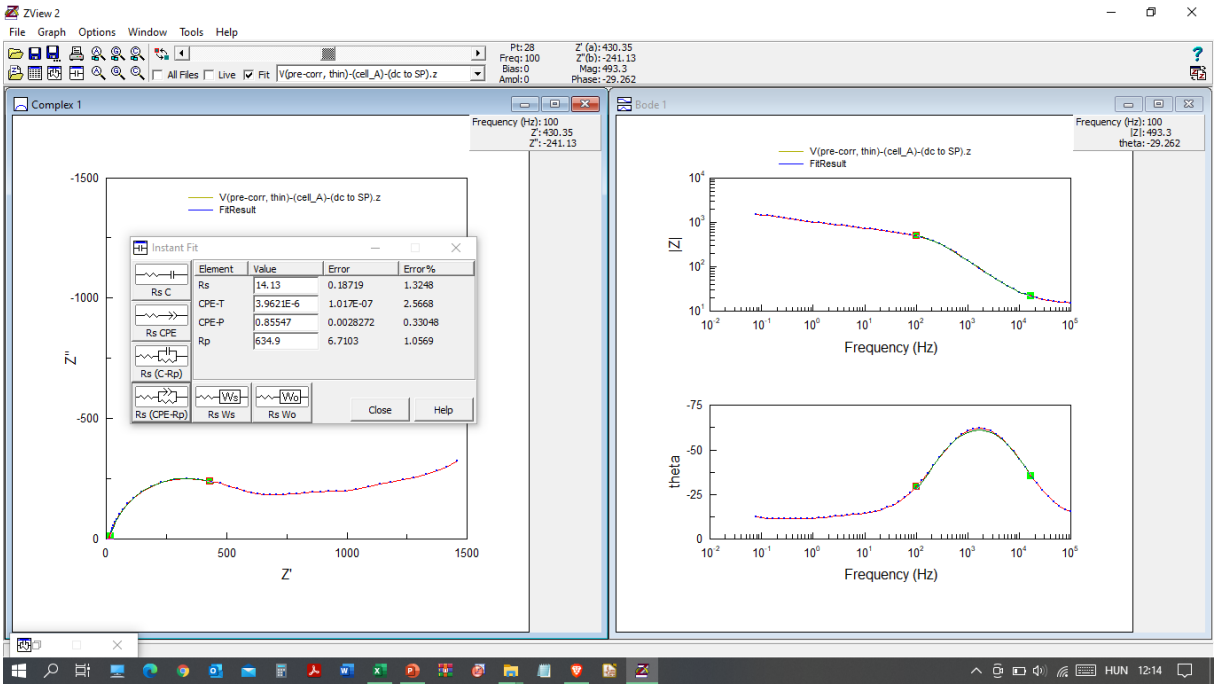

Figure A.89. The PMMA-CE characterised ‘A’ area of the pre-corroded (V) type ‘thin red’ coating sample in exposed state, measured with direct wire connection to the substrate (one cell configuration).

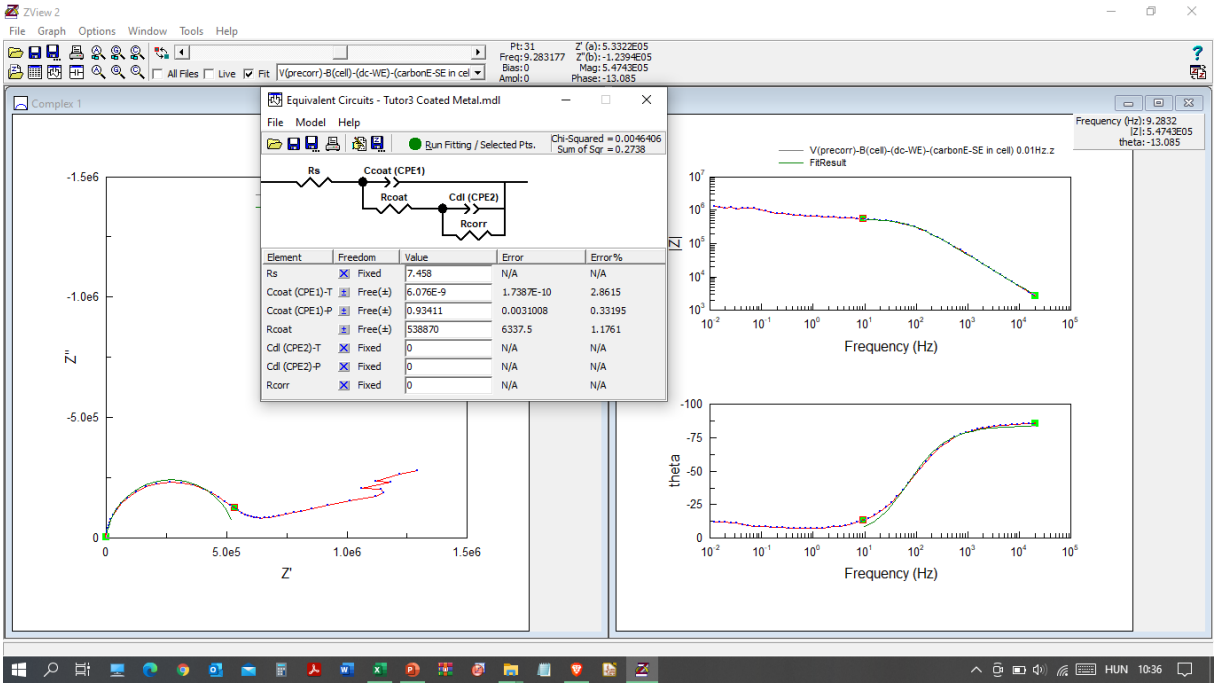

Figure A.90. The PMMA-CE characterised ‘B’ area of the pre-corroded (V) type ‘thin red’ coating sample in intact state, measured with direct wire connection to the substrate (one cell configuration).

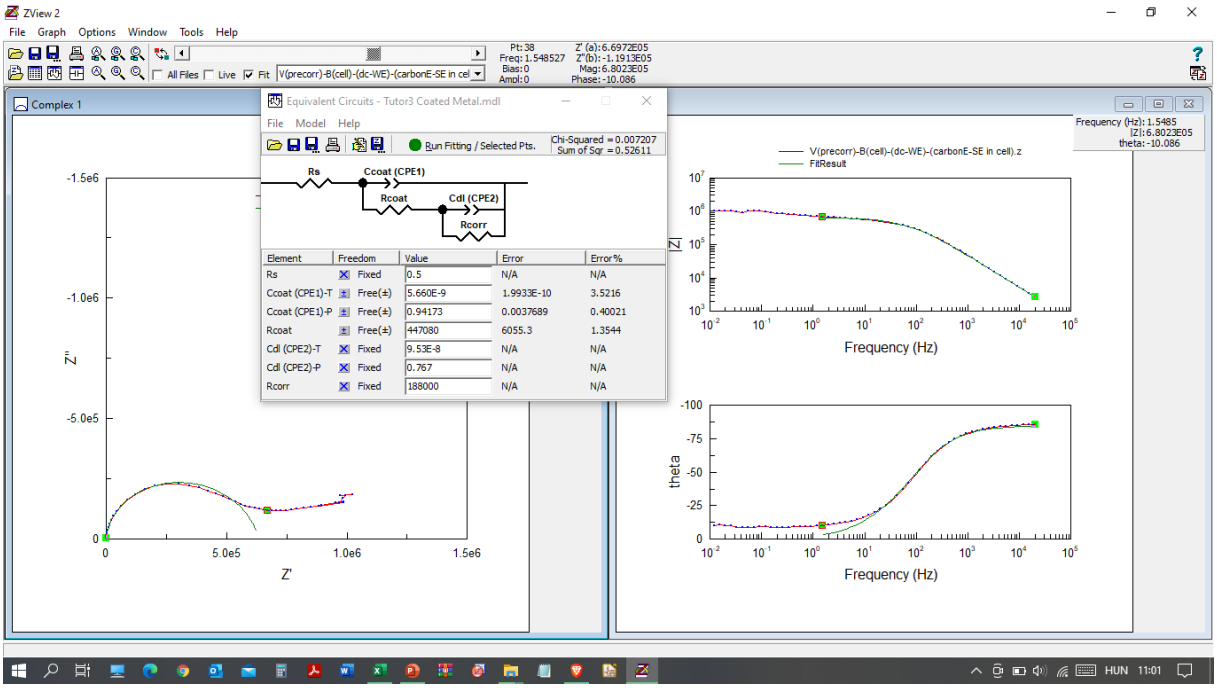

Figure A.91. The PMMA-CE characterised ‘B’ area of the pre-corroded (V) type ‘thin red’ coating sample in medium exposed state, measured with direct wire connection to the substrate (one cell configuration).

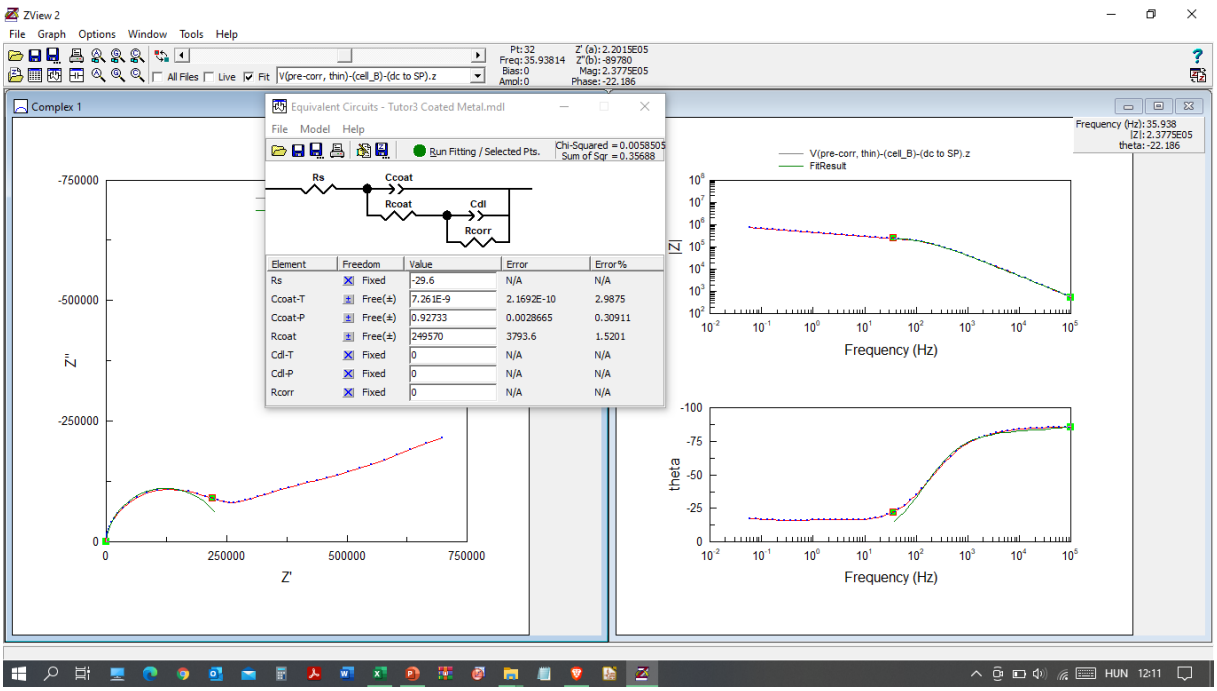

Figure A.92. The PMMA-CE characterised ‘B’ area of the pre-corroded (V) type ‘thin red’ coating sample in exposed state, measured with direct wire connection to the substrate (one cell configuration).

The mono-IDE impedance test results are summarised hereinafter.

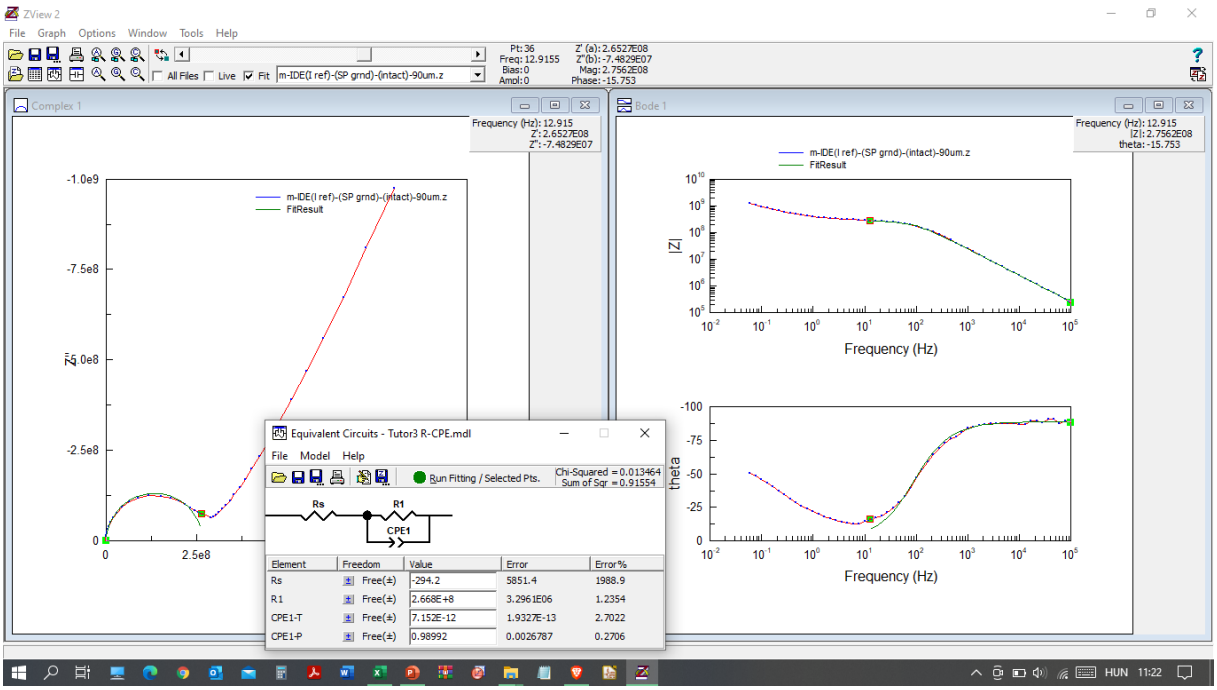

Figure A.93. The mono-IDE characterised reference (I) type ‘thin red’ coating sample in intact state.

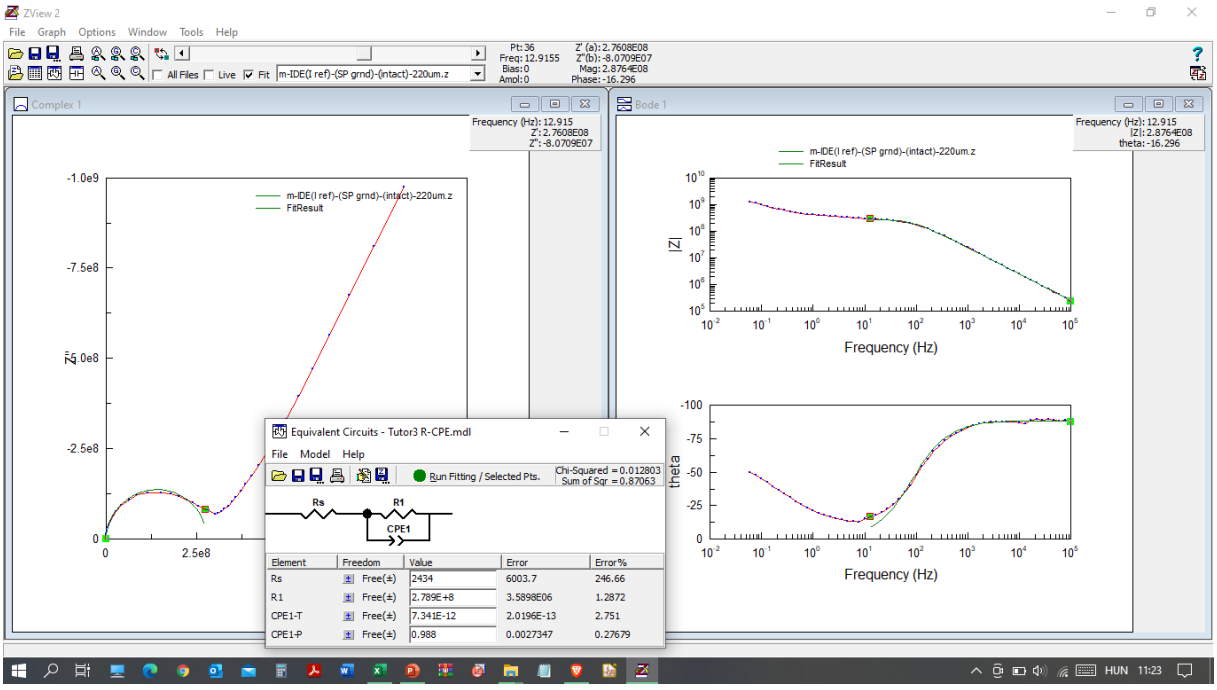

Figure A.94. The mono-IDE characterised reference (I) type ‘thin red’ coating sample in intact state.

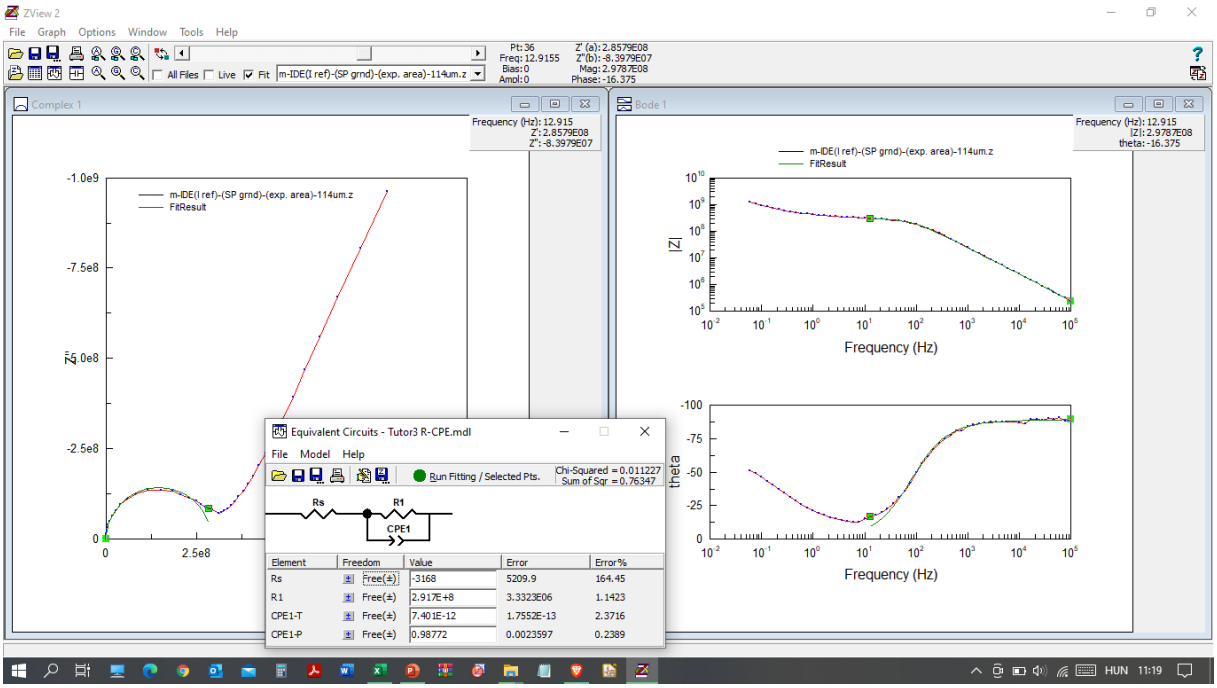

Figure A.95. The mono-IDE characterised reference (I) type ‘thin red’ coating sample in exposed state.

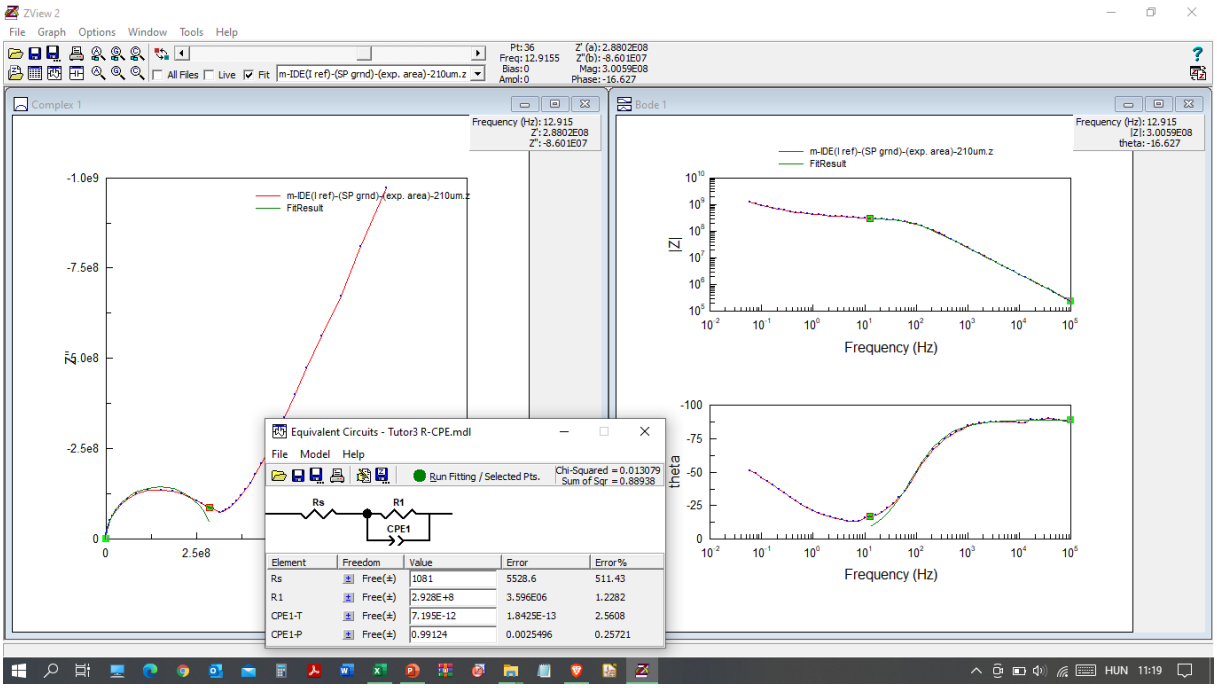

Figure A.96. The mono-IDE characterised reference (I) type ‘thin red’ coating sample in exposed state.

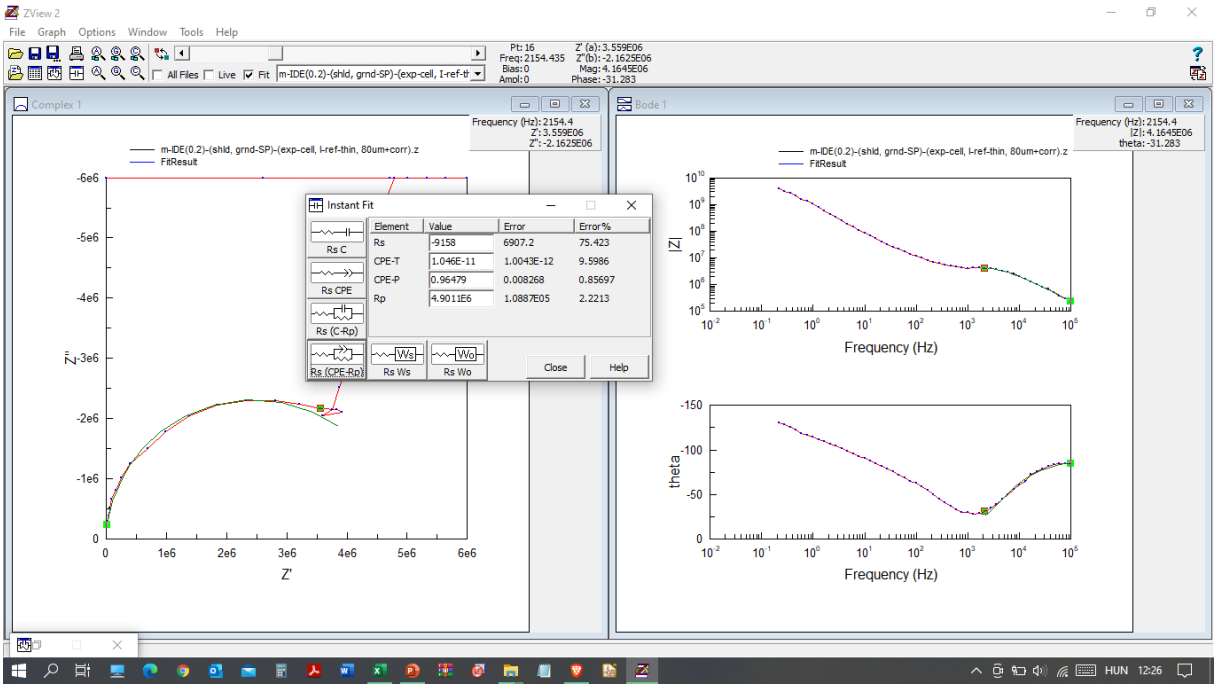

Figure A.97. The mono-IDE characterised reference (I) type ‘thin red’ coating sample in exposed state.

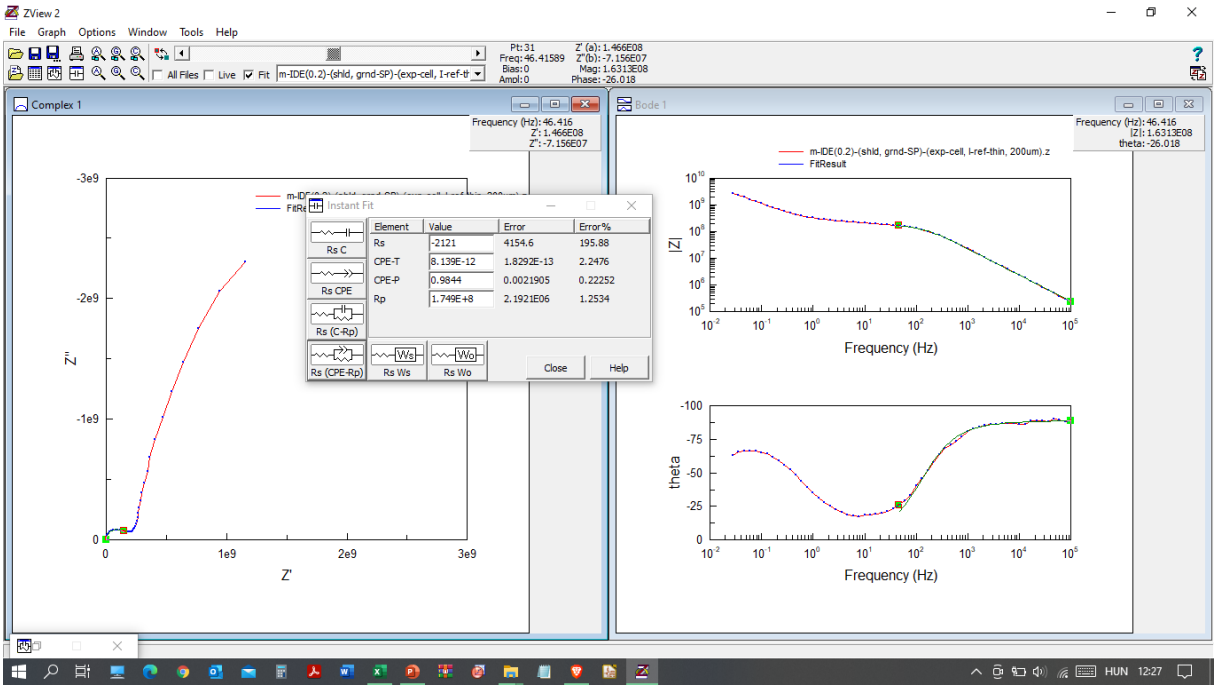

Figure A.98. The mono-IDE characterised reference (I) type ‘thin red’ coating sample in exposed state, high frequency part fitted.

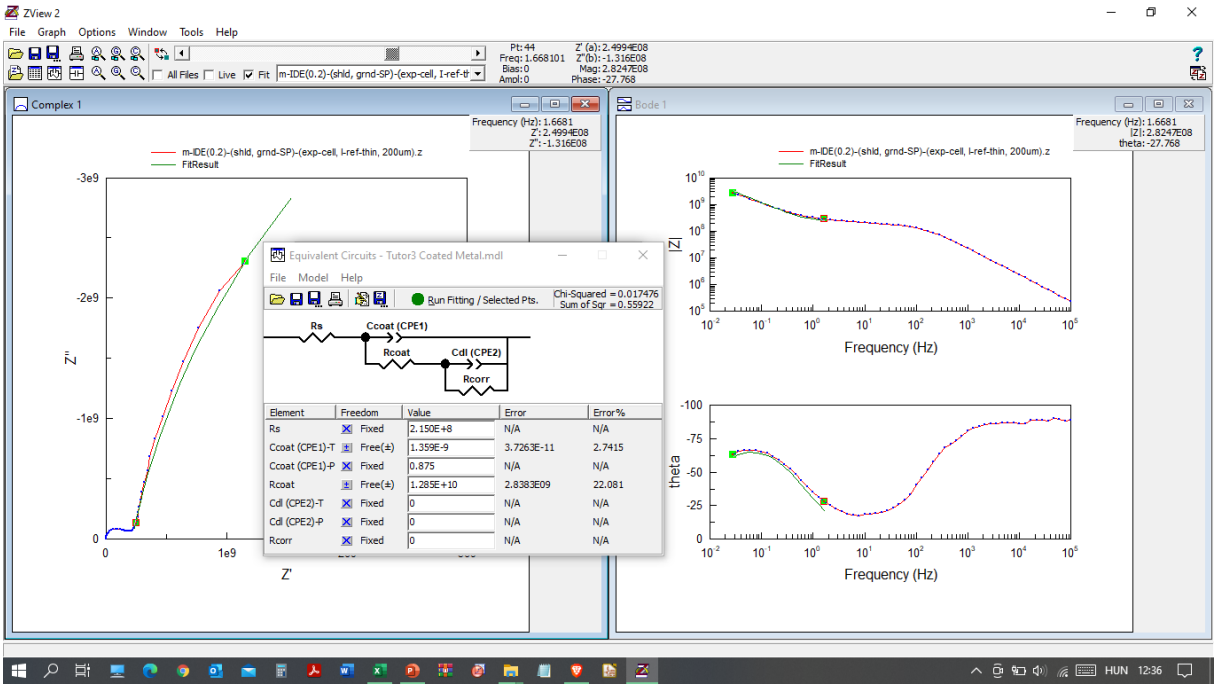

Figure A.99. The mono-IDE characterised reference (I) type ‘thin red’ coating sample in exposed state, low frequency part fitted.

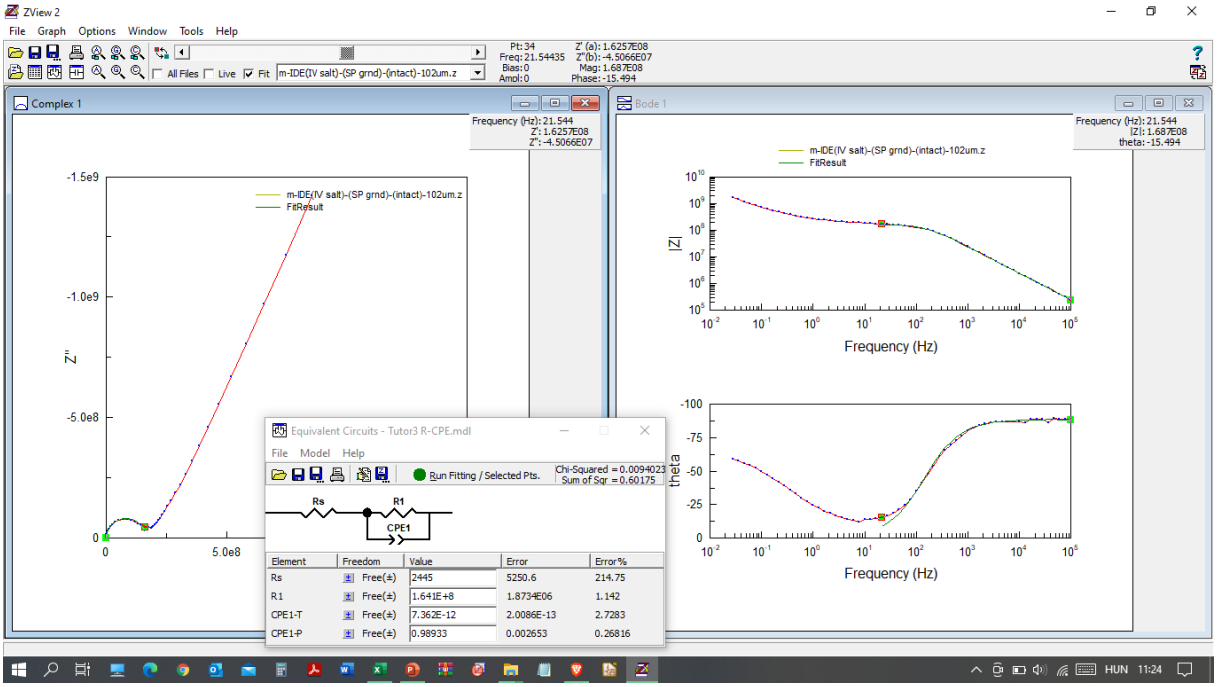

Figure A.100. The mono-IDE characterised salt contaminated (IV) type ‘thin red’ coating sample in intact state, low frequency part fitted.

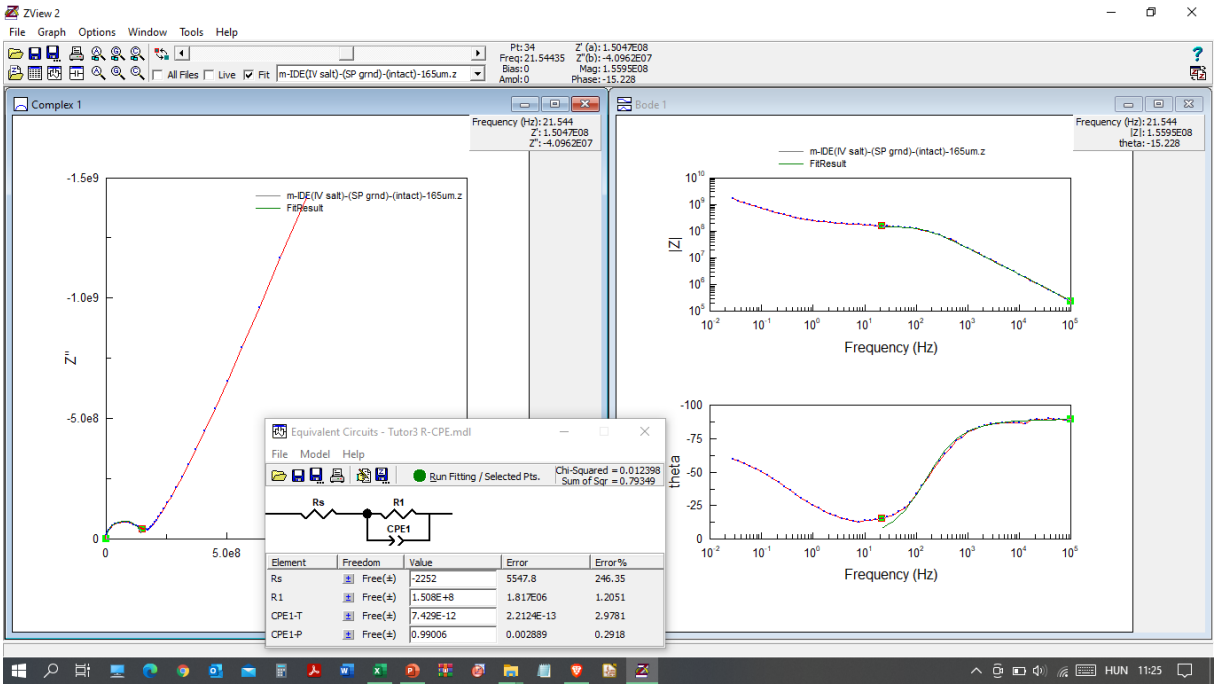

Figure A.101. The mono-IDE characterised salt contaminated (IV) type ‘thin red’ coating sample in intact state.

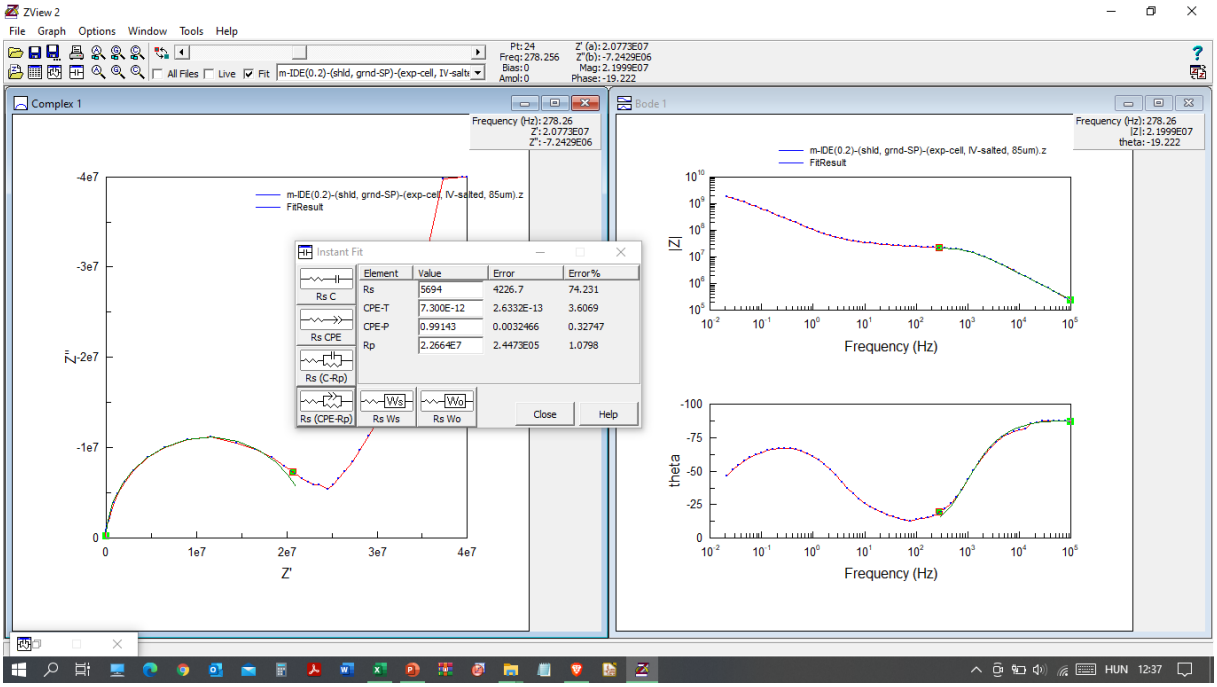

Figure A.102. The mono-IDE characterised salt contaminated (IV) type ‘thin red’ coating sample in exposed state, high frequency range fitted.

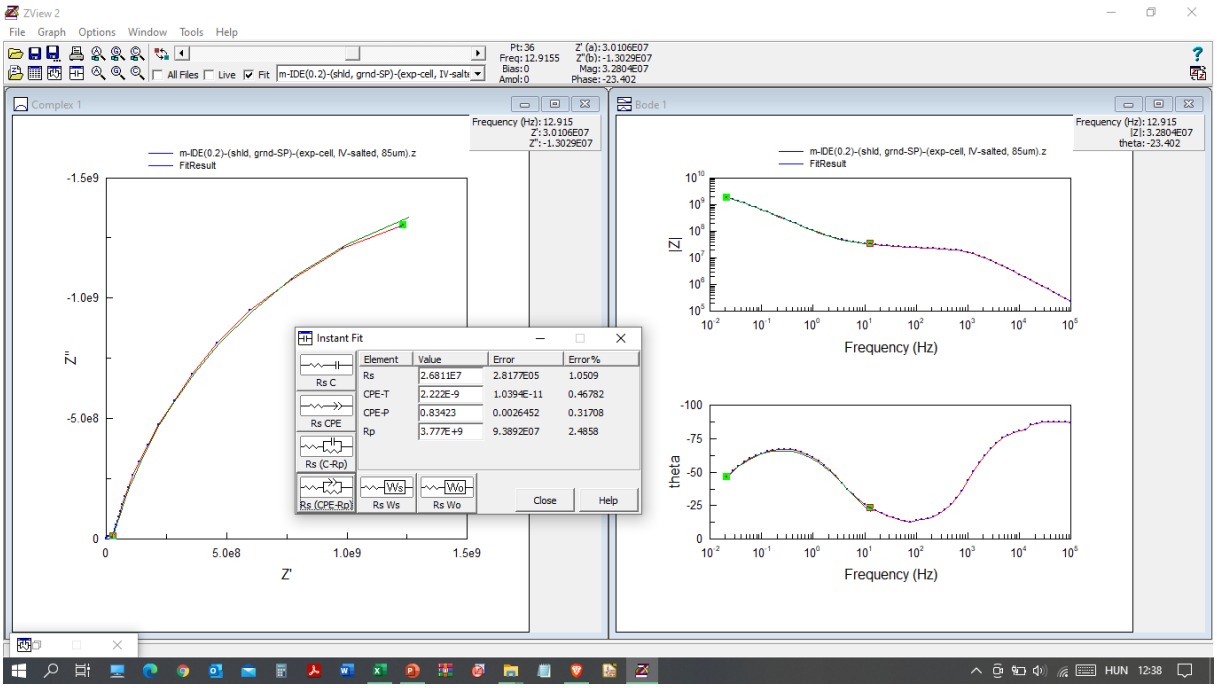

Figure A.103. The mono-IDE characterised salt contaminated (IV) type ‘thin red’ coating sample in exposed state, low frequency range fitted.

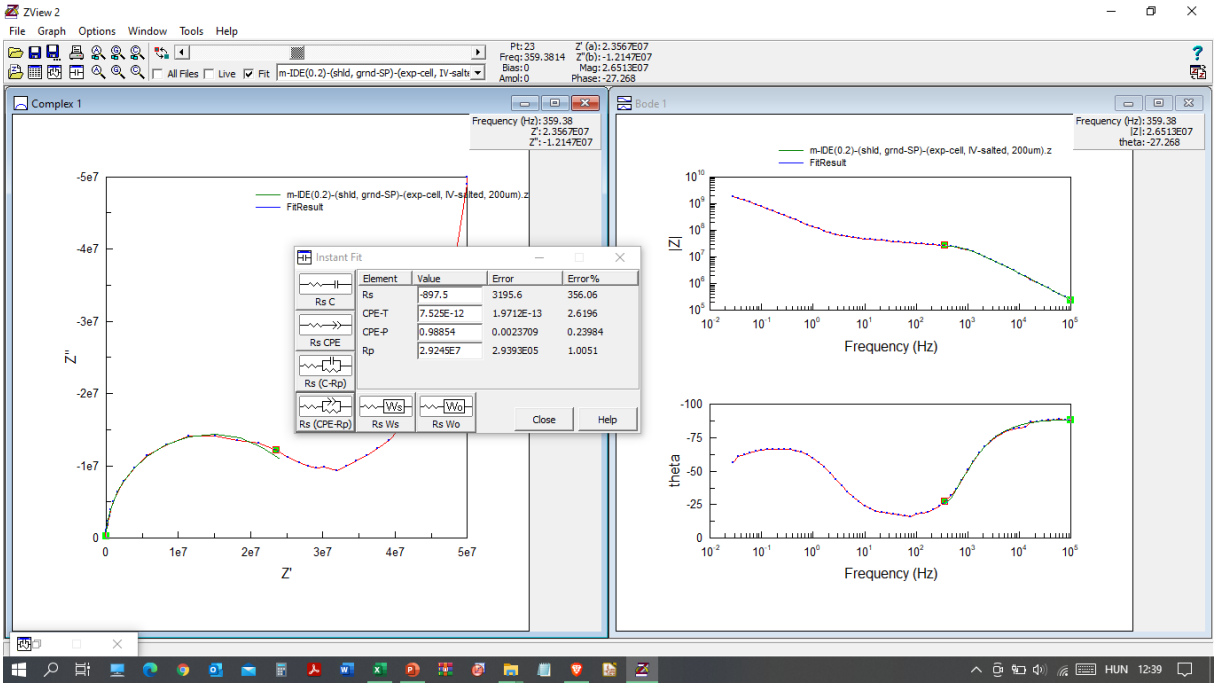

Figure A.104. The mono-IDE characterised salt contaminated (IV) type ‘thin red’ coating sample in exposed state, high frequency range fitted.

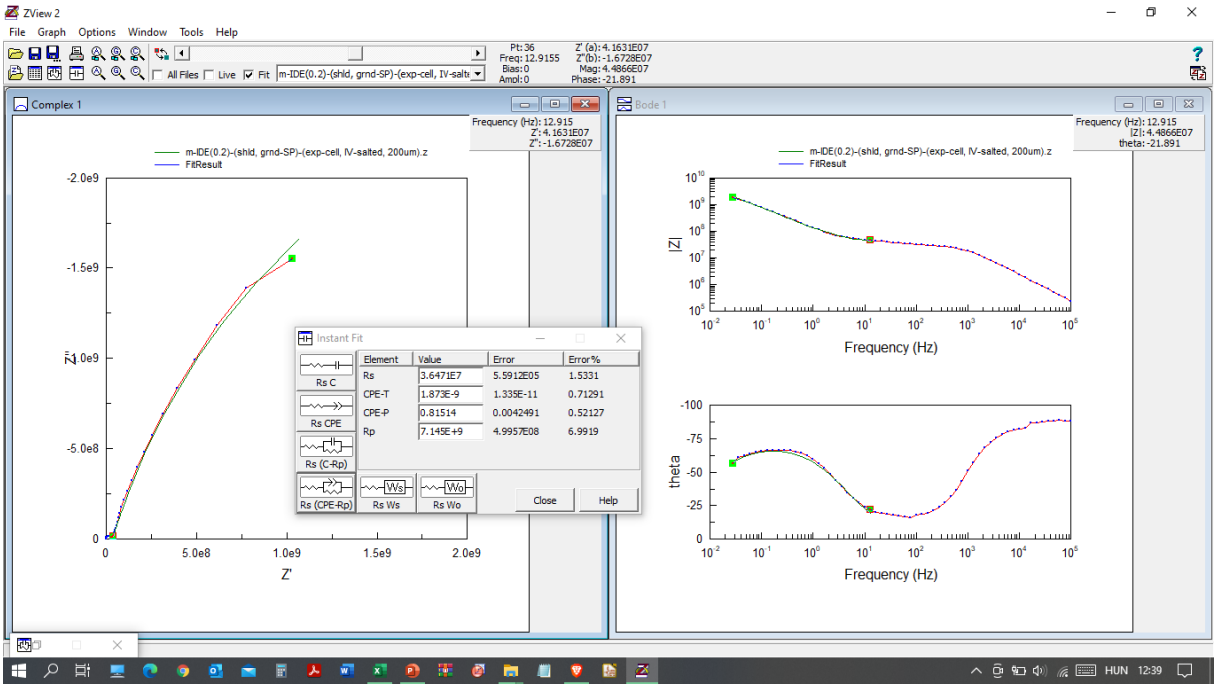

Figure A.105. The mono-IDE characterised salt contaminated (IV) type ‘thin red’ coating sample in exposed state, low frequency range fitted.

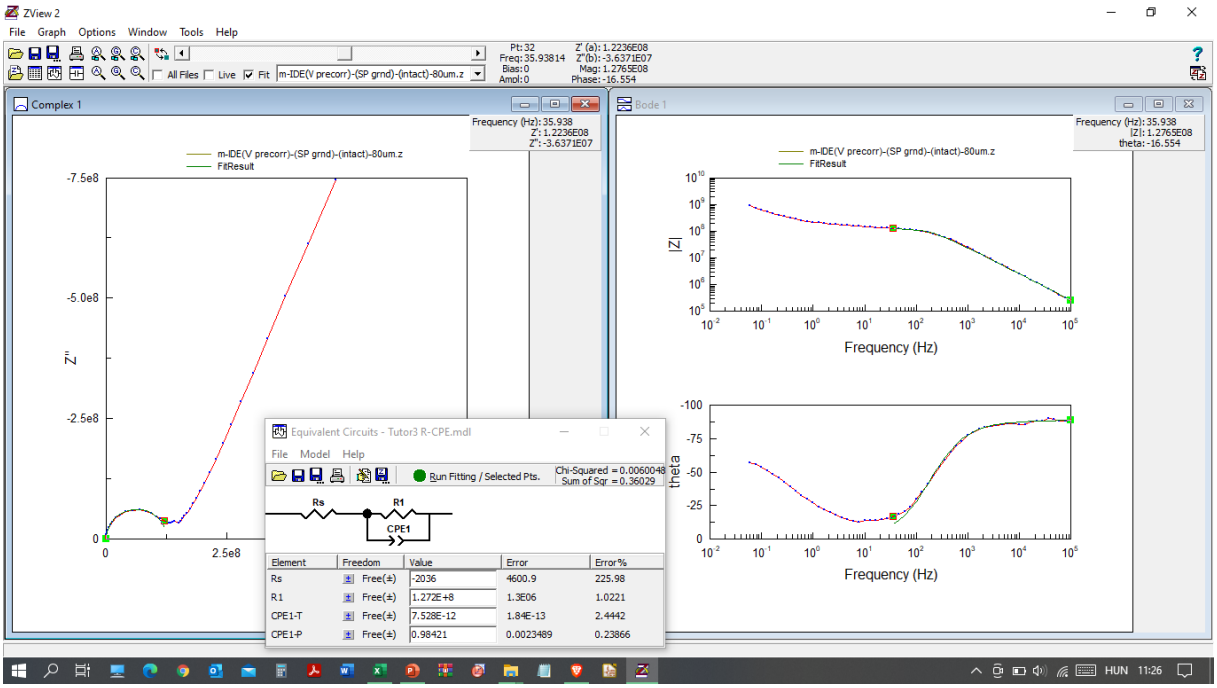

Figure A.106. The mono-IDE characterised pre-corroded (V) type ‘thin red’ coating sample in intact state.

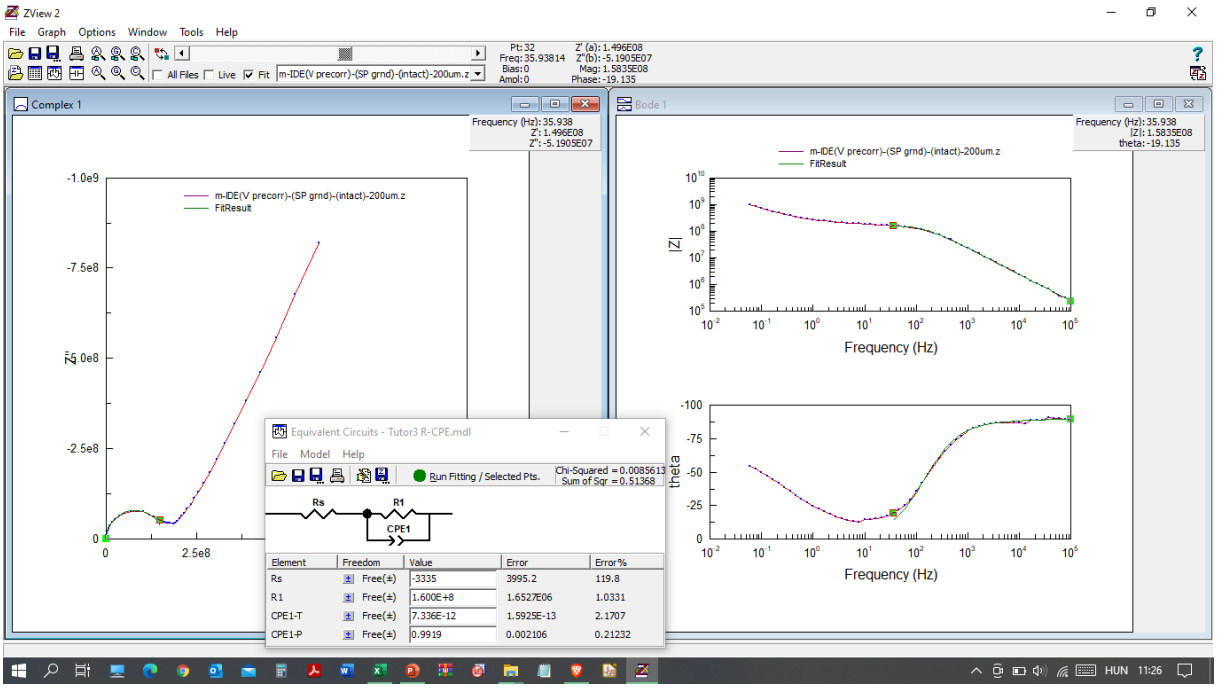

Figure A.107. The mono-IDE characterised pre-corroded (V) type ‘thin red’ coating sample in intact state.

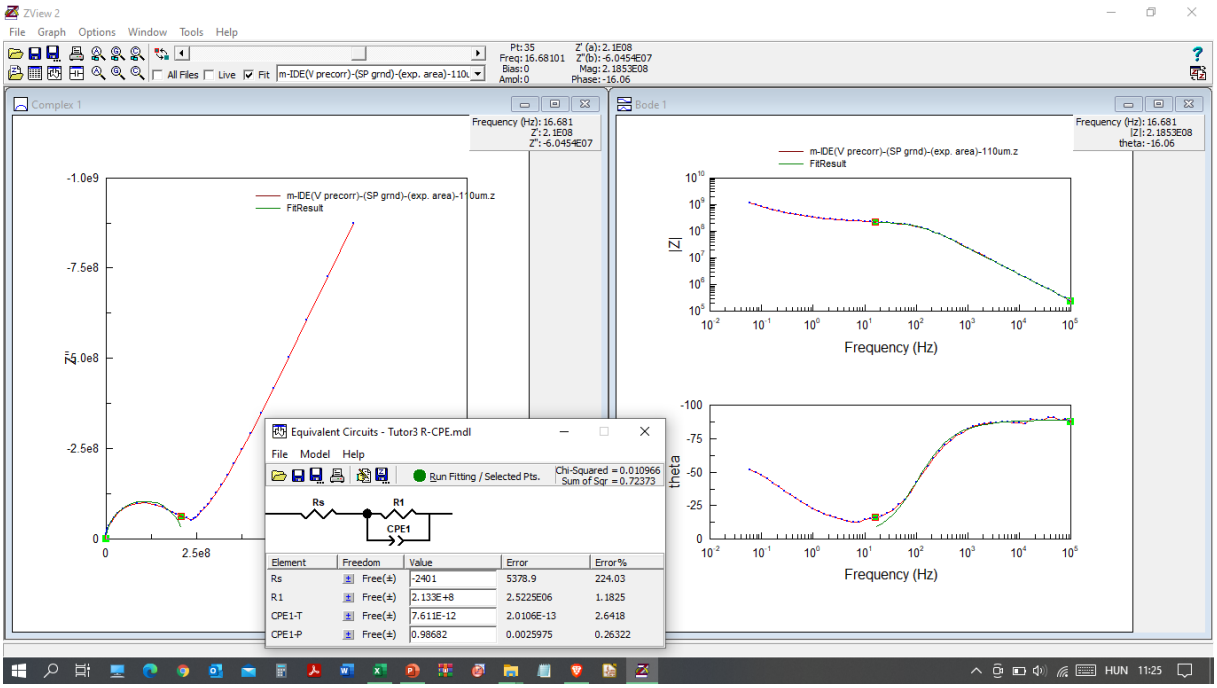

Figure A.108. The mono-IDE characterised pre-corroded (V) type ‘thin red’ coating sample in exposed state.

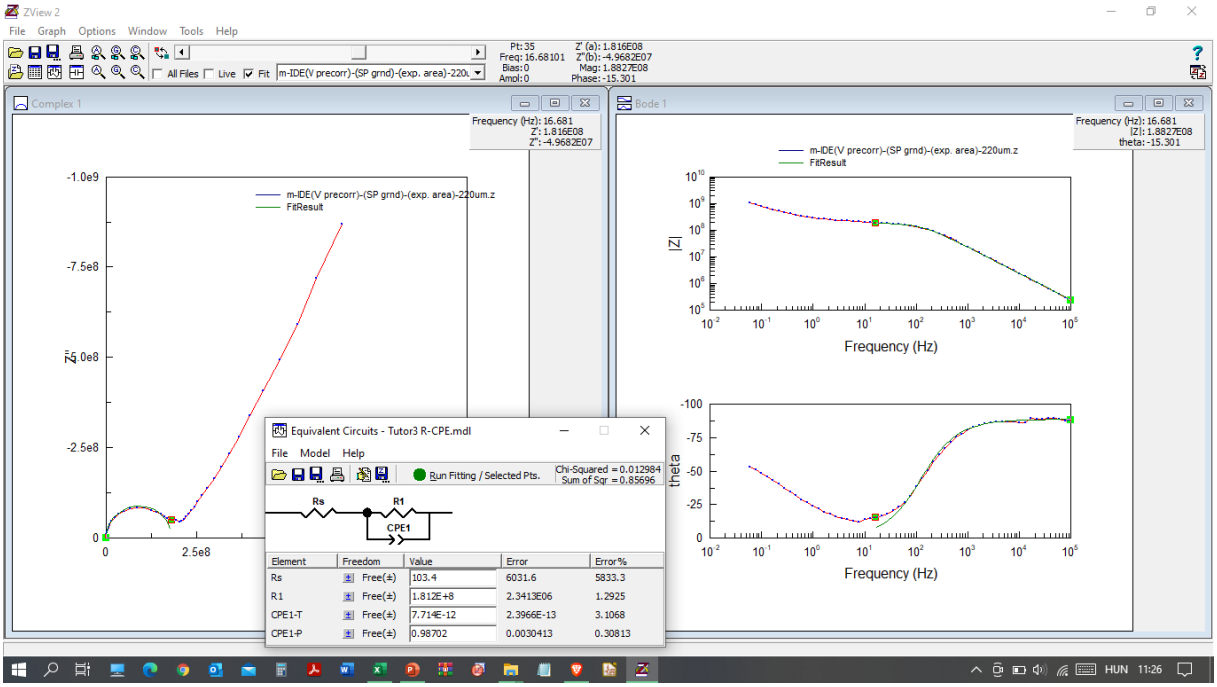

Figure A.109. The mono-IDE characterised pre-corroded (V) type ‘thin red’ coating sample in exposed state.

The quad-IDE impedance test results are summarised hereinafter.

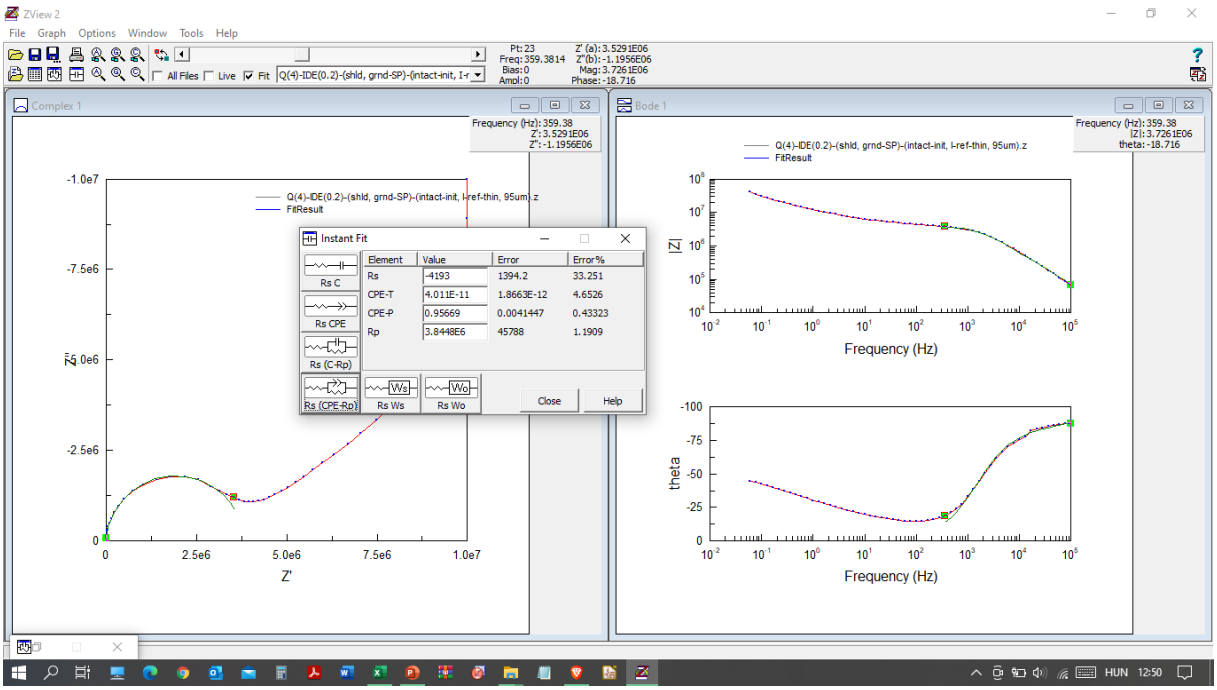

Figure A.110. The quad-array IDE characterised reference (I) type ‘thin red’ coating sample in intact state.

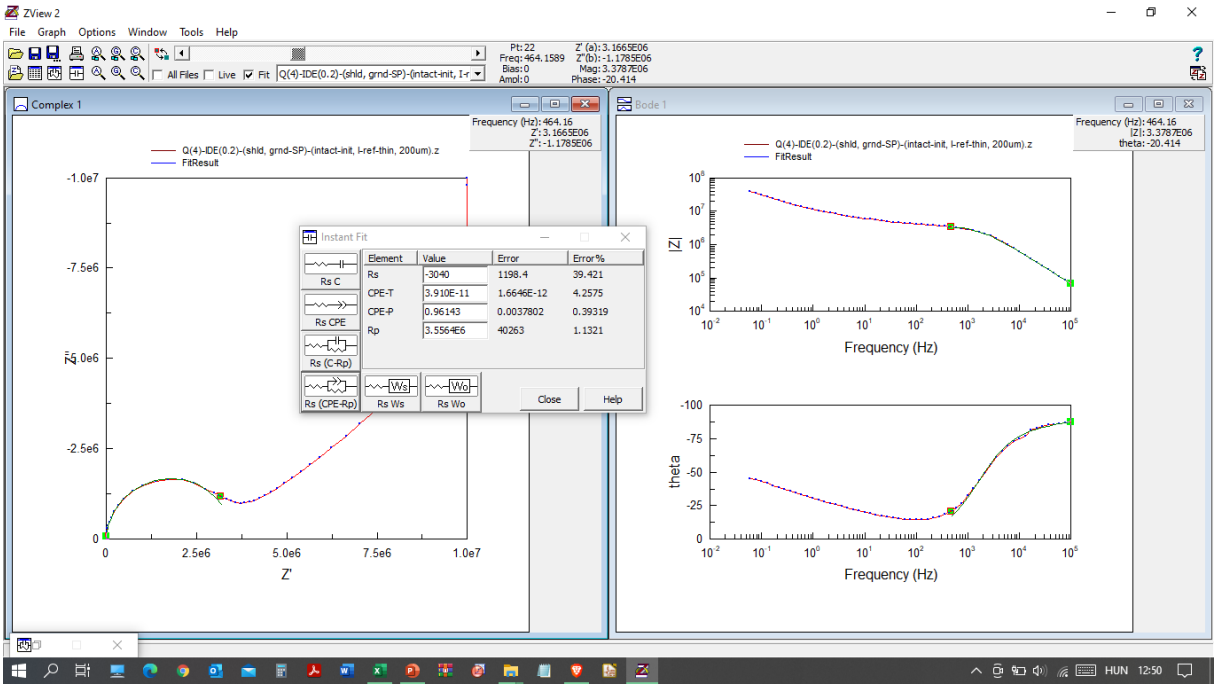

Figure A.111. The quad-array IDE characterised reference (I) type ‘thin red’ coating sample in intact state.

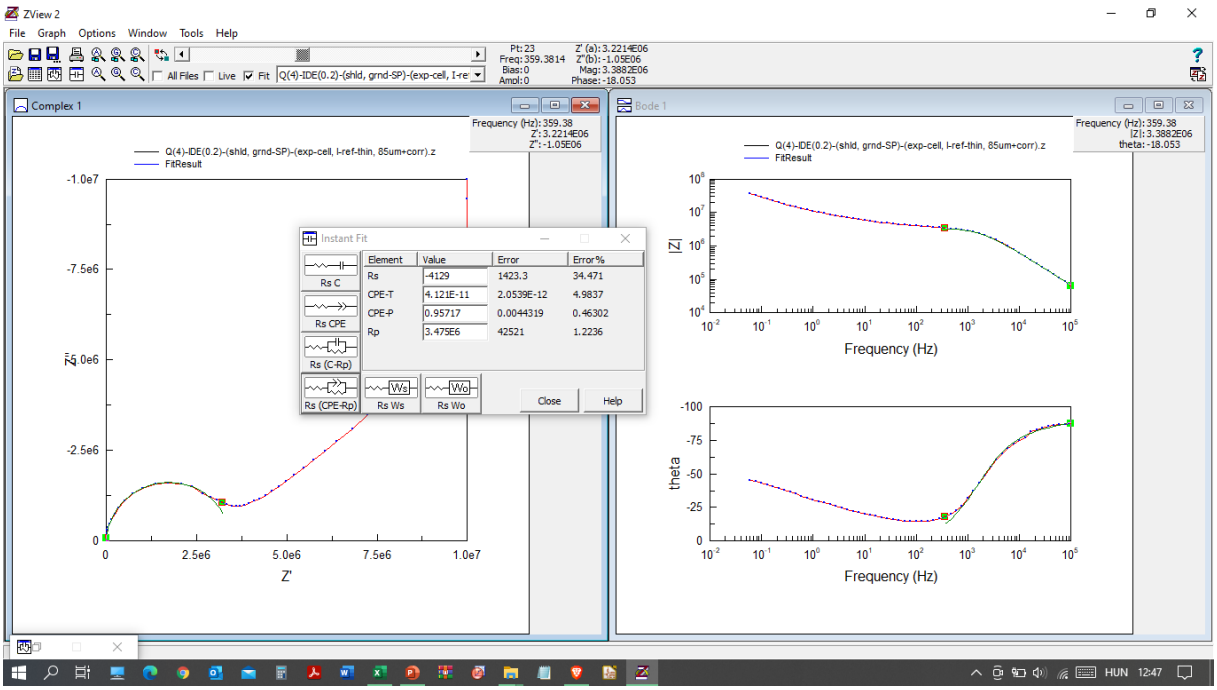

Figure A.112. The quad-array IDE characterised reference (I) type ‘thin red’ coating sample in exposed state.

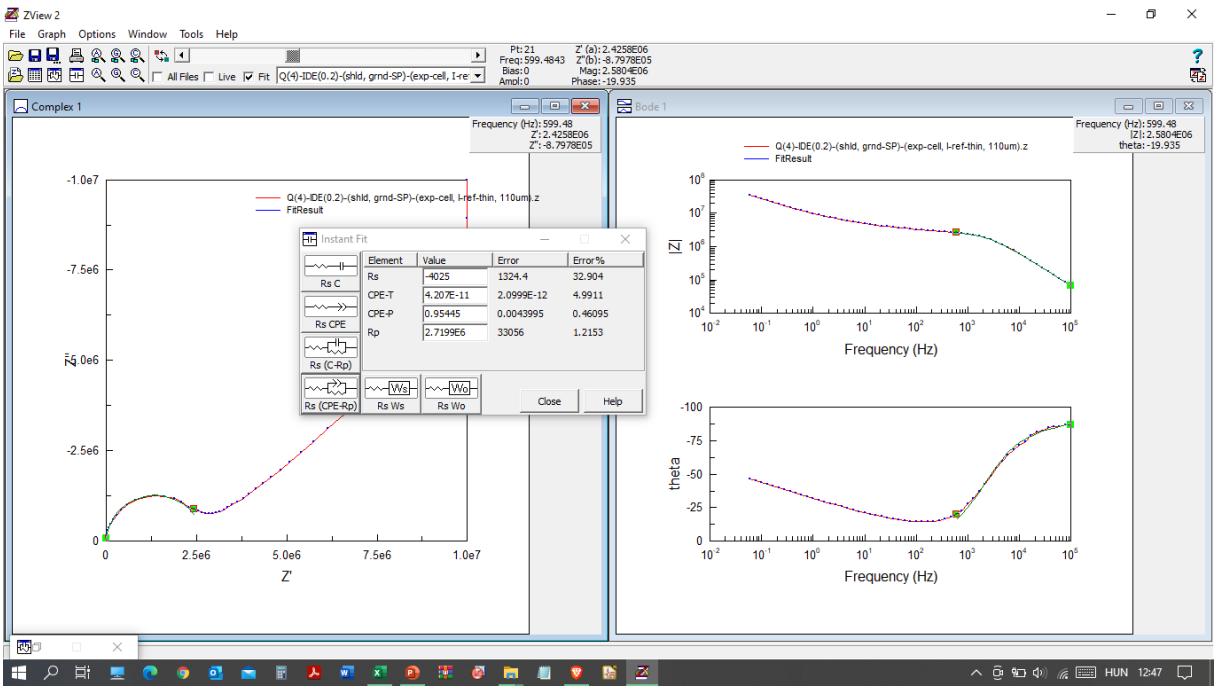

Figure A.113. The quad-array IDE characterised reference (I) type ‘thin red’ coating sample in exposed state.

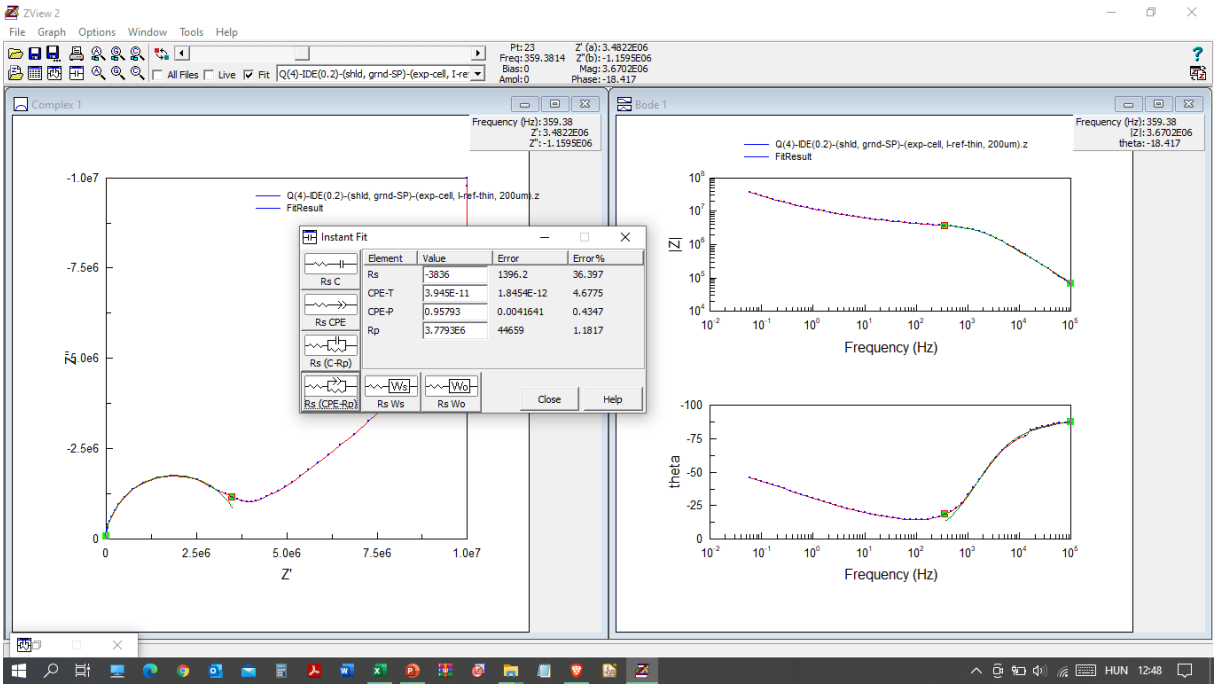

Figure A.114. The quad-array IDE characterised reference (I) type ‘thin red’ coating sample in exposed state.

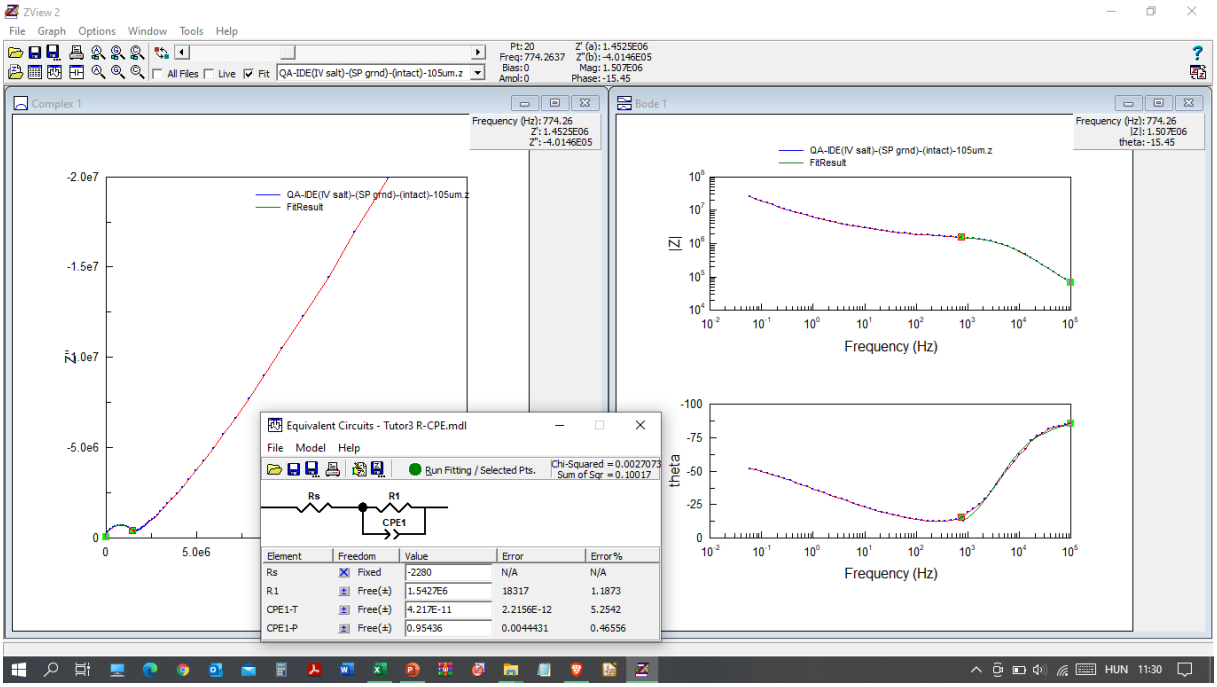

Figure A.115. The quad-array IDE characterised salt contaminated (IV) type ‘thin red’ coating sample in intact state.

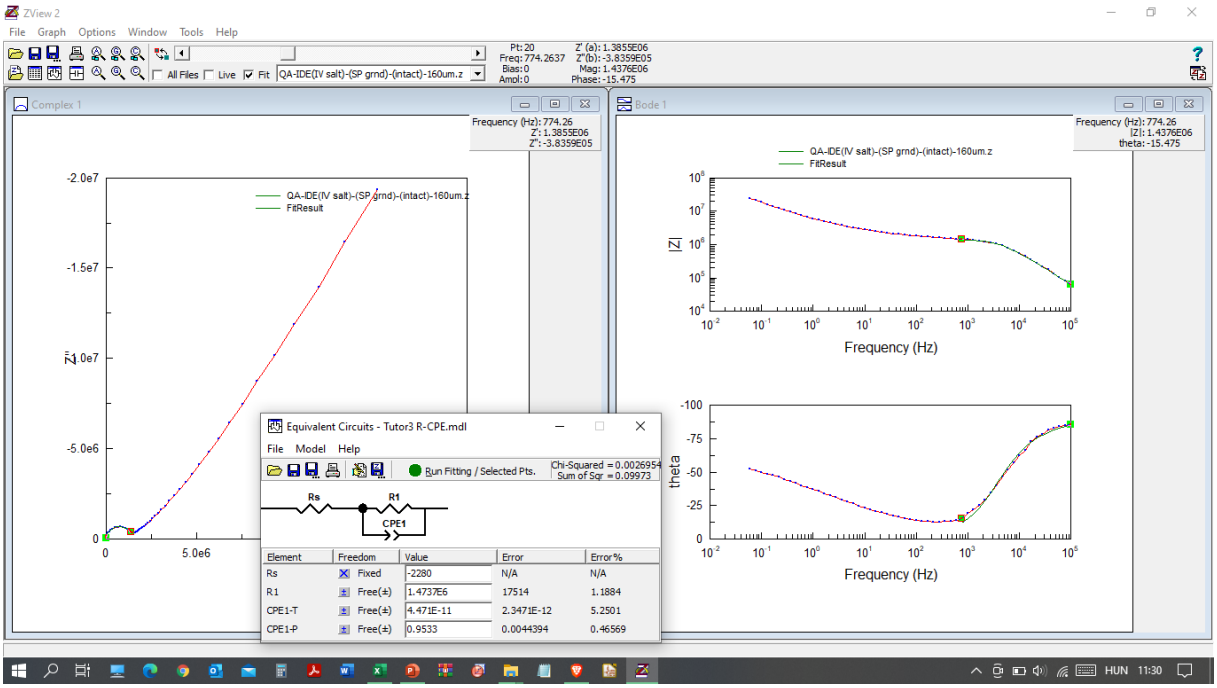

Figure A.116. The quad-array IDE characterised salt contaminated (IV) type ‘thin red’ coating sample in intact state.

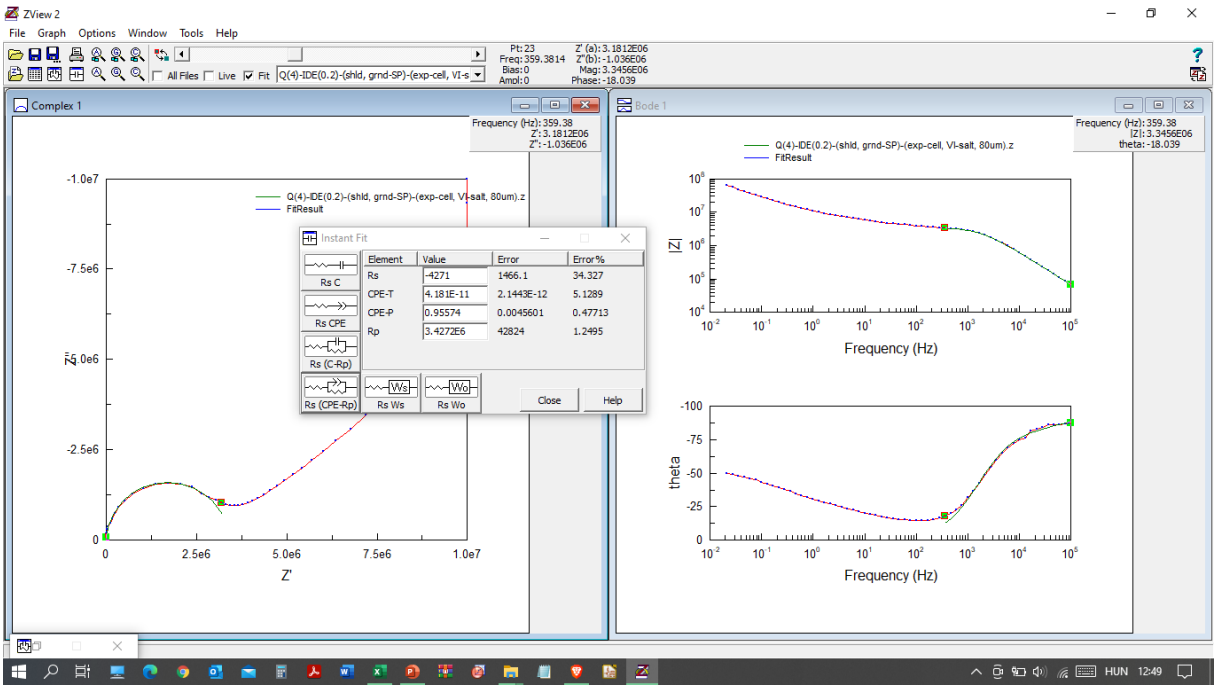

Figure A.117. The quad-array IDE characterised salt contaminated (IV) type ‘thin red’ coating sample in exposed state.

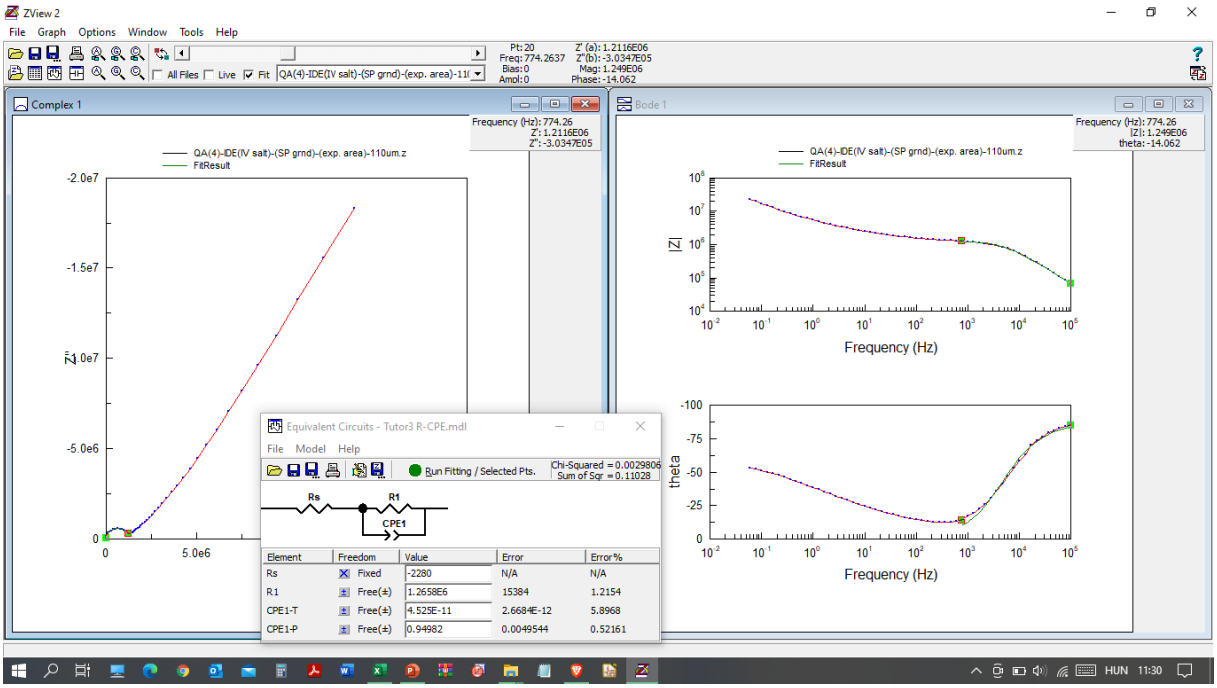

Figure A.118. The quad-array IDE characterised salt contaminated (IV) type ‘thin red’ coating sample in exposed state.

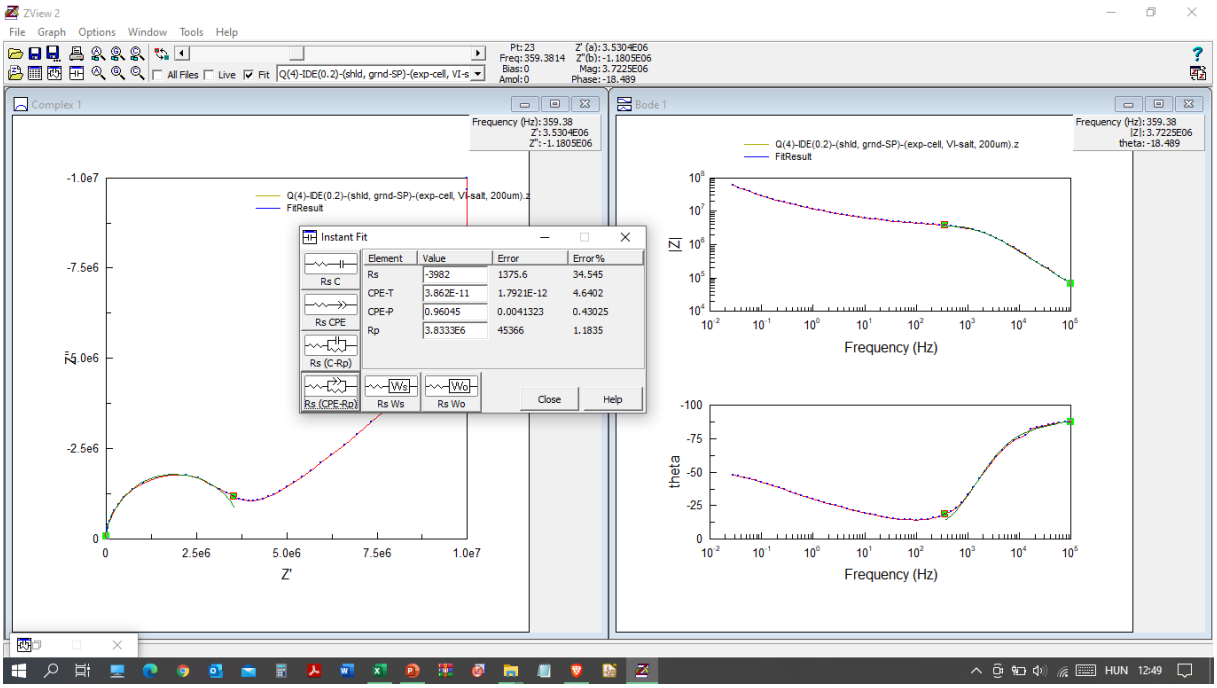

Figure A.119. The quad-array IDE characterised salt contaminated (IV) type ‘thin red’ coating sample in exposed state.

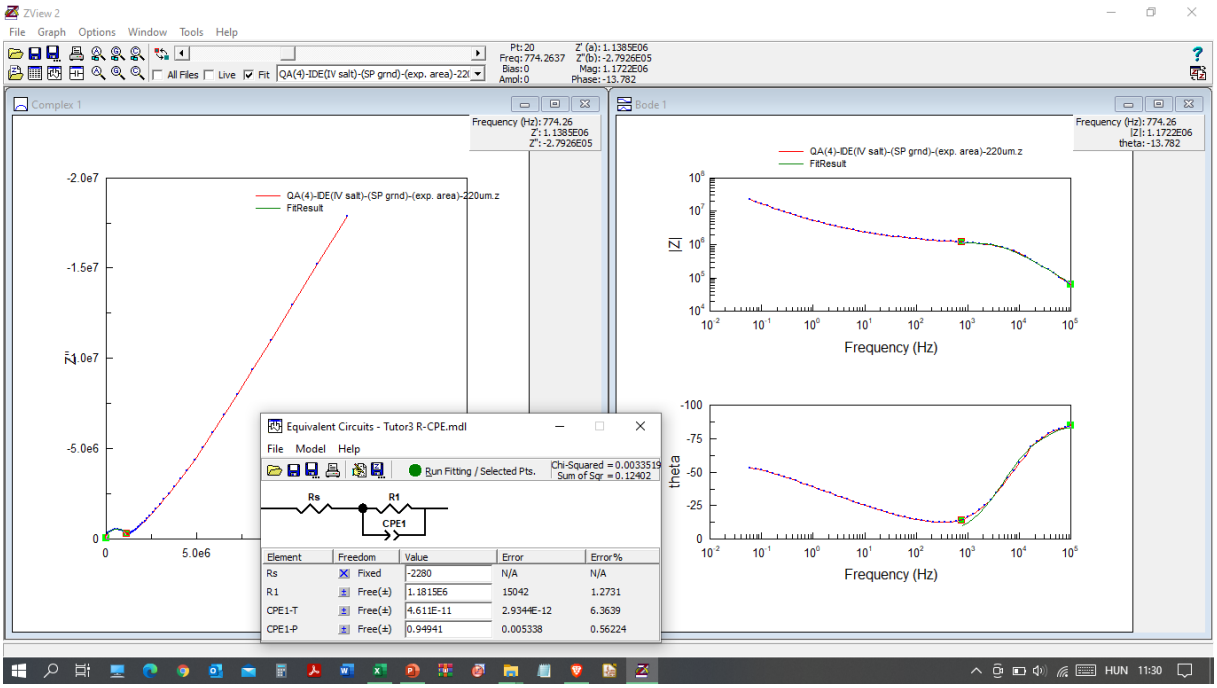

Figure A.120. The quad-array IDE characterised salt contaminated (IV) type ‘thin red’ coating sample in exposed state.

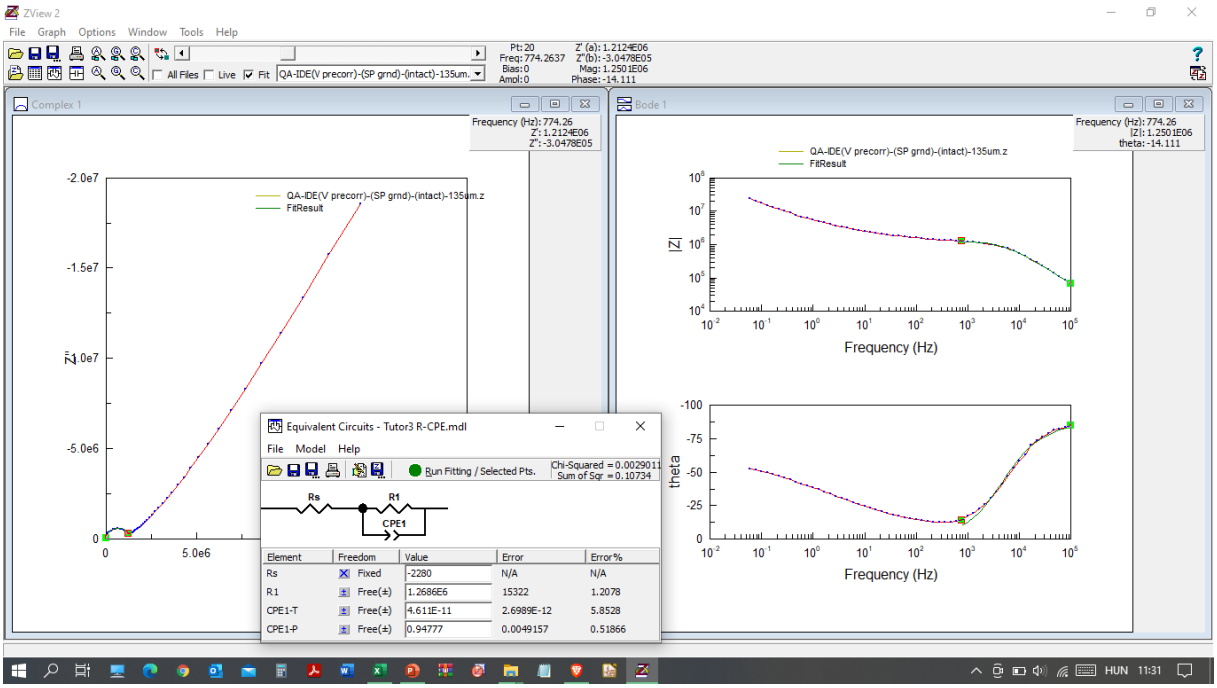

Figure A.121. The quad-array IDE characterised pre-corroded (V) type ‘thin red’ coating sample in intact state.

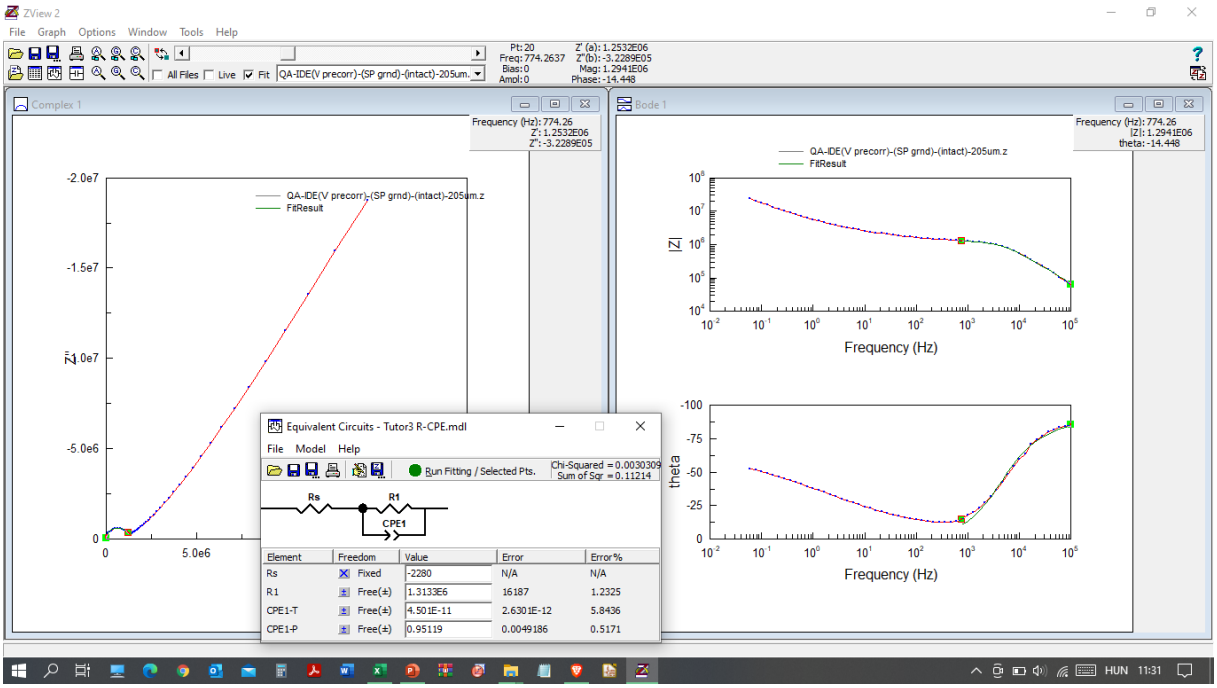

Figure A.122. The quad-array IDE characterised pre-corroded (V) type ‘thin red’ coating sample in intact state.

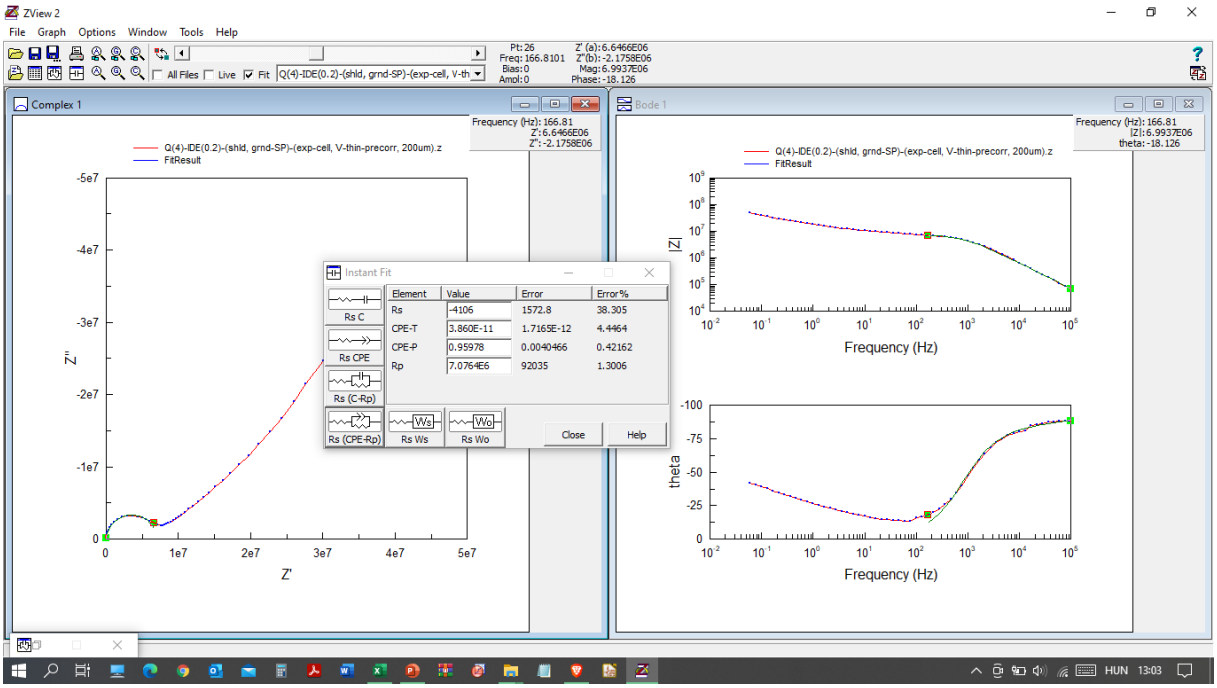

Figure A.123. The quad-array IDE characterised pre-corroded (V) type ‘thin red’ coating sample in exposed state.

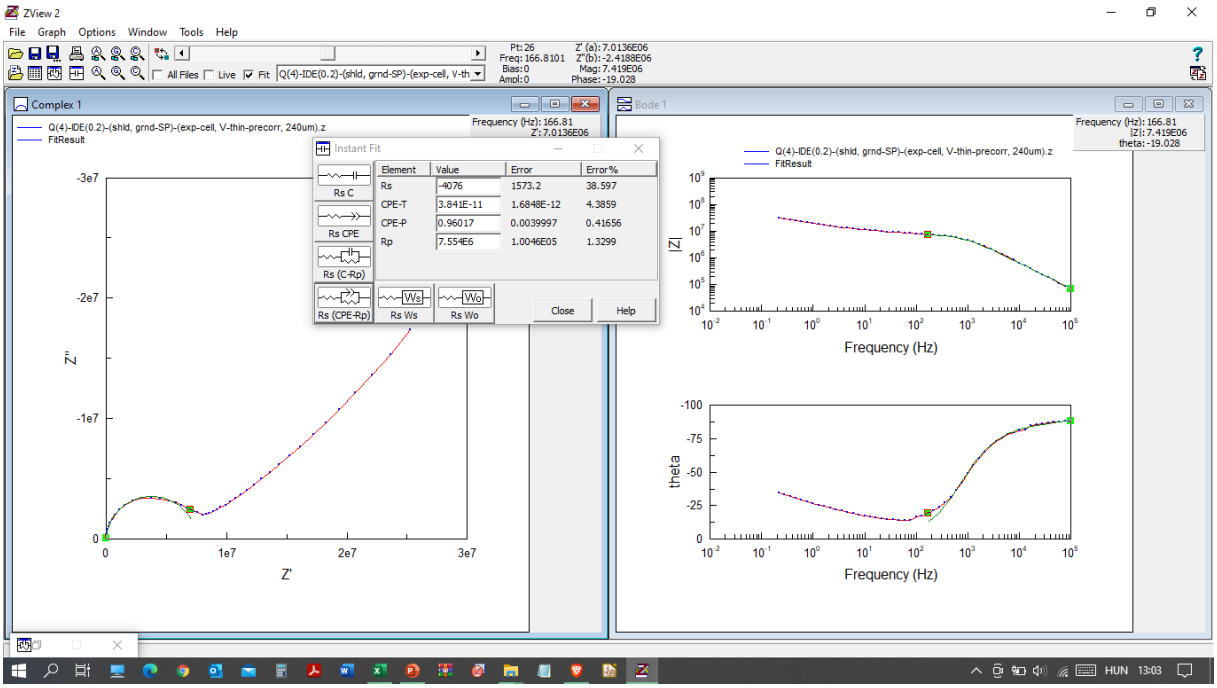

Figure A.124. The quad-array IDE characterised pre-corroded (V) type ‘thin red’ coating sample in exposed state.

The hexa-IDE impedance test results are summarised hereinafter.

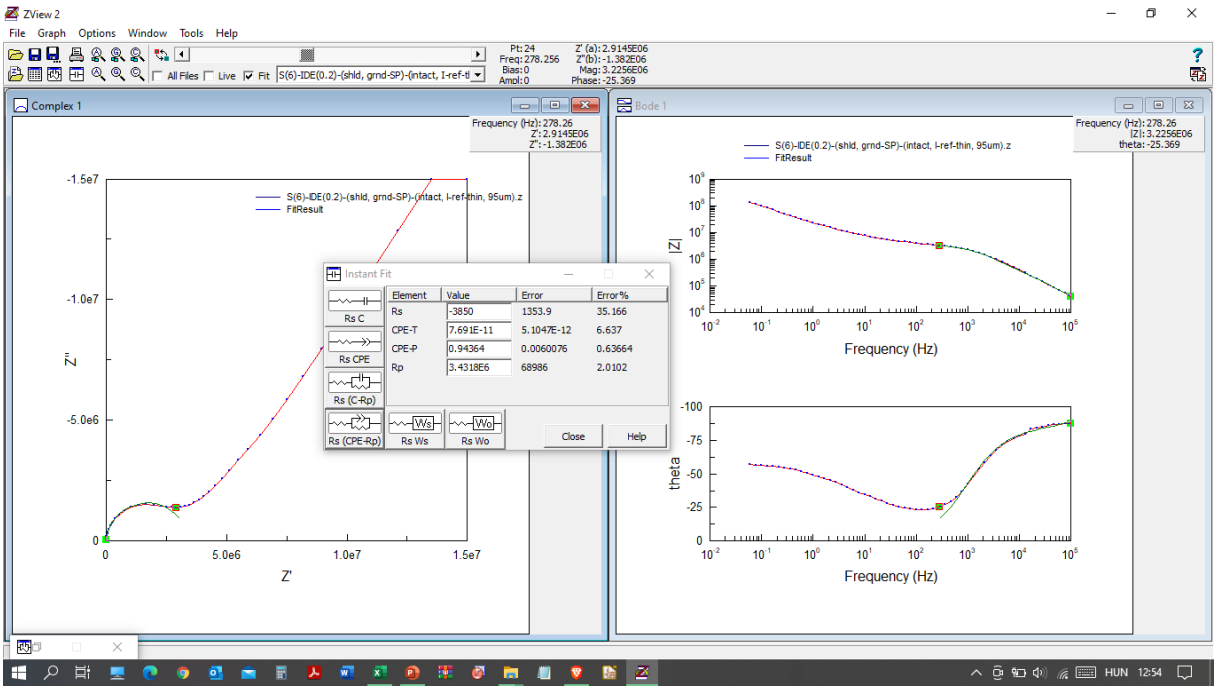

Figure A.125. The hexa-array IDE characterised reference (I) type ‘thin red’ coating sample in intact state.

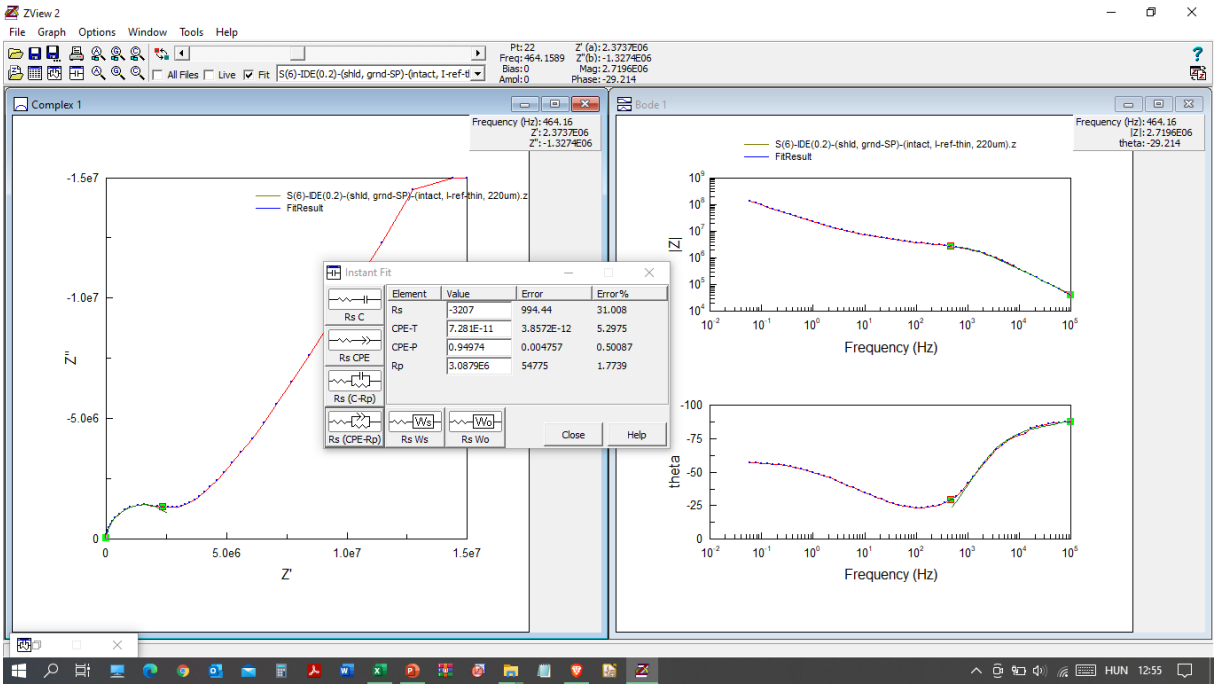

Figure A.126. The hexa-array IDE characterised reference (I) type ‘thin red’ coating sample in intact state.

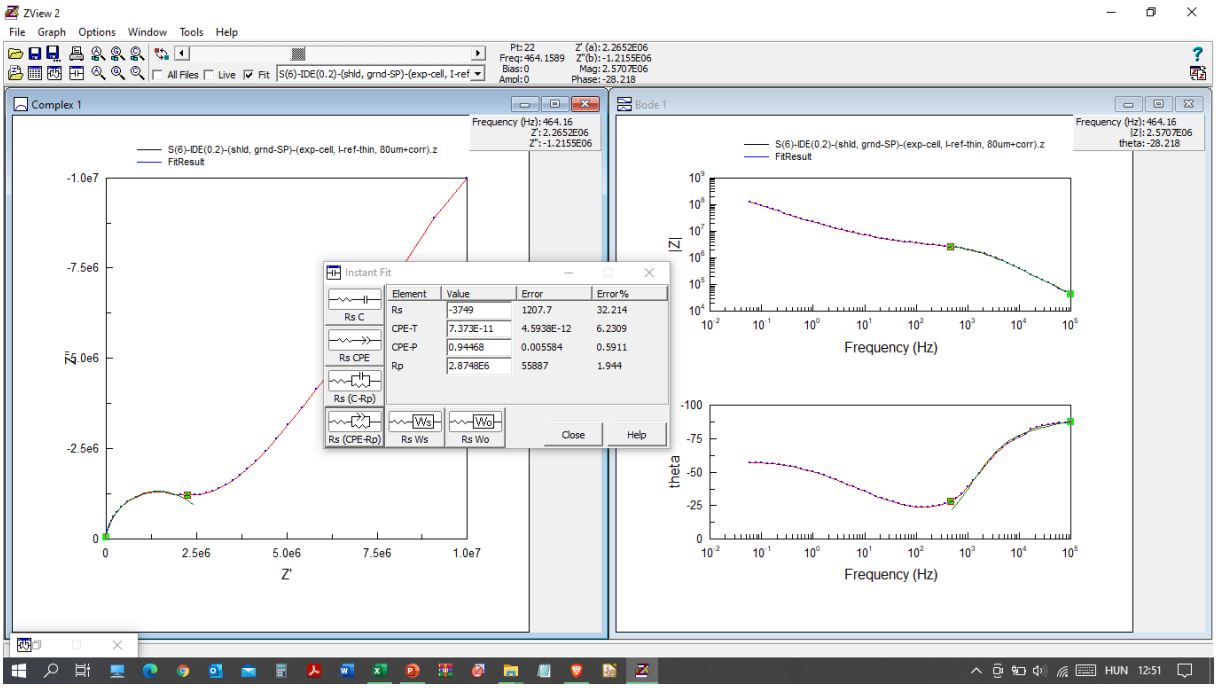

Figure A.127. The hexa-array IDE characterised reference (I) type ‘thin red’ coating sample in exposed state.

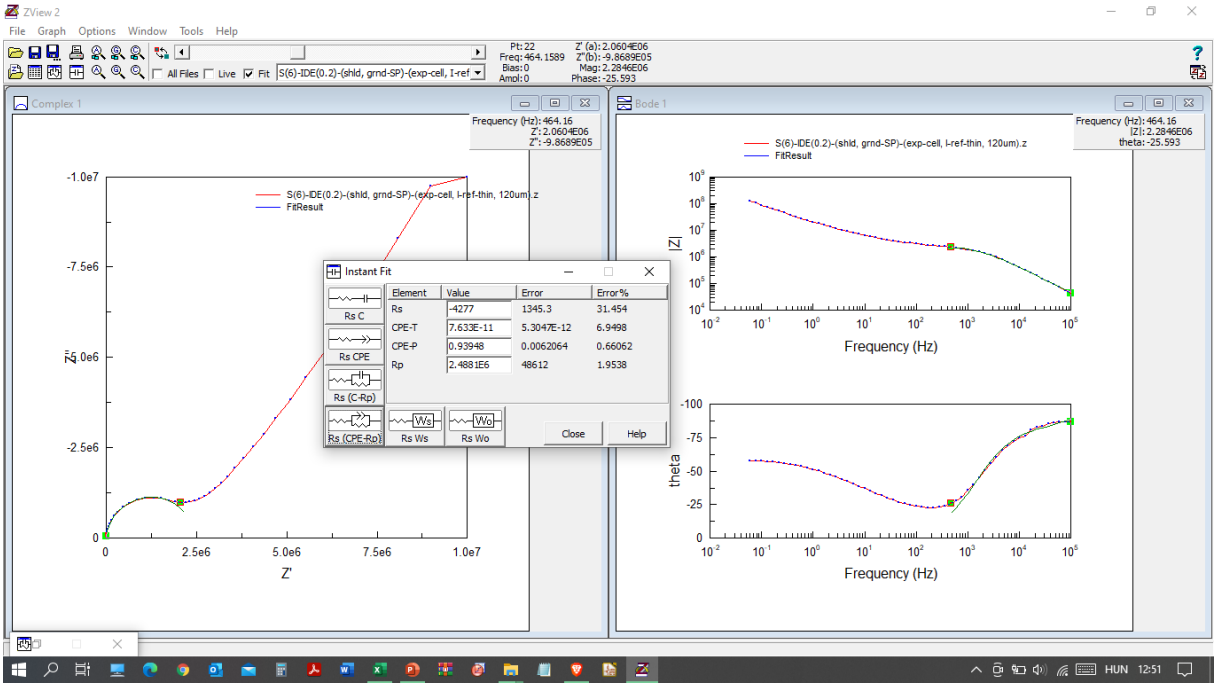

Figure A.128. The hexa-array IDE characterised reference (I) type ‘thin red’ coating sample in exposed state.

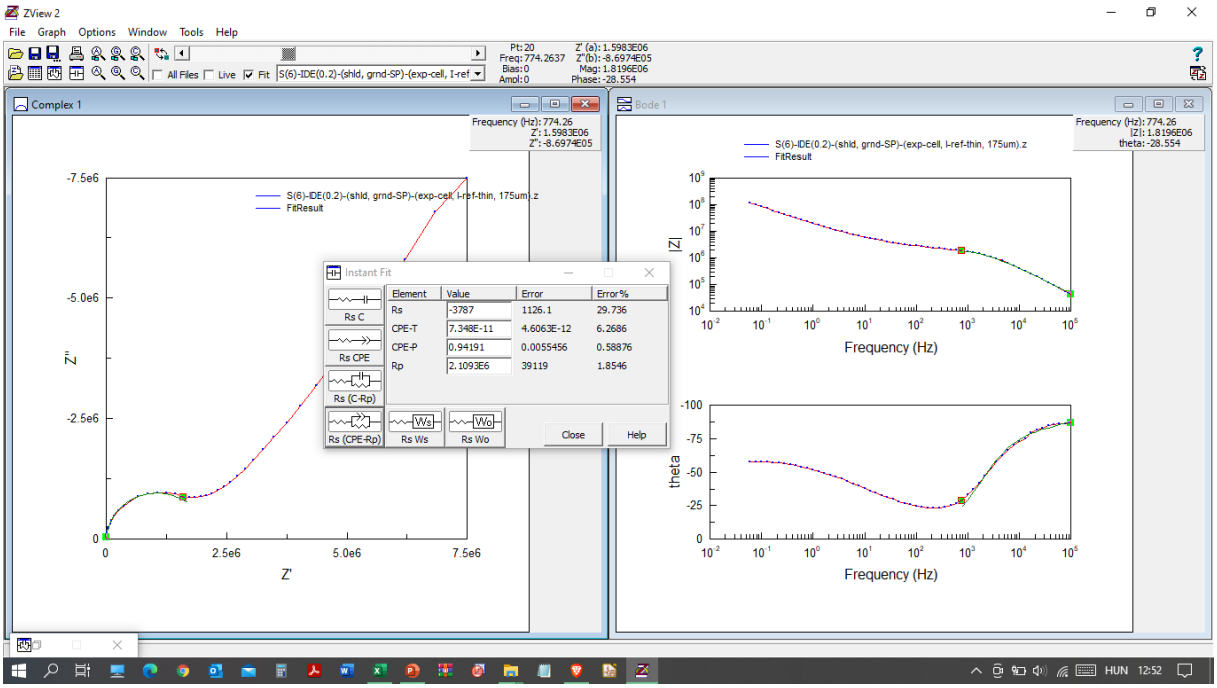

Figure A.129. The hexa-array IDE characterised reference (I) type ‘thin red’ coating sample in exposed state.

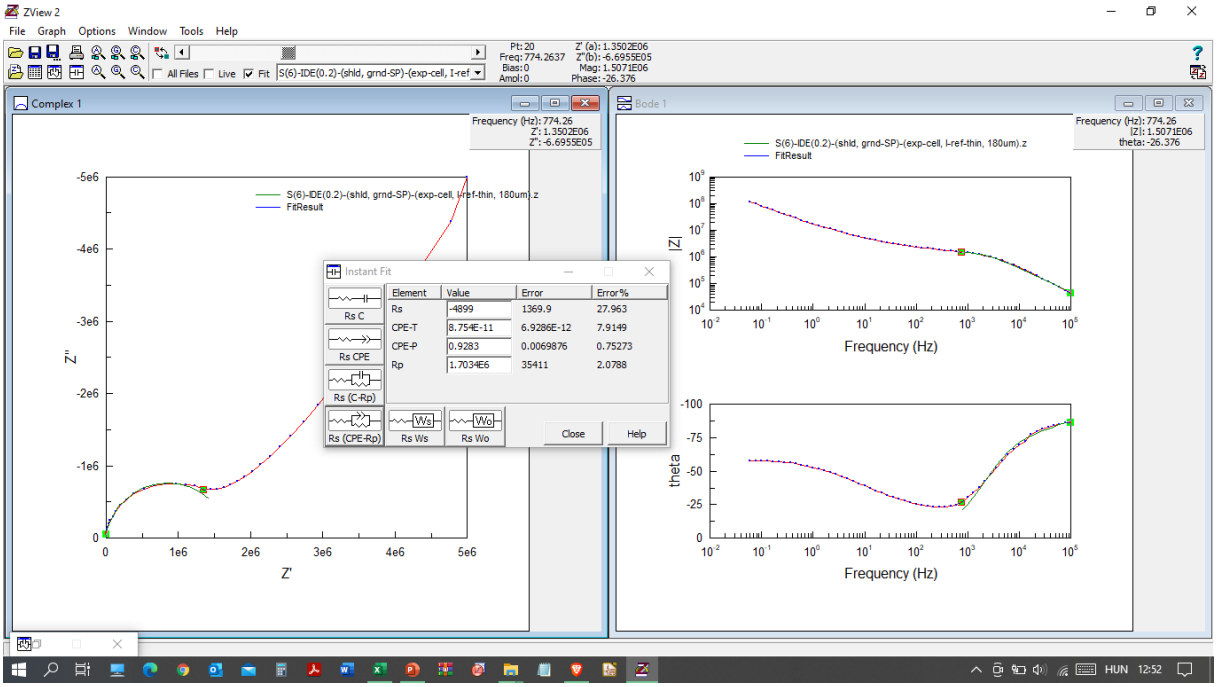

Figure A.130. The hexa-array IDE characterised reference (I) type ‘thin red’ coating sample in exposed state.

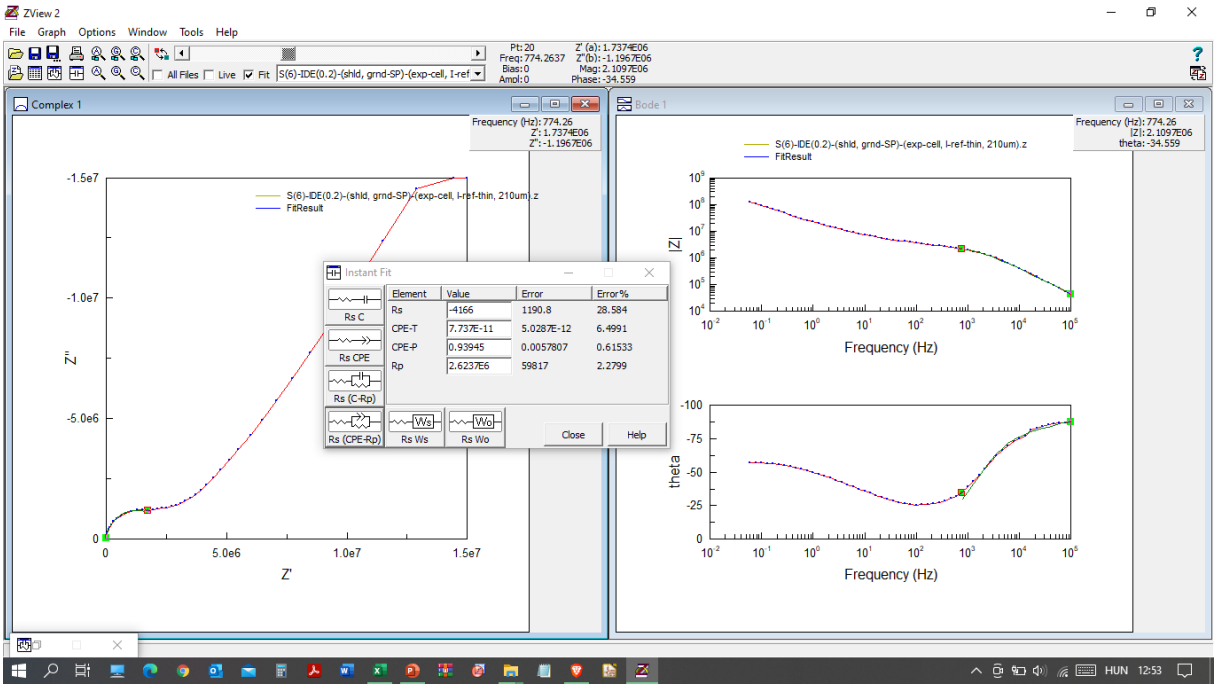

Figure A.131. The hexa-array IDE characterised reference (I) type ‘thin red’ coating sample in exposed state.

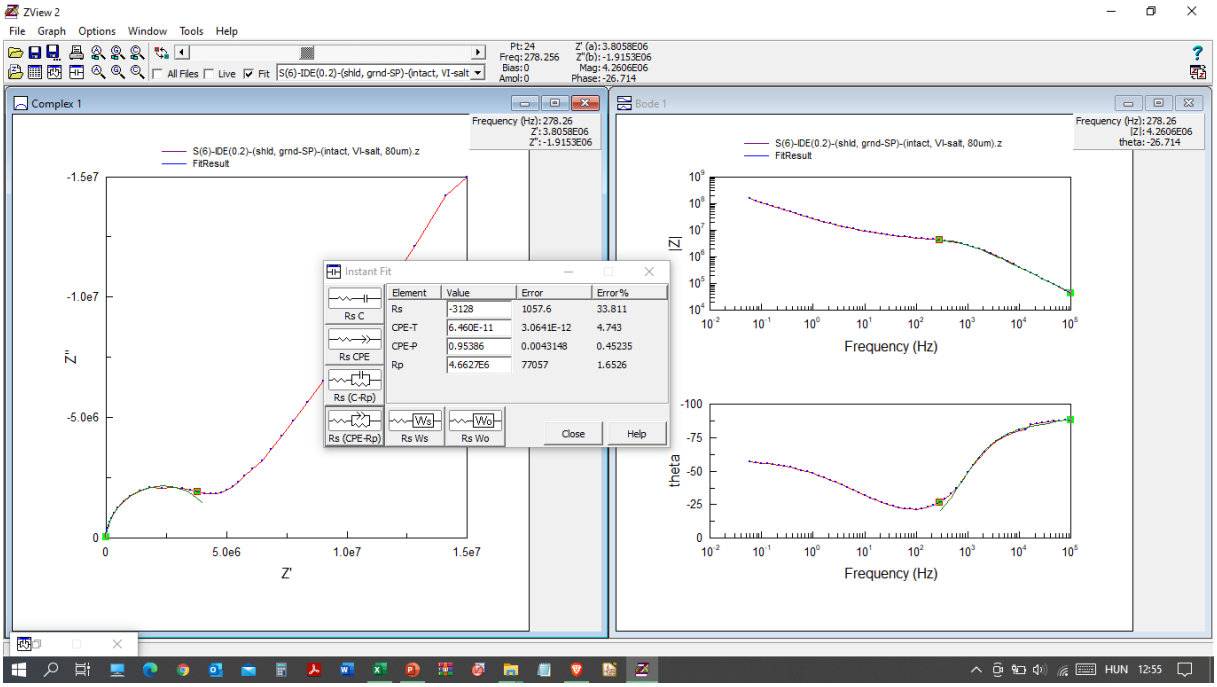

Figure A.132. The hexa-array IDE characterised salt contaminated (IV) type ‘thin red’ coating sample in intact state.

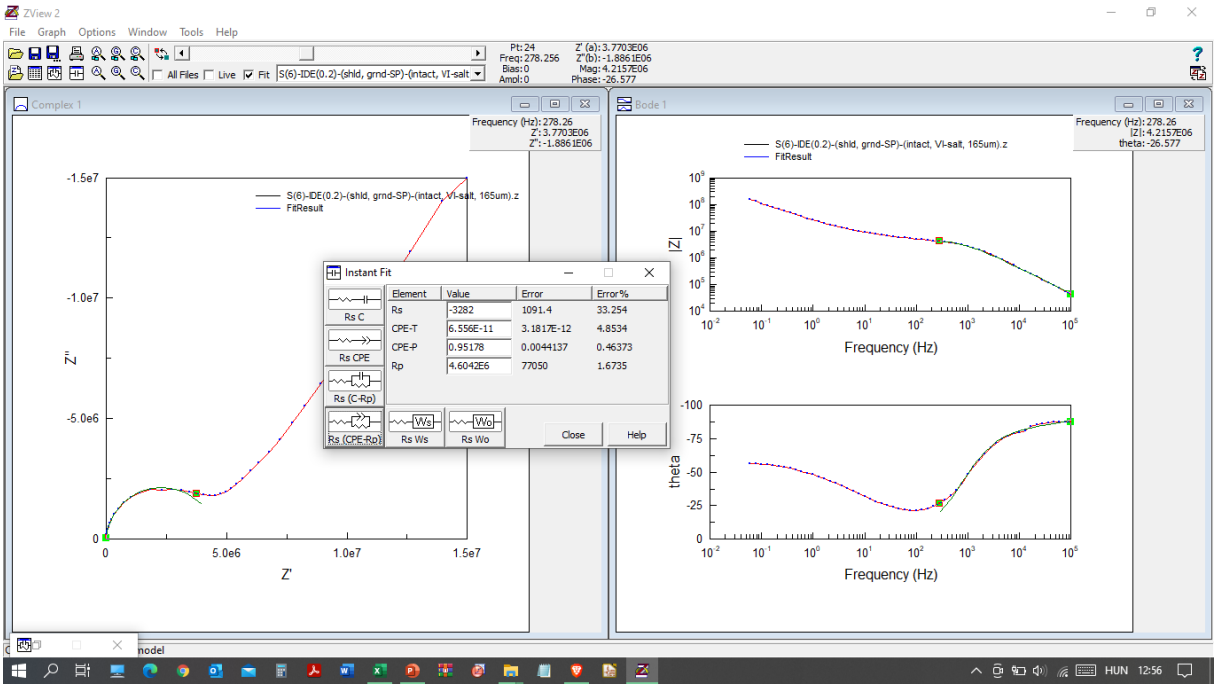

Figure A.133. The hexa-array IDE characterised salt contaminated (IV) type ‘thin red’ coating sample in intact state.

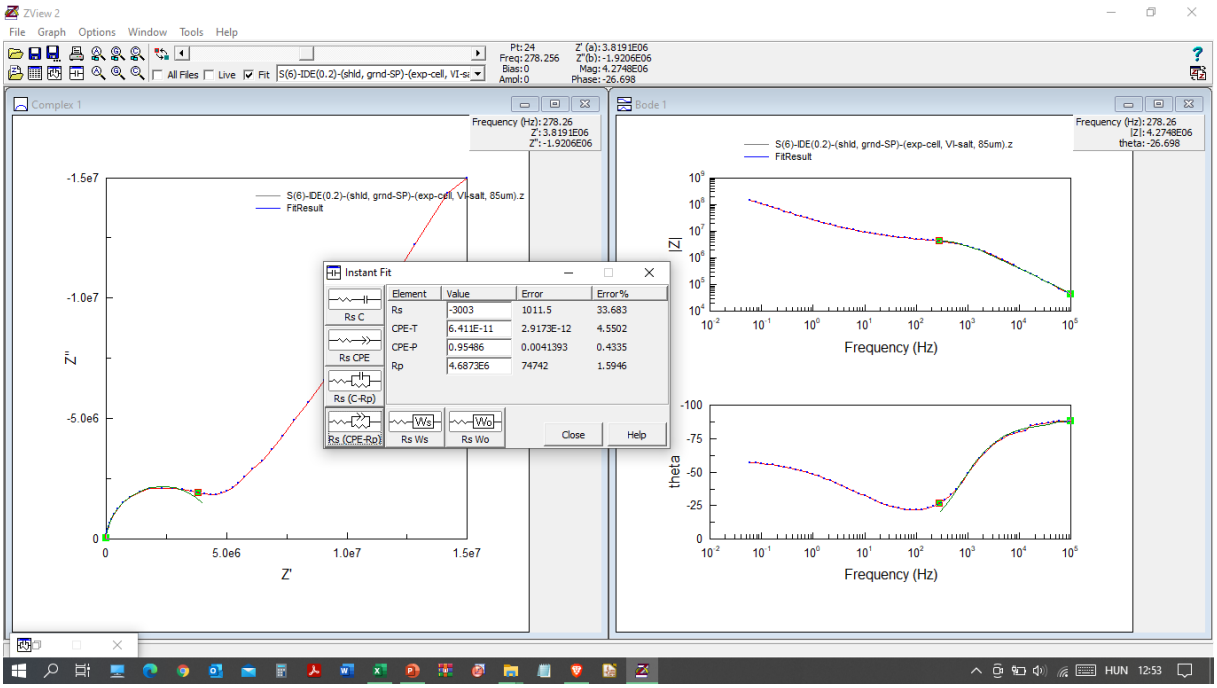

Figure A.134. The hexa-array IDE characterised salt contaminated (IV) type ‘thin red’ coating sample in exposed state.

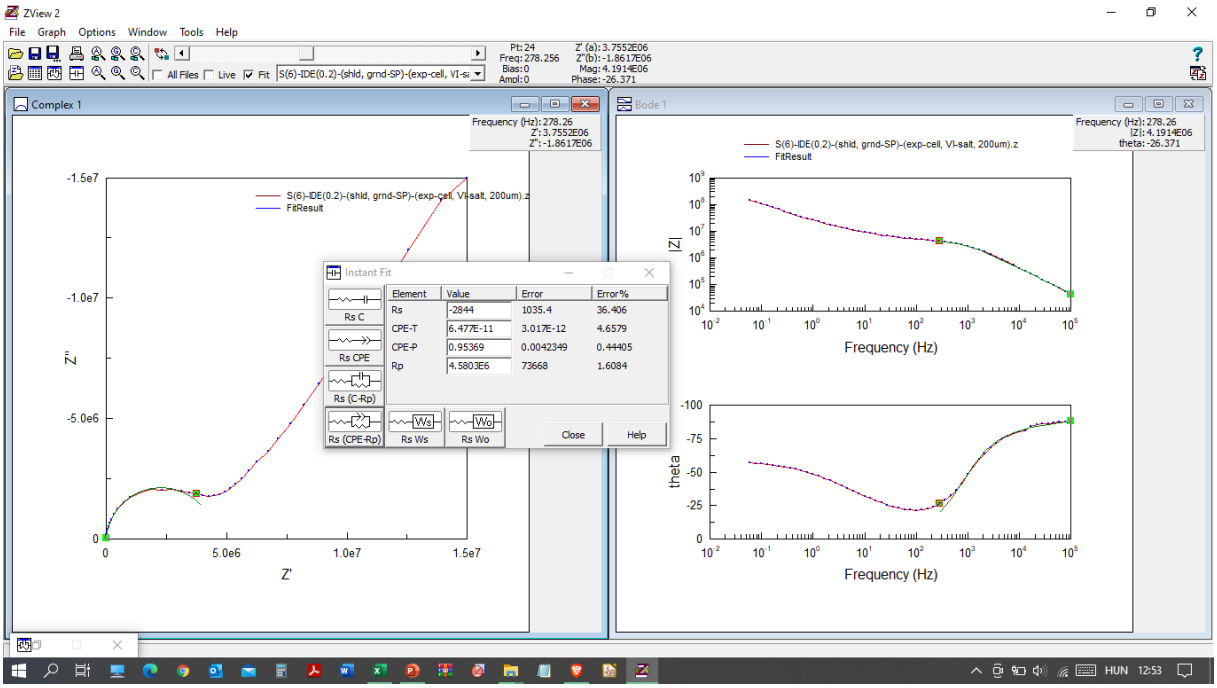

Figure A.135. The hexa-array IDE characterised salt contaminated (IV) type ‘thin red’ coating sample in exposed state.

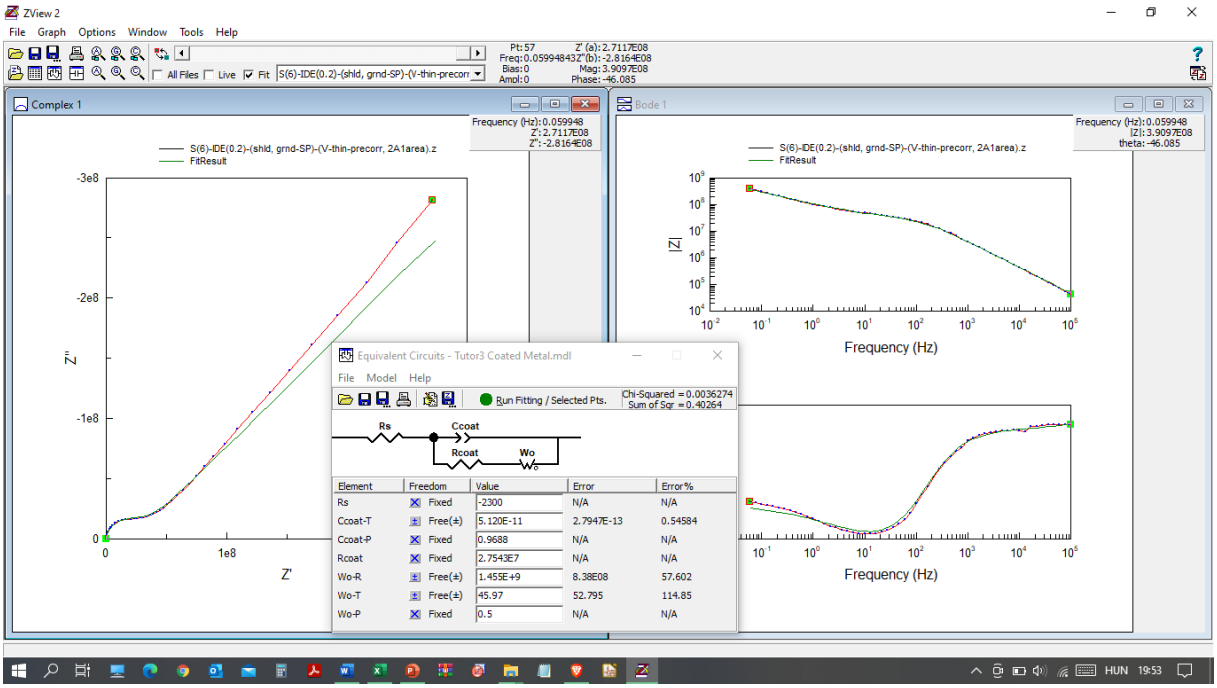

Figure A.136. The hexa-array IDE characterised pre-corroded (V) type ‘thin red’ coating sample in intact state.

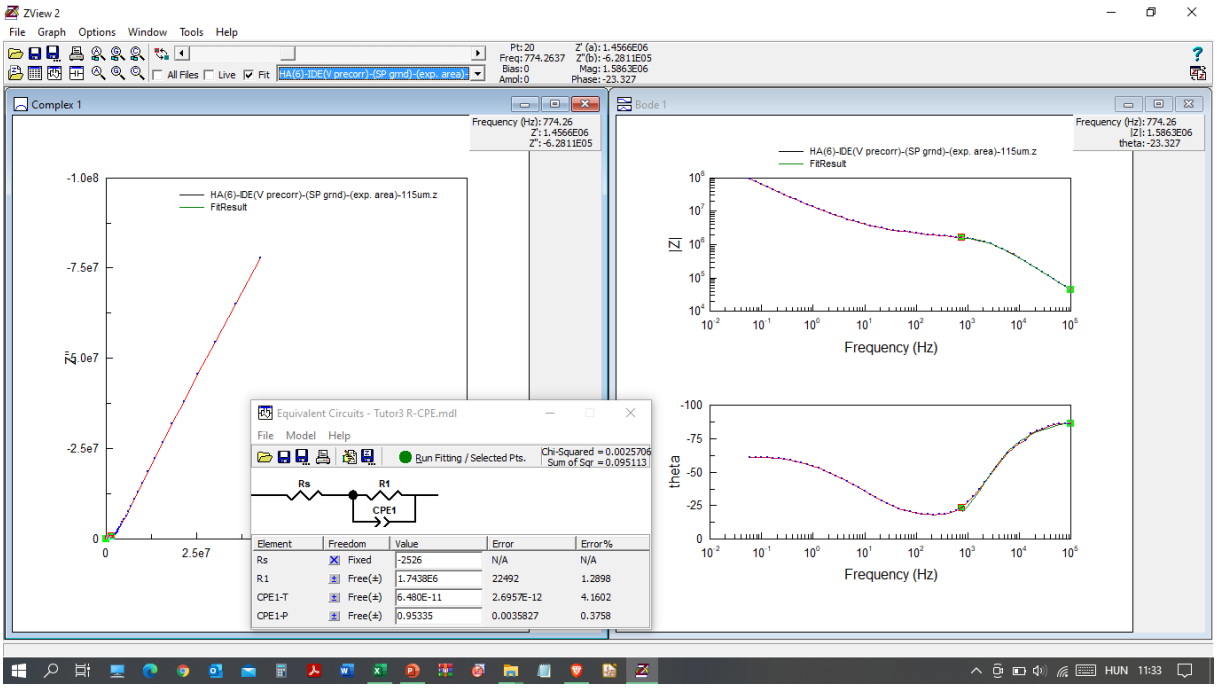

Figure A.137. The hexa-array IDE characterised pre-corroded (V) type ‘thin red’ coating sample in exposed state.

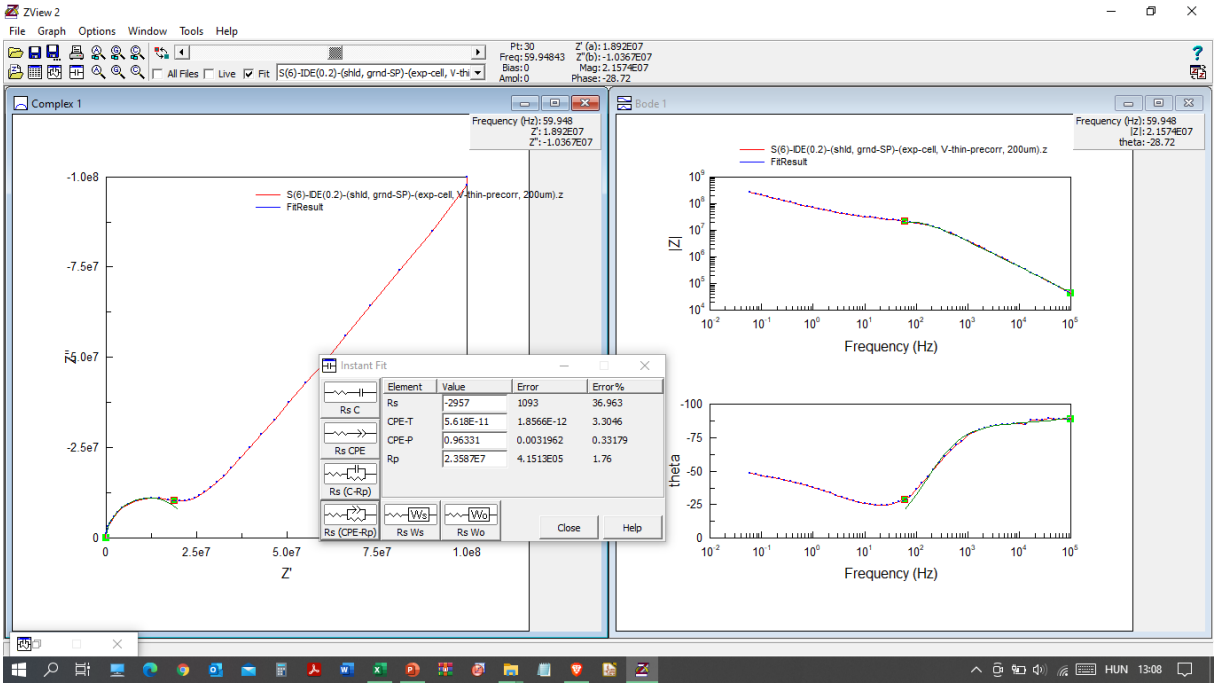

Figure A.138. The hexa-array IDE characterised pre-corroded (V) type ‘thin red’ coating sample in exposed state.

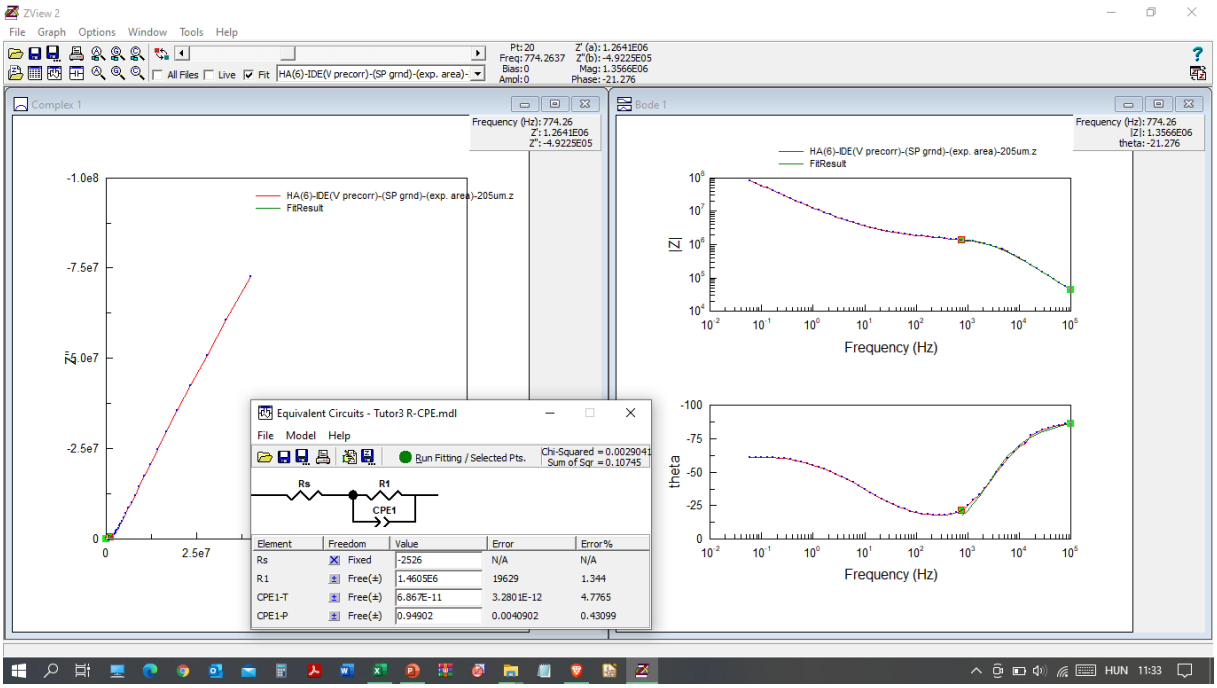

Figure A.139. The hexa-array IDE characterised pre-corroded (V) type ‘thin red’ coating sample in exposed state.

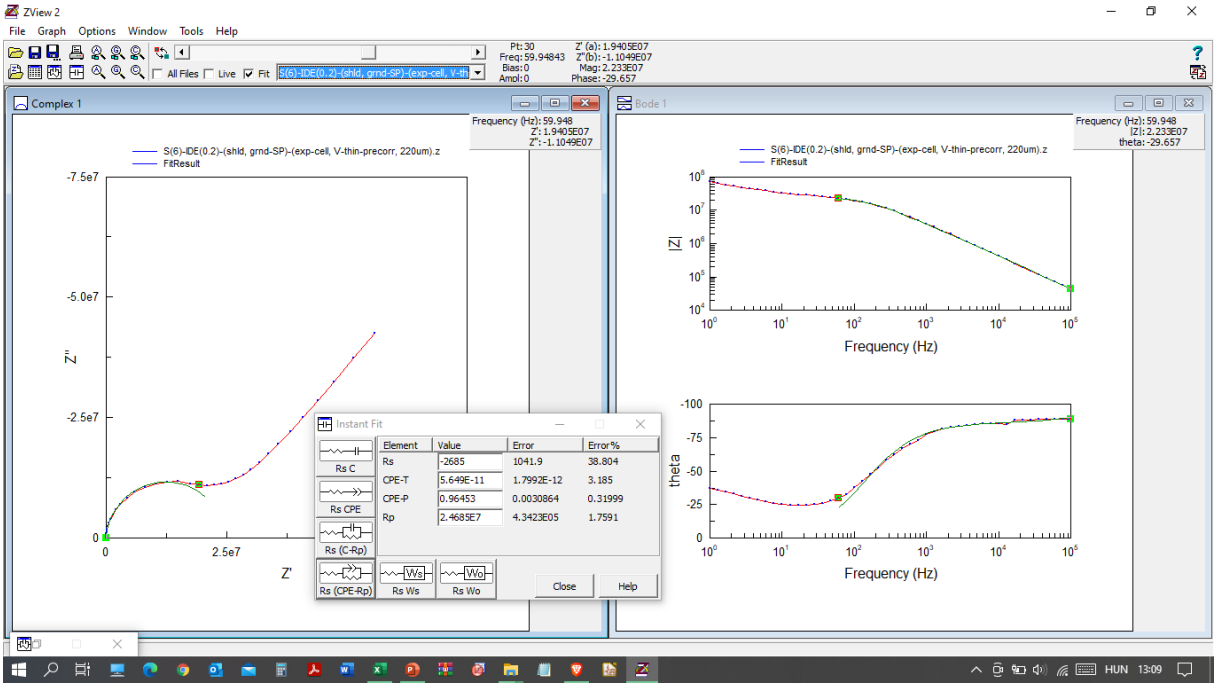

Figure A.140. The hexa-array IDE characterised pre-corroded (V) type ‘thin red’ coating sample in exposed state.

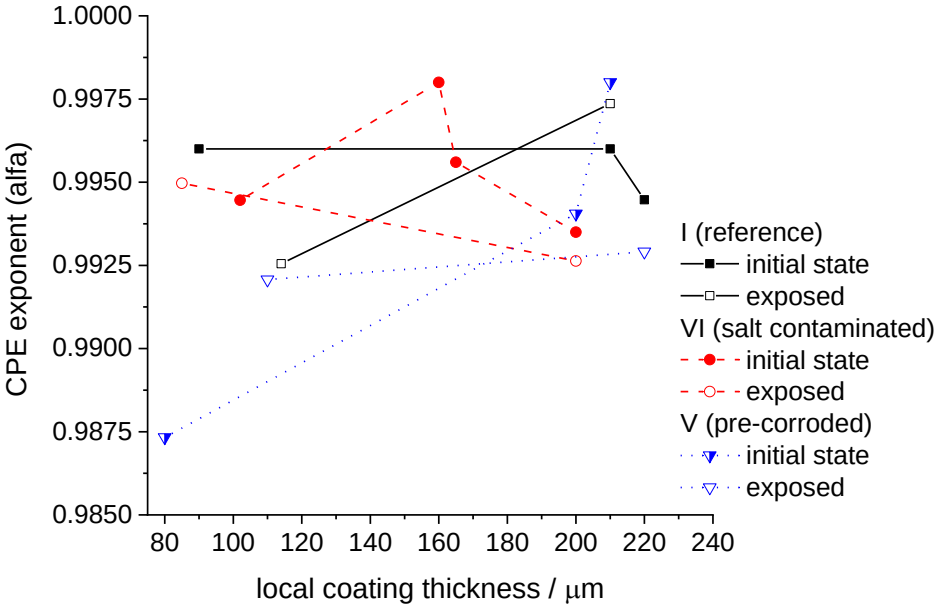

Figure A.141. CPE exponent assessed in intact and exposed (after 984 hours) states of the test panels with the mono-IDE(0.2).

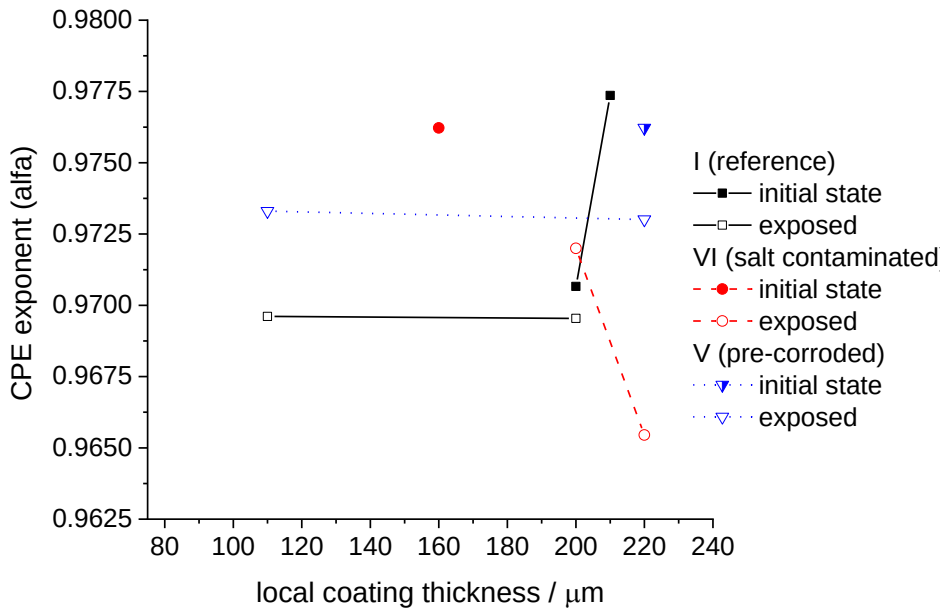

Figure A.142. CPE exponent of the test panels assessed in intact and exposed (after 984 hours) states of the test panels with the quad-array IDE(0.2).

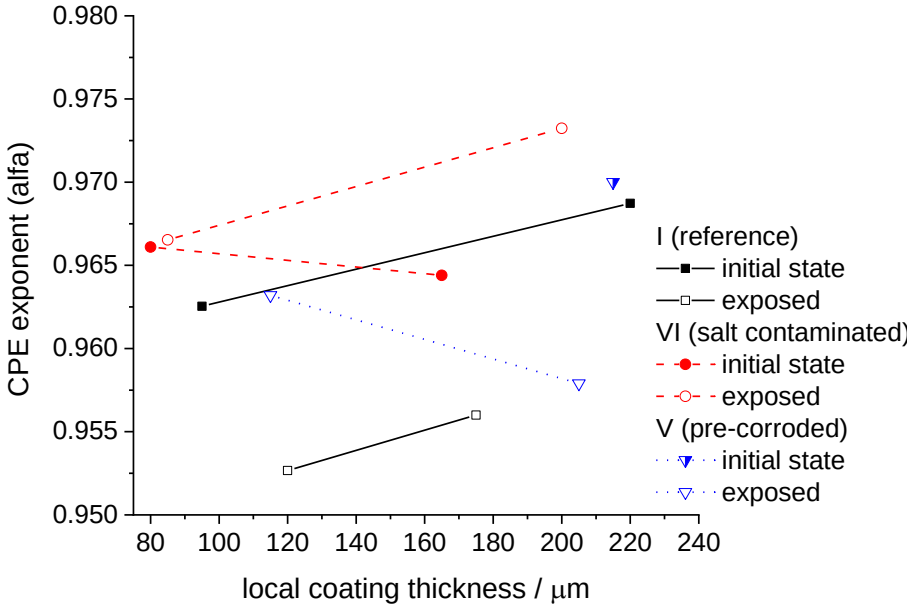

Figure A.143. CPE exponent of the test panels assessed in intact and exposed (after 984 hours) states of the test panels with the hexa-array IDE(0.2).

Appendix 3 Design Cycle III – Final Design

A3.1 Preliminary Prototypes

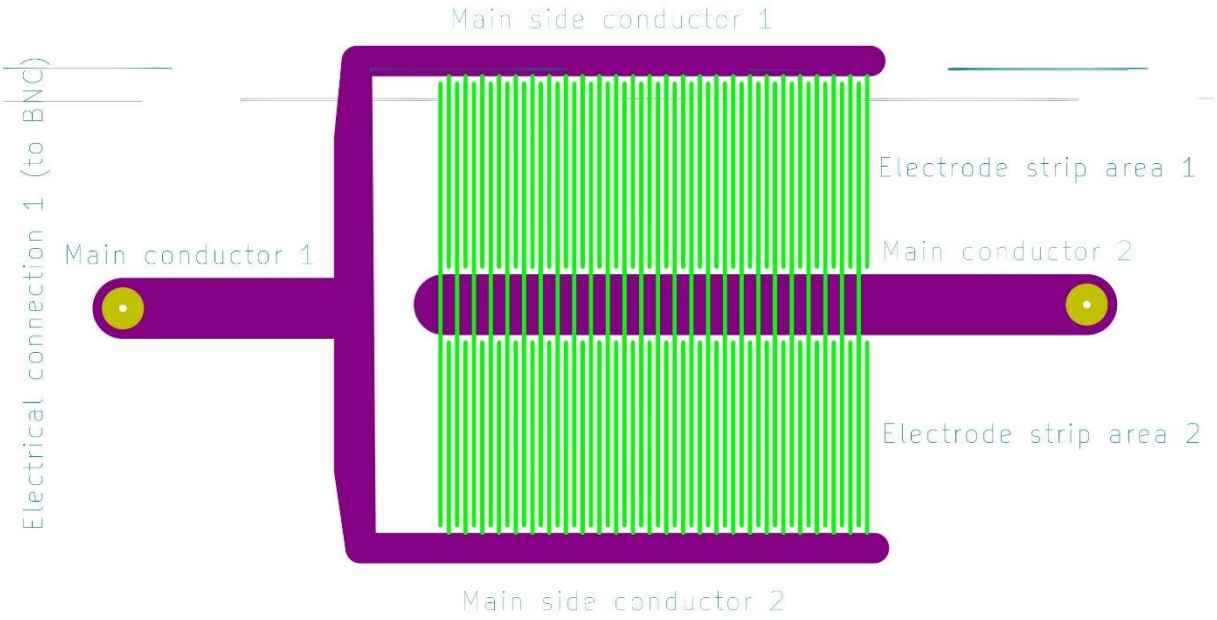

Figure A.144. The 1st initial design of IDE sensor with wide distance of pads for wire connection of driver and sensing electrodes without grounded lateral shielding electrode around the perimeter region.

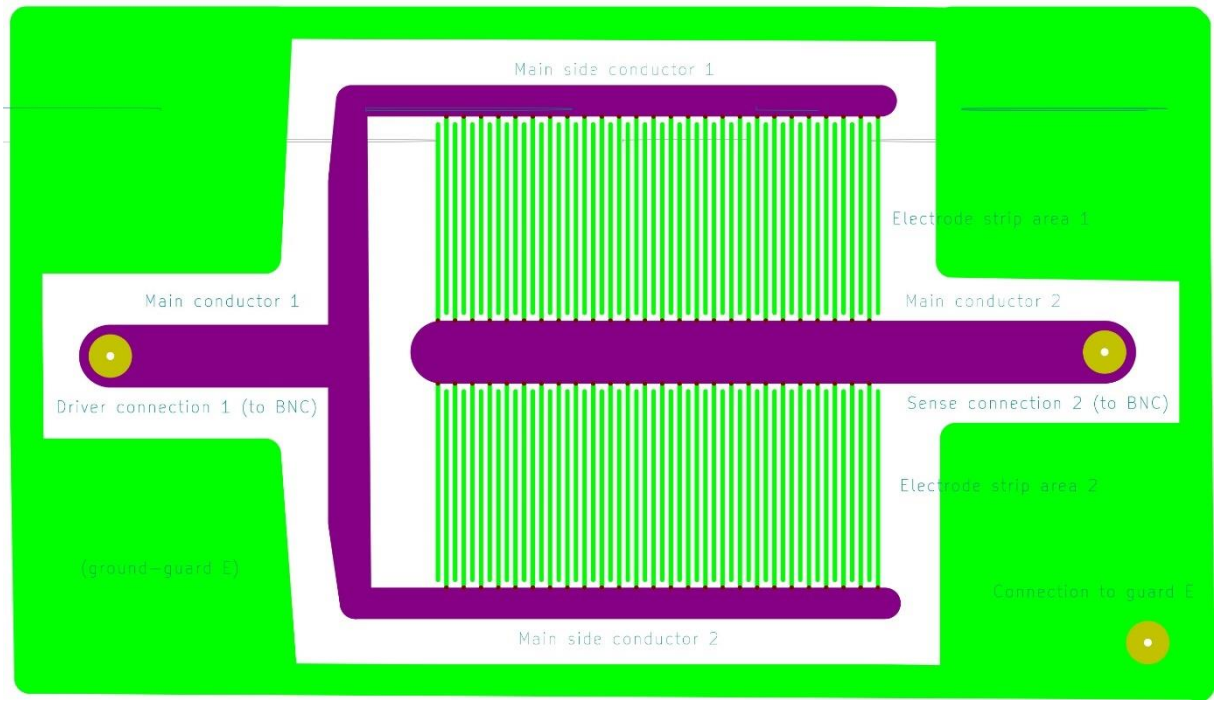

Figure A.145. The 2nd initial design of IDE sensor with wide distance of pads for wire connection of driver and sensing electrodes with grounded lateral shielding electrode around the perimeter region.

A3.2 Experimental Results

Impedance fitting results obtained to the reference type (1.5) ‘black’ coating with the concentric array sensor at low test voltage (0.1 V) are summarised in Figure A.146. Despite the low test voltage amplitude, only low noise accumulation was found in the spectra, which did not impede proper fitting and extrapolation to the LF and DC current range.

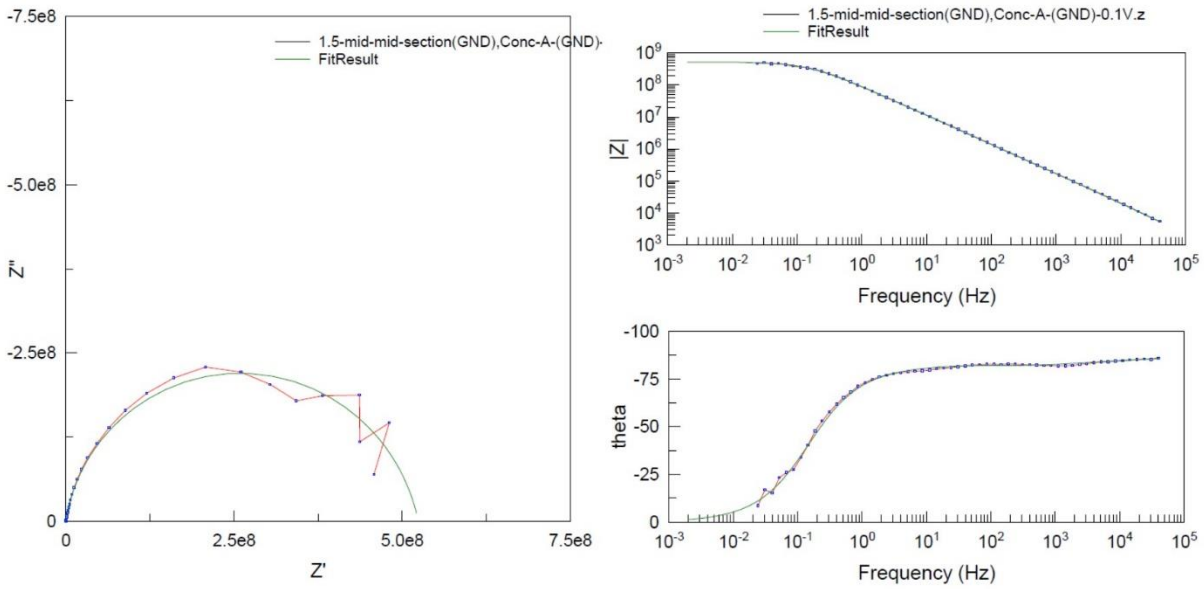

Figure A.146. Impedance fitting results of the spectra, plotted in Nyquist (left) and Bode representations (right), measured with the concentric array (CA) sensor (prototype I) by testing reference type, real maritime modelling coating ‘black’ assigned with reference number of ‘1.5’ at test voltage of 0.1 V rms.

Impedance fitting results obtained to the pre-corroded type (2.4) ‘black’ coating with the concentric array sensor at low test voltage (0.1 V) are summarised in Figure A.147, A.148 and A.149. At low test voltage, repeatability of measured data was well acceptable with the concentric array sensor. Only, the impedance magnitude, derived coating resistance was questionably high compared to the reference sample (Figure A.146). By now, excessive coating resistance estimation is known to arise by low test voltage and superposition of high resistance by the coatings and corroded layers.

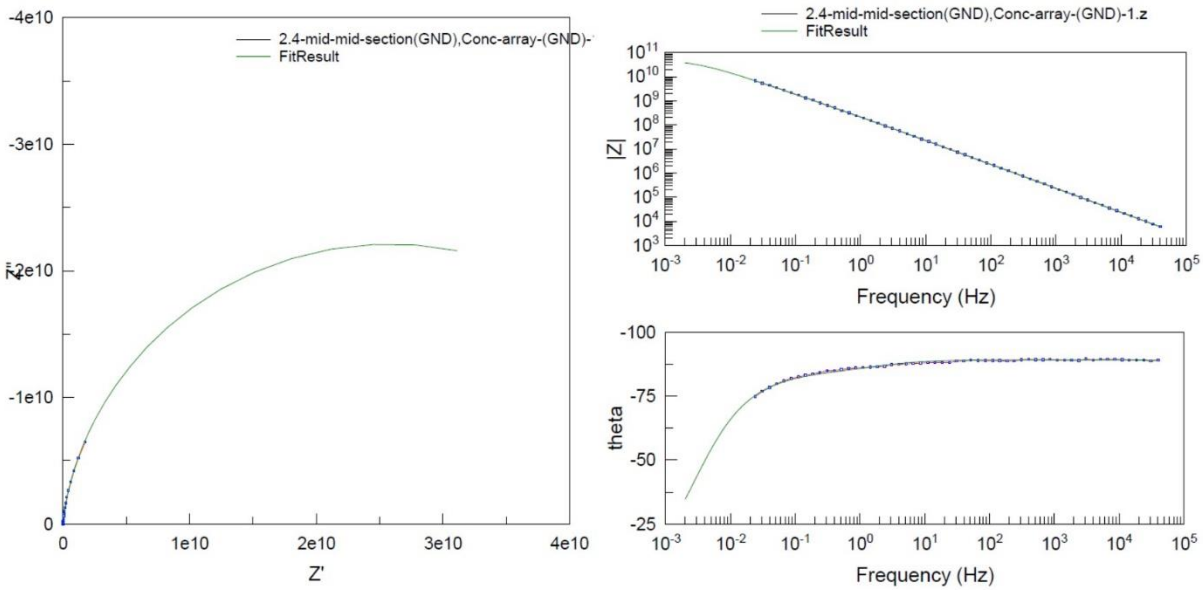

Figure A.147. Impedance fitting results of the spectra, plotted in Nyquist (left) and Bode representations (right), measured with the concentric array (CA) sensor (prototype I) by testing real maritime modelling coating 'black' assigned with reference number of '2.4' at test voltage of 0.1 V rms (parallel 1).

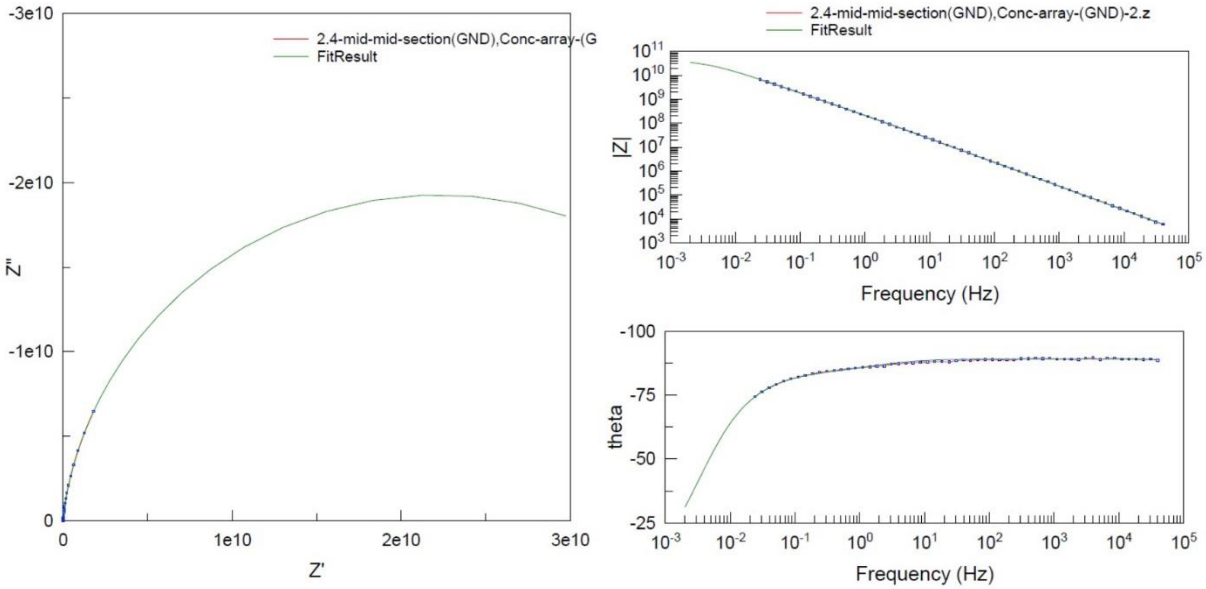

Figure A.148. Impedance fitting results of the spectra, plotted in Nyquist (left) and Bode representations (right), measured with the concentric array (CA) sensor (prototype I) by testing real maritime modelling coating 'black' assigned with reference number of '2.4' at test voltage of 0.1 V rms (parallel 2).

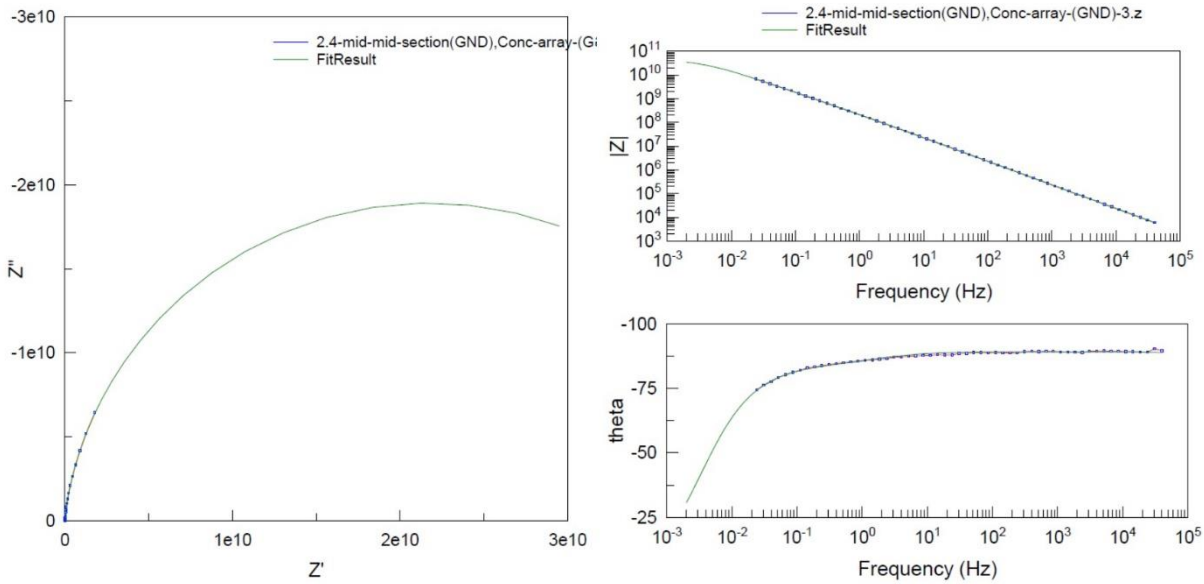

Figure A.149. Impedance fitting results of the spectra, plotted in Nyquist (left) and Bode representations (right), measured with the concentric array (CA) sensor (prototype I) by testing real maritime modelling coating 'black' assigned with reference number of '2.4' at test voltage of 0.1 V rms (parallel 3).

Fitting results obtained to the reference type (1.5) 'black' coating with the concentric array sensor with increasing test voltages (between 0.1 & 0.8 V) are summarised in Figure A.150, A.151, A.152 and A.153. Acceptable noise loading in the spectra was only experienced at the lowest test voltage (0.1 V). Anywhere between the test voltages of 0.2 and 0.8 V, noiseless impedance results were obtained. The steady magnitude and phase data are in agreement with initial condition of the coating and the absence of semiconductor layer under the coating.

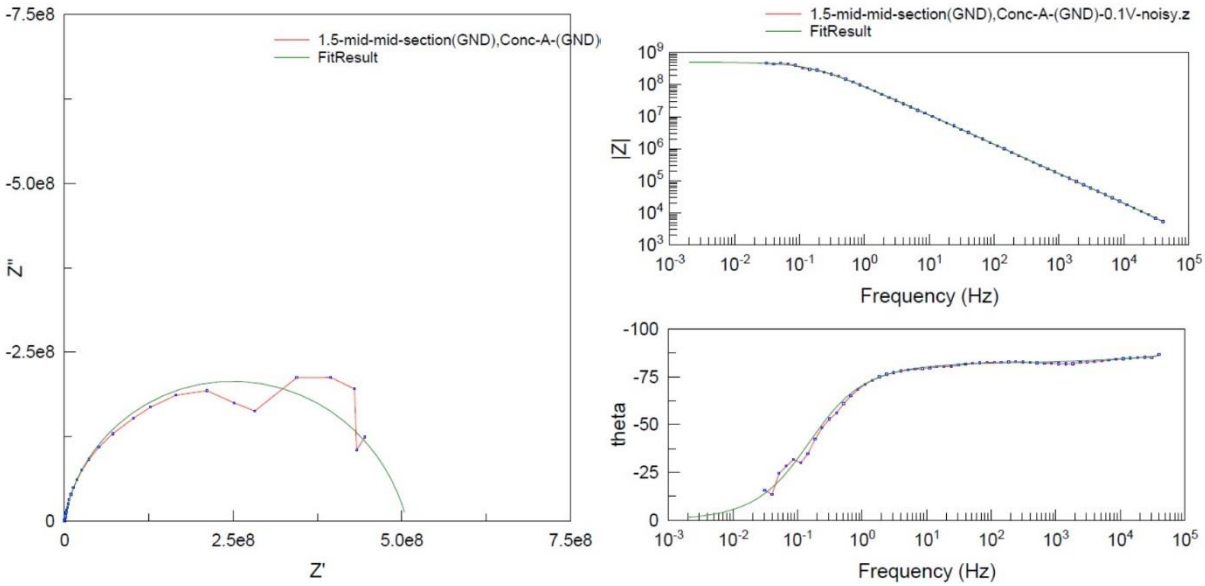

Figure A.150. Impedance fitting results of the spectra, plotted in Nyquist (left) and Bode representations (right), measured with the concentric array (CA) sensor (prototype I) by testing real maritime modelling coating 'black' assigned with reference number of '1.5' at test voltage of 0.1 V rms.

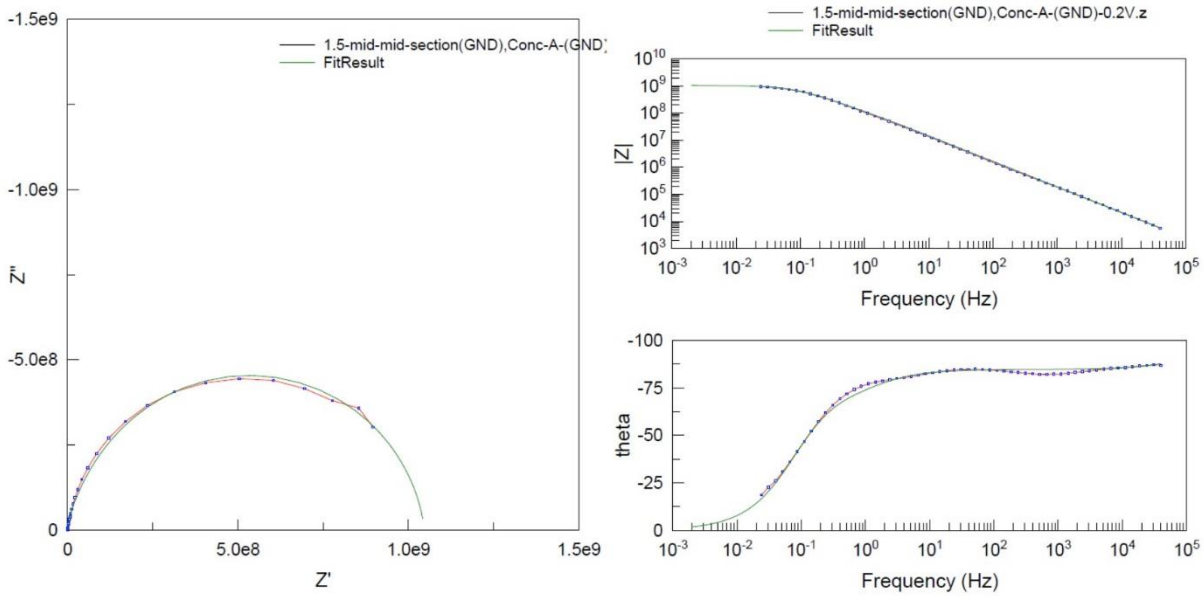

Figure A.151. Impedance fitting results of the spectra, plotted in Nyquist (left) and Bode representations (right), measured with the concentric array (CA) sensor (prototype I) by testing real maritime modelling coating 'black' assigned with reference number of '1.5' at test voltage of 0.2 V rms.

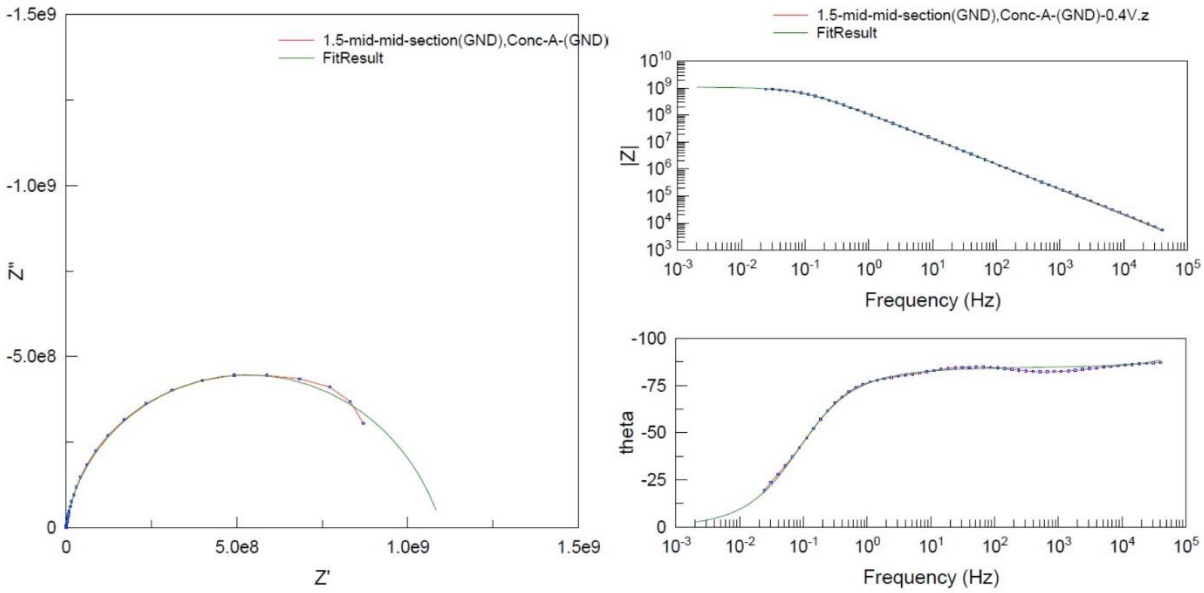

Figure A.152. Impedance fitting results of the spectra, plotted in Nyquist (left) and Bode representations (right), measured with the concentric array (CA) sensor (prototype I) by testing real maritime modelling coating 'black' assigned with reference number of '1.5' at test voltage of 0.4 V rms.

Fitting results obtained to the pre-corroded type (2.4) 'black' coating with the concentric array sensor with increasing test voltages (between 0.1 & 0.8 V) are summarised in Figure A.154, A.155, A.156 and A.157.

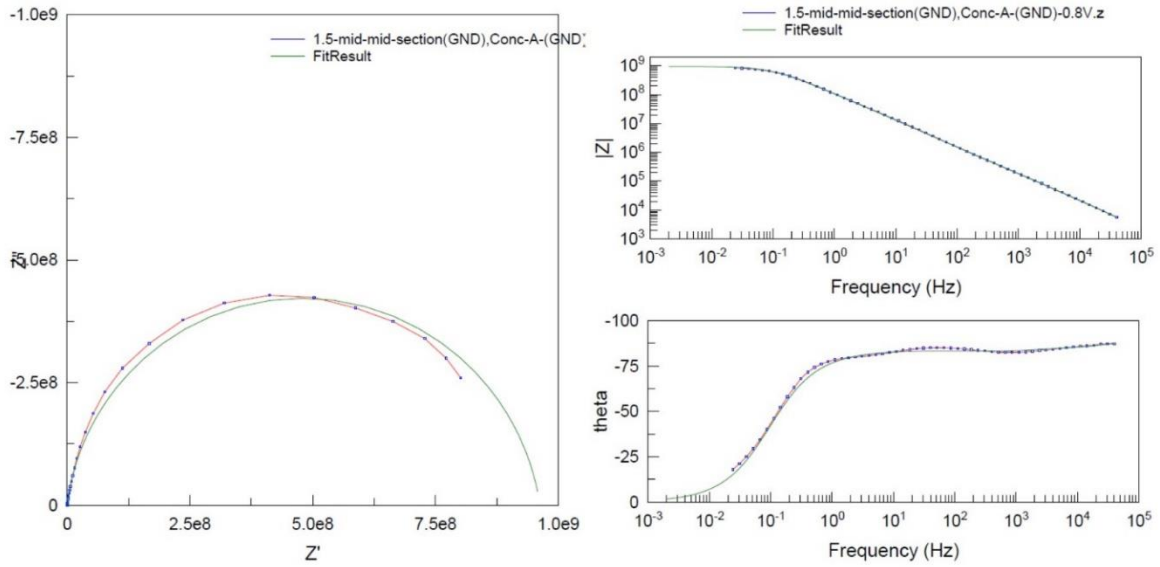

Figure A.153. Impedance fitting results of the spectra, plotted in Nyquist (left) and Bode representations (right), measured with the concentric array (CA) sensor (prototype I) by testing real maritime modelling coating 'black' assigned with reference number of '1.5' at test voltage of 0.8 V rms.

The spectra were noiseless at all test voltages (between 0.1 and 0.8 V). According to semiconductor nature of dry corroded metal oxide layers under coatings, increasing test voltages led to decreasing resistance of the entire system noticed as largely reduced impedance magnitude partly related to the coating. Except for data obtained at the lowest test voltage (0.1 V), all impedance magnitude, coating resistance results were lower compared to the dataset measured to the reference type coating.

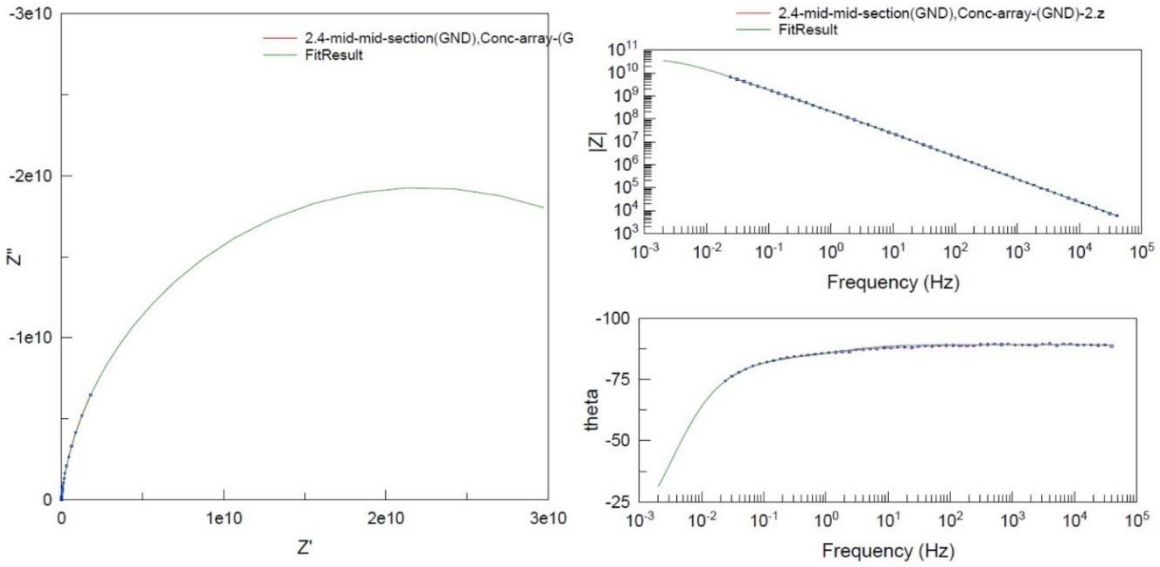

Figure A.154. Impedance fitting results of the spectra, plotted in Nyquist (left) and Bode representations (right), measured with the concentric array (CA) sensor (prototype I) by testing real maritime modelling coating 'black' assigned with reference number of '2.4' at test voltage of 0.1 V rms.

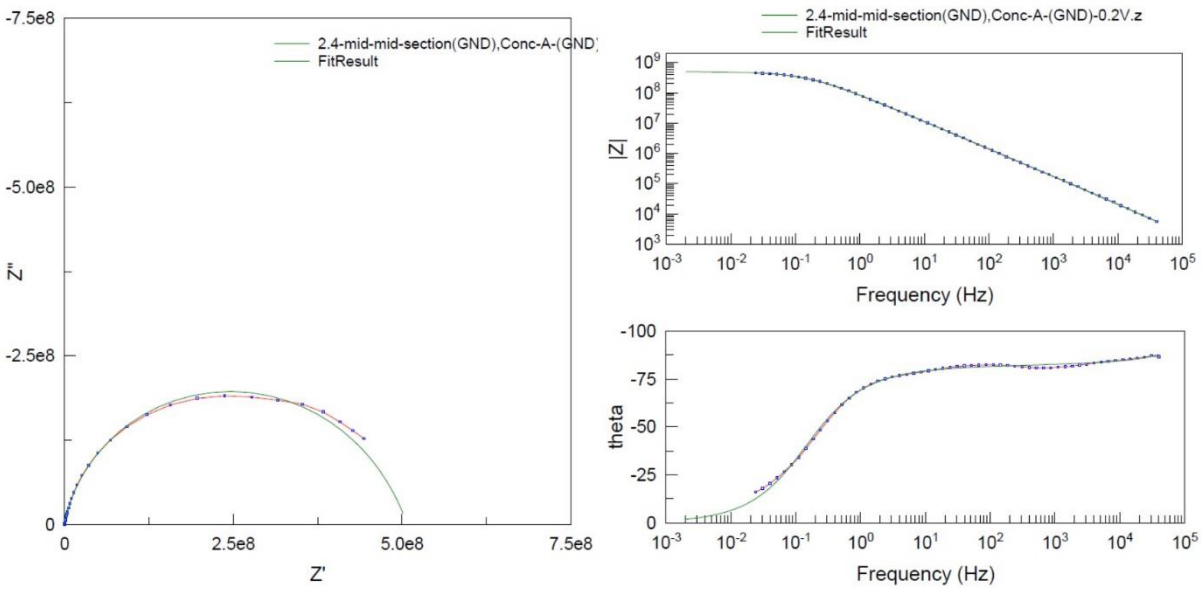

Figure A.155. Impedance fitting results of the spectra, plotted in Nyquist (left) and Bode representations (right), measured with the concentric array (CA) sensor (prototype I) by testing real maritime modelling coating 'black' assigned with reference number of '2.4' at test voltage of 0.2 V rms.

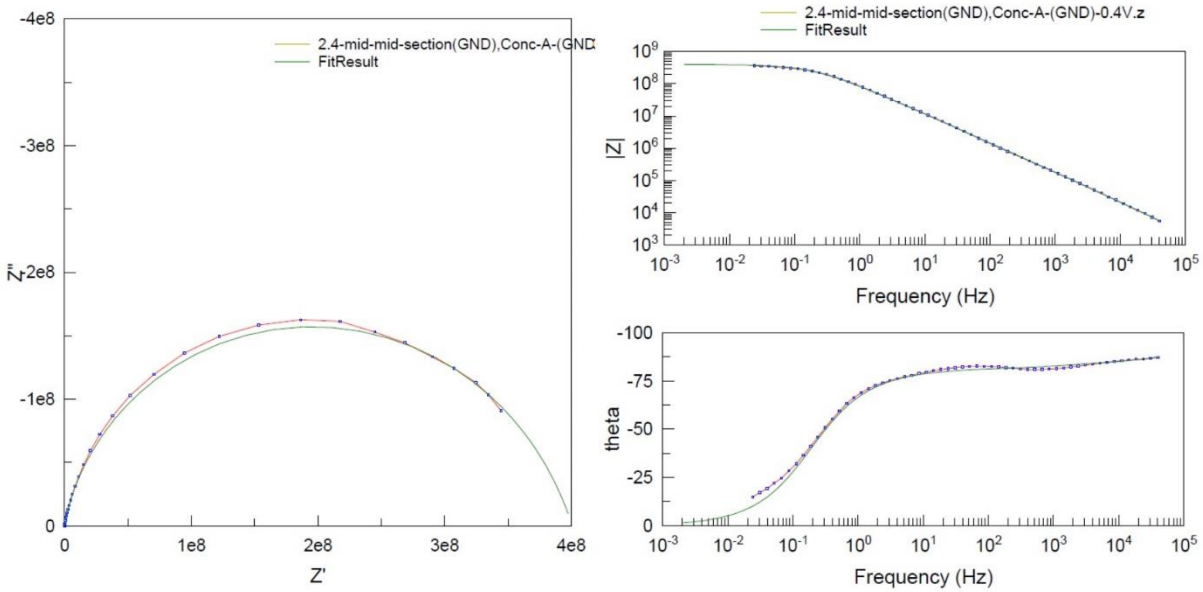

Figure A.156. Impedance fitting results of the spectra, plotted in Nyquist (left) and Bode representations (right), measured with the concentric array (CA) sensor (prototype I) by testing real maritime modelling coating 'black' assigned with reference number of '2.4' at test voltage of 0.4 V rms.

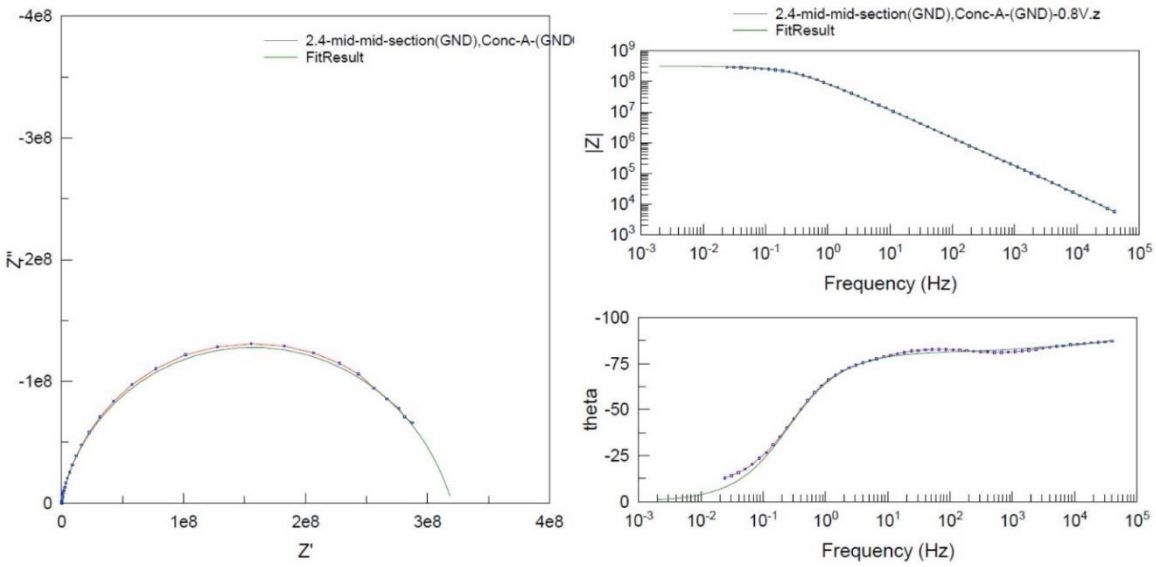

Figure A.157. Impedance fitting results of the spectra, plotted in Nyquist (left) and Bode representations (right), measured with the concentric array (CA) sensor (prototype I) by testing real maritime modelling coating 'black' assigned with reference number of '2.4' at test voltage of 0.8 V rms.

Fitting results obtained to the salt contaminated type (3.5) 'black' coating with the concentric array sensor with increasing test voltages (between 0.1 & 0.8 V) are summarised in Figure A.158, A.159, A.160 and A.161. Similar to other cases, spectra were noiseless in the main frequency range at all test voltages (between 0.1 and 0.8 V). Minor semiconductor effect in the form of decreasing coating resistance was found with the increasing test voltages, due to the presence of chemical contaminants under coating. With this sample, all coating resistance results were lower compared to the dataset measured to the reference type coating (1.5).

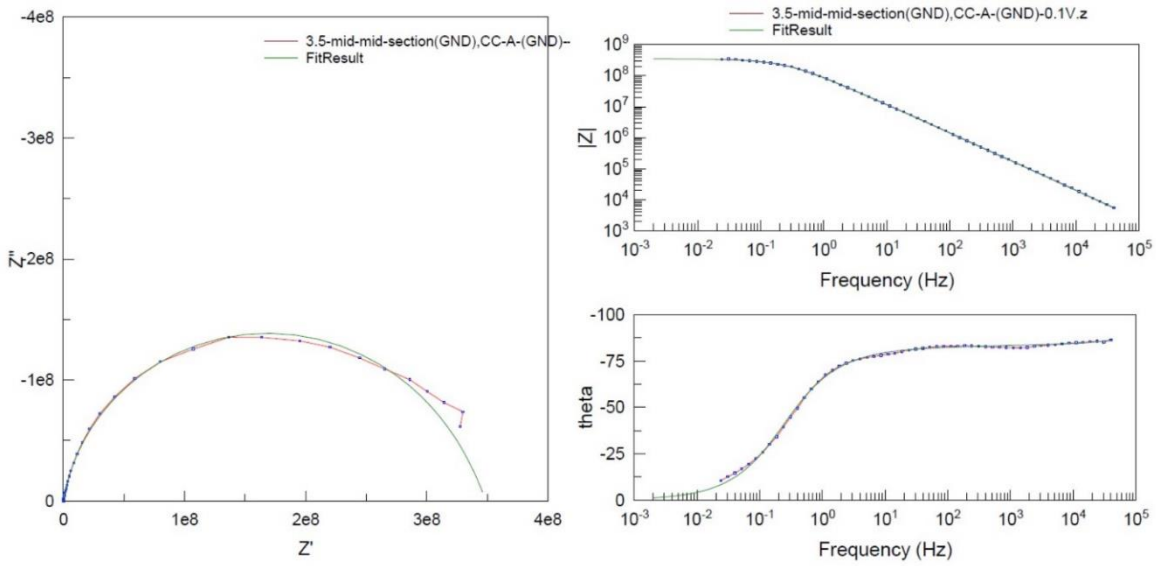

Figure A.158. Impedance fitting results of the spectra, plotted in Nyquist (left) and Bode representations (right), measured with the concentric array (CA) sensor (prototype I) by testing real maritime modelling coating 'black' assigned with reference number of '3.5' at test voltage of 0.1 V rms.

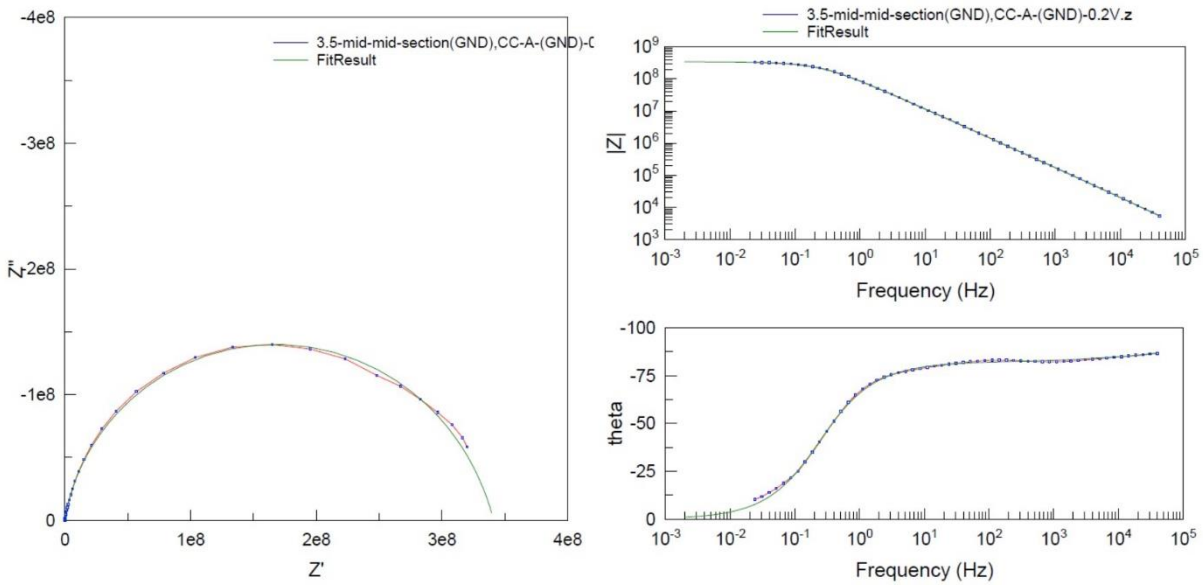

Figure A.159. Impedance fitting results of the spectra, plotted in Nyquist (left) and Bode representations (right), measured with the concentric array (CA) sensor (prototype I) by testing real maritime modelling coating 'black' assigned with reference number of '3.5' at test voltage of 0.2 V rms.

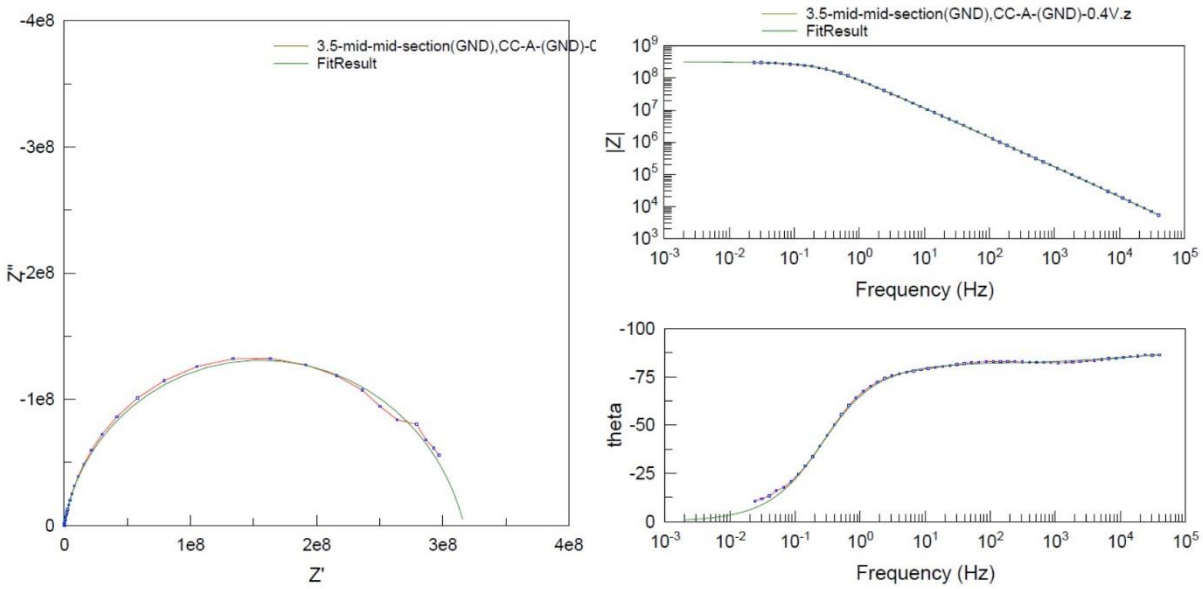

Figure A.160. Impedance fitting results of the spectra, plotted in Nyquist (left) and Bode representations (right), measured with the concentric array (CA) sensor (prototype I) by testing real maritime modelling coating 'black' assigned with reference number of '3.5' at test voltage of 0.4 V rms.

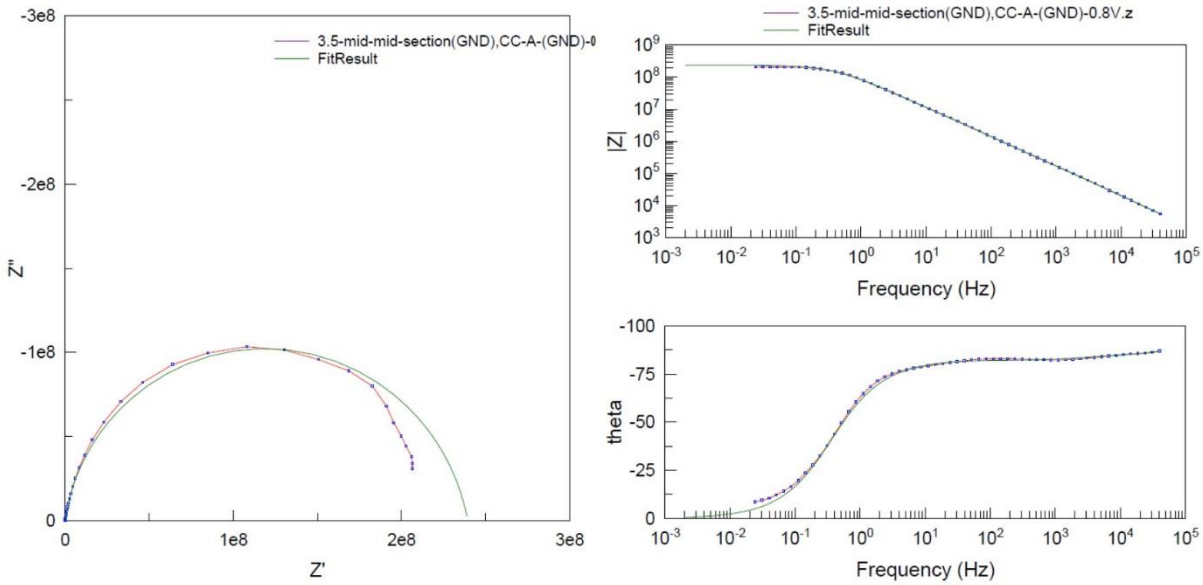

Figure A.161. Impedance fitting results of the spectra, plotted in Nyquist (left) and Bode representations (right), measured with the concentric array (CA) sensor (prototype I) by testing real maritime modelling coating 'black' assigned with reference number of '3.5' at test voltage of 0.8 V rms.

Moderate repeatability of the wet phase setup at the beginning of electrical testing was experienced as exhibited in changing impedance magnitudes in Figure A.162 and A.163.

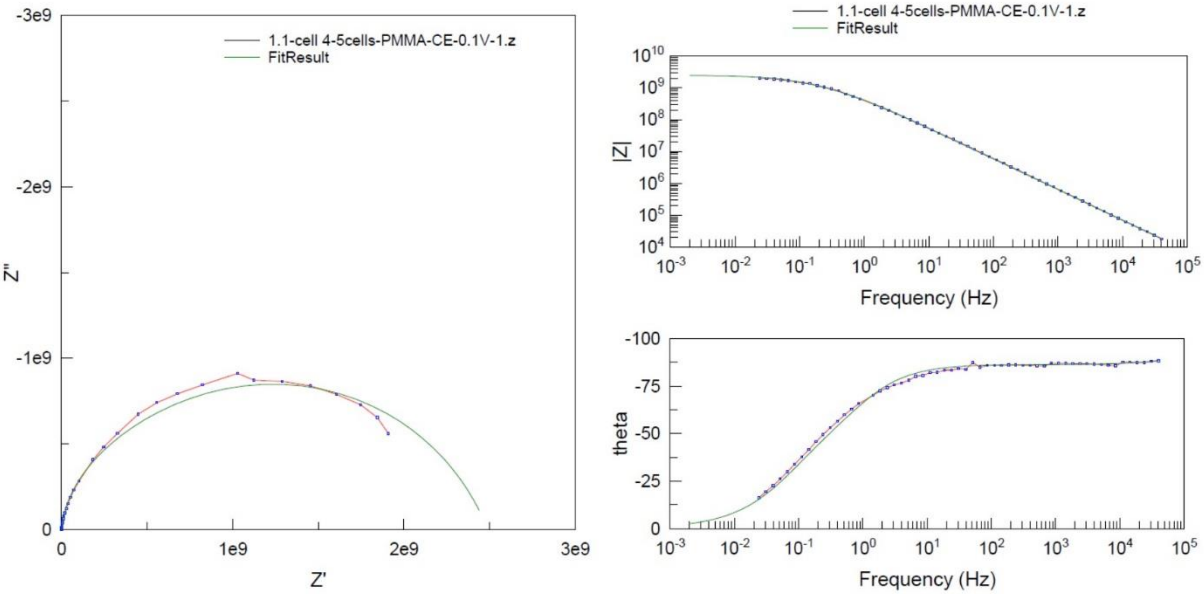

Figure A.162. Impedance fitting results of the spectra, plotted in Nyquist (left) and Bode representations (right), measured with the PMMA-CE by testing real maritime modelling neat, reference coating 'black' assigned with reference number of '1.1' at test voltage of 0.1 V rms (parallel 1).

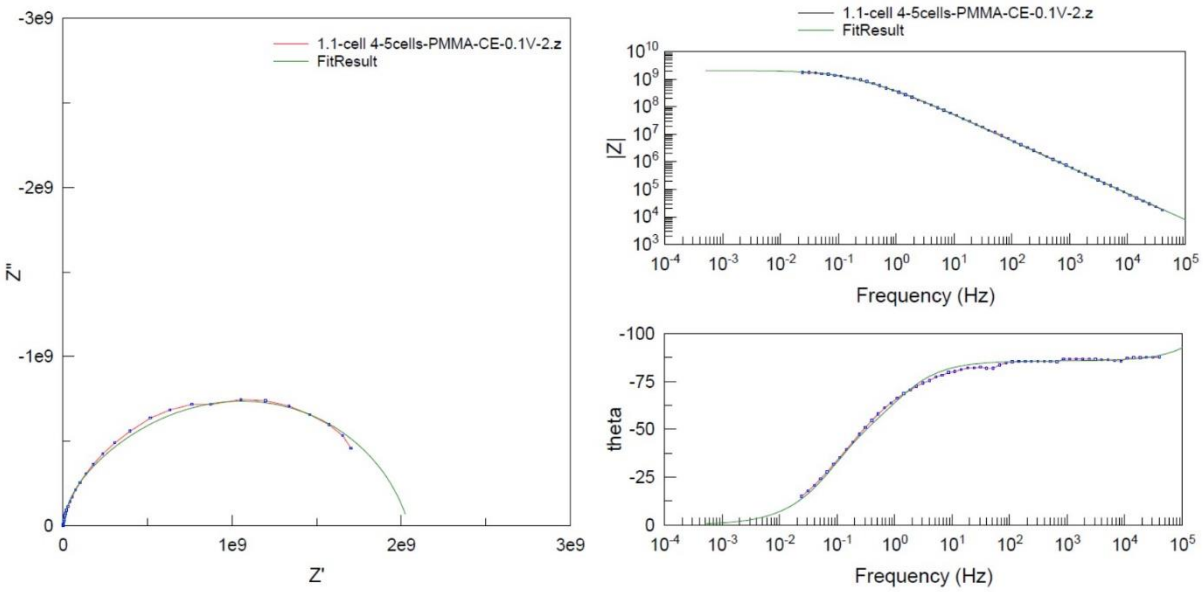

Figure A.163. Impedance fitting results of the spectra, plotted in Nyquist (left) and Bode representations (right), measured with the PMMA-CE by testing real maritime modelling neat, reference coating 'black' assigned with reference number of '1.1' at test voltage of 0.1 V rms (parallel 2).

The pre-corroded coating samples could still be well fitted with two time-constants type, ladder type electrical circuit topology, even though multiple layer scaling of the coating and corroded layer with various electrolyte infiltration degree led to widely extended frequency ranges of the time constants, as a superposition to the unavoidable dispersion by the two-cells effect. Fitting results are presented in Figure A.164 and A.165.

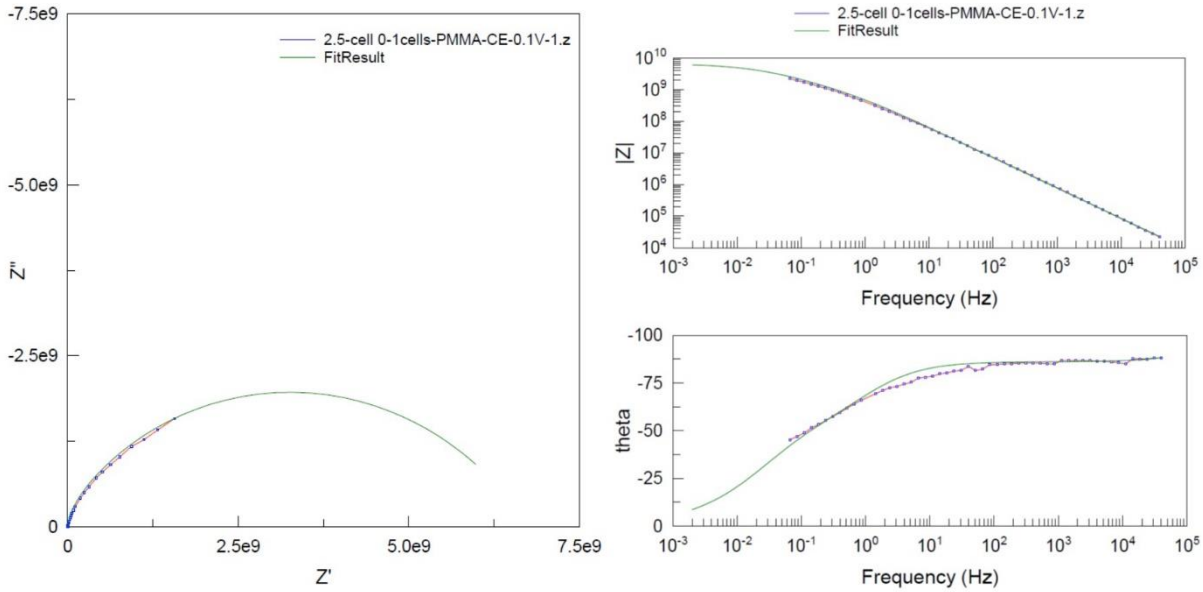

Figure A.164. Impedance fitting results of the spectra, plotted in Nyquist (left) and Bode representations (right), measured with the PMMA-CE by testing real maritime modelling pre-corroded coating 'black' assigned with reference number of '2.5' at test voltage of 0.1 V rms (parallel 1).

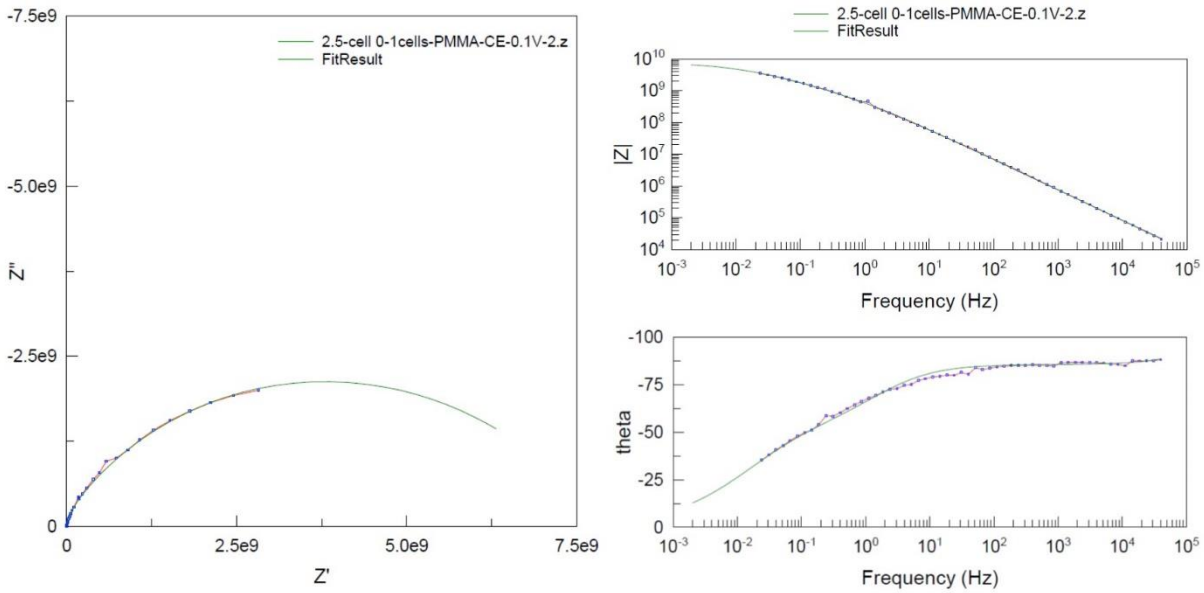

Figure A.165. Impedance fitting results of the spectra, plotted in Nyquist (left) and Bode representations (right), measured with the PMMA-CE by testing real maritime modelling pre-corroded coating 'black' assigned with reference number of '2.5' at test voltage of 0.1 V rms (parallel 2).

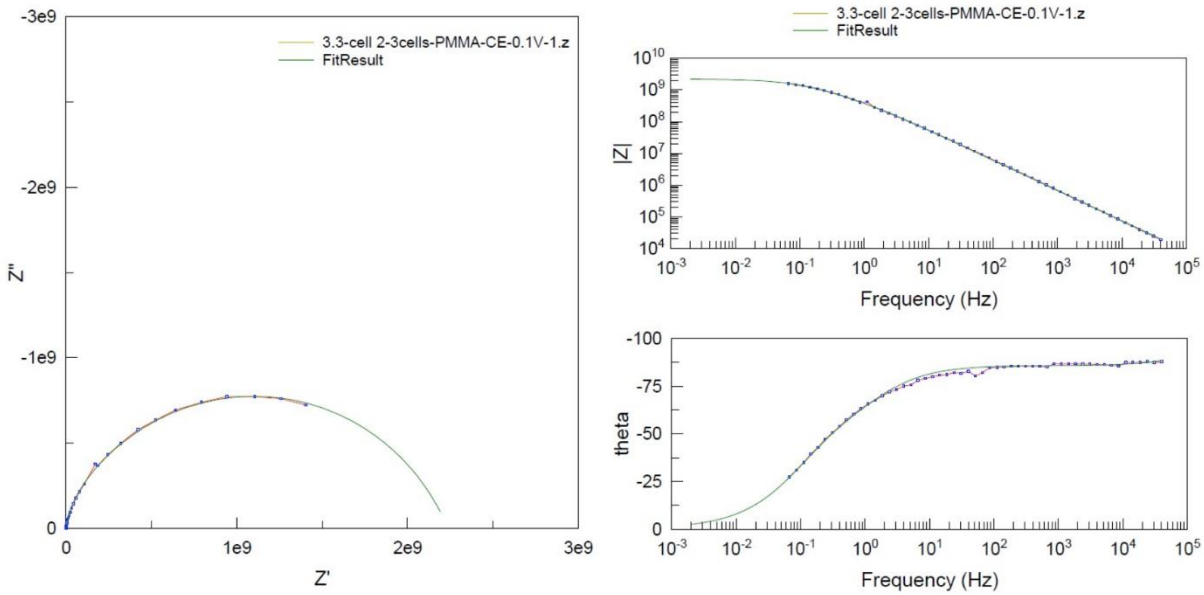

Figure A.166. Impedance fitting results of the spectra, plotted in Nyquist (left) and Bode representations (right), measured with the PMMA-CE by testing real maritime modelling salt-contaminated coating 'black' assigned with reference number of '3.3' at test voltage of 0.1 V rms (parallel 1).

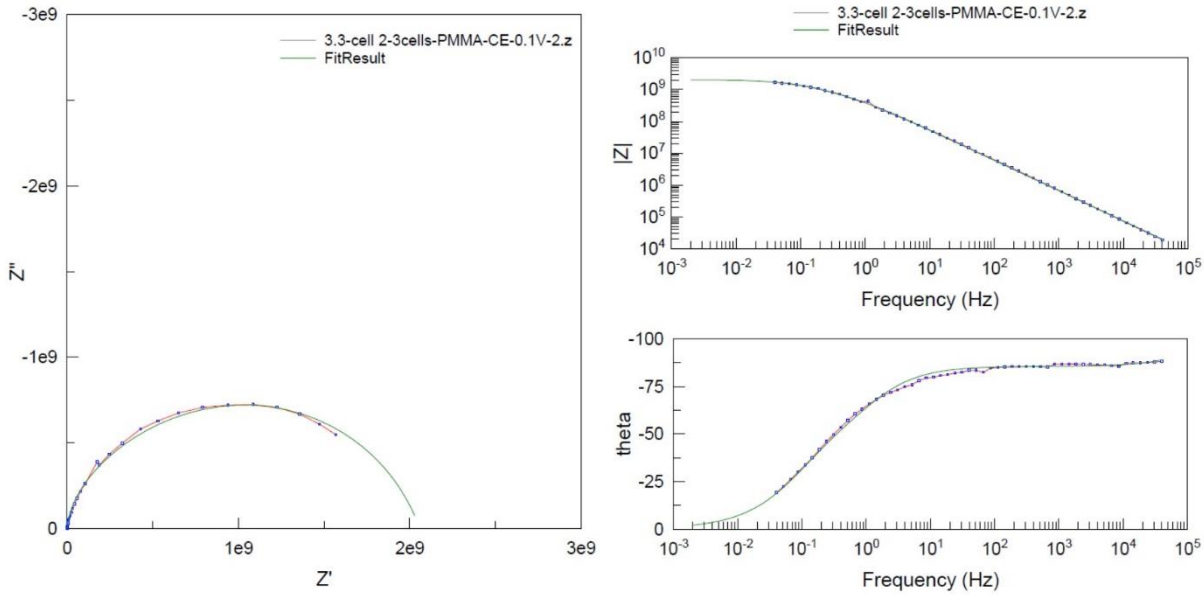

Figure A.167. Impedance fitting results of the spectra, plotted in Nyquist (left) and Bode representations (right), measured with the PMMA-CE by testing real maritime modelling salt-contaminated coating 'black' assigned with reference number of '3.3' at test voltage of 0.1 V rms (parallel 2).

Similar to other areas on the surface (Figure A.166 and A.167), repeatability of the wet phase test setup with the salt contaminated 'black' coating sample is given in Figure A.168, A.169 and A.170. The spectra were noiseless and the detected current was in the well measurable range, ensuring easy and reliable extrapolation to the LF range. Magnitude difference between the first and the second and all subsequent spectra could be noticed, which remained within acceptable limits.

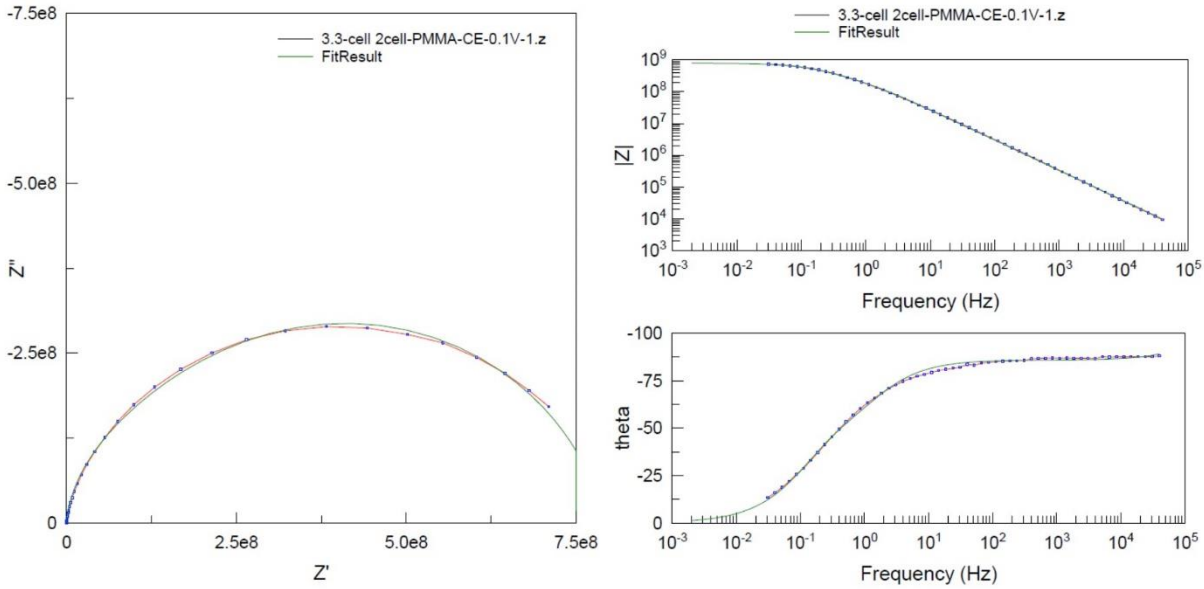

Figure A.168. Impedance fitting results of the spectra, plotted in Nyquist (left) and Bode representations (right), measured with the PMMA-CE by testing real maritime modelling salt-contaminated coating 'black' assigned with reference number of '3.3' at test voltage of 0.1 V rms (parallel 1).

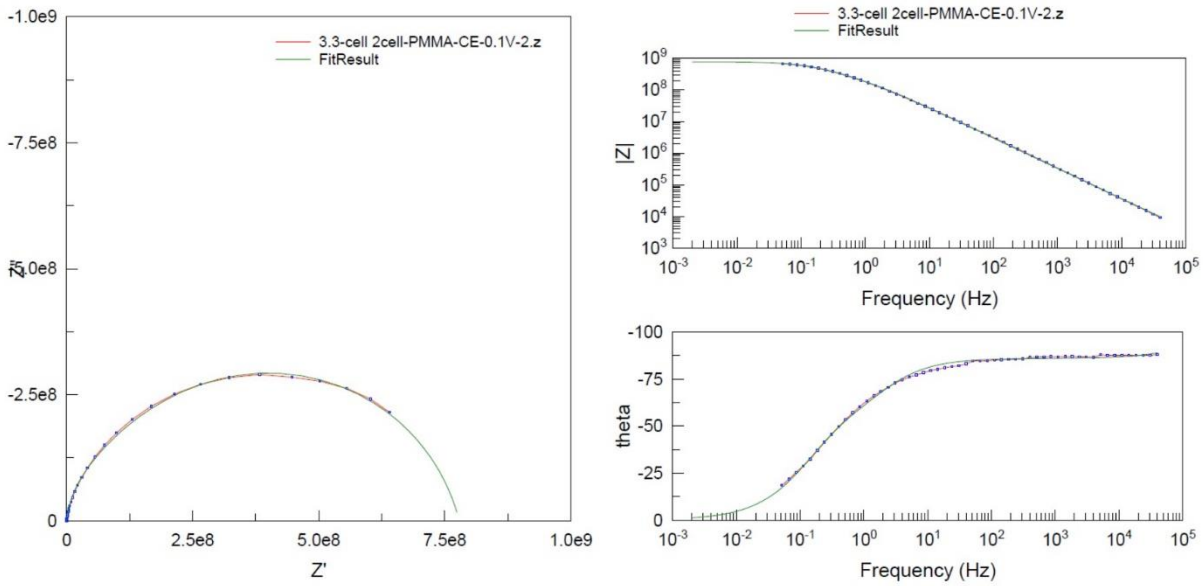

Figure A.169. Impedance fitting results of the spectra, plotted in Nyquist (left) and Bode representations (right), measured with the PMMA-CE by testing real maritime modelling salt-contaminated coating 'black' assigned with reference number of '3.3' at test voltage of 0.1 V rms (parallel 2).

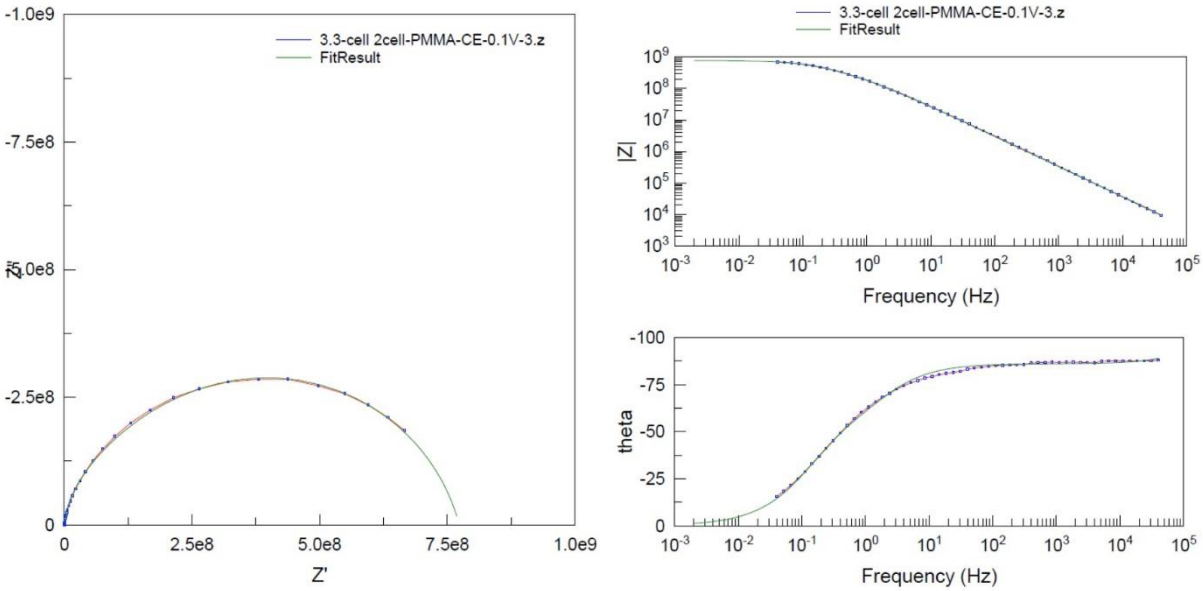

Figure A.170. Impedance fitting results of the spectra, plotted in Nyquist (left) and Bode representations (right), measured with the PMMA-CE by testing real maritime modelling salt-contaminated coating 'black' assigned with reference number of '3.3' at test voltage of 0.1 V rms (parallel 3).

Impedance data of the long-term exposed and unconditioned state of the 'white' coating tested with the IDE-0.55 and the IDE-1.1 sensors are presented in Figure A.171 and A.172, respectively. In case of the IDE-0.55, the best quality impedance spectrum could only be used for evaluation of the LF range. Not any other measurement data were comparable and informative for coating assessment, due to heavy

noise loading in the spectra. In comparison with the IDE-1.1 sensor, increased sensitivity to detect capacitive character of the coatings with the IDE-0.55 is plausible.

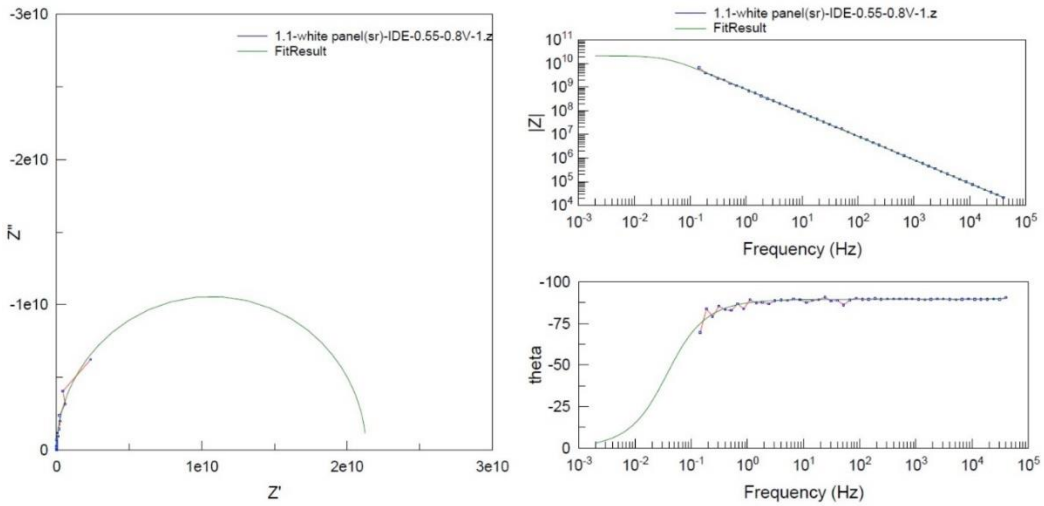

Figure A.171. Impedance fitting results of the spectra, plotted in Nyquist (left) and Bode representations (right), measured with the IDE-0.55 by testing exposed real maritime sample coating 'white' at a test voltage of 0.8 V rms (the least noisy parallel 1 from the many spectra).

The IDE-1.1 sensor provided very low capacitive signals and so remained sensitive to noise, which lead to erroneous detected impedance signals, magnitude and phase data. By learning expected outcome by the IDE-0.55 sensor, impedance data provided by the IDE-1.1 could only be fitted with probably accepted error whilst excluding effect of the medium and LF range noise and erroneous scatter of data. Therefore, none of the IDE type sensors are recommended for high resistance maritime coatings and field application.

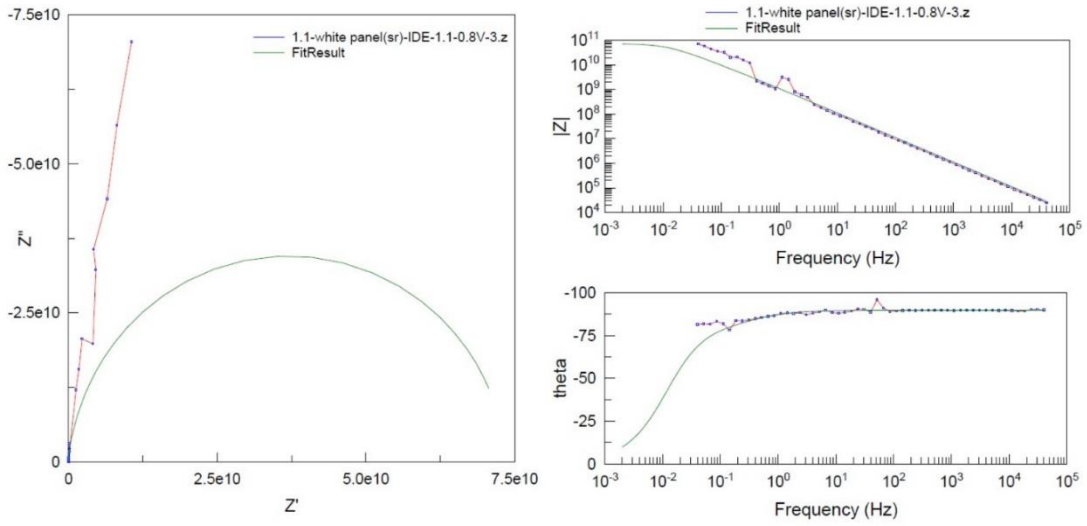

Figure A.172. Impedance fitting results of the spectra, plotted in Nyquist (left) and Bode representations (right), measured with the IDE-1.1 sensor by testing exposed real maritime sample coating 'white' at a test voltage of 0.8 V rms (the least noisy parallel 1 from the many spectra).

Impedance data of the long-term exposed and unconditioned state of the ‘white’ coating tested with the concentric array sensor with only 0.1V rms perturbation voltage are presented in Figure A.173, A.174 and A.175. All spectra obtained with a low test voltage (0.1 V) were moderately noise loaded. This noise is primarily developed by the limited electrical contact of the sensor on top surface of the coating and the low test voltage did not result in overcoming the threshold required for sufficient electrification and transmission. Despite the practical limitations, the sensor provided evaluable impedance data which can be fitted well and extrapolated to the LF range to derive coating properties. Although this type of testing was achieved in a controlled laboratory environment while leading to easily evaluable results (similar to wet phase test setup provided data), field application certainly requires greater test voltage to ensure expected degree of transmission and electrification of the coating.

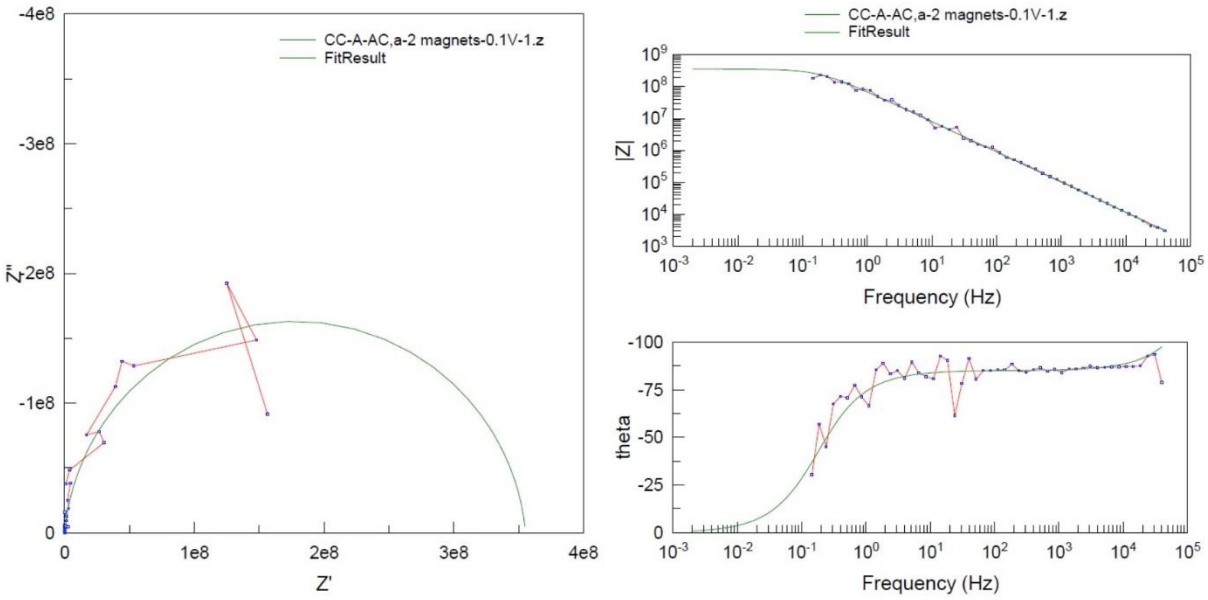

Figure A.173. Impedance fitting results of the spectra, plotted in Nyquist (left) and Bode representations (right), measured with the concentric array (CA) sensor (prototype I) by testing exposed real maritime sample coating ‘white’ at a test voltage of 0.1 V rms (the least noisy parallel 1 from the many spectra).

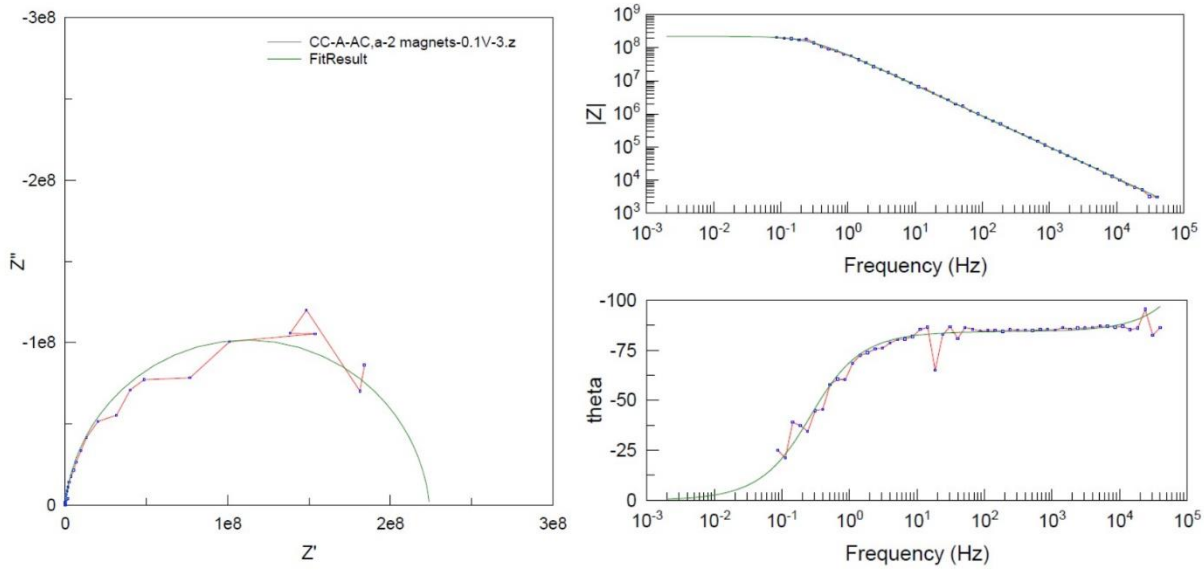

Figure A.174. Impedance fitting results of the spectra, plotted in Nyquist (left) and Bode representations (right), measured with the concentric array (CA) sensor (prototype I) by testing exposed real maritime sample coating 'white' at a test voltage of 0.1 V rms (the least noisy parallel 3 from the many spectra).

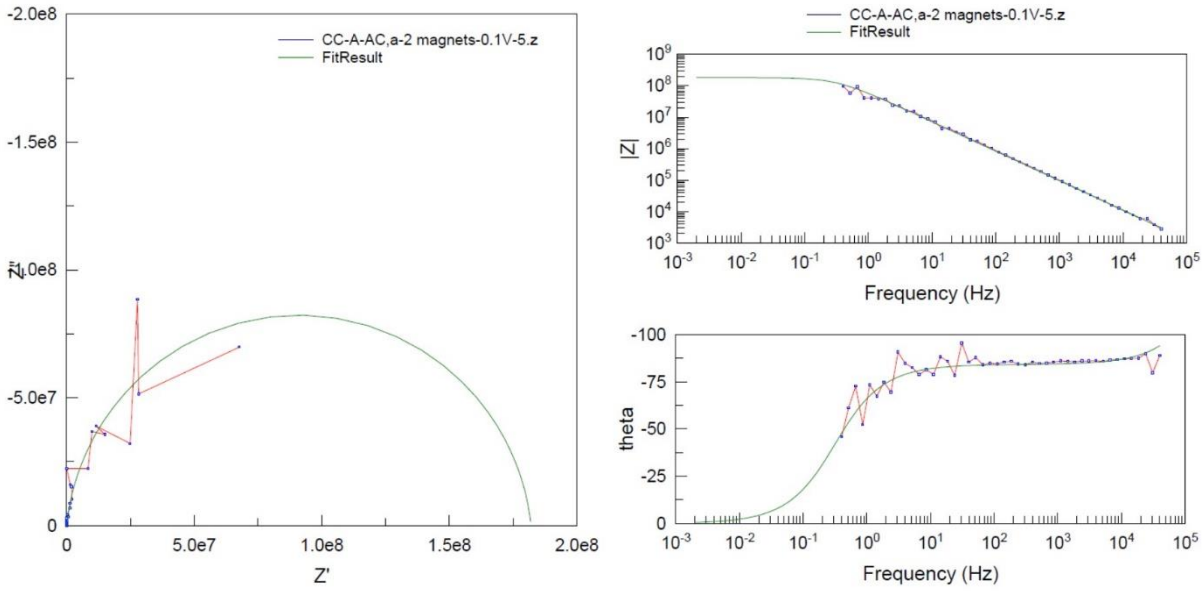

Figure A.175. Impedance fitting results of the spectra, plotted in Nyquist (left) and Bode representations (right), measured with the concentric array (CA) sensor (prototype I) by testing exposed real maritime sample coating 'white' at a test voltage of 0.1 V rms (the least noisy parallel 5 from the many spectra).

Impedance data of the long-term exposed and unconditioned state of the 'white' coating tested with the concentric array sensor with 1V rms perturbation voltage are presented in Figure A.176, A.177, A.178 and A.179. These impedance data generally feature well distinguishable HF and LF ranges for fittings along with relatively easy separation of two time-constants (location of two global and local maxima). In addition, spectra feature low noise which ensures partly high probability, creditable fitting and

assessment of data. It overall means high throughput for the number of measurements over time unit, besides reliability of testing and evaluation of the measure data. In general and in comparison with the previously presented results, electrical contact issues did not arise in the small air-gap as these were easily overcome by the large perturbation voltage in this test series. Such a proper setting for coating testing would assure credible and fast results with ease of interpretation of the spectra, condition of the tested coating.

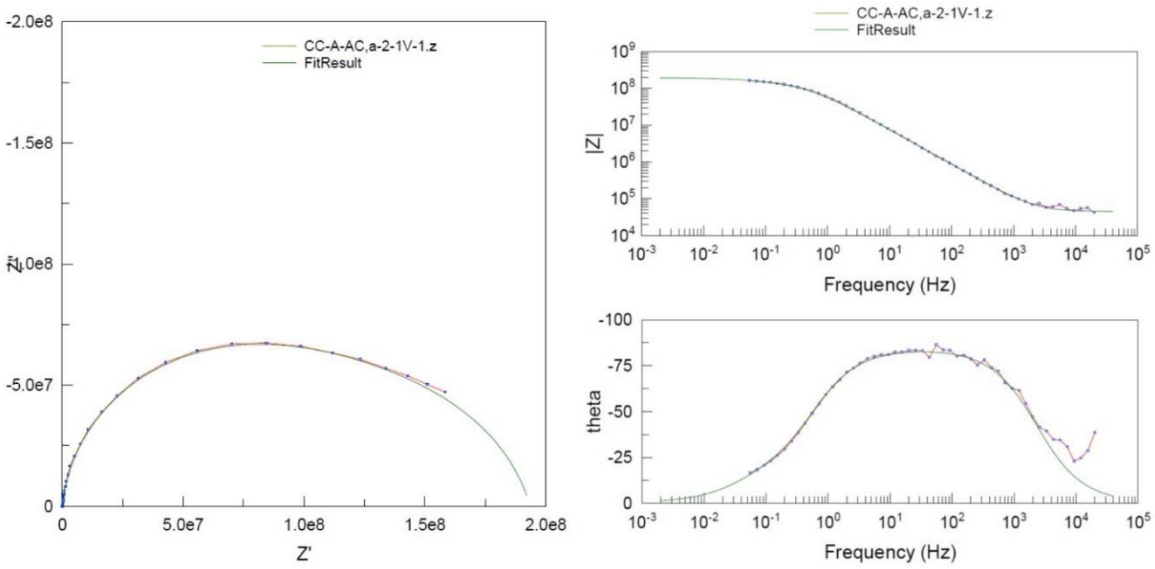

Figure A.176. Impedance fitting results of the spectra, plotted in Nyquist (left) and Bode representations (right), measured with the concentric array (CA) sensor (prototype I) by testing exposed real maritime sample coating ‘white’ at a test voltage of 1 V rms.

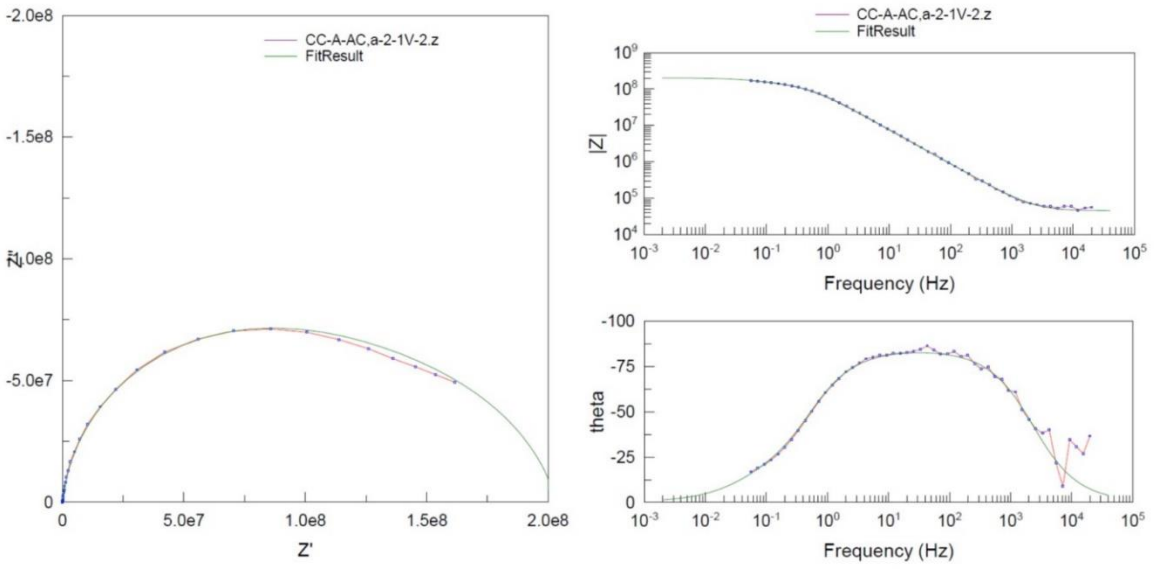

Figure A.177. Impedance fitting results of the spectra, plotted in Nyquist (left) and Bode representations (right), measured with the concentric array (CA) sensor (prototype I) by testing exposed real maritime sample coating ‘white’ at a test voltage of 1 V rms.

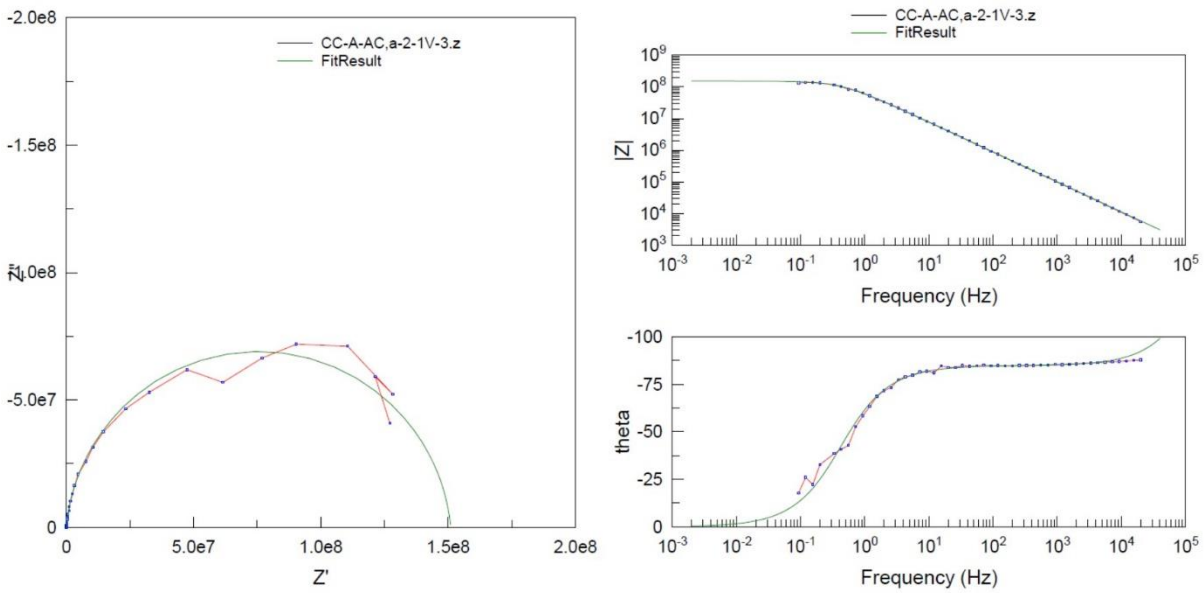

Figure A.178. Impedance fitting results of the spectra, plotted in Nyquist (left) and Bode representations (right), measured with the concentric array (CA) sensor (prototype I) by testing exposed real maritime sample coating ‘white’ at a test voltage of 1 V rms.

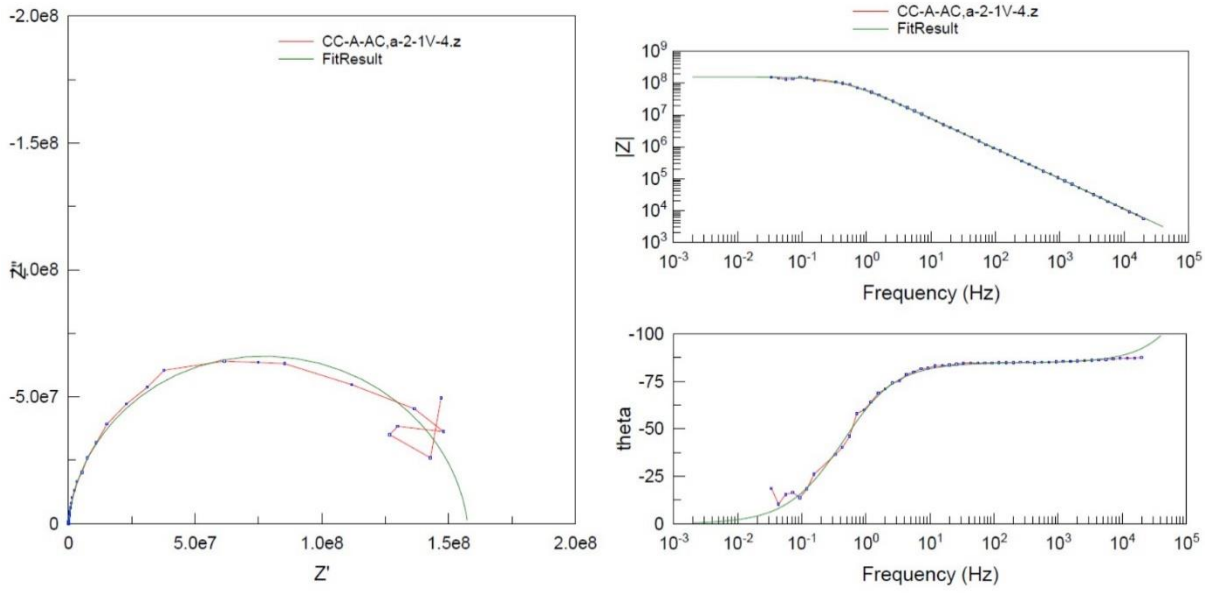

Figure A.179. Impedance fitting results of the spectra, plotted in Nyquist (left) and Bode representations (right), measured with the concentric array (CA) sensor (prototype I) by testing exposed real maritime sample coating ‘white’ at a test voltage of 1 V rms.

In comparison, impedance data of the long-term exposed and unconditioned state of the ‘white’ coating tested with the wet phase setup are presented in Figure A.180, A.181 and A.182. Despite the low perturbation test voltage, the large size test electrodes (PMMA-CE) assured noiseless detection of sensor

readings. Nonetheless, LF range of the spectra was less clearly converging towards a certain DC resistance (unlike in hydrated state by conditioning) and fitted with a simple electrical circuit topology, due to the gradually changing hydrated state of the coating along with its cross-section. In comparison with the concentric array sensor data, the low measured current and so the not distinctly converging LF range requires long-term impedance testing for proper DC extrapolation, which is a clear disadvantage for both theoretical (unaffected system with sensor readings) and practical reasons (the number of test to perform).

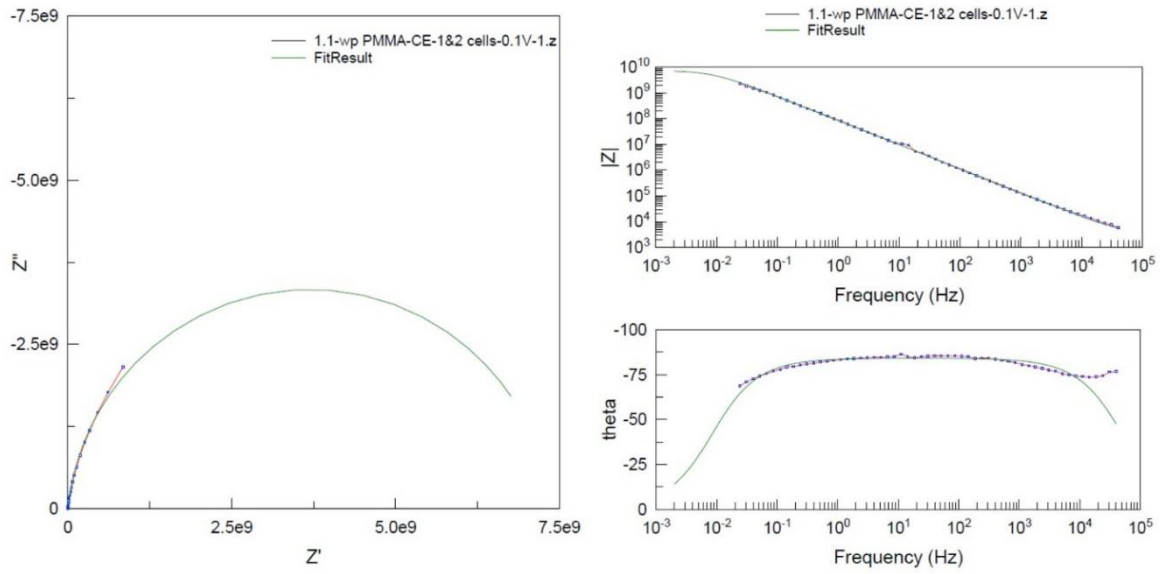

Figure A.180. Impedance fitting results of the spectra, plotted in Nyquist (left) and Bode representations (right), measured with the PMMA-CE sensor by testing exposed real maritime sample coating ‘white’ at a test voltage of 0.1 V rms.

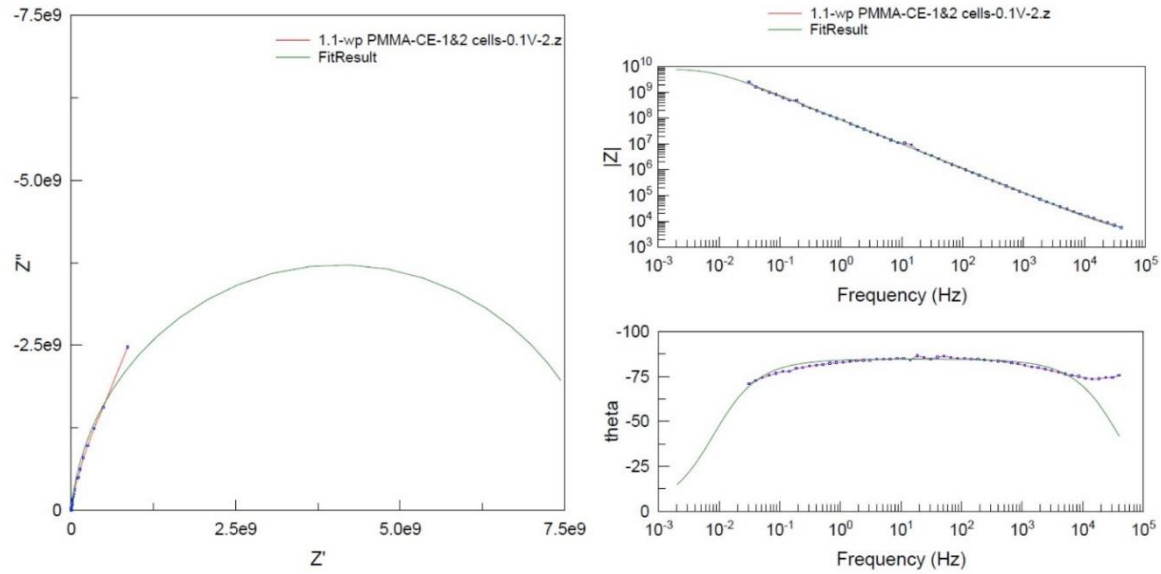

Figure A.181. Impedance fitting results of the spectra, plotted in Nyquist (left) and Bode representations (right), measured with the PMMA-CE sensor by testing exposed real maritime sample coating ‘white’ at a test voltage of 0.1 V rms.

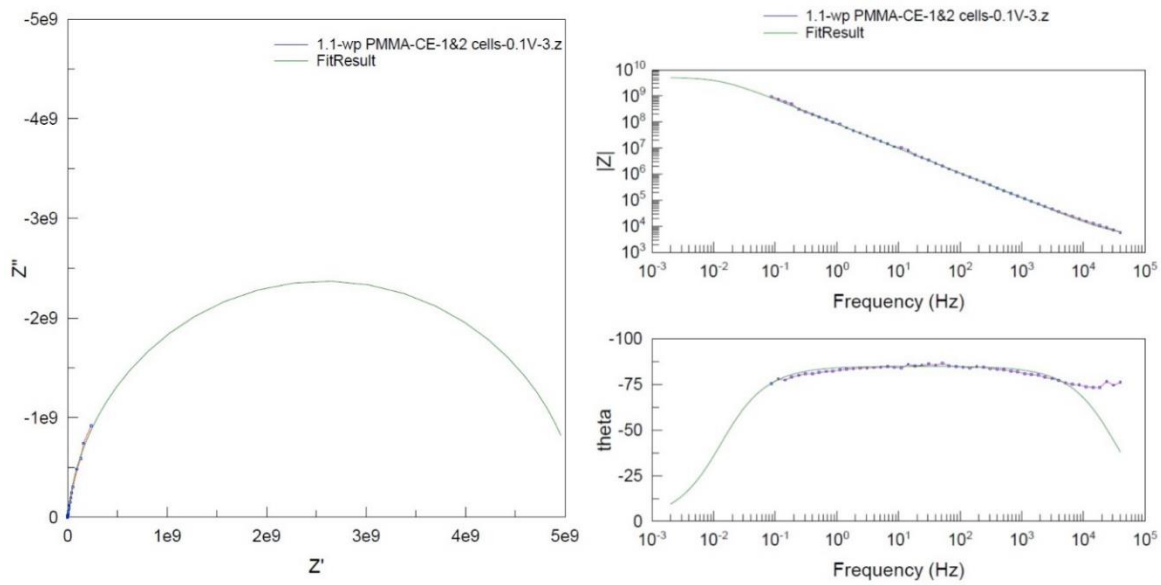

Figure A.182. Impedance fitting results of the spectra, plotted in Nyquist (left) and Bode representations (right), measured with the PMMA-CE sensor by testing exposed real maritime sample coating 'white' at a test voltage of 0.1 V rms.

Impedance test results measured after a day hydration of the tested 'white' coating are given in Figure A.183, A.184 and A.185. In comparison with the unhydrated results (previous series in Figure A.180, A.181 and A.182), medium frequency range of the spectra was affected by wet phase conditioning and so was easier to extrapolate to LF range and estimate DC resistance of the coating. It is also clear even the reference coating without an interface effect requires complex topology electrical circuit for fitting of the at least two highly overlapping time constants.

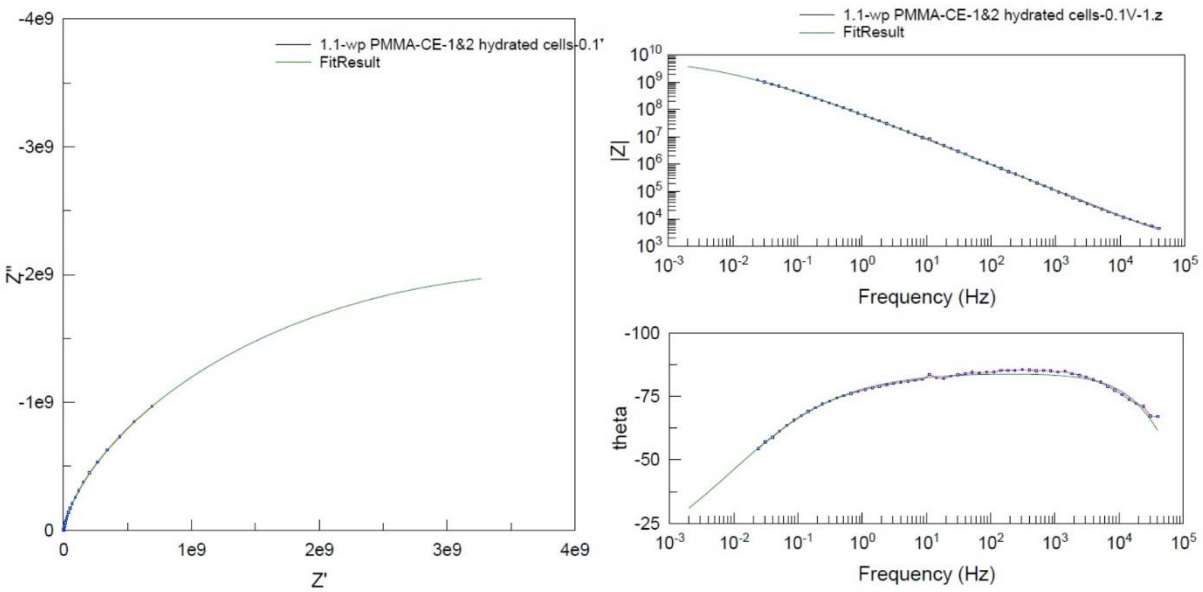

Figure A.183. Impedance fitting results of the spectra, plotted in Nyquist (left) and Bode representations (right), measured with the PMMA-CE sensor by testing exposed real maritime sample coating 'white' (on pre-hydrated area) at a test voltage of 0.1 V rms.

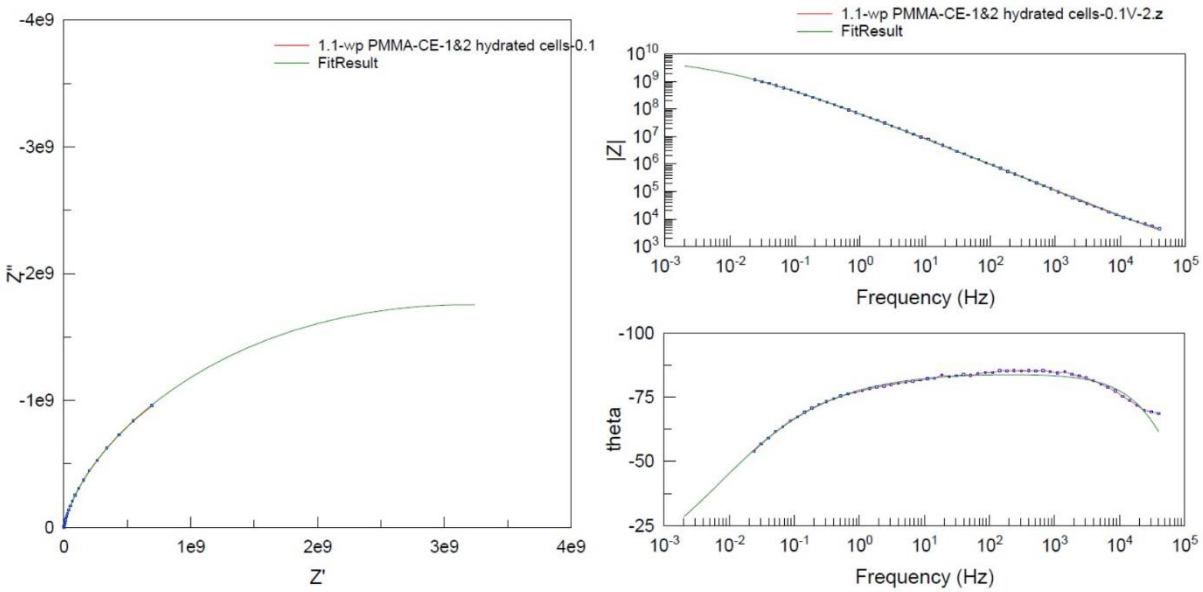

Figure A.184. Impedance fitting results of the spectra, plotted in Nyquist (left) and Bode representations (right), measured with the PMMA-CE sensor by testing exposed real maritime sample coating 'white' (on pre-hydrated area) at a test voltage of 0.1 V rms.

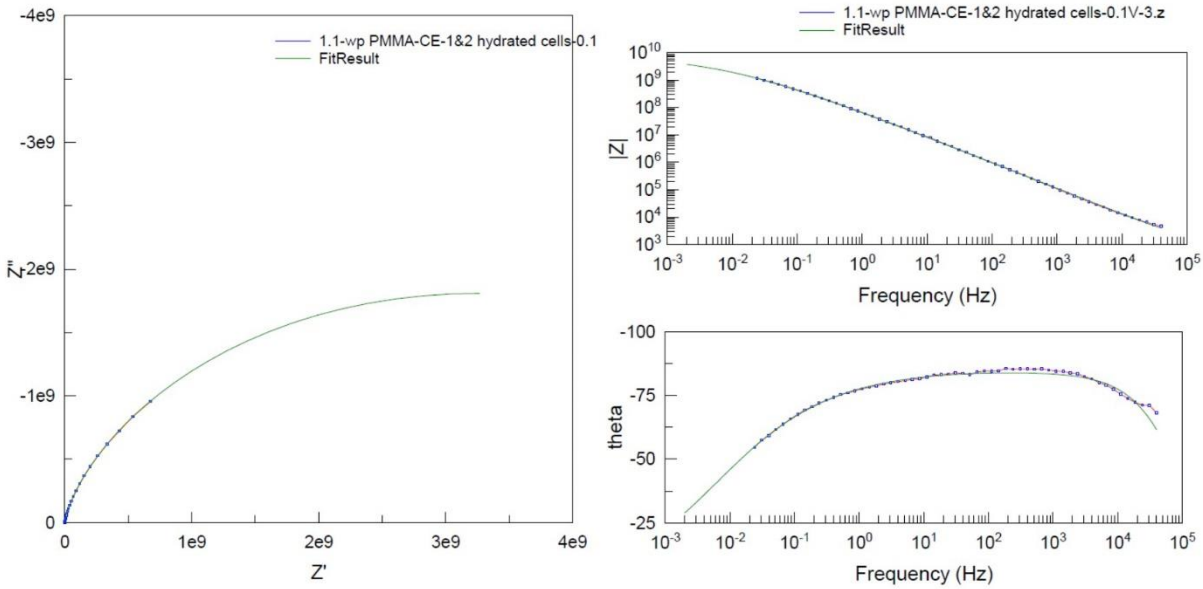

Figure A.185. Impedance fitting results of the spectra, plotted in Nyquist (left) and Bode representations (right), measured with the PMMA-CE sensor by testing exposed real maritime sample coating 'white' (on pre-hydrated area) at a test voltage of 0.1 V rms.

Results from the Mono-pylon at the Endures BV

Parallel spectra and impedance fitting results on the mono-pylon coating tested with the concentric array sensor are summarised in Figure A.186, A.187 and A.188. As it is seen on all Nyquist and Bode representations, the two time-constants, which is typical for long-immersed coatings, are not clearly distinguishable and separable, owing to the moderate magnitude of noise in the spectra. Although scatter

of data was far inferior to the extent experienced in measure data obtained by the traditional wet phase setup, repeated measurements were beneficial to increase probability of proper evaluation of impedance data. The assessment was performed with the simplest topology circuit containing the least number of passive elements while try to reproduce the most probable spectra without noise.

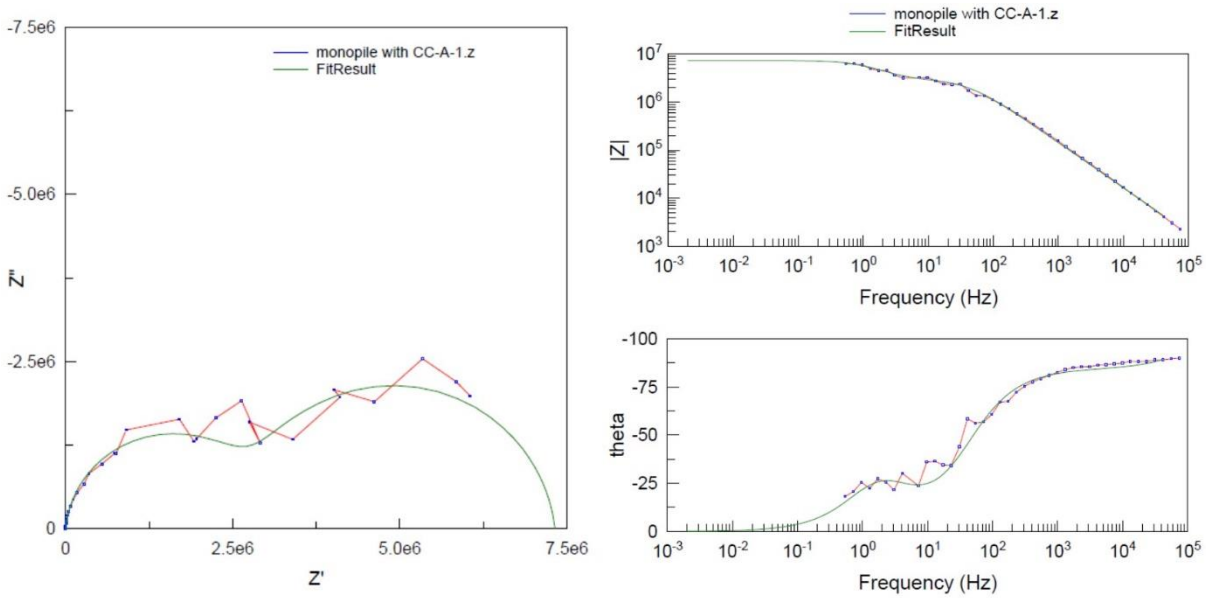

Figure A.186. Impedance fitting results of the spectra, plotted in Nyquist (left) and Bode representations (right), measured with the concentric array (CA) sensor (prototype I) by testing exposed real maritime sample coating 'yellow' (applied on mono-pylon at Endures BV) at a test voltage of 1 V rms (parallel 1).

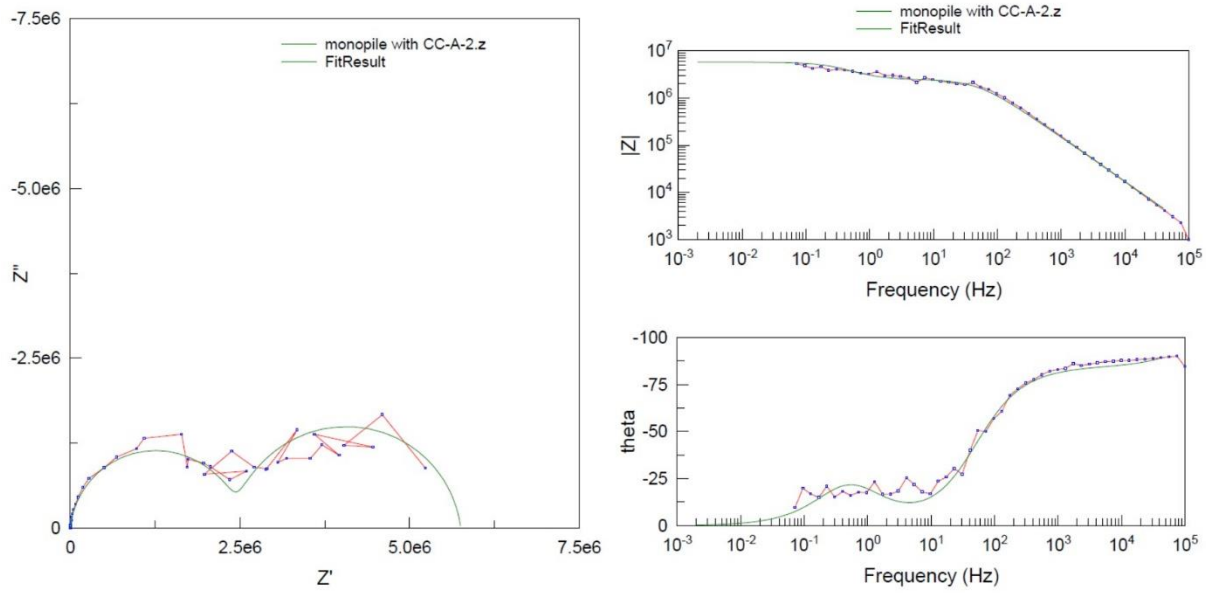

Figure A.187. Impedance fitting results of the spectra, plotted in Nyquist (left) and Bode representations (right), measured with the concentric array (CA) sensor (prototype I) by testing exposed real maritime sample coating 'yellow' (applied on mono-pylon at Endures BV) at a test voltage of 1 V rms (parallel 2).

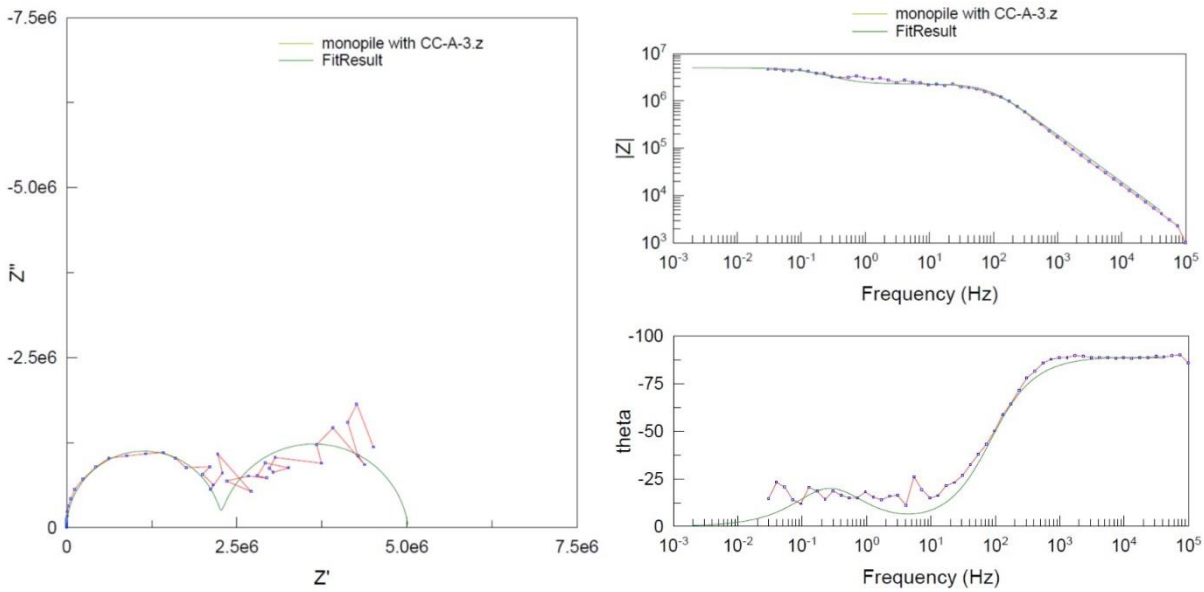

Figure A.188. Impedance fitting results of the spectra, plotted in Nyquist (left) and Bode representations (right), measured with the concentric array (CA) sensor (prototype I) by testing exposed real maritime sample coating 'yellow' (applied on mono-pylon at Endures BV) at a test voltage of 1 V rms (parallel 3).

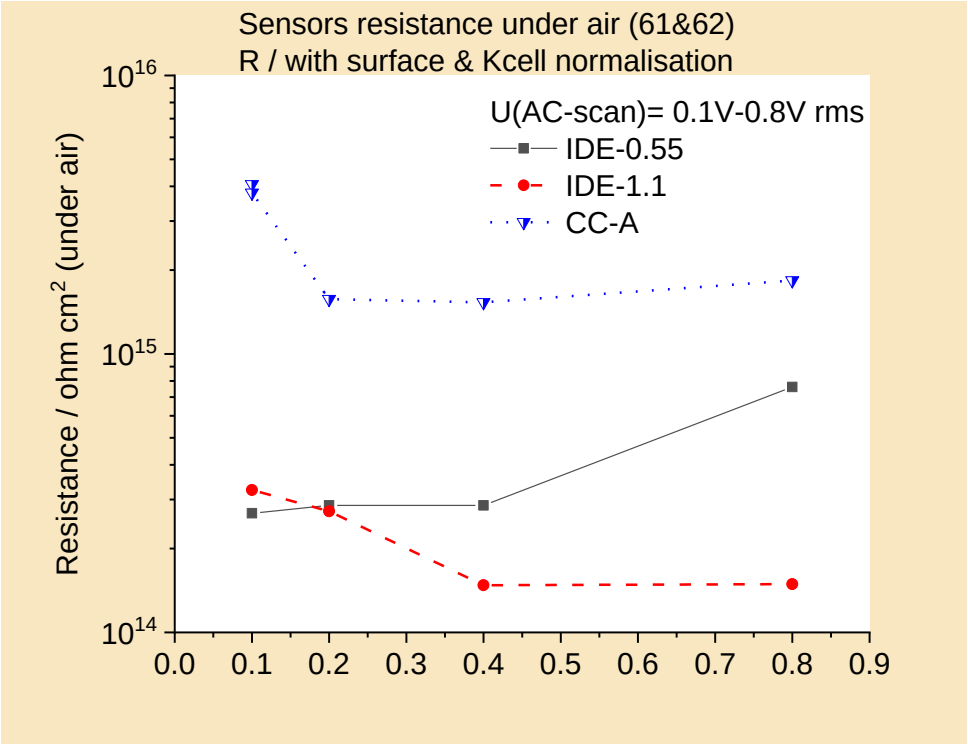

Figure A.189. Resistance response of the prototype sensors under air as a function of test voltage.

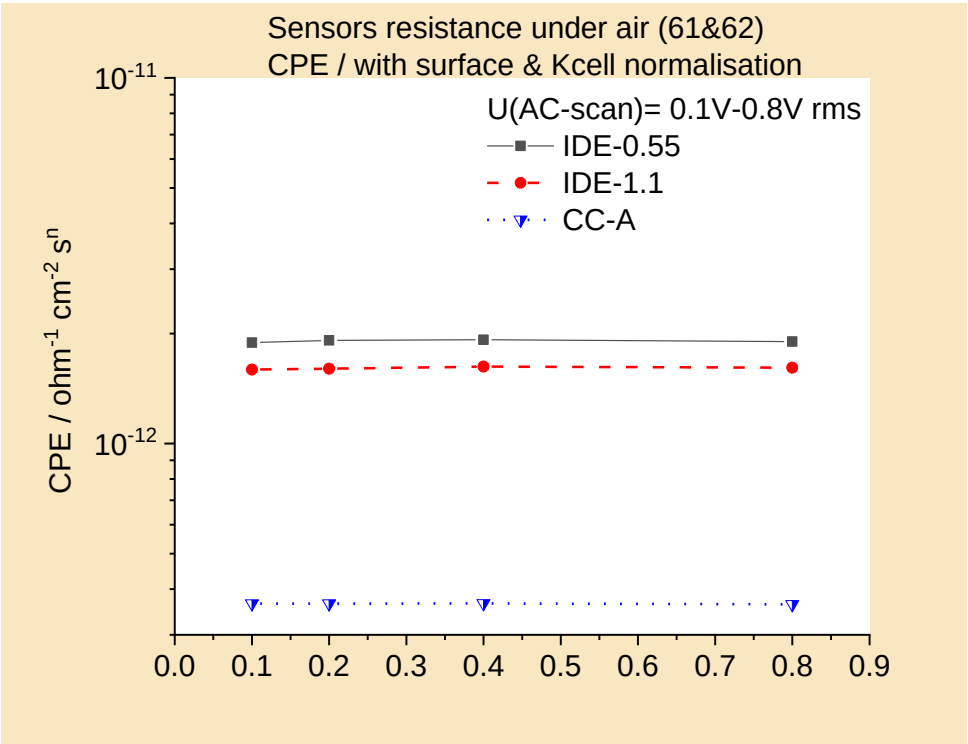

Figure A.190. Capacitive character of the prototype sensors under air as a function of test voltage.

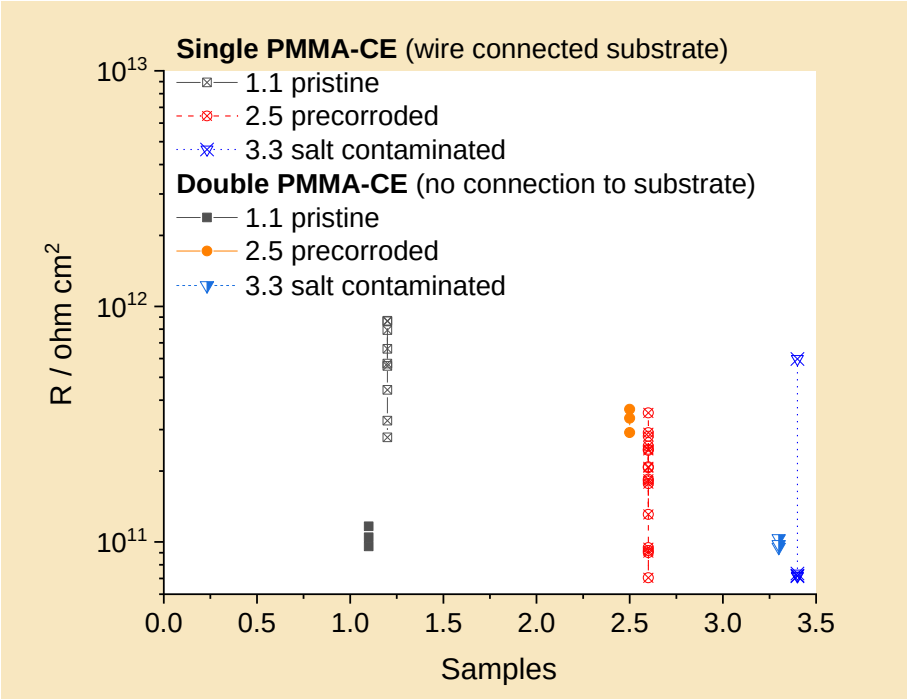

Figure A.191. Resistance of neat (1.1), pre-corroded (2.5), and salt contaminated (3.3) steel-coating substrates fitted with planar carbon electrodes: one and two, used in wire connected (single PMMA-CE) and no connection (double PMMA-CE) to substrate modes.

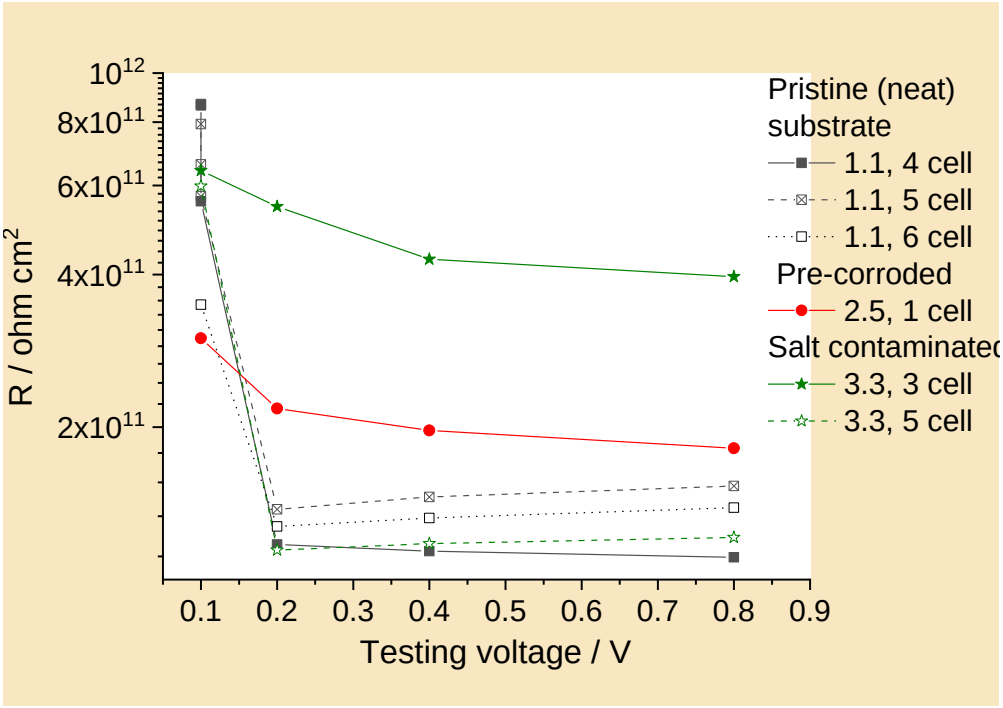

Figure A.151. Resistance of neat (1.1), pre-corroded (2.5), and salt contaminated (3.3) steel-coating substrates (measured with planar carbon electrodes) as a function of test voltage: one and two, used in wire connected (single PMMA-CE) and no connection (double PMMA-CE) to substrate modes.

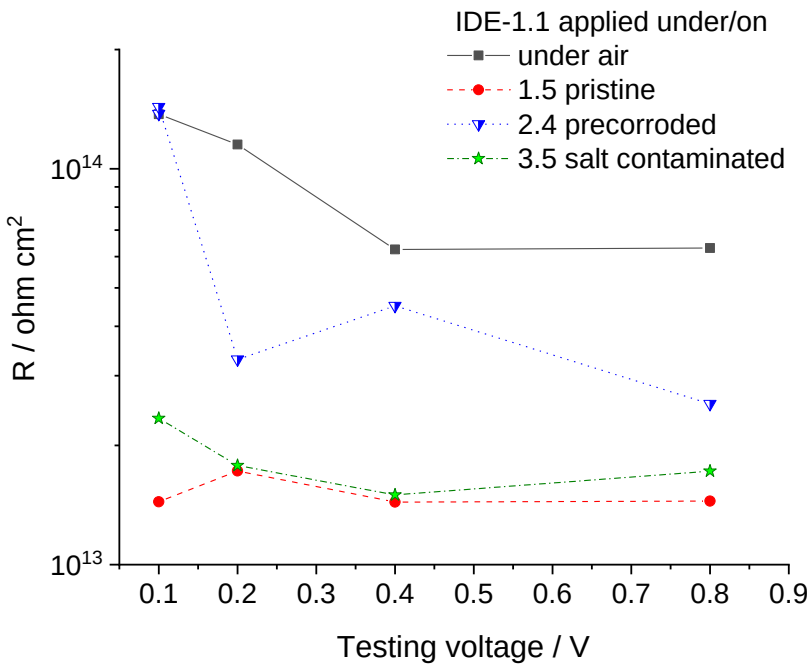

Figure A.152. Resistance of the pristine (1.5), pre-corroded (2.4), and salt contaminated (3.5) steel-coating substrates measured with the interdigitated strip-line (IDE-1.1) sensor and data normalized with cell constant and geometrical surface area in inner section of the disk-ring electrodes.

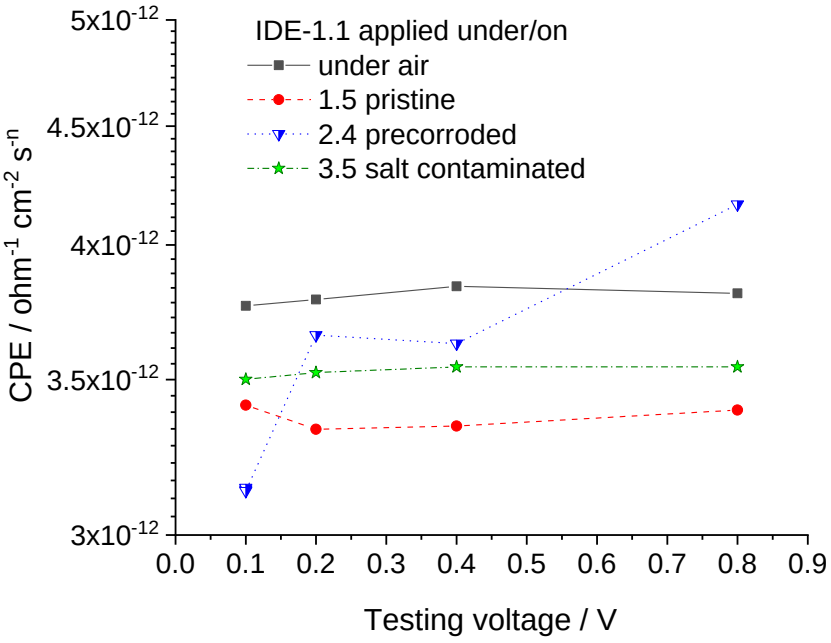

Figure A.153. Constant phase element of the pristine (1.5), pre-corroded (2.4), and salt contaminated (3.5) steel-coating substrates measured with the interdigitated strip-line (IDE-1.1) sensor and data normalized with cell constant and geometrical surface area in inner section of the disk-ring electrodes.

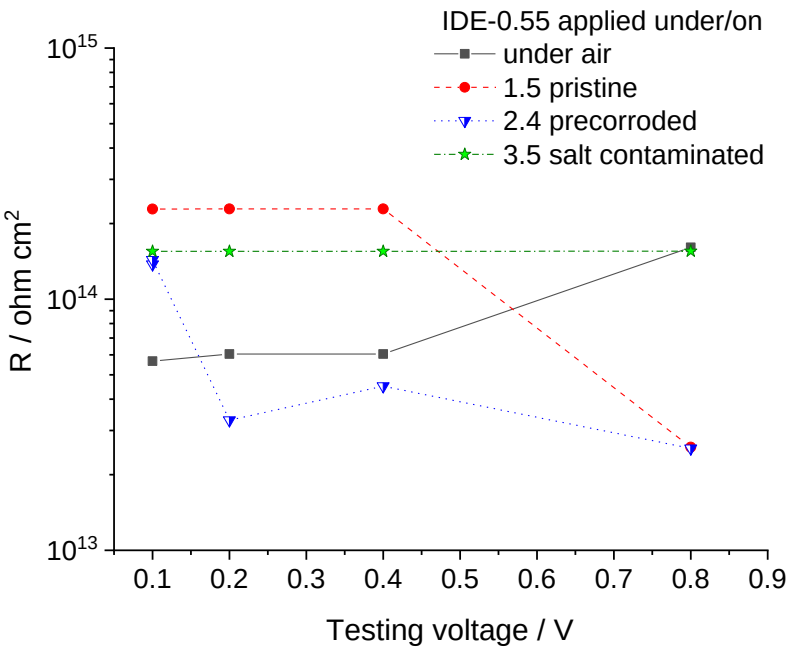

Figure A.154. Resistance of the pristine (1.5), pre-corroded (2.4), and salt contaminated (3.5) steel-coating substrates measured with the interdigitated strip-line (IDE-0.55) sensor. Sensor readings were normalized with cell constant and geometrical surface area in inner section of the disk-ring electrodes.

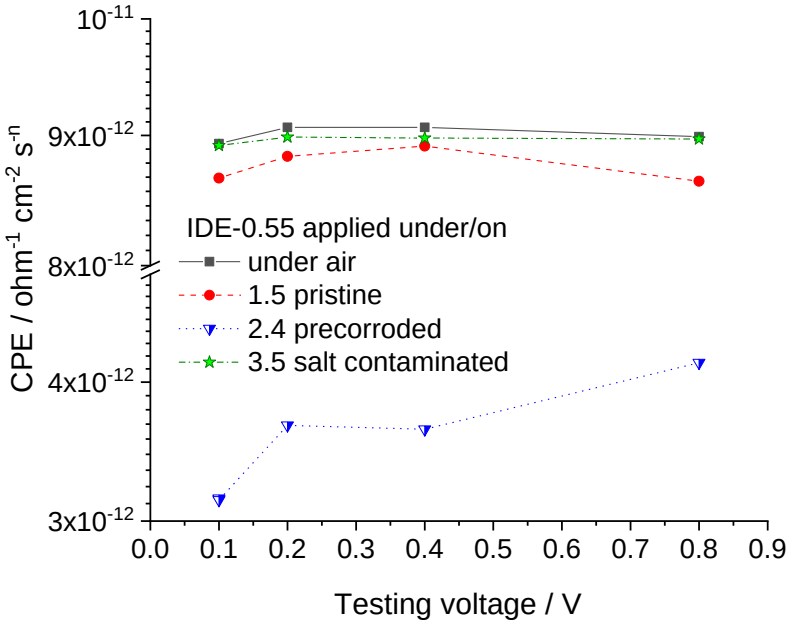

Figure A.155. Constant phase element of the pristine (1.5), pre-corroded (2.4), and salt contaminated (3.5) steel-coating substrates measured with the interdigitated strip-line (IDE-0.55) sensor. Sensor readings were normalized with cell constant and geometrical surface area in inner section of the disk-ring electrodes.

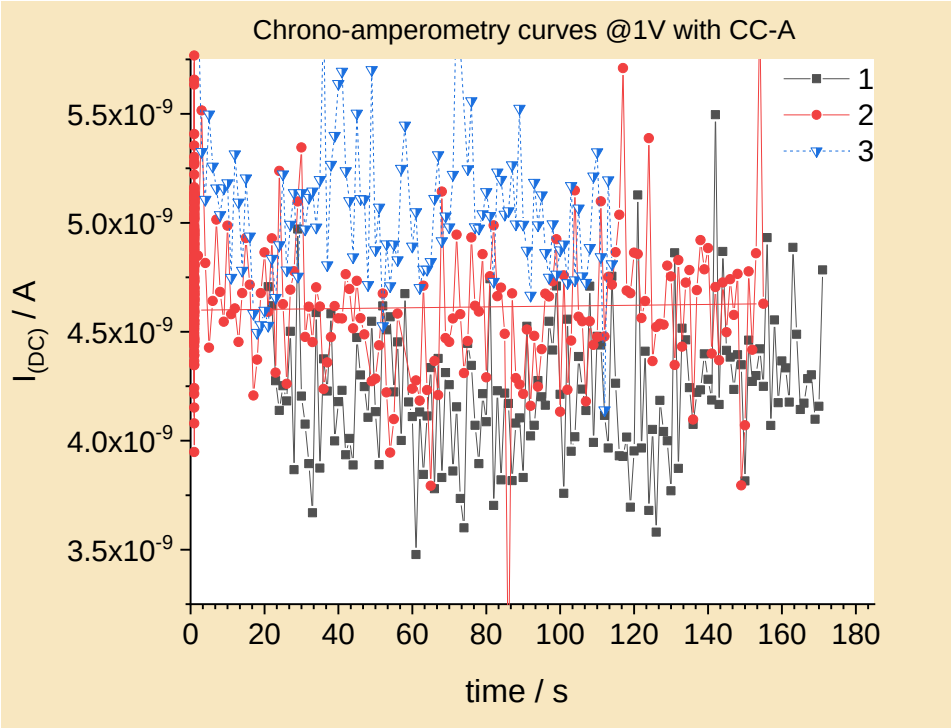

Figure A.156. Chrono-amperometry curves measured in response to 1 V with the concentric array prototype on the long-term immersion exposed real maritime modelling 'white' coating sample.

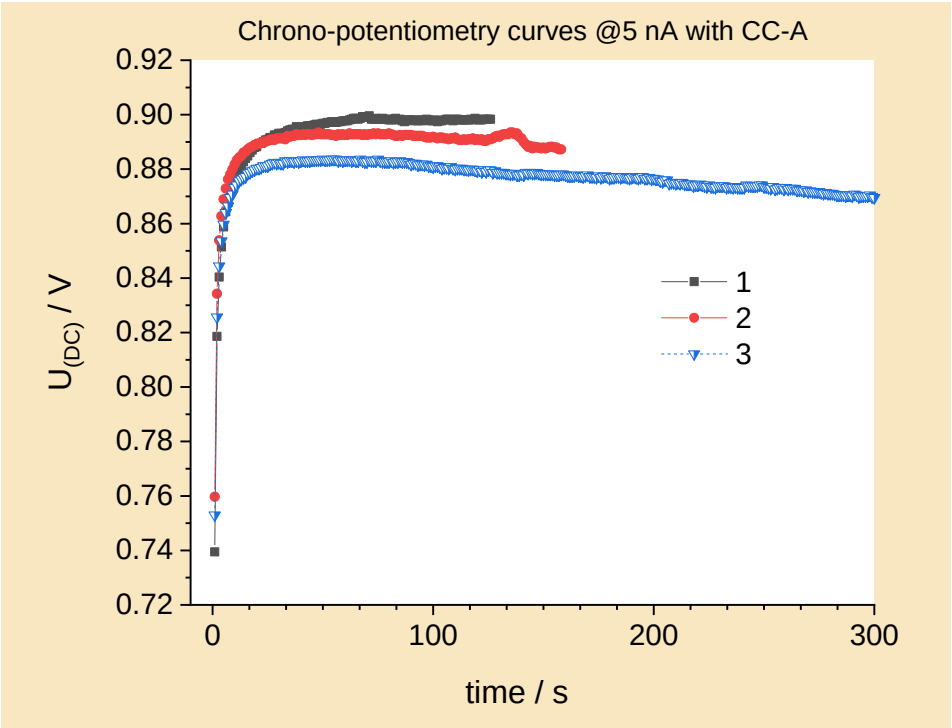

Figure A.157. Chrono-potentiometry curves measured in response to 5 nA with the concentric array prototype on the long-term immersion exposed real maritime modelling 'white' coating sample.

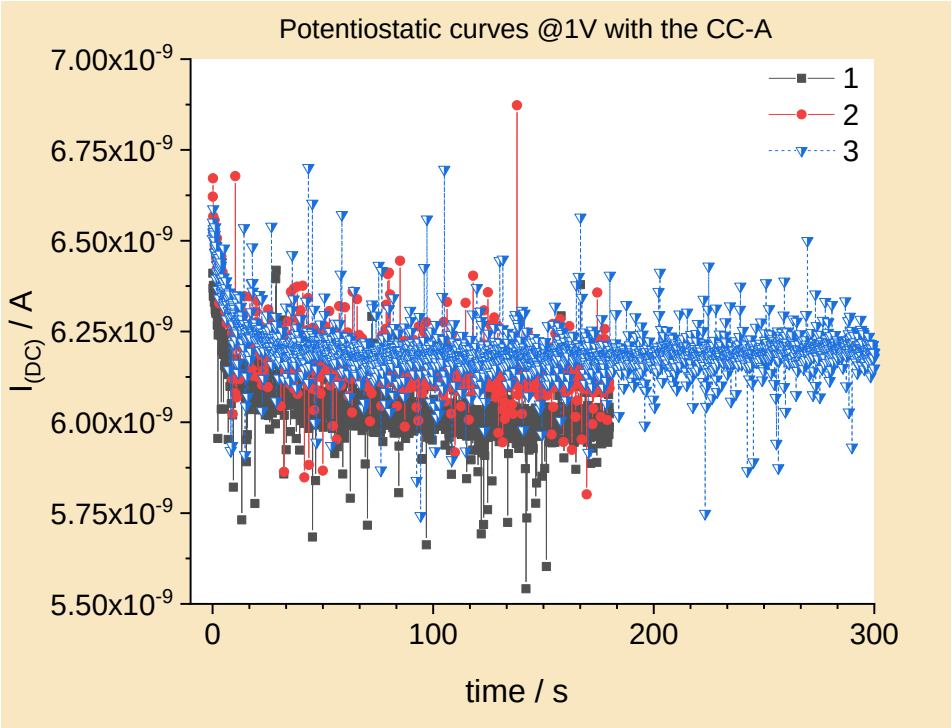

Figure A.158. Potentiometry curves measured in response to 1 V with the concentric array prototype on the long-term immersion exposed real maritime modelling ‘white’ coating sample.